DESIGN AND DEVELOPMENT OF NANOPARTICULATE FORMULATION OF ANTICANCER DRUGS FOR BREAST TUMOR TARGETING

A thesis submitted to

THE MAHARAJA SAYAJIRAO UNIVERSITY OF BARODA

For the award of the degree of

DOCTOR OF PHILOSOPHY
in
PHARMACY

By

ABHINESH KUMAR

Under the guidance of

PROF. KRUTIKA K. SAWANT

Pharmacy Department,
Faculty of Technology and Engineering,
The Maharaja Sayajirao University of Baroda,
Vadodara - 390 001
MAY 2014

DECLARATION

In accordance with University ordinance number ACED-309 Ph.D., I, the undersigned states that, the work presented in this thesis entitled "Design and Development of Nanoparticulate Formulation of Anticancer Drugs for Breast Tumor Targeting" comprise independent investigations carried out by me. Wherever references have been made to the work of others, it has been clearly indicated with the source of information under the title of references at end of each chapter.

Date:

Place: Vadodara (Abhinesh Kumar)

Certified by and forwarded through research guide,

Prof. Krutika K. Sawant,
Pharmacy Department,
Faculty of Technology and Engineering,
The Maharaja Sayajirao University of Baroda,
Vadodara - 390 001

CERTIFICATE

This is to certify that the thesis entitled "Design and Development of Nanoparticulate Formulation of Anticancer Drugs for Breast Tumor Targeting" submitted for the Ph. D. Degree in Pharmacy by Mr. Abhinesh Kumar incorporates the original research work carried out by him under my supervision and no part of this work has been previously submitted for any degree.

Guide
Prof. Krutika. K. Sawant

Head
Pharmacy Department

DEAN
Faculty of Technology & Engineering,
The Maharaja Sayajirao University of Baroda,
Vadodara -390 001

CONTENTS

1. Introduction
   1.1 Introduction
   1.2 Aims to be achieved from the present study
   1.3 Hypothesis
   1.4 Objectives
   1.5 Plan of work
   1.6 References

2. Literature review
   2.1 Cancer
      2.1.1 Cancer statistics
   2.2 Tumor physiology
      2.2.1 Tumor growth
      2.2.2 Tumor vasculature and lymphatic system
      2.2.3 Barriers to drug delivery in tumors
         2.2.3.1 Reticuloendothelial system and mononuclear phagocytic system
         2.2.3.2 First pass renal filtering
         2.2.3.3 Heterogeneous blood flow
         2.2.3.4 High tumor interstitial pressure
         2.2.3.5 Extracellular matrix
         2.2.3.6 Intracellular transport
   2.3 Breast Cancer
      2.3.1 Antiestrogens
      2.3.2 EGFR and HER2/ Neu and Antiestrogen resistance
      2.3.3 Aromatase inhibitors
      2.3.4 Mechanisms of resistance
      2.3.5 Role of progesterone receptor and HER2/Neu
   2.4 Treatment of breast cancer
      2.4.1 Treatment options by stage
      2.4.2 Surgery
      2.4.3 Radiation therapy
      2.4.4 Chemotherapy

2.5 Targeted therapy
2.5.1 Nanoparticulate drug delivery system
2.5.1.1 Polymeric nanoparticles (Nanospheres and nanocapsules)
2.5.1.2 Liposomes
2.5.1.3 Micelles
2.5.1.4 Dendrimers
2.6 Targeting
2.6.1 Passive targeting
2.6.1.1 Size
2.6.1.2 Particle shape
2.6.1.3 Surface characteristics
2.6.1.4 PEGylation
2.6.1.5 Limitations of passive targeting
2.6.2 Active targeting
2.6.2.1 Folate
2.6.2.2 Transferrin
2.6.2.3 Aptamers
2.6.2.4 Antibodies (monoclonal antibodies)
2.6.2.5 Peptides
2.6.2.6 Limitations of active targeting
2.7 Poly lactic-co-glycolic acid (PLGA)
2.8 Polycaprolactone
2.9 Anastrozole
2.10 Exemestane
2.11 References

3. Analytical methods
3.1 Materials
3.2 Estimation method for anastrozole
3.2.1 High performance liquid chromatography
3.2.2 Preparation of standard stock solutions
3.2.3 Preparation of calibration curve
3.2.4 Analytical method validation

3.2.4.1 Linearity
3.2.4.2 Accuracy
3.2.4.3 Precision
3.2.5 Estimation of anastrozole in nanoparticulate formulations
3.3 Estimation method for exemestane
3.3.1 High performance liquid chromatography
3.3.2 Preparation of standard stock solutions
3.3.3 Preparation of calibration curve
3.3.4 Analytical method validation
3.2.4.1 Linearity
3.2.4.2 Accuracy
3.2.4.3 Precision
3.3.5 Estimation of exemestane in nanoparticulate formulations
3.4 References

4. Formulation, optimization and characterization of nanoparticulate formulation
4.1 Introduction
4.2 Materials
4.3 Synthesis of polymer and conjugates
4.3.1 Synthesis of PLGA-PEG conjugate
4.3.2 Synthesis of cPCL
4.3.3 Synthesis of PCL-PEG conjugate
4.4 Characterization of polymer and conjugates
4.4.1 FTIR spectroscopy
4.4.2 NMR spectroscopy
4.4.3 Molecular weight determination
4.5 Formulation and optimization of ATZ loaded PLGA NPs
4.5.1 Preparation of ATZ loaded PLGA NPs
4.5.2 Drug content and percentage drug entrapment
4.5.3 Particle size
4.5.4 Preliminary optimization of ATZ loaded PLGA NPs
4.5.4.1 Selection of organic solvent
4.5.4.2 Selection of volume of organic solvent

4.5.4.3 Selection of surfactant
4.5.5 Optimization
4.5.5.1 Experimental design for optimization of key formulation variables
4.5.5.2 Contour plots
4.5.5.3 Response surface plots
4.5.5.4 Check point analysis
4.5.5.5 Desirability criteria
4.5.5.6 Normalized error determination
4.5.6 Lyophilization and optimization of cryoprotectant
4.6 Formulation and optimization of ATZ loaded cPCL NPs
4.6.1 Preparation of ATZ loaded cPCL NPs
4.6.2 Drug content and percentage drug entrapment
4.6.3 Particle size
4.6.4 Preliminary optimization of ATZ loaded cPCL NPs
4.6.4.1 Selection of organic solvent
4.6.4.2 Selection of volume of organic solvent
4.6.4.3 Selection of surfactant
4.6.5 Optimization
4.6.5.1 Experimental design for optimization of key formulation variables
4.6.5.2 Contour plots
4.6.5.3 Response surface plots
4.6.5.4 Check point analysis
4.6.5.5 Desirability criteria
4.6.5.6 Normalized error determination
4.6.6 Lyophilization and optimization of cryoprotectant
4.7 Formulation and optimization of EXE loaded PLGA NPs
4.7.1 Preparation of EXE loaded PLGA NPs
4.7.2 Drug content and percentage drug entrapment
4.7.3 Particle size
4.7.4 Preliminary optimization of EXE loaded PLGA NPs
4.7.4.1 Type of organic solvent
4.7.4.2 Selection of surfactant
4.7.4.3 Concentration of surfactant

4.7.5 Optimization
4.7.5.1 Experimental design for optimization of key formulation variables
4.7.5.2 Contour plots
4.7.5.3 Response surface plots
4.7.5.4 Check point analysis
4.7.5.5 Desirability criteria
4.7.5.6 Normalized error determination
4.7.6 Lyophilization and optimization of cryoprotectant
4.8 Formulation and optimization of EXE loaded cPCL NPs
4.8.1 Preparation of EXE loaded cPCL NPs
4.8.2 Drug content and percentage drug entrapment
4.8.3 Particle size
4.8.4 Preliminary optimization of EXE loaded cPCL NPs
4.8.4.1 Type of organic solvent
4.8.4.2 Selection of surfactant
4.8.4.3 Concentration of surfactant
4.8.5 Optimization
4.8.5.1 Experimental design for optimization of key formulation variables
4.8.5.2 Contour plots
4.8.5.3 Response surface plots
4.8.5.4 Check point analysis
4.8.5.5 Desirability criteria
4.8.5.6 Normalized error determination
4.8.6 Lyophilization and optimization of cryoprotectant
4.9 Characterization of optimized nanoparticulate formulation
4.9.1 Zeta potential
4.9.2 Transmission electron microscope studies
4.9.3 Differential scanning calorimetric (DSC) studies
4.9.4 In vitro drug release studies
4.9.5 Stability studies
4.10 Results and discussion
4.10.1 Characterization of PLGA-PEG conjugate
4.10.2 Characterization of cPCL

4.10.3 Characterization of PCL-PEG conjugate
4.11Formulation and optimization of ATZ loaded PLGA NPs
4.11.1 Preliminary optimization of ATZ loaded PLGA NPs
4.11.1.1 Selection of organic solvent
4.11.1.2 Selection of volume of organic solvent
4.11.1.3 Selection of surfactant
4.11.2 Optimization of ATZ loaded PLGA NPs using 3^3 factorial design
4.11.2.1 Contour plots
4.11.2.2 Response surface plots
4.11.2.3 Desirability criteria
4.11.2.4 Checkpoint analysis and normalized error
4.11.3 Lyophilization and optimization of cryoprotectants
4.12 Formulation and optimization of ATZ loaded cPCL NPs
4.12.1 Preliminary optimization of ATZ loaded cPCL NPs
4.12.1.1 Selection of organic solvent
4.12.1.2 Selection of volume of organic solvent
4.12.1.3 Selection of surfactant
4.12.2 Optimization of ATZ loaded cPCL NPs using 3^3 factorial design
4.12.2.1 Contour plots
4.12.2.2 Response surface plots
4.12.2.3 Desirability criteria
4.12.2.4 Checkpoint analysis and normalized error
4.12.3 Lyophilization and optimization of cryoprotectants
4.13 Formulation and optimization of EXE loaded PLGA NPs
4.13.1 Preliminary optimization of EXE loaded PLGA NPs
4.13.1.1 Selection of organic solvent
4.13.1.2 Selection of surfactant
4.13.1.3 Selection of surfactant concentration
4.13.2 Optimization of EXE loaded PLGA NPs using BBD
4.13.2.1 Contour plots
4.13.2.2 Response surface plots
4.13.2.3 Desirability criteria
4.13.2.4 Checkpoint analysis and normalized error

4.13.3 Lyophilization and optimization of cryoprotectants
4.14Formulation and optimization of EXE loaded cPCL NPs
4.14.1 Preliminary optimization of EXE loaded cPCL NPs
4.14.1.1 Selection of organic solvent
4.14.1.2 Selection of surfactant
4.14.1.3 Selection of surfactant concentration
4.14.2 Optimization of EXE loaded cPCL NPs using BBD
4.14.2.1 Contour plots
4.14.2.2 Response surface plots
4.14.2.3 Desirability criteria
4.14.2.4 Checkpoint analysis and normalized error
4.14.3 Lyophilization and optimization of cryoprotectants
4.15 Characterization of ATZ loaded PLGA NPs
4.15.1 Zeta potential
4.15.2 Transmission electron microscopy (TEM)
4.15.3 Differential scanning calorimetry (DSC)
4.15.4 In vitro drug release studies
4.15.5 Stability studies
4.16 Characterization of ATZ loaded cPCL NPs
4.16.1 Zeta potential
4.16.2 Transmission electron microscopy (TEM)
4.16.3 Differential scanning calorimetry (DSC)
4.16.4 In vitro drug release studies
4.16.5 Stability studies
4.17 Characterization of EXE loaded PLGA NPs
4.17.1 Zeta potential
4.17.2 Transmission electron microscopy (TEM)
4.17.3 Differential scanning calorimetry (DSC)
4.17.4 In vitro drug release studies
4.17.5 Stability studies
4.18 Characterization of EXE loaded cPCL NPs
4.18.1 Zeta potential
4.18.2 Transmission electron microscopy (TEM)

4.18.3 Differential scanning calorimetry (DSC)
4.18.4 In vitro drug release studies
4.18.5 Stability studies
4.19 References

5. Pegylation and surface functionalization
5.1 Materials
5.2 Cell lines
5.3 Methods
5.3.1 Pegylation of nanoparticles
5.3.2 Phagocytic uptake
5.3.3 Surface functionalization of NPs with ER antibody
5.4 Results and discussion
5.4.1 Physicochemical characterization of ATZ loaded PLGA NPs
5.4.2 Optimization of ATZ loaded PLGA NPs containing different PEG ratio based on PDE, PS and phagocytic uptake studies
5.4.3 Physicochemical characterization of ImmunoNPs
5.4.4 Physicochemical characterization of EXE loaded PCL NPs
5.4.5 Optimization of EXE loaded PCL NPs containing different PEG ratio based on PDE, PS and phagocytic uptake studies
5.4.6 Physicochemical characterization of ImmunoNPs
5.5 References

6. Cell culture studies
6.1 Introduction
6.1.1 Cellular uptake
6.1.2 Cytotoxicity studies
6.1.3 Apoptosis
6.1.4 Cell cycle analysis
6.2 Materials
6.3 Cell lines
6.4 Methods
6.4.1 Receptor expression analysis by Western Blot
6.4.2 Qualitative cellular uptake by fluorescent microscopy

6.4.3 Quantitative cellular uptake by flow cytometry
6.4.4 In vitro cytotoxicity studies by MTT Assay
6.4.5 In vitro apoptosis study
6.4.6 Cell cycle analysis by flow cytometry
6.5 Results and discussion
6.5.1 Receptor expression in cell lines
6.5.2 Qualitative and quantitative cellular uptake
6.5.3 In vitro cytotoxicity studies by MTT Assay
6.5.4 Apoptosis studies
6.5.5 Cell cycle analysis
6.6 References

7. In vivo biodistribution studies
7.1 Introduction
7.2 Materials
7.3 Methods
7.3.1 Radioiodination of antibody
7.3.2 Determination of labeling efficiency by electrophoresis
7.3.3 Purification of radiolabeled antibody
7.3.4 Conjugation of iodinated antibody and TME on NPs
7.3.5 Stability of radiolabelled conjugates
7.3.6 Biodistribution studies
7.3.7 Statistical analysis
7.4 Results and discussion
7.4.1 Stability of radioiodinated complexes
7.4.2 Biodistribution studies
7.4.2.1 Biodistribution of ^{125}I-Tyr PLGA NPs and ^{125}I-ER Ab PLGA NPs
7.4.2.2 Biodistribution of ^{125}I-Tyr PCL NPs and ^{125}I-ER Ab PCL NPs
7. 5 References

8. Summary and Conclusion
8.1 Summary
8.2 Conclusion

List of Figures

Figure 2.1	Growth of cells	14
Figure 2.2	Nanoparticulate platforms for the targeted and controlled delivery of drugs, (a) liposome, (b) polymeric nanoparticle, (c) lipid polymer hybrid nanoparticle and (d) dendrimer.	37
Figure 2.3	Particle schematics, (A) nanosphere, (B) nanocapsule (C) liposome, (D) micelle, (E) dendrimers functionalized with completed (left) and encapsulated drug molecules.	38
Figure 2.4	Targeted particles: (A) example of a folate receptor targeted particle. Liposome functionalized with PEG tethers to impart STEALTH characteristics and folate for tumor targeting, (B) folate-conjugated PLGA-PGA polymeric micelle loaded with encapsulated doxorubicin and (C) cRGD-functionalized PCL–PEG polymeric micelle containing encapsulated doxorubicin.	48
Figure 2.5	Molecular structure of lactide and glycolide based biodegradable polymer	55
Figure 2.6	Different methods for preparation of PLGA NPs.	57
Figure 2.7	Degradation of polycaprolactone.	61
Figure 3.1	Regressed calibration curve of ATZ by HPLC at 215 nm. Data presented as Mean ± SD, n=3 (some error bars are too small to be shown).	93
Figure 3.2	Chromatogram of ATZ solution by HPLC at 215 nm.	94
Figure 3.3	Regressed calibration curve of EXE by HPLC at 247 nm. Data presented as Mean ± SD, n = 3 (some error bars are too small to be shown).	98
Figure 3.4	Chromatogram of EXE solution by HPLC at 247 nm.	99
Figure 4.1	FTIR spectra of polymers, A: PLGA; B: PEG and C: PLGA-PEG.	127
Figure 4.2	NMR spectra of pegylated PLGA.	128
Figure 4.3	Gel permeation chromatogram of pegylated PLGA.	128
Figure 4.4	FTIR spectra of cPCL.	129
Figure 4.5	Gel permeation chromatogram of cPCL.	130

Figure 4.6	FTIR spectra of polymers, A: cPCL; B: PEG and C: PCL-PEG.	131
Figure 4.7	NMR spectra of pegylated PCL.	131
Figure 4.8	Gel permeation chromatogram of pegylated PCL.	132
Figure 4.9	Contour plots showing effect of (A) X_1 vs X_2 (at -1 level of X_3), (B) X_1 vs X_3 (at -1 level of X_2) and (C) X_2 vs X_3 (at -1 level of X_1) on PDE of ATZ loaded PLGA NPs.	140
Figure 4.10	Contour plots showing effect of (A) X_1 vs X_2 (at -1 level of X_3), (B) X_1 vs X_3 (at -1 level of X_2) and (C) X_2 vs X_3 (at -1 level of X_1) on PS of ATZ loaded PLGA NPs.	140
Figure 4.11	Response surface plot showing effect of (A) X_1 vs X_2 (at -1 level of X_3), (B) X_1 vs X_3 (at -1 level of X_2) and (C) X_2 vs X_3 (at -1 level of X_1) on PDE of ATZ loaded PLGA NPs.	141
Figure 4.12	Response surface plot showing effect of (A) X_1 vs X_2 (at -1 level of X_3), (B) X_1 vs X_3 (at -1 level of X_2) and (C) X_2 vs X_3 (at -1 level of X_1) on PS of ATZ loaded PLGA NPs.	141
Figure 4.13	Particle size distribution of ATZ loaded PLGA NPs	142
Figure 4.14	Contour plots showing effect of (A) X_1 vs X_2 (at -1 level of X_3), (B) X_1 vs X_3 (at -1 level of X_2) and (C) X_2 vs X_3 (at -1 level of X_1) on PDE of ATZ loaded cPCL NPs.	152
Figure 4.15	Contour plots showing effect of (a) X_1 vs X_2 (at -1 level of X_3), (b) X_1 vs X_3 (at -1 level of X_2) and () X_2 vs X_3 (at -1 level of X_1) on PS of ATZ loaded cPCL NPs.	152
Figure 4.16	Response surface plot showing effect of (A) X_1 vs X_2 (at -1 level of X_3), (B) X_1 vs X_3 (at -1 level of X_2) and (C) X_2 vs X_3 (at -1 level of X_1) on PDE of ATZ loaded cPCL NPs.	153
Figure 4.17	Response surface plot showing effect of (A) X_1 vs X_2 (at -1 level of X_3), (B) X_1 vs X_3 (at -1 level of X_2) and (C) X_2 vs X_3 (at -1 level of X_1) on PS of ATZ loaded cPCL NPs.	153
Figure 4.18	Particle size distribution of ATZ loaded cPCL NPs	154
Figure 4.19	Contour plots showing effect of (A) X_1 vs X_2 (at -1 level of X_3), (B) X_1 vs X_3 (at -1 level of X_2) and (C) X_2 vs X_3 (at -1 level of X_1) on PDE of EXE loaded PLGA NPs.	163
Figure 4.20	Contour plots showing effect of (A) X_1 vs X_2 (at -1 level of	163

	X_3), (B) X_1 vs X_3 (at -1 level of X_2) and (C) X_2 vs X_3 (at -1 level of X_1) on PS of EXE loaded PLGA NPs.	
Figure 4.21	Response surface plot showing effect of (A) X_1 vs X_2 (at -1 level of X_3), (B) X_1 vs X_3 (at -1 level of X_2) and (C) X_2 vs X_3 (at -1 level of X_1) on PDE of EXE loaded PLGA NPs.	165
Figure 4.22	Response surface plot showing effect of (A) X_1 vs X_2 (at -1 level of X_3), (B) X_1 vs X_3 (at -1 level of X_2) and (C) X_2 vs X_3 (at -1 level of X_1) on PS of EXE loaded PLGA NPs.	165
Figure 4.23	Particle size of EXE loaded PLGA NPs	175
Figure 4.24	Contour plots showing effect of (A) X_1 vs X_2 (at -1 level of X_3), (B) X_1 vs X_3 (at -1 level of X_2) and (C) X_2 vs X_3 (at -1 level of X_1) on PDE of EXE loaded cPCL NPs.	175
Figure 4.25	Contour plots showing effect of (A) X_1 vs X_2 (at -1 level of X_3), (B) X_1 vs X_3 (at -1 level of X_2) and (C) X_2 vs X_3 (at -1 level of X_1) on PS of EXE loaded cPCL NPs.	175
Figure 4.26	Response surface plot showing effect of (A) X_1 vs X_2 (at -1 level of X_3), (B) X_1 vs X_3 (at -1 level of X_2) and (C) X_2 vs X_3 (at -1 level of X_1) on PDE of EXE loaded cPCL NPs.	176
Figure 4.27	Response surface plot showing effect of (A) X_1 vs X_2 (at -1 level of X_3), (B) X_1 vs X_3 (at -1 level of X_2) and (C) X_2 vs X_3 (at -1 level of X_1) on PS of EXE loaded cPCL NPs.	176
Figure 4.28	Particle size distribution of EXE loaded cPCL NPs	177
Figure 4.29	Zeta potential of ATZ loaded PLGA NPs	179
Figure 4.30	TEM image of ATZ loaded PLGA NPs	180
Figure 4.31	DSC thermogram of ATZ (A), ATZ loaded PLGA NPs (B), Sucrose (C), PLGA (D) and Physical mixture (E).	181
Figure 4.32	Drug release profile of ATZ from plain drug suspension, PLGA NPs and pegylated PLGA NPs across semi-permeable membrane using the dialysis bag diffusion technique in phosphate buffered saline (pH 7.4). The values represent mean ± S.D. of three batches.	182
Figure 4.33	Effect of different storage conditions on drug content and PS of ATZ loaded PLGA NPs.	183

Figure 4.34	Zeta potential of ATZ loaded cPCL NPs	184
Figure 4.35	TEM image of ATZ loaded cPCL NPs	185
Figure 4.36	DSC thermogram of ATZ (A), ATZ loaded cPCL NPs (B), Sucrose (C), cPCL (D) and Physical mixture (E).	186
Figure 4.37	Drug release profile of ATZ from plain drug suspension, cPCL NPs and pegylated PCL NPs across semi-permeable membrane using the dialysis bag diffusion technique in phosphate buffered saline (pH 7.4). The values represent mean ± S.D. of three batches.	187
Figure 4.38	Effect of different storage conditions on drug content and PS of ATZ loaded cPCL NPs.	188
Figure 4.39	Zeta potential of EXE loaded PLGA NPs	189
Figure 4.40	TEM image of EXE loaded PLGA NPs	190
Figure 4.41	DSC thermogram of EXE loaded PLGA NPs (A), EXE (B), Sucrose (C), PLGA (D) and Physical mixture (E).	191
Figure 4.42	Drug release profile of EXE from plain drug suspension, PLGA NPs and pegylated PLGA NPs across semi-permeable membrane using the dialysis bag diffusion technique in phosphate buffered saline (pH 7.4). The values represent mean ± S.D. of three batches.	192
Figure 4.43	Effect of different storage conditions on drug content and PS of ATZ loaded cPCL NPs.	193
Figure 4.44	Zeta potential of EXE loaded cPCL NPs	194
Figure 4.45	TEM image of EXE loaded cPCL NPs	195
Figure 4.46	DSC thermogram of EXE loaded cPCL NPs (A), EXE (B), cPCL (C), Sucrose (D) and Physical mixture (E).	196
Figure 4.47	Drug release profile of EXE from plain drug suspension, PCL NPs and pegylated PCL NPs across semi-permeable membrane using the dialysis bag diffusion technique in phosphate buffered saline (pH 7.4). The values represent mean ± S.D. of three batches.	197
Figure 4.48	Effect of different storage conditions on drug content and PS of ATZ loaded cPCL NPs.	198

Figure 5.1	Phagocytic uptake histograms of 6-Coumarin loaded NP formulations by human acute monocytic leukemia cell line (THP1) after incubation for (a) 60, (b) 120 and (c) 240 min using FACS.	212
Figure 5.2	Phagocytic uptake of 6-Coumarin loaded PLGA and pegylated PLGA NPs using Human acute monocytic leukemia cell line, THP1 after incubation for 60, 120 and 240 min using FACS. Data presented as Mean ± SD, n=3	212
Figure 5.3	Drug release profile of ATZ from plain drug suspension, PLGA NPs and pegylated PLGA NPs across semi-permeable membrane using the dialysis bag diffusion technique in phosphate buffered saline (pH 7.4). The values represent mean ± S.D. of three batches.	213
Figure 5.4	TEM image of ATZ loaded pegylated PLGA ImmunoNPs.	214
Figure 5.5	Phagocytic uptake histograms of 6-Coumarin loaded NP formulations by human acute monocytic leukemia cell line (THP1) after incubation for (a) 60, (b) 120 and (c) 240 min using FACS.	216
Figure 5.6	Phagocytic uptake of 6-coumarin loaded PCL and pegylated PCL NPs using Human acute monocytic leukemia cell line, THP-1 after incubation for 60, 120 and 240 min using FACS. Data presented as Mean ± SD, n=3.	217
Figure 5.7	Drug release profile of EXE from plain drug suspension, PCL NPs and pegylated PCL NPs across semi-permeable membrane using the dialysis bag diffusion technique in phosphate buffered saline (pH 7.4). The values represent mean ± S.D. of three batches.	218
Figure 5.8	TEM image of EXE loaded pegylated PCL ImmunoNPs.	219
Figure 6.1	Schematic presentation of principle for cell cycle analysis using DNA intercalating florescence probe in flow cytometry.	224
Figure 6.2	Receptor expression analyses in cell lines.	228
Figure 6.3	Quantitative intracellular uptake histograms of 6-Coumarin	229

	loaded PLGA NPs, pegylated PLGA NPs and ER antibody conjugated ImmunoNPs by MCF7 cells using flow cytometry.	
Figure 6.4	Quantitative intracellular uptake of 6-Coumarin loaded PLGA NPs, pegylated PLGA NPs and ER antibody conjugated ImmunoNPs by MCF7 cells using flow cytometry. Uptake was calculated by measuring MFI and represented as mean ± S.D. (n=3)	230
Figure 6.5	Quantitative intracellular uptake histograms of 6-Coumarin loaded PCL NPs, pegylated PCL NPs and ER antibody conjugated ImmunoNPs by MCF7 cells using flow cytometry.	231
Figure 6.6	Quantitative intracellular uptake of 6-Coumarin loaded PCL NPs, pegylated PCL NPs and ER antibody conjugated ImmunoNPs by MCF7 cells using flow cytometry. Uptake was calculated by measuring MFI and represented as mean ± S.D. (n=3)	231
Figure 6.7	Qualitative cellular uptake of PLGA NPs, pegylated PLGA and ImmunoNPs using fluorescent microscope. (A-C) ImmunoNPs; (D-F) pegylated PLGA NPs; (G-I) PLGA NPs; (J-L) 6-Coumarin dye solution; (B, E, H and K) nucleus stained using Hoechst 33342; (C, F, I and L) overlapping images.	232
Figure 6.8	Qualitative cellular uptake of PCL NPs, pegylated PCL NPs and ImmunoNPs using fluorescent microscope. (A-C) ImmunoNPs; (D-F) pegylated PCL NPs; (G-I) PCL NPs; (J-L) 6-Coumarin dye solution; (B, E, H and K) nucleus stained using Hoechst 33342; (C, F, I and L) overlapping images.	233
Figure 6.9	Cytotoxicity of ATZ loaded formulations (solution, PLGA NPs, PLGA PEG NPs, ImmunoNPs) and blank PLGA PEG NPs on MCF7 (A,B,C) and MDAMB231 (D,E,F) cells after exposure for 6 h (A, D), 24 h (B, E) and 48 h (C, F).	235
Figure 6.10	Cytotoxicity of ATZ loaded formulations (solution, PCL NPs,	236

	PCL PEG NPs, ImmunoNPs) and blank PCL PEG NPs on MCF7 (A,B,C) and MDAMB231 (D,E,F) cells after exposure for 6 h (A, D), 24 h (B, E) and 48 h (C, F).	
Figure 6.11	Cytotoxicity of EXE loaded formulations (solution, PLGA NPs, PLGA PEG NPs, ImmunoNPs) and blank PLGA PEG NPs on MCF7 (A,B,C) and MDAMB231 (D,E,F) cells after exposure for 6 h (A, D), 24 h (B, E) and 48 h (C, F).	238
Figure 6.12	Cytotoxicity of EXE loaded formulations (solution, PCL NPs, PCL PEG NPs, ImmunoNPs) and blank PCL PEG NPs on MCF7 (A,B,C) and MDAMB231 (D,E,F) cells after exposure for 6 h (A, D), 24 h (B, E) and 48 h (C, F).	239
Figure 6.13	Apoptosis estimation in MCF7 cell line after exposure of Control (PBS), A; ATZ Solution, B; ATZ PLGA NPs, C; ATZ PLGA-PEG NPs, D; and ATZ PLGA-PEG ImmunoNPs, E; for 24 and 48 h by Annexin V-FITC and PI staining using FACS technique. Necrotic cells FITC (-) PI (+), Late apoptosis FITC (+) PI (+), Live FITC (-) PI (-), Early apoptotis FITC (+) PI (-).	243
Figure 6.14	Apoptosis estimation in MCF7 cell line after exposure of Control (PBS), A; ATZ Solution, B; ATZ PCL NPs, C; ATZ PCL-PEG NPs, D; and ATZ PCL-PEG ImmunoNPs, E; for 24 and 48 h by Annexin V-FITC and PI staining using FACS technique. Necrotic cells FITC (-) PI (+), Late apoptosis FITC (+) PI (+), Live FITC (-) PI (-), Early apoptotis FITC (+) PI (-).	244
Figure 6.15	Apoptosis estimation in MCF7 cell line after exposure of Control (PBS), A; EXE Solution, B; EXE PLGA NPs, C; EXE PLGA-PEG NPs, D; and EXE PLGA-PEG ImmunoNPs, E; for 24 and 48 h by Annexin V-FITC and PI staining using FACS technique. Necrotic cells FITC (-) PI (+), Late apoptosis FITC (+) PI (+), Live FITC (-) PI (-), Early apoptotis FITC (+) PI (-).	245
Figure 6.16	Apoptosis estimation in MCF7 cell line after exposure of	246

	Control (PBS), A; EXE Solution, B; EXE PCL NPs, C; EXE PCL-PEG NPs, D; and EXE PCL-PEG ImmunoNPs, E; for 24 and 48 h by Annexin V-FITC and PI staining using FACS technique. Necrotic cells FITC (-) PI (+), Late apoptosis FITC (+) PI (+), Live FITC (-) PI (-), Early apoptotis FITC (+) PI (-).	
Figure 6.17	Effect of ATZ, ATZ PLGA PEG NPs and ImmunoNPs exposure on cell cycle distribution in MCF7 cells using FACS as an estimation technique.	247
Figure 6.18	Effect of ATZ, ATZ PCL PEG NPs and ImmunoNPs exposure on cell cycle distribution in MCF7 cells using FACS as an estimation technique.	248
Figure 6.19	Effect of EXE, EXE PLGA PEG NPs and ImmunoNPs exposure on cell cycle distribution in MCF7 cells using FACS as an estimation technique.	249
Figure 6.20	Effect of EXE, EXE PCL PEG NPs and ImmunoNPs exposure on cell cycle distribution in MCF7 cells using FACS as an estimation technique.	250
Figure 7.1	Biodistribution of ^{125}I labeled Tyrosine and ER antibody conjugated PLGA NPs and the radioactivity was measured after 3 and 24 h post injection. The values represented as mean ± SD. Radioactivity is expressed as percent of administered dose per gram of tissue or organ.	261
Figure 7.2	Biodistribution of ^{125}I labeled Tyrosine and ER antibody conjugated PCL NPs and the radioactivity was measured after 3 and 24 h post injection. The values represented as mean ± SD. Radioactivity is expressed as percent of administered dose per gram of tissue or organ.	264

List of Tables

Table 2.1	Available antibody-based cancer treatments.	51
Table 3.1	Calibration curve of ATZ by HPLC at 215 nm, Data presented as Mean ± SD, n=3.	93
Table 3.2	Accuracy of ATZ measurement using mobile phase at 215 nm.	96
Table 3.3	Precision of ATZ measurement using mobile phase at 215 nm, Data presented as Mean, n=3.	96
Table 3.4	Calibration curve of EXE by HPLC at 247 nm, Data presented as Mean ± SD, n=3.	98
Table 3.5	Accuracy of EXE measurement using mobile phase at 247 nm.	99
Table 3.6	Precision of EXE measurement using mobile phase at 247 nm, Data presented as Mean, n=3.	99
Table 4.1	Selection of organic phase in preliminary optimization of ATZ loaded PLGA NPs	132
Table 4.2	Selection of volume of organic solvent in preliminary optimization of ATZ loaded PLGA NPs	133
Table 4.3	Selection of surfactant in preliminary optimization of ATZ loaded PLGA NPs	133
Table 4.4	Coded values of the formulation parameters of ATZ loaded PLGA NPs	134
Table 4.5	Layout of 3^3 full factorial design for ATZ loaded PLGA NPs	135
Table 4.6	Model coefficients estimated by multiple regression analysis for percentage drug entrapment of ATZ loaded PLGA NPs	136
Table 4.7	Model coefficients estimated by multiple regression analysis for particle size of ATZ loaded PLGA NPs	136
Table 4.8	Analysis of Variance (ANOVA) of full and reduced models for PDE of ATZ loaded PLGA NPs	137
Table 4.9	Analysis of Variance (ANOVA) of full and reduced models for PS of ATZ loaded PLGA NPs	137
Table 4.10	Check point analysis, t test analysis and normalized error determination	143

Table 4.11	Effect of cryoprotectants and their concentration on PS of lyophilized NPs after re-dispersion in distilled water	143
Table 4.12	Selection of organic phase in preliminary optimization of ATZ loaded cPCL NPs	144
Table 4.13	Selection of volume of organic solvent in preliminary optimization of ATZ loaded cPCL NPs	144
Table 4.14	Selection of surfactant in preliminary optimization of ATZ loaded cPCL NPs	145
Table 4.15	Coded values of the formulation parameters of ATZ loaded cPCL NPs	146
Table 4.16	Layout of 3^3 full factorial design for ATZ loaded cPCL NPs	147
Table 4.17	Model coefficients estimated by multiple regression analysis for percentage drug entrapment of ATZ loaded cPCL NPs	148
Table 4.18	Model coefficients estimated by multiple regression analysis for particle size of ATZ loaded cPCL NPs	148
Table 4.19	Analysis of Variance (ANOVA) of full and reduced models for PDE of ATZ loaded cPCL NPs	149
Table 4.20	Analysis of Variance (ANOVA) of full and reduced models for PS of ATZ loaded cPCL NPs	149
Table 4.21	Check point analysis, t test analysis and normalized error determination	154
Table 4.22	Effect of cryoprotectants and their concentration on PS of lyophilized NPs after re-dispersion in distilled water	155
Table 4.23	Selection of organic phase in preliminary optimization of EXE loaded PLGA NPs	156
Table 4.24	Selection of surfactant phase in preliminary optimization of EXE loaded PLGA NPs	156
Table 4.25	Selection of surfactant concentration in preliminary optimization of EXE loaded PLGA NPs	157
Table 4.26	Coded values of the formulation parameters of EXE loaded PLGA NPs	157
Table 4.27	Box Behnken experimental design with measured responses for EXE loaded PLGA NPs	158

Table 4.28	Model coefficients estimated by multiple regression analysis for PDE of EXE loaded PLGA NPs	159
Table 4.29	Model coefficients estimated by multiple regression analysis for PS of EXE loaded PLGA NPs	159
Table 4.30	Analysis of Variance (ANOVA) of full and reduced models for PDE of EXE loaded PLGA NPs	160
Table 4.31	Analysis of Variance (ANOVA) of full and reduced models for PS of EXE loaded PLGA NPs	161
Table 4.32	Check point analysis, t test analysis and normalized error determination	164
Table 4.33	Effect of cryoprotectants and their concentration on PS of lyophilized NPs after re-dispersion in distilled water	167
Table 4.34	Selection of organic phase in preliminary optimization of EXE loaded cPCL NPs	167
Table 4.35	Selection of surfactant in preliminary optimization of EXE loaded cPCL NPs	168
Table 4.36	Selection of surfactant concentration in preliminary optimization of EXE loaded cPCL NPs	168
Table 4.37	Coded values of the formulation parameters of EXE loaded cPCL NPs	169
Table 4.38	Box Behnken experimental design with measured responses for EXE loaded cPCL NPs	169
Table 4.39	Model coefficients estimated by multiple regression analysis for PDE of EXE loaded cPCL NPs	171
Table 4.40	Model coefficients estimated by multiple regression analysis for PS of EXE loaded cPCL NPs	171
Table 4.41	Analysis of Variance (ANOVA) of full and reduced models for PDE of EXE loaded cPCL NPs	172
Table 4.42	Analysis of Variance (ANOVA) of full and reduced models for PS of EXE loaded cPCL NPs	172
Table 4.43	Check point analysis, t test analysis and normalized error determination	178
Table 4.44	Effect of cryoprotectants and their concentration on PS of	178

	lyophilized NPs after re-dispersion in distilled water	
Table 4.45	Stability data of ATZ loaded PLGA NPs stored at different temperature conditions	183
Table 4.46	Stability data of ATZ loaded cPCL NPs stored at different temperature conditions	188
Table 4.47	Stability data of EXE loaded PLGA NPs stored at different temperature conditions	193
Table 4.48	Stability data of EXE loaded cPCL NPs stored at different temperature conditions	198
Table 5.1	Physicochemical characterization of ATZ loaded PLGA NPs, pegylated PLGA NPs and ImmunoNPs	210
Table 5.2	Physicochemical characterization of EXE loaded cPCL NPs, pegylated PCL NPs and ImmunoNPs	215
Table 6.1	Intracellular uptake of 6-Coumarin loaded PLGA NPs, pegylated PLGA NPs and ER antibody conjugated ImmunoNPs by MCF7 cells using flow cytometry. Uptake was calculated by measuring MFI and represented as mean ± S.D. (n=3)	230
Table 6.2	Intracellular uptake of 6-Coumarin loaded PCL NPs, pegylated PCL NPs and ER antibody conjugated ImmunoNPs by MCF7 cells using flow cytometry. Uptake was calculated by measuring MFI and represented as mean ± S.D. (n=3)	231
Table 6.3	Cytotoxicity of formulations loaded with ATZ and tested on MCF7 cell line	236
Table 6.4	Cytotoxicity of formulations loaded with EXE and tested on MCF7 cell line	238
Table 6.5	Apoptosis studies in MCF7 cell line after treatment of (a) Control (PBS), (b) ATZ solution, ATZ loaded (c) PLGA, (d) PLGA-PEG NPs and (d) PLGA-PEG ImmunoNPs using FACS technique.	241
Table 6.6	Apoptosis studies in MCF7 cell line after treatment of (a) Control (PBS), (b) ATZ solution, ATZ loaded (c) PCL, (d) PCL-PEG NPs and (d) PCL-PEG ImmunoNPs using FACS	241

	technique.	
Table 6.7	Apoptosis studies in MCF7 cell line after treatment of (a) Control (PBS), (b) EXE solution, EXE loaded (c) PLGA, (d) PLGA-PEG NPs and (d) PLGA-PEG ImmunoNPs using FACS technique.	242
Table 6.8	Apoptosis studies in MCF7 cell line after treatment of (a) Control (PBS), (b) EXE solution, EXE loaded (c) PCL, (d) PCL-PEG NPs and (d) PCL-PEG ImmunoNPs using FACS technique.	242
Table 6.9	Cell cycle analysis in MCF7 cell line after treatment of (a) Control (PBS), (b) ATZ solution, ATZ loaded (c) PLGA-PEG NPs and (d) PLGA-PEG ImmunoNPs by PI staining using FACS technique.	248
Table 6.10	Cell cycle analysis in MCF7 cell line after treatment of (a) Control (PBS), (b) ATZ solution, ATZ loaded (c) PCL-PEG NPs and (d) PCL-PEG ImmunoNPs by PI staining using FACS technique.	249
Table 6.11	Cell cycle analysis in MCF7 cell line after treatment of (a) Control (PBS), (b) EXE solution, EXE loaded (c) PLGA-PEG NPs and (d) PLGA-PEG ImmunoNPs by PI staining using FACS technique.	250
Table 6.12	Cell cycle analysis in MCF7 cell line after treatment of (a) Control (PBS), (b) EXE solution, EXE loaded (c) PCL-PEG NPs and (d) PCL-PEG ImmunoNPs by PI staining using FACS technique.	251
Table 7.1	Approximate half life of various radioisotopes.	255
Table 7.2	Stability of iodinated complexes after 24 h.	259
Table 7.3	Biodistribution of ^{125}I labeled Tyrosine and ER antibody conjugated PLGA NPs and the radioactivity was measured after 3 and 24 h post injection. The values represented as mean ± SD. Radioactivity is expressed as percent of administered dose per gram of tissue or organ.	260
Table 7.4	Different ratio between the tissue/organ of ^{125}I labeled Tyrosine	261

	and ER antibody conjugated PLGA NPs.	
Table 7.5	Biodistribution of ^{125}I labeled Tyrosine and ER antibody conjugated PCL NPs and the radioactivity was measured after 3 and 24 h post injection. The values represented as mean ± SD. Radioactivity is expressed as percent of administered dose per gram of tissue or organ.	262
Table 7.6	Different ratio between the tissue/organ of ^{125}I labeled Tyrosine and ER antibody conjugated PCL NPs.	263

List of Abbreviations

ATZ	Anastrozole
EXE	Exemestane
PLGA	Poly lactic-co-glycolic acid
cPCL	Carboxylated polycaprolactone
PEG	Poly ethylene glycol
ER	Estrogen receptor
NPs	Nanoparticles
PDE	Percentage drug entrapment
PS	Particle size
FM	Full model
RM	Reduced model
HPLC	High pressure liquid chromatography
FTIR	Fourier transform infrared spectroscopy
NMR	Nuclear magnetic resonance
GPC	Gel permeation chromatography
MRA	Multiple regression analysis
FFD	Full factorial design
BBD	Box behnken design
CCD	Central composite design
TEM	Transmission electron microscopy
DSC	Differential scanning calorimetry
FBS	Fetal bovine serum
PBS	Phosphate buffered saline
MTT	[3-(4,5-dimethylthiazoyl-2-yl)-2,5-diphenyltetrazolium bromide]
FACS	Fluorescence activated cell sorting
MFI	Mean fluorescent index
TME	α-Methyl tyrosine ester

Chapter 1

INTRODUCTION

1.1 Introduction

Cancer is a major cause of death in India. Every year about 8,50,000 new cancer cases are diagnosed in India resulting in about 5,80,000 cancer related death every year. In females, Cervical (30%) and Breast cancers (19%) are the two main causes of cancer related illnesses and death. Despite the significant progress in the development of anticancer technology, there is still no common cure for patients with malignant diseases. In addition, the long-standing problem of chemotherapy is the lack of tumor-specific treatments. Traditional chemotherapy relies on the premise that rapidly proliferating cancer cells are more likely to be killed by a cytotoxic agent. In reality, however, cytotoxic agents have very little or no specificity as very less concentration of drug reaches tumor site, which leads to systemic toxicity.

The causes of breast cancer are still unknown, but there is a combination of risk factors including lifestyle factors, environmental factors, genetic factors, and hormonal factors that may be responsible for breast cancer. Although many risk factors are associated with breast cancer, it is not yet known exactly how these risk factors cause normal breast cells to become cancerous. The molecular biology of breast cancer is complex as multiple factors contribute in the development of breast cancer such as genetic mutations in BRCA1, BRCA2 and p53 and cross-talks between different signalling pathways. Cell-signalling pathways allow normal programs of proliferation, transcription, growth, migration, differentiation and death in the normal cell. But in the case of breast cancer cells, these normal programs are altered by altering cell-signalling pathways. Various signalling pathways that play an important role in development and progression of breast cancer are initiated by the interaction between growth factors and their receptors, such as human epidermal growth factor receptors (HER2 and VEGF) and their ligands, as well as insulin-like growth factor (IGF) and IGF-1R.

Specific molecular targets having critical roles in cancer proliferation are interfered by targeting drugs. Some important therapeutic targets in breast cancer are HER-2, vascular endothelial growth factor (VEGF), insulin-like growth factor binding proteins-3 (IGFBP-3), estrogen receptor (ER), gene silencing by siRNA and aptamer.

Estrogens and progesterone are important growth regulators in the development of breast cancer. In breast cancer, the majority of tumors found in postmenopausal women contain ER while tumors in younger women often lack this protein. Approximately 70% of all breast cancers retain the estrogen receptor α (ERα, encoded by ESR1) and the

progesterone receptor (PR) [Arpino 2005]. ER is a protein normally found in various reproduction-related tissues such as the breast and uterus. When estrogen receptor binds estrogen, it becomes activated and can interact with the genes of the cell, resulting in the activation of selected sets of responsive genes. This results in changes in the synthesis of specific RNA's and proteins involved in the regulation of cell proliferation, differentiation and physiologic function. Although normal breast tissue also makes ER, the amount of this protein produced in positive breast carcinomas is significantly higher. This may account for some of the differences seen in the abnormal growth of various tumors and tumor cell lines when compared to normal breast tissue development [Kocbek P 2007].

Clinical data indicates ER^+/PR^- breast cancer are more likely to have an aggressive phenotype to express HER-1 and over express HER-2. These tumors are more frequent in older patient, larger in size and have a higher S-phase fraction. Recurrence rate of tumor is higher in ER^+/PR^- than ER^+/PR^+ [Bonneterre J 2001]. There was little difference in the recurrence rate of PR^+ versus PR^- tumors in patients treated with anastrozole. The patients with ER^+/PR^- tumors respond nearly as well to anastrozole as those with ER^+/PR^+ tumors suggesting that the ER signalling pathway is functional in many ER^+/PR^- tumors and these tumors are still dependent on estrogen for growth despite having somewhat lower ER levels. ER^+/PR^- tumors were three times more likely than ER^+/PR^+ tumors to express HER-1 (25% versus 8%, respectively), and the levels of HER-1 in ER^+/PR^- tumors (40 fmol/mg protein) were nearly twice those in ER^+/PR^+ tumors (24 fmol/mg protein). ER^+/PR^- tumors were also statistically significantly more likely to over express HER-2 (21% for ER^+/PR^- versus 14% for ER^+/PR^+). Both HER-1 and HER-2 are markers of tumor aggressiveness, and therefore, are more likely to have an intermediate or high S-phase fraction than tumors negative for these two growth factors, regardless of PR status.

Endocrine therapies are effective in reducing recurrence, increasing overall survival, and reducing contralateral breast cancer up to 50%. However, about 50% of patients with ERα-positive breast cancer have intrinsic resistance to antiestrogen therapy and therefore do not benefit. In contrast to patients with intrinsically resistant tumors, there are patients who do initially respond to antiestrogen therapy; however, most of these patients develop acquired resistance during the treatment regimen. Therefore, the current goal in breast cancer research is to elucidate the mechanisms of both intrinsic

and acquired resistance to tamoxifen and the aromatase inhibitors in order to develop new therapeutic strategies to prevent and/or treat resistant breast cancer.

An alternate strategy to endocrine therapy, which specifically inhibits binding of E2 to the ER, is to inhibit the production of E2 by blocking the cytochrome p450 aromatase enzyme, the rate-limiting enzyme that converts androgens (i.e., testosterone and androstenedione) to estrogens (i.e., E2 and estrone) in the adrenal gland, surrounding stroma, and adipose tissue of the breast tumor. The main drugs of this type are aromatase inhibitors, which include Type I (steroidal) or Type II (nonsteroidal). Steroidal inhibitors are competitive-substrate mimics of androstenedione. These include formestane and exemestane, which are irreversible inhibitors that bind with high affinity to the binding site of aromatase and are converted to a covalently bound intermediate. Nonsteroidal inhibitors include the first-generation aromatase inhibitor aminoglutethimide and the second-generation compounds anastrozole and letrozole. All nonsteroidal aromatase inhibitors act by binding reversibly to the enzyme and competitively inhibiting binding of the substrate androstenedione. The benefits of using aromatase inhibitors over tamoxifen are believed to be the complete deprivation of E2 and thus better efficacy for ERα-positive breast cancer. Recent clinical data have clearly demonstrated that anastrozole is more effective than tamoxifen as first-line treatments in patients with metastatic breast cancer.

Two very small trials demonstrated a significantly increased clinical response rate in patients with ER-positive, HER2-positive cancers treated with preoperative aromatase inhibitors compared to preoperative tamoxifen. This led to a widely accepted hypothesis that aromatase inhibitors were a better choice than tamoxifen in patients with ER-positive, HER2-positive cancers. Treatment of breast cancer has included efforts to decrease estrogen levels, by ovariectomy pre-menopausally and by use of anti-estrogens and progestational agents both pre- and post-menopausally; and these interventions lead to decreased tumor mass or delayed progression of tumor growth in some women. Tamoxifen is a selective estrogen-receptor modulator [Leserman], which blocks estrogen from attaching to estrogen receptors on breast cancer cells and acts as an anti-estrogen. Tamoxifen increases the risks of uterine cancer, thromboembolism, and tamoxifen resistance. In postmenopausal women, ovaries do not produce estrogen. A small amount of estrogen is produced by the adrenal glands. Aromatase inhibitors block estrogen production [Sharaf 2006]. Anastrozole, a product of aromatase

inhibitors, has fewer side-effects than tamoxifen but it causes joint pain or bone fractures.

Currently, various conventional therapies like radiation therapy, chemotherapy, hormonal therapy, and immunotherapy are used for the treatment of breast cancer. Cancer cells that may not be seen during surgery can be killed by radiation to reduce the risk of local recurrence of cancer. Radiation therapy is a process in which cancer cells are exposed to high levels of radiation directly. Radiation therapy after surgery shrinks the tumor in combination with chemotherapy. But there are some side-effects of radiation therapy, such as decreased sensation in the breast tissue or under the arm, skin problems in the treated area (including soreness, itching, peeling, and/or redness) and at the end of treatment the skin may become moist and weepy. In chemotherapy cytotoxic drugs are administered to kill cancer cells. Chemotherapy may be recommended as adjuvant chemotherapy or neoadjuvant chemotherapy. Adjuvant chemotherapy is the systemic therapy given to patients after surgery to treat undetected breast cancer cells. Neoadjuvant chemotherapy is given before surgery to shrink large cancers so that they can easily be removed by lumpectomy. It is reported clinically that chemotherapy is most effective when given in combinations of more than one drug. The most common side-effects are hair loss, mouth sores, loss of appetite, nausea, vomiting, increased chance of infections (due to low white blood cell counts), easy bleeding (due to low blood platelet counts) and fatigue.

The purpose of hormonal therapy is either adding or blocking hormones. The female hormones estrogen and progesterone can promote the growth of some breast cancer cells. Therefore hormone therapy is required to block or lower the levels of estrogen and progesterone to prevent growth of cancer cells. Several types of hormonal drugs used for primary breast cancer include Tamoxifen, Toremifene, Arimidex, Zoladex, etc. These targeted therapies should allow action with high efficacy and less toxicity. Several nanotechnological approaches have been used to improve targeted delivery of a potent anticancer drug to breast cancer cells with minimum toxic effects on healthy tissues while maintaining efficacy. Nanotechnology is developing a new generation of more effective therapies by using nanocarriers that are capable of overcoming the biological, biophysical, and biomedical barriers in treatment of breast cancer. Nanocarriers show much promising breast cancer therapy by selectively reaching the desired specific sites due to their small size and surface modifying properties with multifunctionality. This

article highlights recent approaches that can be targeted and are clinically applicable for treatment of breast cancer.

An ideal drug-delivery system should possess two elements: the ability to target and to control the drug release. Targeting will ensure high efficiency of the drug and reduce the side effects, especially when dealing with drugs that are presumed to kill cancer cells but can also kill healthy cells when delivered to them. The reduction or prevention of side effects can also be achieved by controlled release. Nanoparticulate drug delivery systems provide a better penetration of the particles inside the body as their size allows delivery via intravenous injection or other routes. The nanoscale size of these particulate systems also minimizes the irritant reactions at the injection site. Nanoparticles (NPs) may be targeted to the growing vasculature serving the growing cancer or to the cancer cells themselves. Targeted delivery utilizes unique phenotypic features of diseased tissues and cells in order to concentrate the drug at the location where it is needed. Targeted delivery can be divided into passive and active targeting. Passive targeting tries to minimize nonspecific interactions between the drug carrier and nontarget sites in the body by detailing the physiochemical properties of the aberrant tissue such as size, morphology, hydrophilicity, and surface charge. When targeting tumor tissue, the enhanced permeability and retention effect (EPR) is an example of passive targeting approach; it allows passage of drug carriers ranging in size from 10 to 500 nm through the highly permeable blood vessels that supply growing tumors and leads to entrapment of large molecules as a result of deficient lymphatic drainage.

It is known that plasma retention time of the NPs is one of the primary driving forces for tumor accumulation by EPR [Modi et al. 2006]. In fact, one prerequisite for the EPR effect to manifest in mice is that the plasma concentration of the drug must remain high for more than 6 h [Iyer et al. 2006]. Because of their size, PEGylated NPs not only remain in circulation longer, giving them more time to accumulate in the tumor by EPR effect, but also take longer to leave the tumor and return to circulation. This extended tumor cell contact time can conceivably allow more of the ligand conjugated NP complex to bind to the tumor cells. Concomitantly, the polyethylene glycol (PEG) complex also takes longer to return to circulation [Bartlett et al. 2007; Kirpotin et al. 2006]. Support for this theory can be found in a publication by Khalid et al., who reported that tumor localization of a lipid NPs carrying docetaxel was not only

enhanced by inclusion of PEG but also increased with the PEG density on the particle over a range of 6 to 15 mol % [Khalid et al. 2006]. Similarly, Fang et al. reported that the peak tumor concentration, as well as the peak accumulation time, of NPs delivered ^{125}I labeled recombinant human tumor necrosis factor-a (rHuTNF-a) varied with the PEG molecular weight, surface density and the size of the NPs. In fact, it has been reported that the intra-cellular openings in vascular endothelium of tumor blood vessels can be up to 2 mm in diameter and that the vessel leakiness in tumor vasculature can be up to an order of magnitude higher than that of normal blood vessels [Fang 2006]. Active targeting utilizes biologically specific interactions including antigen–antibody and ligand–receptor binding and may seek drug uptake by receptor mediated endocytosis through association of the drug or drug carrier with such antigen or ligand.

Targeted therapy of cancer is based on the use of specific carriers to deliver cytotoxic agents, including chemotherapeutic drugs, radioisotopes, or toxins, to their preferred site of action (i.e., tumors). For targeted delivery of cytotoxic agents, it is important to select a carrier that can be delivered selectively to tumor cells. The most widely investigated and advanced polymers in regard to available toxicological and clinical data are the aliphatic polyesters based on lactic and glycolic acids, like poly(lactic acid) and poly (lactic co-glycolic acid) (PLGA). Other biodegradable polymers which are used in nanoparticulate drug delivery systems are poly (ε-caprolactone) (PCL), poly (alkylcyanoacrylate), etc. The drug loaded polymeric NPs can be attached to this carrier by a number of synthetic or biochemical means to form a tumor-selective conjugate. Administration of such conjugate should lead to the accumulation of drug loaded NPs preferentially in the tumor without significant distribution to normal tissues, followed by selective damage to the tumor cells. Several classes of specific carriers have been evaluated for the selective delivery of drugs to tumors. Such specific carriers include antibodies [Ghose et al. 1985], cytokines such as interleukin-2 (IL-2) and granulocyte-macrophage colony-stimulating factor (GM-CSF), growth factors such as epidermal growth factor (EGF) and vascular endothelial growth factor (VEGF), and hormones such as gonadotropin releasing hormone.

The use of antibodies as carriers of cytotoxic drugs is particularly attractive because of their unique specificity and high affinity for tumor antigens. The monoclonal antibodies (MAbs) are preferred over the conventional polyclonal antibodies (PAbs) due to defined specificity, homogeneity, and availability of MAbs in practically unlimited quantities.

These properties of MAbs render them as the most attractive carriers for the selective delivery of therapeutic agents to malignant tumors. To date, numerous MAbs have been produced against virtually every malignant tumor of human tissues. Many of these MAbs have been used as tumor specific carriers of cytotoxic agents and evaluated either in animal models and/or patients [Zhu Z. 2004].

Three major classes of MAbs have been developed as cancer therapeutics:

1. Antibodies that act as molecular antagonists that modulate the function of key regulatory molecules on tumor cells, such as blocking growth factor/receptor interaction and/or downregulating expression of oncogenic proteins (or receptors) on the cell surface;
2. Antibodies that recruit effector mechanisms of the immune system, such as the antibody-dependent cellular cytotoxicity (ADCC) and complement-mediated cytotoxicity (CMC), and
3. Antibodies used as targeting devices (immunoconjugates) to specifically deliver cytotoxic agents to tumor sites. Functional blockade is thought to be one of the main antitumor mechanisms for several antibodies, including those directed against EGF receptor (also called HER1) and HER2 (erbB2 / neu) on tumor-cell surface,[3] and receptors for VEGF on endothelial-cell surface. By interfering with important growth factor / receptor pathways, these antibodies can influence the growth and survival of tumor cells. In addition, antibodies that inhibit function of regulatory pathways may potentiate the cytotoxic effects of chemotherapeutic drugs and radiation.

Different conjugation techniques are used for targeting cancer cells using MAbs. Examples of such approaches are as follows;

Kocbek et al. applied two strategies for attaching MAbs to PLGA NPs: covalent and non-covalent [Kocbek P 2007]. In covalent attachment, a spacer or linker like EDC (1-ethyl-3-(3-dimethylaminopropyl)-carbodiimide) can be used to conjugate the primary amine group of MAb with the free carboxylic end group of PLGA NPs, forming a connecting amide bond. Non-covalently, NPs were incubated with MAb to allow non-specific adsorption onto their surface. Lu et al. have developed a new surface tethering technology that can attach ligands to PLGA particles at very high density [Lu et al. 2011]. Using this technology doxorubicin was encapsulated in PLGA, and targeted thus making it more efficacious than untargeted doxorubicin particles or free drug in Non-

Hodgkins lymphoma in vitro studies. Kirpotin et al. have described evidence for a novel mechanism of monoclonal antibody (MAb)–directed NPs (immunoliposome) targeting to solid tumors in vivo [Kirpotin et al. 2006]. Long-circulating immunoliposomes targeted to HER2 (ErbB2, Neu) were prepared by the conjugation of anti-HER2 MAb fragments (Fab' or single chain Fv) to liposome-grafted polyethylene glycol chains. Sahoo et al prepared rapamycin loaded PLGA NPs that were surface conjugated with antibodies to epidermal growth factor receptor (EGFR), using EDC and N-hydroxysuccinimide (NHS) mediated cross linking agents [Acharya et al. 2009]. *In vitro* cytotoxicity of native rapamycin, rapamycin loaded NPs and EGFR antibody conjugated rapamycin loaded NPs were evaluated on malignant MCF7 breast cancer cell lines. IC50 doses as determined by 3-(4,5-dimethylthiazol-2-yl)-2,5-diphenyl tetrazolium (MTT) assay. Cell cycle arrest and cellular apoptosis induced by the formulations were confirmed by flow cytometry. Molecular basis of apoptosis was studied by western blotting. It was concluded that EGFR-Rapa-NPs provide an efficient and targeted delivery of anticancer drugs, presenting a promising active targeting carrier for tumor selective therapeutic treatment.

1.2 Aims to be achieved from the present study

The study aims;

i. at formulating a delivery system for Anastrozole and Exemestane, capable of delivering drugs to its site of action (breast) to improve disease condition.
ii. at developing an effective formulation to minimize the associated side effects with currently available drug treatment.
iii. to provide comparative evaluation of different nanoparticulate formulations, which will help to optimize formulation for breast tumor targeting.
iv. at developing a nanoparticulate formulation for anticancer drugs to provide better alternative to currently available tablet formulation, as these are not having site specificity.
v. to reduce dose of drugs and dosage frequency by sustaining the release of drug from nanoparticulate formulation.

1.3 Hypothesis

Targeted delivery of nanoparticulate formulation containing drug (anastrozole, or exemestane) surface engineered with antibody specifically to estrogen receptor positive breast tumor will facilitate high tumor uptake and retention. Targeting will improve therapy, reduce systemic side effects and prevent metastases.

1.4 Objectives

The prime objective of the study is to develop intravenously delivered nanoparticulate drug delivery system composed of synthetic polymers which are biocompatible and biodegradable (PLGA or PCL) conjugated with hetero-bifunctional PEG loaded with anticancer drugs (anastrozole or exemestane) for enhancing tumor uptake by ligand (antibody for estrogen receptor) specific breast tumor targeting with the following objectives;

Reducing systemic side effects,
Site specific drug delivery,
Sustained release of drug,
Reduced dose and dosing frequency,
Improved disease condition,
Patient compliance.

1.5 Plan of work

a. Literature survey, procurement of APIs and excipients.
b. Formulation and optimization: To prepare various nanoparticulate formulations using suitable formulation techniques and their optimization by applying statistical design of experiments for achieving optimum excipient concentration and process parameters to prepare best formulation.
c. Physicochemical characterization:
    i. Particle size and Zeta potential.
    ii. Assay/Entrapment efficiency.
    iii. Compatibility studies by Differential Scanning Calorimetry (DSC).
    iv. Transmission Electron Microscopy.
    v. In vitro release studies.

d. Conjugation of hetero-bifunctional PEG to polymers (PLGA or PCL) and confirmation of reaction steps using TLC, FTIR, NMR and GPC.
e. Phagocytic uptake studies on THP1 cells using flow cytometer.
f. Lyophilization.
g. Surface engineering of optimized formulation with monoclonal antibody.
h. Stability studies.
i. In vitro cytotoxic studies using MCF7 and MDAMB-231 cell lines.
j. Cellular uptake studies of native 6-Coumarin, 6-Coumarin loaded NPs and ER antibody conjugated 6-Coumarin NPs on MCF7 cell line using flow cytometer.
k. Cellular targeting of 6-Coumarin, 6-Coumarin loaded NPs and ER antibody conjugated 6-Coumarin NPs by fluorescence microscopy.
l. Cell cycle analysis and apoptosis studies on MCF7 cell line using flow cytometer.
m. In vivo biodistribution studies by radiolabelling in tumor bearing mice.

1.6 References

Acharya S, Dilnawaz F, Sahoo SK. 2009. Targeted epidermal growth factor receptor nanoparticle bioconjugates for breast cancer therapy. Biomaterials 30(29):5737-5750.

Arpino G, Weiss, H, Lee, AV, Schiff, R, De Placido, S, Osborne, CK, Elledge, RM. 2005. Estrogen receptor–positive, progesterone receptor–negative breast cancer: Association with growth factor receptor expression and tamoxifen resistance. J. Nat. Cancer Inst. 97(17):1254-1261.

Bartlett DW, Su H, Hildebrandt IJ, Weber WA, Davis ME. 2007. Impact of tumor-specific targeting on the biodistribution and efficacy of siRNA nanoparticles measured by multimodality in vivo imaging. Proc. Natl. Acad. Sci. U S A 104(39):15549-15554.

Bonneterre J BA, Nabholtz JM, Robertson JF, Thürlimann B, von Euler M, Sahmoud T, Webster A, Steinberg M. 2001. Anastrozole is superior to tamoxifen as first-line therapy in hormone receptor positive advanced breast carcinoma. Cancer 92:2247-2258.

Fang C, Shi B, Pei YY, Hong MH, Wu J, Chen HZ. 2006. In vivo tumor targeting of tumor necrosis factor-α-loaded stealth nanoparticles: effect of MePEG molecular weight and particle size. Eur. J. Pharm. Sci. 27:27-36.

Ghose T, Blair AH, Uadia P, Kulkarni PN, Goundalkar A, Mezei M, Ferrone S. 1985. Antibodies as carriers of cancer chemotherapeutic agents. Ann. N. Y. Acad. Sci. 446:213-227.

Iyer AK, Khaled G, Fang J, Maeda H. 2006. Exploiting the enhanced permeability and retention effect for tumor targeting. Drug Discov. Today 11(17-18):812-818.

Khalid MN, Simard P, Hoarau D, Dragomir A, Leroux JC. 2006. Long circulating poly(ethylene glycol)-decorated lipid nanocapsules deliver docetaxel to solid tumors. Pharm. Res. 23(4):752-758.

Kirpotin DB, Drummond DC, Shao Y, Shalaby MR, Hong K, Nielsen UB, Marks JD, Benz CC, Park JW. 2006. Antibody targeting of long-circulating lipidic nanoparticles does not increase tumor localization but does increase internalization in animal models. Cancer Res. 66(13):6732-6740.

Kocbek P, Obermajer N, Cegnar M, Kos J, Kristl J. 2007. Targeting cancer cells using PLGA nanoparticles surface modified with monoclonal antibody. J. Controlled Rel. 120(1-2):18-26.

Leserman LD, Barbet J, Kourilsky F, Weinstein JN. 1980. Targeting to cells of fluorescent liposomes covalently coupled with monoclonal antibody or protein A. Nature 288:602-604.

Lu RM, Chang YL, Chen MS, Wu HC. 2011. Single chain anti-c-Met antibody conjugated nanoparticles for in vivo tumor-targeted imaging and drug delivery. Biomaterials 32(12):3265-3274.

Modi S, Prakash Jain J, Domb AJ, Kumar N. 2006. Exploiting EPR in polymer drug conjugate delivery for tumor targeting. Curr. Pharm. Des. 12(36):4785-4796.

Sharaf LH. 2006. Current trends and recent advances in breast cancer drug therapy. Can. Therapy 4:183-192.

Zhu Z, Hicklin DJ. 2004. Antibody-mediated drug delivery in cancer therapy: In: Lu DR, Oie S, eds. Cellular drug delivery: Principles and practice. Totowa, Humana Press Inc., 312-315.

Chapter 2

LITERATURE REVIEW

2.1 Cancer

Cancer begins in cells, the body's basic unit of life. The body is made up of different types of cells. These cells grow and divide in a controlled way to produce more cells which are needed to keep the body in healthy conditions. When cells become old or when they are damaged, they die and are replaced with new cells. However, sometimes this orderly process goes wrong. When the genetic material (DNA) of a cell is damaged or changed, producing mutations that affect normal cell growth and division. When mutation occurs, cells do not die when they should and the new cells form when the body does not need them (Figure 2.1). These extra cells forms a mass of tissue called a tumor. Not all tumors are cancerous; tumors can be benign or malignant [Anand 2008].

- Benign tumors aren't cancerous. They can often be removed, and, in most cases, they do not come back. Cells in benign tumors do not spread to other parts of the body.
- Malignant tumors are cancerous. Cells in these tumors can invade nearby tissues and spread to other parts of the body. The spread of cancer from one part of the body to another is called metastasis.

Some cancers do not form tumors. For example, leukemia is a cancer of the bone marrow and blood.

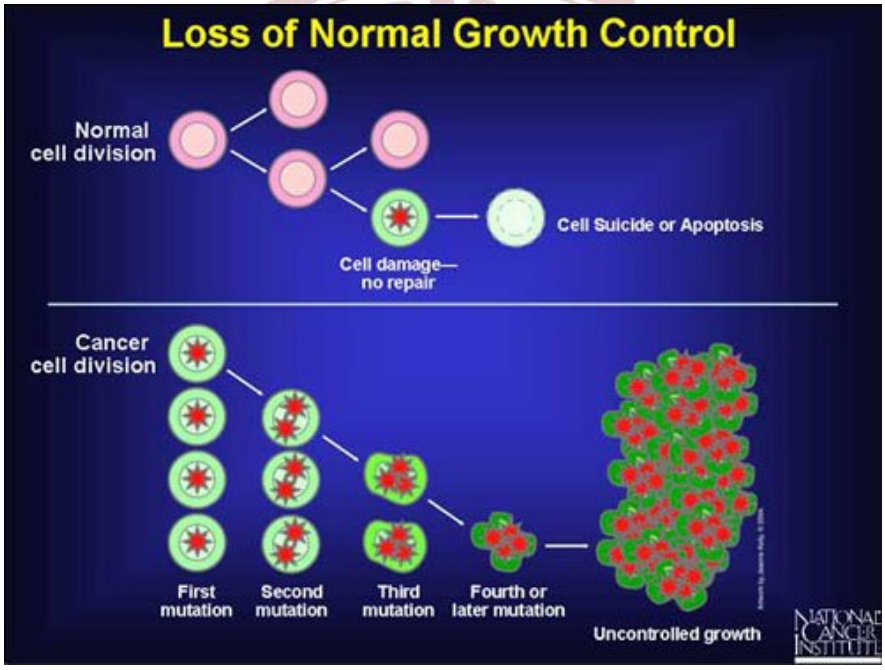

Figure 2.1 Growth of cells

Cancer is a disease in which abnormal cells divide without control and are able to invade other tissues. Cancer cells can spread to other parts of the body through the blood and lymph systems. Cancer is not just one disease but many diseases. There are more than 100 different types of cancer. Most cancers are named for the organ or type of cell in which they start - for example, cancer that begins in the breast is called breast cancer; cancer that begins in melanocytes of the skin is called melanoma [Jemal 2011]. Cancer types can be grouped into broader categories. The main categories of cancer include:

- Carcinoma - cancer that begins in the skin or in tissues that line or cover internal organs. There are a number of subtypes of carcinoma, including adenocarcinoma, basal cell carcinoma, squamous cell carcinoma, and transitional cell carcinoma.
- Sarcoma - cancer that begins in bone, cartilage, fat, muscle, blood vessels, or other connective or supportive tissue.
- Leukemia - cancer that starts in blood-forming tissue such as the bone marrow and causes large numbers of abnormal blood cells to be produced and enter the blood.
- Lymphoma and myeloma - cancers that begin in the cells of the immune system.
- Central nervous system cancers - cancers that begin in the tissues of the brain and spinal cord.

Cancer cells can also spread to other parts of the body. For example, cancer cells in the lung can travel to the bones and grow there. When cancer cells spread, it is called metastasis. Cancers can sometimes recur (or come back) after treatment, mostly at the site where they started but sometimes at a distant site like lungs, liver, brain, or bone. Some cancers tend to grow and spread very quickly. Others grow more slowly. Cancers also respond to treatment in different ways. Some types are best treated with surgery. Others do better with drugs called chemotherapy. Often 2 or more treatments are used to get the best results. Most cancers form a lump that doctors call a tumor or a growth. Not all tumors (lumps) are cancer. Doctors have to take out a piece of the lump and look at it to find out if it is cancer. Lumps that are not cancer are called benign. Lumps that are cancer are called malignant. There are also a few kinds of cancer, like leukemia (cancer of the blood), that do not form tumors. They grow in the blood or other cells of

the body. The most common treatments for cancer are surgery, chemotherapy, and radiation. Surgery is used to remove the cancer when it is confined to the organ where it started. The surgeon might also take part or the entire organ it affects. For breast cancer, part (or all) of the breast might be removed. For prostate cancer, the prostate gland might be removed. But surgery is not used for all types of cancer.

Chemotherapy is the use of drugs to kill cancer cells or to slow their growth. Some chemotherapy is given by IV (put into a vein using a needle), some as a shot, and others are swallowed as a pill or liquid. Because chemotherapeutic drugs travel to nearly all parts of the body, they are useful for cancer that has spread. Radiation treatment is also used to kill or slow the growth of cancer cells. It can be used alone or with surgery or chemo. Radiation treatment is like getting x-rays. Or sometimes it can be given by placing "seeds" that give off radiation inside the tumor.

2.1.1 Cancer statistics

Cancer is one of the leading causes of adult deaths worldwide. In India, the International Agency for Research on Cancer estimated indirectly that about 6,35,000 people died from cancer in 2008, representing about 8% of all estimated global cancer deaths and about 6% of all deaths in India [Ferlay et al. 2010]. Every year about 8,50,000 new cancer cases are diagnosed in India resulting in about 5,80,000 cancer related death every year. In females, cervical (30%) and breast cancers (19%) are the two main causes of cancer related illnesses and death [Causes of death in India 2009; Jemal 2011]. The absolute number of cancer deaths in India is projected to increase because of population growth and increasing life expectancy [Causes of death in India 2009]. Rates of cancer deaths are expected to rise, particularly, from increases in the age-specific cancer risks of tobacco smoking, which increase the incidence of several types of cancer [Jha 2009].

In 2010, more than 5,56,000 cancer deaths were estimated in India for people of all ages, and 71.1% occurred in people aged 30–69 years. Cancer deaths accounted for 8.0% of the 2.5 million total male deaths and 12.3% of the 1.6 million total female deaths at age 30–69 years. In 2010, at all ages, the rates of cancer deaths were about 59 per 100000 for men and about 52 per 1,00,000 for women. However, the rates of cancer deaths per 1,00,000 rose sharply with age and at age 30–69 years were about 98 for men and 95 for women. Based on the actual death rates and the hypothetical absence of other causes of death, a 30 year old man in India had a 4.7% chance of dying from

cancer before the age of 70 years. The respective risk for a 30-year-old woman was 4.4% [Dikshit et al. 2012].

The latest WHO statistics suggests about 45% increase in the global cancer deaths by 2030, of which 70% would be contributed from developing countries like India **[Thun 2010]**. With continuous up-gradation in the field of science and technology, the need for addressing the practical problems associated with the drug therapies increased proportionately. The major portion of cancer therapy till the last couple of decades was based on parenteral route of administration [O'Neill 2002; Ruddy 2009]. However, looking at the quality of life and need of follow-up therapy after the diagnosis of the disease, oral route has gained major focus as compared to the parenteral route [Jeanneret 2011; O'Neill 2002; Partridge 2002].

2.2 Tumor physiology

Tumor biology plays an important role in drug delivery. The growth, structure, and physiology of a tumor all impact the ability of nanoparticle (NP) drug carriers to be delivered successfully. Understanding which aspects of tumor biology are beneficial and which are detrimental to delivery leads to the development of more effective and efficient drug carriers.

2.2.1 Tumor growth

A tumor grows from a single cell that undergoes some mutation that blocks its apoptotic signaling pathway causing it to uncontrollably proliferate. The rapidly replicating cells displace their healthy counterparts due to an increased demand for nutrients and subsequent waste product elimination [Brannon-Peppas 2004]. During the initial stages of tumor growth the cells rely solely on diffusion to obtain nutrients limiting their size to approximately 2 mm^3 [Jones 1998]. To bypass their diffusion-limited size the tumor cells must begin to recruit new blood vessels in a process called angiogenesis [Brannon-Peppas 2004; Brown 1998].

2.2.2 Tumor vasculature and lymphatic system

Once a tumor mass is able to initiate angiogenesis, the blood vessels continue to rapidly grow producing an unorganized and aberrant vasculature [Haley and Frenkel 2008]. Consequently, the tumor contains regions with extensive vasculature and rich blood supply and regions with poor vasculature and little blood supply. The variance in level of vasculature and the tendency of the vessels to have dead-ends and little-to-no smooth

muscle or nerve innervation results in significantly heterogeneous blood flow through the tumor tissue [Brown 1998]. Tumor vessels are also inherently leaky due to abnormal basement membranes and incomplete endothelial linings caused by the inability of pericytes to fully line the quickly proliferating cells forming the vessel walls [Baban and Seymour 1998; Haley and Frenkel 2008].

Tumors also have a reduced ability to drain fluid and waste from the interstitial space [Brannon-Peppas 2004]. The reduction in drainage is due to a poorly-defined lymphatic system caused by the demand of the quickly proliferating tumor cells [Haley and Frenkel 2008]. Unlike healthy tissue which can rapidly remove macromolecules and lipids from its interstitium, a tumor will accumulate these molecules and retain them for extended periods of time [Maeda 2001].

Additional factors present at high levels in tumor cells contribute notably to angiogenesis and vessel permeability. These factors include vascular endothelial growth factor [Roberts and Palade 1995], basic fibroblast growth factor [Dellian 1996], bradykinin [Matsumura 1988], and nitric oxide [Wu 1998]. Vascular endothelial growth factor (VEGF) increases the permeability of blood vessels by increasing both the size and quantity of fenestrations between cells [Roberts and Palade 1995]. Elevated concentrations of bradykinin and depletion of nitric oxide both result in increased extravasation of macromolecules through the tumor vasculature [Matsumura 1988; Wu 1998]. Basic fibroblast growth factor (bFGF) is active in angiogenesis as it recruits endothelial cells and increases cellular proliferation [Roberts and Palade 1995].

Combined, the highly permeable vasculature, poorly-defined lymphatic system, and elevated levels of the aforementioned factors, result in a phenomenon called the enhanced permeability and retention effect (EPR). This effect was first defined by Maeda and colleagues and explains the observed accumulation of drugs, lipids and other macromolecules (MW > 50 kDa) at the tumor site [Maeda 2001]. The EPR has been the focus of much research due to its ability to passively target macromolecules including NPs.

2.2.3 Barriers to drug delivery in tumors

Most chemotherapeutic drugs are given via a systemic injection and circulate in the bloodstream prior to reaching the tumor site. A disadvantage of this type of delivery scheme is that the agent is allowed to come into contact with both healthy tissue and the tumor. This interaction between healthy tissue and the chemotherapeutic agent is what

often leads to the debilitating side effects that accompany treatment. Another detriment to systemic delivery is that the agent will encounter numerous extra-and intracellular barriers prior to reaching the tumor site. Furthermore, the drug must retain its biological activity and reach the target site at high enough concentrations to have therapeutic efficacy. In this section we will examine the significant systemic, extra- and intracellular barriers therapeutic agents encounter.

2.2.3.1 Reticuloendothelial system and mononuclear phagocytic system

The reticuloendothelial system (RES) also known as the mononuclear phagocytic system [Kurokawa] are a group of organs and circulating macrophages whose primary function is to rid the body of foreign objects, such as bacteria [Owens 2006a]. NPs that enter the bloodstream are also subject to rapid clearance by the RES/MPS. These foreign bodies are not directly recognized by the macrophages, typically liver macrophages or Kupffer cells, and must first be coated by a layer of proteins in a process called opsonization. The proteins involved in this process are termed opsonins, a class of proteins available in the circulation. Opsonins include immunoglobulins, components of the complement system (C3, C4, and C5), fibronectin, type I collagen, and many others. These proteins, when encountering a foreign particle, adhere by a variety of interactions such as ionic, electrostatic, hydrophobic, hydrophilic and van der Waals forces [Owens 2006a]. The macrophages then identify the surface layer of bound opsonin proteins coating the foreign body and proceed to engulf the particle by phagocytosis, “cell-eating”, then degrading it within an intracellular vesicle such as the lysosome [Jones and Harris 1998].

2.2.3.2 First pass renal filtering

The human body is a carefully designed system that is particularly adept at recognizing and removing foreign particles from circulation. The renal system is an essential component in the purification of the blood and is an important consideration when designing carriers for drug delivery. The kidneys filter blood through a structure known as the glomerular capillary wall. Particles with a diameter of less than 10 nm are subject to first pass renal filtration through this structure [Davis 2008; Venturoli 2005].

2.2.3.3 Heterogeneous blood flow

As mentioned previously, due to the rapid proliferation of tumor tissue, tumor vasculature is highly aberrant and unorganized. In conjunction with irregular vasculature structure is a lack of nerve enervation and smooth muscle which leads to a

heterogeneous and variable blood flow. This becomes a barrier to systemic drug delivery as the macromolecular therapeutic agent will not be evenly dispersed throughout the tumor tissue [Jang 2003]. It has been shown that areas of tumor tissue with poor blood flow are often resistant to treatment [Hori 1991].

2.2.3.4 High tumor interstitial pressure

The tumor interstitium comprises the bulk of tumor mass and consists of a collagen network and highly viscous fluid [Haley and Frenkel 2008]. The fluid within the interstitium has some quantifiable pressure that increases with tumor size and proximity to the tumor center. This pressure increase is due to a combination of factors such as rapid cellular proliferation in a confined area, high vascular permeability into the interstitium, and lack of lymphatic drainage from the interstitium [Jain 1987; Jain 1998]. Drug diffusion into the interstitium is depleted as the pressure increases. For this reason, there tends to be a lack of drug accumulation in the center of the tumor mass where the interstitial pressure is the highest [Haley and Frenkel 2008; Jain 1998].

2.2.3.5 Extracellular matrix (ECM)

The extracellular matrix is composed of fibrous proteins such as collagen and elastin, as well as a highly viscous polysaccharide-containing fluid. Its primary functions are to maintain cellular structure and integrity, modulate cellular interaction with the external milieu – including neighboring cells, regulate macromolecular transport and serve as a barrier to bacterial infiltration. In the context of drug transport, and, more specifically chemotherapeutic agent delivery, the ECM poses a formidable physical barrier. The tightly woven fibrous proteins and highly viscous ECM fluid, containing both hyaluronan and proteoglycans, each serve to reduce the diffusivity and spatial distribution of drug molecules within the tumor interstitium [Jain 1987; Jang 2003].

2.2.3.6 Intracellular transport

Once the drug component reaches the cell it must be internalized. This internalization process is termed phagocytosis, or cell eating, and consists of actin protrusions of the cellular membrane surrounding and engulfing a particle [Jones and Harris 1998]. The particle is now contained within an intracellular vesicle for transport through the cytoplasm. The particle is shuttled from the early endosome to the late endosome and finally the lysosome for degradation. Throughout this pathway the pH decreases from 7.4 to approximately 5.0. Additionally, contained within the intracellular components

are enzymes that aid in foreign body degradation. The drug must maintain its activity through both decreased pH and rampant enzymatic activity [Jones and Harris 1998].

2.3 Breast Cancer

Breast cancer is a disease in which malignant (cancer) cells form in the tissues of the breast. The breast is made up of lobes and ducts. Each breast has 15 to 20 sections called lobes, which have many smaller sections called lobules. Lobules end in dozens of tiny bulbs that can make milk. The lobes, lobules, and bulbs are linked by thin tubes called ducts. Each breast also has blood vessels and lymph vessels. The lymph vessels carry almost colorless fluid called lymph. Lymph vessels lead to organs called lymph nodes. Lymph nodes are small bean-shaped structures that are found throughout the body. They filter substances in fluid called lymph and help fight infection and disease. Clusters of lymph nodes are found near the breast in the axilla (under the arm), above the collarbone, and in the chest [Sariego 2010].

The most common type of breast cancer is ductal carcinoma, which begins in the cells of the ducts. Cancer that begins in the lobes or lobules is called lobular carcinoma and is more often found in both breasts than are other types of breast cancer. Inflammatory breast cancer is an uncommon type of breast cancer in which the breast is warm, red, and swollen. Breast cancer is sometimes caused by inherited gene mutations. The genes in cells carry the hereditary information that is received from a person's parents. Hereditary breast cancer makes up about 5 to 10% of all breast cancer. Some mutated genes related to breast cancer are more common in certain ethnic groups. Women who have certain gene mutations, such as a *BRCA1* or *BRCA2* mutation, have an increased risk of breast cancer. Also, women who had breast cancer in one breast have an increased risk of developing breast cancer in the other breast. These women also have an increased risk of ovarian cancer, and may have an increased risk of other cancers.

Breast cancer cells have receptors on their surface and in their cytoplasm and nucleus. Chemical messengers such as hormones bind to receptors, and this causes changes in the cell. Breast cancer cells may or may not have three important receptors: estrogen receptor (ER), progesterone receptor (PR), and HER2 [Petit 2011]. ER+ cancer cells depend on estrogen for their growth, so they can be treated with drugs to block estrogen effects (e.g. tamoxifen), and generally have a better prognosis. HER2+ breast

cancer has a worse prognosis, but HER2+ cancer cells respond to drugs such as the monoclonal antibody trastuzumab (in combination with conventional chemotherapy), and this has improved the prognosis significantly [Gabriel 2005; Spigel 2002]. Cells with none of these receptors are called triple-negative although they frequently express receptors for other hormones such as androgen receptor and prolactin receptor.

Discovery of ER is critical for the development of endocrine therapy in breast cancer. Expression of ERα, the predominant isoform, in breast tumors of both premenopausal and postmenopausal women is a highly predictive marker for response to antiestrogen treatment in women with ERα-positive breast cancer [Nahta 2003]. Today, endocrine therapies include the use of antiestrogens such as tamoxifen and aromatase inhibitors such as anastrozole, exemestane, and letrozole. Tamoxifen, the first antiestrogen to be used for the treatment of ERα-positive breast cancer, competitively blocks the actions of 17β-estradiol (E_2), the female hormone that binds and activates ERα in tumors. In postmenopausal women, peripheral aromatization of androgens to estrogens is the major source of plasma estrogen. Aromatase inhibitors inhibit this reaction and consequently suppress the production of circulating estrogen in postmenopausal women [Fisher et al. 1986]. Endocrine therapies are effective at reducing recurrence, increasing overall survival, and reducing contralateral breast cancer up to 50%. However, about 50% of patients with ERα-positive breast cancer have intrinsic resistance to antiestrogen therapy and therefore do not benefit [Bonneterre 2001]. In contrast to patients with intrinsically resistant tumors, there are patients who do initially respond to antiestrogen therapy; however, most of these patients develop acquired resistance during the treatment regimen. Therefore, the current goal in breast cancer research is to elucidate the mechanisms of both intrinsic and acquired resistance to tamoxifen and the aromatase inhibitors in order to develop new therapeutic strategies to prevent and/or treat resistant breast cancer.

2.3.1 Antiestrogens

Nonsteroidal antiestrogens were initially developed as contraceptives in the 1960s. Walpole and colleagues synthesized tamoxifen (termed ICI 46, 474), a potent antiestrogen with antifertility properties in rats. However, in humans, tamoxifen induced ovulation in subfertile women. Therefore, the development of tamoxifen as a contraceptive was terminated. However, Walpole also patented the application of tamoxifen as a drug treatment for hormone dependent cancers. Thus, clinical trials were

started to evaluate tamoxifen against the standard endocrine treatment at the time, diethylstilbestrol, for the treatment of advanced breast cancer in postmenopausal women [Cole et al. 1971]. Tamoxifen not only was as effective as diethylstilbestrol for the treatment of advanced breast cancer but also had fewer side effects. Therefore, the advantage of tamoxifen over diethylstilbestrol was crucial for its subsequent evaluation as a treatment for all stages of breast cancer.

In 1962, Jensen and colleagues discovered ERα. Jensen demonstrated that E_2, the circulating female hormone that promoted breast cancer growth, binds to diverse tissue sites around a woman's body but is retained in estrogen target tissues, for example, the uterus and vagina [Jensen EV 1962]. The identification of ERα as the target of E2 action in the breast and antiestrogens blocking the binding of E_2 to ERα provided a therapeutic target and an approach for the treatment of breast cancer. Although many antiestrogens were discovered and tested during the 1960s and 1970s, only tamoxifen was considered safe enough for extensive clinical evaluation [Jordan and Dowse 1976]. Clinical trials ultimately demonstrated that patients with ERα-positive breast cancer benefited the most from tamoxifen therapy, whereas women with ERα-negative breast cancer were found to be unaffected. During subsequent clinical trials, five years of adjuvant tamoxifen treatment was found to be more effective than less than five years of treatment in improving time to tumor recurrence and overall survival [Fisher et al. 1986]. In contrast to the beneficial effects of tamoxifen as a treatment for breast cancer, both laboratory and clinical results showed that tamoxifen increased the risk of endometrial cancer in the uterus four fold in postmenopausal women compared with untreated women [Fisher et al. 1994; Gottardis et al. 1988]. These results strongly indicated that tamoxifen was not a pure antiestrogen but had selective functions depending on the target tissue.

2.3.2 EGFR and HER2/ Neu and Antiestrogen resistance

Numerous laboratory and clinical studies indicate that overexpression and/or aberrant activity of the HER2/neu (erbB2) signalling pathway is associated with antiestrogen resistance in breast cancer [Kurokawa and Arteaga 2003]. The HER2/neu receptor is a member of the EGFR family of receptor tyrosine kinases, which include HER3 (erbB3) and HER4 (erbB4) [Yarden 2001a; Yarden 2001b; Yarden and Sliwkowski 2001]. Upon dimerization, the tyrosine kinase domains located within the COOH-terminal regions of receptors are activated by an autophosphorylation cascade on specific tyrosine

residues, which activate downstream effectors, such as MAPK and Akt, which promote cellular proliferation, survival, anti-apoptosis, and transformation. HER2/neu is overexpressed and/or amplified in 25 to 30% of breast tumors and is associated with a more aggressive phenotype and poor prognosis [Spigel DR 2002]. Patients with breast tumors overexpressing HER2/neu exhibit much lower response rates to antiestrogen therapy [Spigel DR 2002]. Thus, it is suggested that one possible mechanism of resistance to tamoxifen is overexpression of HER2/neu in ERα-positive breast cancers. In addition, overexpression of EGFR and its ligands are observed in several human cancers including breast cancer [Klijn JG 1994; Tang et al. 2000]. The increased expression of EGFR is frequently associated with tumor progress ion and resistance to antiestrogens. These data suggest that EGFR and/or HER2/neu are possible targets for preventing or treating antiestrogen resistance in breast cancer. Strategies to target EGFR and HER2/neu include the use of humanized monoclonal antibodies to the receptors [Slamon DJ 2001], tyrosine kinase inhibitors that block reduction of adenosine triphosphate (ATP) to adenosine diphosphate (ADP) + Pi, and receptor antisense molecules [Nahta R 2003]. Gefitinib, (ZD 1839, Iressa®), an EGFR-specific tyrosine kinase inhibitor, has been shown to inhibit growth of breast cancer cell lines in vitro that are resistant to tamoxifen. More importantly, the combination of gefitinib and tamoxifen was shown to prevent resistance [Johnston et al. 2003], demonstrating that EGFR might be a key player in the development of antiestrogen resistance and inhibiting the activity of this receptor might be therapeutically beneficial in preventing resistance to antiestrogens. In addition to gefitinib, trastuzumab (Herceptin®) is a humanized monoclonal antibody directed against the ectodomain of the HER2/neu receptor. It has been shown to restore breast cancer cell sensitivity to tamoxifen in HER2/neu overexpressing cells [Kurokawa 2000].

2.3.3 Aromatase inhibitors

An alternate strategy to endocrine therapy, which specifically inhibits binding of E_2 to the ER, is to inhibit the production of E_2 by blocking the cytochrome p450 aromatase enzyme, the rate-limiting enzyme that converts androgens (i.e., testosterone and androstenedione) to estrogens (i.e., E_2 and estrone) in the adrenal gland, surrounding stroma, and adipose tissue of the breast tumor. The main drugs of this type are aromatase inhibitors, which include Type I (steroidal) or Type II (nonsteroidal). Steroidal inhibitors are competitive-substrate mimics of androstenedione. These

include formestane and exemestane, which are irreversible inhibitors that bind with high affinity to the binding site of aromatase and are converted to a covalently bound intermediate. Nonsteroidal inhibitors include the first-generation aromatase inhibitor aminoglutethimide and the second-generation compounds anastrozole and letrozole. All nonsteroidal aromatase inhibitors act by binding reversibly to the enzyme and competitively inhibiting binding of the substrate androstenedione. The benefits of using aromatase inhibitors over tamoxifen are believed to be the complete deprivation of E_2 and thus better efficacy for ERα-positive breast cancer [Johnston 2003]. Recent clinical data have clearly demonstrated that anastrozole [Bonneterre 2001], letrozole [Mouridsen 2001], and exemestane [Paridaens 2003] are more effective than tamoxifen as first-line treatments in patients with metastatic breast cancer. On the basis of clinical results [Bonneterre 2001; Mouridsen 2001], currently both anastrozole and letrozole are approved by the Food and Drug Administration for first-line treatment of postmenopausal, ERα-positive advanced breast cancer. The data from advanced breast cancer trials provided the rationale to perform large scale clinical trials to determine whether there is an advantage of using aromatase inhibitors over tamoxifen in the adjuvant setting. The anastrozole, tamoxifen, and the combination of anastrozole and tamoxifen (ATAC) trial has sufficient follow-up data to confirm that anastrozole is superior to tamoxifen as a first-line adjuvant therapy in ERα-positive breast cancer with regard to disease-free survival and incidence of contralateral breast cancer [Baum 2002]. The Breast International Group [Paridaens] 1-98 study demonstrated a similar improvement in event -free survival to confirm that letrozole is superior to tamoxifen as first-line adjuvant hormonal therapy [Thürlimann 2005]. Other trials have demonstrated an improved outcome for post menopausal patient s with early- stage breast cancer treated with two to three years of tamoxifen, followed by an aromatase inhibitor, compared with five years of tamoxifen [Coombes 2007; Kaufmann 2007].

2.3.4 Mechanisms of resistance

Clinically, patients that relapse after a previous response to tamoxifen usually have a clinical response to aromatase inhibitors [Buzdar et al. 1996; Dombernowsky et al. 1998]. These results strongly indicate that the ERα continues to be expressed and is functional in breast tumors that are resistant to antiestrogens. However, although estrogen deprivation treatment might be more effective than tamoxifen in delaying resistance, eventually resistance to aromatase inhibitors will also develop. To date, it is

unclear whether similar mechanisms of actions that have been identified for tamoxifen resistance are also involved in resistance to aromatase inhibitors. The exact mechanisms contributing to aromatase inhibitor resistance has yet to be fully elucidated. However, in vitro studies have identified mutations within the aromatase gene that confers resistance to aromatase inhibitors [Kao 1996]. These mutations have not yet been identified in human breast carcinomas [Sourdaine 1994]. Other studies have demonstrated that estrogen deprivation super sensitizes the breast cancer cell to low levels of estrogen, thus creating a hypersensitive environment to overcome estrogen deprivation resulting in resistance [Chan 2002; Masamura 1995; Santen 2001]. In addition, results suggest that there is increased cross talk between growth factor receptor signalling pathways and ERα. ERα has been shown to become activated and supersensitized by several different intracellular kinases, including MAPKs, insulin-like growth factors, and the PI3-K/Akt pathway [Campbell et al. 2001; Jeng 2000; Martin et al. 2003]. Therefore, the data suggest that ERα continues to be an integral part of the breast cancer cell signalling pathway even after resistance to aromatase inhibitors has developed.

2.3.5 Role of progesterone receptor and HER2/Neu

There is emerging evidence to suggest that ER-positive cancers that do not express the progesterone receptor (PR) and/or HER2/neu are somewhat intrinsically resist ant to tamoxifen and perhaps hormonal therapy in general. Arpino et al. have demonstrated an increased relapse rate in patients with ER-positive, PR negative cancers compared with ER-positive, PR-positive cancers, treated with tamoxifen [Arpino 2005]. Patients treated with tamoxifen with ER-positive, HER2- positive metastatic breast cancers have a shorter time to treatment failure compared with ER-positive, HER2-negative cancers [De Laurentiis 2005]. In fact, Arpino et al. have demonstrated an increase in both HER1 and HER2 in ER-positive, PR-negative cancers compared to ER-positive, PR-positive cancers, suggesting an interplay between the ER and epidermal growth factor pathways [Arpino 2005].

Two very small trials demonstrated a significantly increased clinical response rate in patients with ER-positive, HER2-positive cancers treated with preoperative aromatase inhibitors compared to preoperative tamoxifen [Ellis 2006; Smith 2005]. This led to a widely accepted hypothesis that aromatase inhibitors were a better choice than tamoxifen in patients with ER-positive, HER2-positive cancers. However, an analysis of

the BIG-1-98 trial demonstrates that letrozole improves outcome compared to tamoxifen in both ER-positive, HER2-positive cancers (HR 0.68) and in ER-positive, HER2-negative cancers (HR 0.72) [Viale 2007]. A recent subanalysis of the ATAC trial demonstrated a significantly improved outcome in ER-positive, HER2-negative cancers (HR 0.66) but not in ER-positive, HER2 positive cancers (HR 0.92), but this may have been due to the small number of patients in the HER positive group [Dowsett 2008]. Are HER2- positive cancers somewhat resistant to not just tamoxifen but also to aromatase inhibitors? As outlined above, a recent trial randomized patients with HR-positive, HER2 positive metastatic breast cancers to anastrozole alone or to anastrozole plus trastuzumab . Although there was no significant difference in overall survival, possibly because patients randomized to anastrozole alone could receive trastuzumab at disease progression, the time to progression was doubled from 2.4 months in the anastrozole-alone arm to 4.8 months in the combined arm (p ¼ 0.0016). The clinical benefit rate in the combination arm was 42% significantly higher than in the anastrozole alone arm. A trial that evaluated single-agent trastuzumab as first-line therapy for patients with HER2-positive cancers demonstrated a clinical benefit rate of 48% [Vogel 2002]. This suggests the intriguing possibility that HR positive, HER2-positive cancers are driven by the HER2 pathway, which renders the cancers partly resistant to hormonal therapies.

An initial evaluation of the ATAC trial using case report forms revealed that TTR was longer for anastrozole in both ER-positive/PR-positive and ER positive/ PR-negative subgroups, but the benefit was more pronounced in the ER positive/ PR-negative subgroup [HR 0.84, 95% confidence interval 0.69-1.02 vs. 0.43, 95% CI 0.31-0.61] [Dowsett 2005]. Importantly, the ER and PR analyses were not performed cent rally. More recently , a central analysis of about 2000 patients on the ATAC trial demonstrated similar improvements with the use of anastrozole compared to tamoxifen, regardless of PR status (HR anastrozole vs. tamoxifen 0.72 for ER-positive, PR-positive subgroups and 0.66 for ER-positive, PR-negative subgroups) [Dowsett 2008]. In the BIG-1-98 trial, similar benefits for letrozole compared to tamoxifen were seen in the ER-positive/PR-positive and ER-positive/ PR-negative subgroups [Viale 2007]. On the basis of this data, decisions regarding whether to start a patient on tamoxifen or an aromatase inhibitor should not be based on PR or HER2 status. Further molecular profiling may help in the future in making decisions regarding optimal hormonal therapies.

2.4 Treatment of breast cancer

2.4.1 Treatment options by stage

- Early Stage Breast Cancer (Stage I and Stage II): Treatment of early stage breast cancer (Stage I and Stage II) may be surgery followed by adjuvant therapy as follows:
- Modified radical mastectomy.
- Breast-conserving surgery: Lumpectomy, partial mastectomy or segmental mastectomy.
- Breast-conserving surgery during pregnancy followed by radiation therapy after the baby is born.
- Surgery during pregnancy followed by chemotherapy after the first t.
- Clinical trials of surgery followed by hormone therapy with or without chemotherapy.

Late Stage Breast Cancer (Stage III and Stage IV): Treatment of late stage breast cancer (Stage III and Stage IV) may include the following:

- Radiation therapy.
- Chemotherapy.

The mainstay of breast cancer treatment is surgery when the tumor is localized, followed by chemotherapy (when indicated), radiotherapy and adjuvant hormonal therapy for ER positive tumors (with tamoxifen or an aromatase inhibitor). Management of breast cancer is undertaken by a multidisciplinary team based on national and international guidelines. Depending on clinical criteria (age, type of cancer, size, metastasis) patients are roughly divided to high risk and low risk cases, with each risk category following different rules for therapy. Treatment possibilities include radiation therapy, chemotherapy, hormone therapy and immune therapy.

2.4.2 Surgery

Depending on the stage and type of the tumor, just a lumpectomy (removal of the lump only) may be all that is necessary, or removal of larger amounts of breast tissue may be necessary. Surgical removal of the entire breast is called mastectomy. Lumpectomy techniques are increasingly utilized for breast-conservation cancer surgery. Studies indicate that for patients with a single tumor smaller than 4 cm, lumpectomy may be as effective as a mastectomy.

However, mastectomy may be the preferred treatment in certain instances:

- Two or more tumors exist in different areas of the breast (a "multifocal" cancer).
- The patient has previously received radiotherapy.
- The tumor is large, relative to the size of the breast.
- The patient has had scleroderma or another disease of the connective tissue, which can complicate radiotherapy.
- The patient lives in an area where radiotherapy is inaccessible.
- The patient is apprehensive about the risk of local recurrence after lumpectomy.

2.4.3 Radiation therapy

Radiation therapy is an adjuvant treatment for most women who have undergone lumpectomy and for some women who have mastectomy surgery. In these cases the purpose of radiation is to reduce the chance that the cancer will recur. Radiation therapy involves using high-energy X-rays or gamma rays that target a tumor or post surgery tumor site. This radiation is very effective in killing cancer cells that may remain after surgery or recur where the tumor was removed [Buchholz 2009].

Radiation therapy eliminates the microscopic cancer cells that may remain near the area where the tumor was surgically removed. The dose of radiation must be strong enough to ensure the elimination of cancer cells. However, radiation affects normal cells and cancer cells alike, causing some damage to the normal tissue around where the tumor was. Healthy tissue can repair itself, while cancer cells do not repair themselves as well as normal cells. For this reason, radiation treatments are given over an extended period, enabling the healthy tissue to heal. Treatments using external beam radiotherapy are typically given over a period of five to seven weeks, performed five days a week. Each treatment takes about 15 minutes. A newer approach, called 'accelerated partial breast irradiation' (APBI), uses brachytherapy to deliver the radiation in a much shorter period of time. APBI delivers radiation to only the immediate region surrounding the original tumor and can typically be completed over the course of one week [Hendrick 2010].

Side effects of radiation therapy

External beam radiation therapy is a non-invasive treatment with some short term and some longer-term side effects. Patients undergoing some weeks of treatment usually experience fatigue caused by the healthy tissue repairing itself and aside from this there can be no side effects at all. However many breast cancer patients develop a suntan-like change in skin color in the exact area being treated. As with a suntan, this darkening of

the skin usually returns to normal in the one to two months after treatment. In some cases permanent changes in color and texture of the skin is experienced. Other side effects sometimes experienced with radiation can include:

- muscle stiffness
- mild swelling
- tenderness in the area
- lymphedema

2.4.4 Chemotherapy

Chemotherapeutic agents are, in the broadest sense, small drug-like molecules that disrupt the normal functioning of a cell by inhibiting replication or inducing apoptosis [Feng 2003]. Due to their proficiency at provoking cytotoxic effects, chemotherapeutic agents have been almost exclusively utilized in the treatment of cancer, where they exhibit the most deleterious effects to rapidly proliferating cells [Feng 2003]. Prominent chemotherapeutic agents include paclitaxel, doxorubicin, daunorubicin, cisplatin, and docetaxel. Paclitaxel and docetaxel are both taxanes, components that function by stabilizing the microtubules and preventing mitosis from progressing from metaphase to anaphase [Rowinsky 1997]. Doxorubicin and daunorubicin belong to a class of chemotherapeutics known as the anthracyclines. These molecules are among the most effective drugs available, inducing the greatest degree of cytotoxicity and used to treat the widest variety of tumor types including aggressive lymphoma, breast cancer, and myeloblastic leukemia [Minotti 2004; Weiss 1992]. Doxorubicin has been shown to target the topoisomerase-II-DNA complex, disrupting the DNA and preventing cellular replication [Hurley 2002]. Similarly, cisplatin, a platinum-compound, modifies cellular DNA which activates signaling pathways that triggers apoptosis [Boulikas 2003].

The primary concern with utilizing the aforementioned chemotherapeutic agents is their inability to differentiate between healthy and tumor tissue [Maeda 2001]. The drugs will attack all cells without discrimination, being particularly harmful to any rapidly proliferating cells in the body such as hair, intestinal epithelial cells, and bone marrow [Feng 2003]. The most cytotoxic agents are the most effective but often result in severe side effects. Doxorubicin is widely considered to be best anti-cancer drug available today but results in side effects such as, nausea, fatigue, and extensive and often fatal cardiotoxicity [Minotti 2004]. Oncologists must, therefore, optimize the balance between the effectiveness of the drug and a patient's ability to tolerate the

accompanying side effects [Feng 2003]. Nanoscale carrier systems designed to target specific disease conditions could be utilized to alleviate some, if not all, of these cytotoxic effects to healthy cells.

However, oral delivery of anticancer drugs is a great challenge owing to their peculiar physicochemical properties, and physiological barriers such as pre-systemic metabolism and gastrointestinal instability. Upon oral administration of such drugs, only a fraction of dose is available to systemic circulation for execution of therapeutic response *e.g.* oral bioavailability of paclitaxel, docetaxel, doxorubicin, tamoxifen, etc. is in the range of 5–20% [Kuppens 2005; Peltier 2006; Troutman 2003]. Broadly, this could be attributed to low aqueous solubility, poor intestinal permeability, high level of P-glycoprotein (P-gp) efflux and pre-systemic metabolism. The P-gp efflux also has a key role in the execution of multidrug resistance in the tumor cells and thereby needs special consideration while designing the formulation of poor biopharmaceutical properties, as the amount which is required to achieve the therapeutic response might be very high ultimately leading to multidrug resistance.

The therapeutic efficacy of the formulation depends upon its capability to deliver the drug at the right place and at the right time in amount adequate enough to yield a therapeutic response. Comparative therapeutic equivalence of oral and intravenous routes has been studied for wide variety of drugs and promising results were observed in most of the cases. Cyclophosphamide yields no statistical significant difference in the area under the plasma disappearance curve (AUC) and generated similar cytotoxic metabolic products upon administration through oral and parenteral routes thereby suggesting the therapeutic equivalence, irrespective of the route of delivery [Struck 1987]. Paclitaxel in nanoparticulate dosage form administered by oral route had shown promising tumor reduction in animals compared to commercially available intravenous formulation at 50% reduced dose [Bhardwaj 2009]. Co-administration of cyclosporin A further potentiated its oral bioavailability, due to inhibition of the P-gp efflux pump and CYP 3A4, both being limitations for oral bioavailability [Asperen 1998]. Similarly, topotecan has also been found to be equally effective irrespective of the route of administration with upper hand in reduced toxicity *via* oral route [Gore 2002; von Pawel 2001]. The other drugs which have been evaluated include docetaxel, paclitaxel, doxorubicin, cisplatin [Urien 2005], ifosfamide/mesna combination [Manegold 1996] and melphalan [Bosanquet 1982] to name a few. The studies suggest that by

virtue of appropriate pharmaceutical/pharmacological interventions, the inherent problems associated with oral route (owing to various physiological barriers) can be overcome in comparison to intravenous route of administration.

2.5 Targeted therapy

In patients whose cancer expresses an over-abundance of the HER2 protein, a monoclonal antibody known as trastuzumab (Herceptin) is used to block the activity of the HER2 protein in breast cancer cells, slowing their growth. In the advanced cancer setting, trastuzumab use in combination with chemotherapy can both delay cancer growth as well as improve the recipient's survival [22]. More recently, several clinical trials have also confirmed that in the adjuvant setting, i.e. postoperative following breast cancer surgery, the use of trastuzumab for up to one year also delays the recurrence of breast cancer and improves survival[23][24][25].

Other types of targeted therapies that are being researched to fight cancer include:

- Angiogenesis inhibitors. These antibodies prevent the growth of new blood vessels, cutting off the supply of oxygen and nutrients to cancer cells.
- Signal transduction inhibitors. These antibodies block signals inside the cancer cell that helps the cells divide, stopping the cancer from growing.
- Antibodies/antagonists for other hormones/receptors such as androgen receptors and prolactin receptors, which are present in a high proportion of breast cancers

Targeted cancer therapies are drugs or other substances that block the growth and spread of cancer by interfering with specific molecules involved in tumor growth and progression. Because scientists often call these molecules “molecular targets,” targeted cancer therapies are sometimes called “molecularly targeted drugs,” “molecularly targeted therapies,” or other similar names. By focusing on molecular and cellular changes that are specific to cancer, targeted cancer therapies may be more effective than other types of treatment, including chemotherapy and radiotherapy, and less harmful to normal cells. Many targeted cancer therapies have been approved by the U. S. Food and Drug Administration (FDA) for the treatment of specific types of cancer. Others are being studied in clinical trials (research studies with people), and many more are in preclinical testing (research studies with animals). Targeted cancer therapies are

being studied for use alone, in combination with other targeted therapies, and in combination with other cancer treatments, such as chemotherapy.

Targeted cancer therapies interfere with cancer cell division (proliferation) and spread in different ways. Many of these therapies focus on proteins that are involved in cell signaling pathways, which form a complex communication system that governs basic cellular functions and activities, such as cell division, cell movement, cell responses to specific external stimuli, and even cell death. By blocking signals that tell cancer cells to grow and divide uncontrollably, targeted cancer therapies can help stop cancer progression and may induce cancer cell death through a process known as apoptosis. Other targeted therapies can cause cancer cell death directly, by specifically inducing apoptosis, or indirectly, by stimulating the immune system to recognize and destroy cancer cells and/or by delivering toxic substances directly to the cancer cells.

The development of targeted therapies, therefore, requires the identification of good targets – that is, targets that are known to play a key role in cancer cell growth and survival. For example, most cases of chronic myeloid leukemia (CML) are caused by the formation of a gene called *BCR-ABL*. This gene is formed when pieces of chromosome 9 and chromosome 22 break off and trade places. One of the changed chromosomes resulting from this switch contains part of the *ABL* gene from chromosome 9 fused to part of the *BCR* gene from chromosome 22. The protein normally produced by the *ABL* gene [Astete] is a signaling molecule that plays an important role in controlling cell proliferation and usually must interact with other signaling molecules to be active. However, Abl signaling is always active in the protein (Bcr-Abl) produced by the *BCR-ABL* fusion gene. This activity promotes the continuous proliferation of CML cells. Therefore, Bcr-Abl represents a good molecule to target.

Once a target has been identified, a therapy must be developed. Most targeted therapies are either small-molecule drugs or monoclonal antibodies. Small-molecule drugs are typically able to diffuse into cells and can act on targets that are found inside the cell. Most monoclonal antibodies cannot penetrate the cell's plasma membrane and are directed against targets that are outside cells or on the cell surface. Candidates for small-molecule drugs are usually identified in studies known as drug screens – laboratory tests that look at the effects of thousands of test compounds on a specific target, such as Bcr-Abl. The best candidates are then chemically modified to produce numerous closely related versions, and these are tested to identify the most effective

and specific drugs. Monoclonal antibodies, by contrast, are prepared first by immunizing animals (typically mice) with purified target molecules. The immunized animals will make many different types of antibodies against the target. Next, spleen cells, each of which makes only one type of antibody, are collected from the immunized animals and fused with myeloma cells. Cloning of these fused cells generates cultures of cells that produce large amounts of a single type of antibody, known as a monoclonal antibody. These antibodies are then tested to find the ones that react best with the target.

Before they can be used in humans, monoclonal antibodies are "humanized" by replacing as much of the animal portion of the antibody as possible with human portions. This is done through genetic engineering. Humanizing is necessary to prevent the human immune system from recognizing the monoclonal antibody as "foreign" and destroying it before it has a chance to interact with and inactivate its target molecule. The first molecular target for targeted cancer therapy was the cellular receptor for the female sex hormone estrogen, which many breast cancers require for growth. When estrogen binds to the estrogen receptor (ER) inside cells, the resulting hormone-receptor complex activates the expression of specific genes, including genes involved in cell growth and proliferation. Research has shown that interfering with estrogen's ability to stimulate the growth of breast cancer cells that have these receptors (ER-positive breast cancer cells) is an effective treatment approach. Several drugs that interfere with estrogen binding to the ER have been approved by the FDA for the treatment of ER-positive breast cancer. Drugs called selective estrogen receptor modulators (SERMs), including tamoxifen and toremifene (Fareston®), bind to the ER and prevent estrogen binding. Another drug, fulvestrant (Faslodex®), binds to the ER and promotes its destruction, thereby reducing ER levels inside cells.

Aromatase inhibitors (AIs) are another class of targeted drugs that interfere with estrogen's ability to promote the growth of ER-positive breast cancers. The enzyme aromatase is necessary to produce estrogen in the body. Blocking the activity of aromatase lowers estrogen levels and inhibits the growth of cancers that need estrogen to grow. AIs are used mostly in women who have reached menopause because the ovaries of premenopausal women can produce enough aromatase to override the inhibition. Three AIs have been approved by the FDA for the treatment of ER-positive breast cancer: Anastrozole (Arimidex®), exemestane (Aromasin®), and letrozole

(Femara®). Targeted cancer therapies have been developed that interfere with a variety of other cellular processes.

2.5.1 Nanoparticulate drug delivery system

Therapeutic NP technologies have revolutionized the drug development process and changed the landscape of the pharmaceutical industry [Allen 2004; Farokhzad 2009; Petros 2010; Wagner 2006]. By virtue of their unique physicochemical properties, NPs have shown promise in delivering a range of molecules at a desired site in the body. Nanoparticulate technologies may improve the therapeutic index of drugs by enhancing their efficacy and/or increasing their tolerability in the body. NPs have also been reported to improve the bioavailability of hydrophobic drugs, protect the active pharmaceutical ingredient from physiological barriers, as well as enable the development of novel classes of bioactive macromolecules like proteins, DNA and siRNA [Shi 2010]. Additionally, the incorporation of imaging contrast agents within NPs allowed us to visualize the site of drug delivery or monitor the in vivo efficacy of the therapeutic agent [Cai 2007]. So far, US Food and Drug Administration (FDA) have approved over two-dozen nanotechnology products for clinical use, and many are under clinical and preclinical development [Davis 2008; Wagner 2006]. Interestingly, the majority of these clinically approved, first-generation nanotechnology products are comprised of liposomal drugs and polymer–drug conjugates, which are relatively simple and generally lack active targeting or controlled drug release components. To develop safer and more effective therapeutic NPs, researchers have designed novel multifunctional NP platforms for cell/tissue-specific targeting, sustained or triggered drug delivery, co-delivery of synergistic drug combinations, etc. Among these functions, targeted delivery is critical for the successful development of next-generation nanotechnology products [Shi 2010].

Targeted drug delivery system can be formulated by conjugating drug-encapsulated NPs with targeting ligands, which could facilitate the preferential delivery of NPs to the sites of interest while reducing undesired side effects elsewhere. Since the first description of cell-specific targeted liposomes in 1980 [Heath 1980; Leserman 1980], targeted NPs have shown some promising clinical and preclinical results in the treatment of different diseases. For tumor cell targeting, the presence of targeting ligands could enhance cellular uptake and retention of drugs via receptor-mediated endocytosis, although tumor accumulation through the enhanced permeability and retention (EPR) effect

[Maeda 2001] is largely determined by the physicochemical properties of NPs and long circulation half-life [Farokhzad 2009]. Active NP targeting is also essential for the delivery of biomacromolecules (e.g., DNA and siRNA) that require intracellular delivery for bioactivity [Farokhzad 2009]. In the case of vascular endothelial targeting for oncology or cardiovascular indications, ligand-mediated targeting may be critically important as NPs localization is not a function of EPR [Dhar 2011; Rothenfluh 2008]. In addition, efforts have been made to transport drugs across tight epithelial and endothelial barriers with nanotherapeutics (e.g., the blood–brain barrier) via ligand-mediated transcytosis. More recently, targeted NPs have been employed in solving the complex problems of multidrug resistance [Davis 2008].

Controlled release polymer technology, resulting in the control of drug exposure, has benefited virtually every branch of medicine over the past 4 decades. Many products utilizing this technology are now in clinical use, including Atridox®, Lupron Depot®, Gliadel®, Zoladex®, Trelstar® Depot, and Sandostatin® LAR® [Farokhzad 2006]. Polymeric NPs can encapsulate drugs and release them at sustained rates in the optimal range of drug concentration, thus enhancing the in vivo therapeutic efficacy, maximizing patient compliance, and facilitating the use of highly toxic, poorly soluble, or relatively unstable drugs [Brigger 2002a; Farokhzad 2006]. In general, drug release can be regulated by diffusion of the drug molecules through the polymer matrix or by differential surface and bulk erosion of the polymer. Alternatively, drug release can be triggered by specific microenvironments in the body (e.g., changes in pH, temperature, and enzymatic activities) or manipulated by external events (e.g., electric field, magnetic field, and ultrasound) [Ganta 2008; Kale 2010; Oh 2007]. By further functionalization with targeting ligands, controlled release polymeric NPs could deliver therapeutic agents in a spatiotemporally regulated fashion, which may be essential to many medical applications.

Over the past few decades, different nanotechnology platforms were studied for their use in therapeutic applications [Davis 2008]. These NPs platforms have been developed to enhance the pharmacological properties and therapeutic index of a myriad of drugs [Allen 2004; Moghimi 2005]. Four major classes of nanoparticulate delivery systems, includes liposomes, polymeric NPs, lipid–polymer hybrid NPs, and dendrimers (figure 2.2).

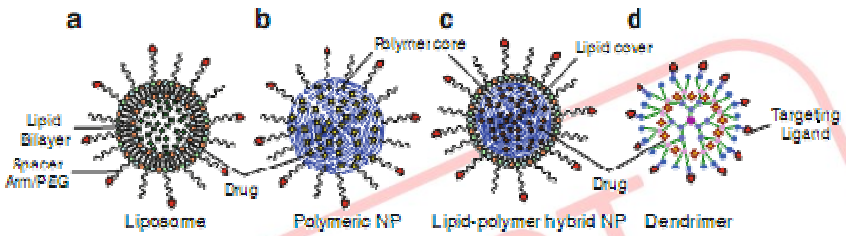

Figure 2.2 Nanoparticulate platforms for the targeted and controlled delivery of drugs, (a) liposome, (b) polymeric nanoparticle, (c) lipid polymer hybrid nanoparticle and (d) dendrimer.

2.5.1.1 Polymeric nanoparticles (Nanospheres and nanocapsules)

Nanospheres consist of a spherical polymeric matrix within which a drug is encapsulated (figure 2.3A). The drug is typically distributed evenly throughout this matrix and released into the environment via diffusion. The composition of the polymer matrix and its ability to imbibe fluids will determine how rapidly the drug will be released [Brigger 2002b].

Nanocapsules are often referred to as reservoir systems as they contain the active ingredient in a core separated from the environment by a polymeric membrane (figure 2.3B) [Haley and Frenkel 2008]. By saturating the core, the active ingredient can diffuse through the membrane with an approximately constant release rate. This release behavior is attractive for drug delivery applications.

The above nanoparticulate systems have been widely explored for diffusion-driven drug release due to their large surface-to-volume ratios, which allow for drug release at feasible and clinically relevant time scales. There is a surge in the development of nanoparticulate systems that do not rely solely on diffusion mechanisms for drug release. Instead, this new class of NPs is able to respond to environmental, chemical, thermal, or biological triggers [Caldorera-Moore 2009; Liechty and Peppas 2012; Schoener 2012]. These 'smart materials' will release their therapeutic payload only when triggered. A more complete review on environmentally responsive carriers was recently published by Liechty et al. Although the diffusion-driven NPs are unable to respond directly to their environment there are means by which these systems can target and accumulate in the tumor interstitium.

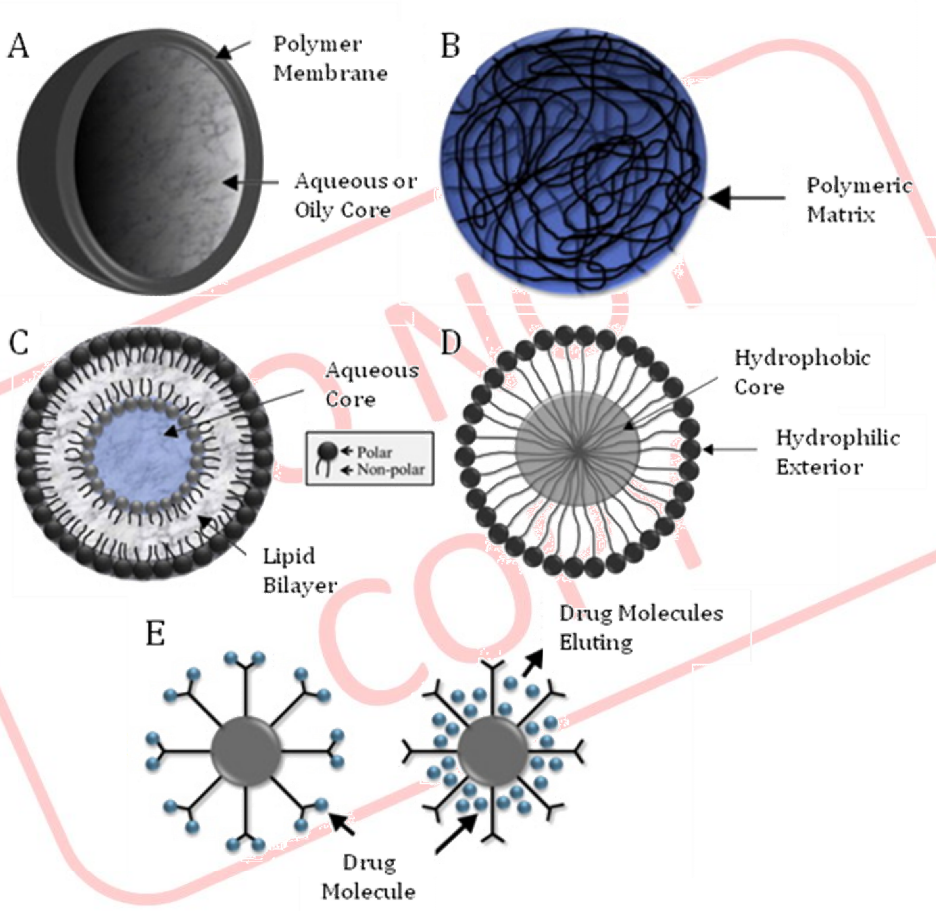

Figure 2.3 Particle schematics, (A) nanosphere, (B) nanocapsule (C) liposome, (D) micelle, (E) dendrimers functionalized with complexed (left) and encapsulated drug molecules.

Polymeric NPs have made a significant clinical impact by improving the pharmaceutical efficacy and dosing of a variety of already approved drugs [Davis 2008; Greco 2009]; however, their drug loading efficiency may be limited by the number of conjugation sites in the polymer, and most of them lack the ability of active targeting or controlling drug release. In order to further enhance the drug loading capacity and incorporate the spatial and/or temporal control over drug delivery, many biocompatible polymeric NPs platforms have been developed [Chan 2010; Napier 2007]. Different polymers like poly lactic-co-glycolic acid (PLGA), poly caprolactone (PCL), poly butyl cyanoacrylate (PBCA), etc. are already used in formulation of nanoparticulate drug delivery systems for anticancer drug delivery. Polymeric micelles have attracted substantial attention for their remarkable potential as therapeutic carriers [Matsumura 2009]. Polymeric

micelles can be formed by self assembly of amphiphilic polymers with two or more polymer chains of different hydrophobicity. In aqueous environments, these block copolymers can spontaneously self-assemble into core-shell nanostructures, with a hydrophobic core and a hydrophilic shell [Chan 2010; Matsumura 2009]. To date several polymeric micelles have reached different stages of clinical development, and these systems have demonstrated enhanced accumulation of therapeutic agents at the target site and/or reduced adverse effects of therapeutic agents [Sutton 2007]. Among them, NK911 [Matsumura 2004] and NK105 utilize PEG-poly(aspartic acid) copolymer to carry and protect the anticancer agents doxorubicin and paclitaxel, respectively. Notably, NK105 was shown to reduce the reported adverse effects of paclitaxel, which include neurotoxicity, myelosuppression, and allergic reactions. A cisplatin-incorporated polymeric micelle-based system, NC-6004, is being examined in Phase I/II clinical trials and has demonstrated several distinct features, including sustained cisplatin release, promoted accumulation of cisplatin in cancer cells, and reduced nephrotoxicity and neurotoxicity associated with cisplatin [Wilson 2008]. Another PEG-poly(glutamic acid) based polymeric micelle, NK012, loaded with 7-ethyl-10-hydroxycamptothecin (SN-38), has been shown to exert more potent antitumor activity against various human tumor xenografts than irinotecan (CPT-11), a water-soluble prodrug of SN-38 [Hamaguchi 2010; Hamaguchi 2005]. More impressively, the nontargeted polymeric micelle composed of poly(l-lactic acid)-PEG (Genexol-PM), for delivery of paclitaxel, was first approved for cancer therapy in Korea in 2007 and is currently being evaluated in a clinical Phase II trial in the United States for the treatment of metastatic pancreatic cancer [Kim 2004; Lee 2008].

The conjugation of polymeric NPs with targeting ligands could also enable drug delivery in a spatially and temporally controlled manner, which may further enhance the therapeutic efficacy of drugs and reduce their toxic side effects. Aptamer-targeted polymeric NPs have been developed and its application in cancer therapy was studied [Dhar 2011; Gao 2010]. For example, A10 RNA aptamer-conjugated PLGA–PEG NPs were developed that can recognize PSMA (prostate-specific membrane antigen), expressed on the cancer cell surface [Farokhzad 2004]. This PLGA–PEG NPs can substantially reduce tumor growth in a human prostate cancer tumor xenograft mouse model. More recently, a strategy was reported for precisely engineering PLGA–PEG NPs with different biophysicochemical properties in a reproducible manner, whereby

enabling the systematic screening of the targeted polymer NPs for optimization [Gu 2008]. Building on these efforts, BIND Biosciences has developed a selfassembled, targeted polymeric NP (BIND-014) and is currently evaluating this nanotherapeutic candidate in Phase I/II clinical trials for the treatment of solid tumors [Service 2010].

2.5.1.2 Liposomes

Liposomes are composed of amphiphilic molecules that are comprised of both polar and nonpolar components that self-assemble into colloidal particles (figure 2.3C). This self-assembly produces a spherical structure with the polar components of the molecule contacting the polar environment and the nonpolar components contacting the nonpolar environment [Lasic 1998]. The most common classification of liposomes is by the number of lipid bilayers present in the colloidal structure, with unilamellar liposomes containing one lipid bilayer and multilamellar liposomes containing multiple lipid bilayers. Due to their amphiphilic nature liposomes are capable of encapsulating both polar and nonpolar compounds for delivery [Lasic 1998].

Liposomes are attractive for drug delivery applications for numerous reasons, including their resemblance to cell membranes in both structure and composition. Additionally, liposomes can be readily formed with nontoxic, nonimmunogenic, natural and biodegradable amphiphilic molecules [Haley and Frenkel 2008; Lasic 1998]. Liposomes by themselves tend to be slightly sterically unstable and are cleared rapidly from the bloodstream. For drug delivery applications, this behavior is remedied by functionalizing the liposomal surface with poly(ethylene glycol) tethers to impart increased steric stabilization [Lasic 1998]. The surface of the liposome can also be modified with ligands for active targeting. A pegylated biodegradable liposome was used to encapsulate doxorubicin and became the first liposome-based treatment for cancer (Doxil) [Haley and Frenkel 2008].

2.5.1.3 Micelles

The micelle is composed of amphiphilic molecules that self-assemble into a structure with a hydrophobic core and a hydrophilic exterior (figure 2.3D) [Liechty 2012]. Micellar structure lends itself well to drug delivery applications for multiple reasons. Micelles typically have diameters of less than 100 nm, allowing them to participate in extravasation through the fenestrations in tumor vessels and limiting their uptake by the MPS/RES system. Their hydrophilic surface characteristics also shield them from immediate recognition and subsequently increase circulation time [Lavasanifar 2002].

Hydrophobic drugs can be loaded into the core of the micellar structure and protected by the hydrophilic corona during transport to the tumor site [Kwon 1995].

2.5.1.4 Dendrimers

Dendrimers are highly branched molecules that display a high degree of monodispersity and a well-defined structure [Hughes 2005]. They are stable and have surfaces that can be readily functionalized with targeting ligands and molecules such as folic acid [Majoros 2006]. Drug molecules can be encapsulated in the dendrimer's multifunctional core and protected by the extensive branching. Drug molecules, such as paclitaxel, can also be attached to the exterior of the dendrimer (figure 2.3E) [Majoros 2006].

2.6 Targeting

One significant challenge for the successful development of therapeutic NPs is its rapid clearance during systemic delivery. When NPs enter the bloodstream, the particle surface may experience nonspecific protein adsorption (opsonization), thereby making them more visible to phagocytic cells [Alexis 2008b; Owens 2006b]. After opsonization, NPs could be rapidly cleared from the bloodstream through phagocytosis by the mononuclear phagocyte system [Kurokawa] in the liver and by spleen filtration [Eisenstein 2006; Ostuni 2001]. Therefore, the factors that could affect the clearance and biodistribution of NPs, such as particle physicochemical properties and targeting ligand functionalization [Alexis 2008b], should be evaluated for the optimal design of therapeutic NPs.

2.6.1 Passive targeting

Passive targeting of NPs takes advantage of the abnormal tumor physiology and structure that results in the EPR effect. The permeability of the vasculature and retention by an insufficient lymphatic system can passively accumulate macromolecules and increase their tumor concentration by 70-fold [Duncan 2003]. This accumulation will only be observed if the macromolecules avoid clearance by mechanisms such as renal clearance and uptake by the MPS/RES. Two of the most important properties of effective nanocarriers are the carriers' ability to (a) remain circulating in the blood stream for a significant amount of time and (b) target specific tissues and cells [Duncan 2003]. Particle circulation time, targeting, and the ability to overcome biological barriers is also dependent on a particle's shape, size, and surface characteristics. The lifespan of a NPs within circulation is modulated by its interactions with the

environment and can be modified by changing its size, particle shape, and surface characteristics [Davis 2008].

2.6.1.1 Size

The size of NPs has an extremely important impact on its interaction with its environment. As stated previously, a particle must be at least 10 nm in diameter to avoid clearance by first pass renal filtration [Davis 2008; Venturoli 2005]. The largest size of NPs to be used for drug delivery to a tumor is determined by a multitude of factors. As passive targeting is entirely dependent on diffusion-mediated transport into the tumor, size is important. Dreher and colleagues have shown that particles on the order of hundreds of nanometers in diameter can accumulate in the tumor tissue. Using dextran as a model macromolecule they showed that increasing the molecular weight from 3.3 kDa to 2 MDa reduced permeability by two orders of magnitude. Larger molecules were able to accumulate but were primarily contained close to the vascular surface within the tumor. Conversely, smaller molecules could penetrate more deeply into the tumor interstitium and achieve a more homogenous distribution. These observed behaviors are attributed to the effective interstitial diffusion coefficient, which decreases as the molecular weight of the diffusing molecule increases [Dreher 2006]. Extrapolating from macromolecules to NPs, it has been determined that the upper bound size for NPs participating in the EPR effect is approximately 400 nm [Alexis 2008a]. Particles larger than 400 nm are simply unable to diffuse through the tumor interstitium in sufficient quantities to have any clinical or therapeutic effect.

While 400 nm is the upper bound for harnessing the effect of EPR there are other important factors that narrow the effective size range of NPs. The leaky vasculature in tumors is highly permeable due to the increased size and quantity of fenestrations as well as incomplete or abnormal basement membranes [Haley and Frenkel 2008; Roberts and Palade 1995]. These fenestrations are typically 50–100 nm in size and, although not the only mechanism of permeating into the tumor interstitium, an important pathway for NP accumulation. Looking solely at clearing mechanisms, it has been shown that particles with diameters less than 200 nm will be cleared much less rapidly than particles with diameters over 200 nm [Alexis 2008a; Matsumura 1988; Moghimi 1993]. With all of the above factors taken into consideration, an approximate upper bound of 150 nm has been determined [Liechty 2012]. Therefore, in order to be an effective drug carrier the NP should have a diameter between 10–150 nm. This size

range will ensure longer circulation time and increased accumulation in the tumor interstitium.

On the basis of physiological parameters such as hepatic filtration, tissue extravasation/diffusion, and kidney excretion, it is clear that particle size plays a key factor in the long circulation and biodistribution of NPs. NPs smaller than 10 nm can be rapidly cleared by the kidneys or through extravasation, while larger NPs may have higher tendency to be cleared by cells of the mononuclear phagocyte system (MPS, also referred to as reticuloendothelial system, RES) [Petros 2010]. For example, in vivo biodistribution results of polystyrene NPs with consistent composition and varying particle size of 50 and 500 nm showed higher level of agglomeration of the larger NPs in the liver [Nagayama 2007]. Another study compared different size ranges of PEGylated spherical NPs (<100 nm, 100–200 nm, and >200 nm) for protein absorption, NP uptake by murine macrophages, and blood clearance kinetics [Fang 2006b]. It was observed that NPs <100 nm have a higher potential to circulate in the blood for long periods of time and experience reduced hepatic filtration. NP size also plays a key role in tumor accumulation through the EPR effect. Several studies have tried to determine the gap size in the leaky vasculature. For example, sterically stabilized liposomes of 100–600 nm were used for transvascular transport, and the cutoff size of the pores was estimated to be 400–600 nm in diameter [Yuan 1995]. In another study, the pore cutoff size was estimated to be between 7 and 100 nm at 34°C and was increased to >400 nm at 42°C, allowing all NPs tested (~7 nm albumin, and 100, 200, and 400 nm liposomes) to be delivered to the tumor interstitium to some degree [Kong 2000]. Therefore, to capitalize on the EPR effect and to efficiently escape from the physiological barriers, many studies advocate the optimal NP size range of approximately 10–250 nm [Alexis 2008b].

2.6.1.2 Particle shape

Development of novel particle fabrication methods that allow for precise control over particle shape and size [Champion 2007; Glangchai 2008; Rolland 2005] has allowed for researchers to explore the effects of particle shape on particle bio-distribution and cellular internalization. The effects of particle shape and potentially the particles' curvature on cellular internalization was shown by Chan et al. [Chithrani 2007]. It was reported that 14 and 75 nm spherical NPs were up-taken by cells 3.75–5 times more than 74-by-14 nm rod-shaped particles. Gratton et al. have also demonstrated the

effects of *in vitro* cellular internalization in HeLa cells. The group reported that cylindrical NPs had the highest percentage of cellular internalization [Gratton 2008]. Specifically, NPs with 150 nm diameter and 450 nm height showed the highest internalization percentage and were taken up 4 times faster than symmetrical particles (aspect ratio of 1200 by 200 nm cubes). These findings suggest that NPs' aspect ratio also plays an important role in cellular uptake. However, in the same studies, 100 nm diameter particles with an aspect ratio of 3 had a lower degree of internalization compared with 150 nm particles with the same aspect ratio. The group also observed that cylindrical-shaped particles with 500 nm or 1 μm diameters and 1 μm height had reduced internalization in comparison with smaller particles but showed higher uptake than micrometer-sized square cross-section particles. This result suggests that the uptake kinetics is probably a function of both size and shape.

2.6.1.3 Surface characteristics

The surface of a particle is the primary medium by which it interacts with its environment. This is of even greater important with NPs because of their large surface-to-volume ratio and relatively large surface area [Storm 1995]. The surface can be modified by polymer content or functionalization which will impact how the environment "sees" the particle. When contemplating the question of drug delivery it is essential to consider how to modify the particle so it remains in circulation for the longest possible time to ensure tumor accumulation. It has been determined that modifying the surface of NPs by adding hydrophilic polymers results in decreased clearance by the MPS/RES system [Storm 1995]. One such hydrophilic polymer is poly(ethylene glycol). When attached to the surface of NPs PEG imparts stealth characteristics by shielding the NPs from opsonin adsorption and subsequent clearance by the MPS/RES [Alexis 2008a]. The shape, density and length of the PEG chains can be modified and have various effects on the rate of clearance. It has been shown that increasing the molecular weight of PEG chains above 2 kDa increases the half-life of the PEGylated particle [Owens 2006a]. A dense covering of PEG chains over the surface, particularly of negative particles easily recognized by the MPS/RES, is also necessary to prevent rapid clearance [Fang 2006a]. It has been established that the surface charge of NPs also could affect their uptake by the MPS cells. Neutrally charged particles have demonstrated much lower opsonization rates than charged particles [Roser 1998; Schwendener 1984]. It was found that positively charged NPs generate a higher

immune response (complement activation and conjugate activation) compared to neutral or negatively charged NP formulations [Salvador-Morales 2009]. For example, NPs with a primary amine at the surface promote higher rates of phagocytic uptake when compared to those having sulfate, hydroxyl, or carboxyl groups at the surface [Alexis 2008b; Salvador-Morales 2009]. In a review study, Davis *et al*. have proposed that the optimal range of NP surface charge should be between -10 and +10 mV for reduced phagocytosis and minimized nonspecific interactions of NPs [Davis 2009].

2.6.1.4 PEGylation

PEG chains as a hydrophilic polymer with a flexible nature can be selected as shell-forming segments, which assemble into dense palisades of tethered chains to achieve unique properties. The biocompatibility was guaranteed by the dense PEG shell, which endows the micelle with a stealth character in the blood compartment, achieving a long circulation [Kataoka 1993]. PEG chains attached to a surface or forming the corona of a nanosphere exhibit rapid chain motion in an aqueous medium and have a large excluded volume. The steric repulsion resulting from a loss of conformational entropy of the bound PEG chains upon the approach of a foreign substance and the low interfacial free energy of PEG in water contribute to the extraordinary physiological properties of nanospheres covered with PEG [Kataoka 1994; Yokoyama 1991].

Drug targeting for efficient accumulation in the body is often hampered by the rapid recognition of carrier system by the RES and by the subsequent kidney and/or hepatic elimination. Moreover, for modulated drug delivery to solid tumors, which locate outside the blood compartment, the carrier is required to exhibit not just a sufficient half-life in the blood compartment, but also the capability of extravasation at the tumor site. Recent developments led to the design of drug carriers with prolonged circulation in the vascular system [Kataoka 1993]. Cancer chemotherapy may cause severe side effects, leaving patients under extreme distress. To overcome this problem, an interest has been raised in the application of block copolymer as novel carrier systems for anticancer agents [Kataoka 1994; Kataoka 1993; Yokoyama 1991].

PEG grafted to surfaces of biomedical devices also proved to increase their biocompatibility and to reduce thrombogenicity [Holmberg 1993]. Surface modification of NPs with PEG, which has favorable intrinsic physicochemical properties (e.g., high flexibility and hydrophilicity, and low toxicity and immunogenicity), was found to reduce NP accumulation in off-target organs such as liver and spleen [Knop 2010]. A

PEG shell on the NP surface shields hydrophobic or charged particles from attachment by blood proteins, leading to prolonged circulation half-life compared to non-PEGylated NPs [Moghimi 2003; Vonarbourg 2006]. The length, shape, and density of PEG chains on the NP surface largely affect its surface hydrophilicity and phagocytosis [Grefa 2000]. For example, at low PEG surface density, the PEG chains would be closer to the surface of the NP with a "mushroom" configuration, while as the density increases, most of the chains are extended away from the surface in a "brush" configuration, which decides the thickness of the PEG shell on the NP corona [Owens 2006b]. It has been postulated that the brush configuration would create more effective blocking or repulsion of opsonins than the mushroom one [Vonarbourg 2006]. In addition to PEG, some other promising hydrophilic polymers are under investigation for the same purpose, including natural polymers (*e.g.*, heparin, dextran, and chitosan) and synthetic polymers (*e.g.*, poly(amino acids), poly(glycerols), poly(2-oxazolines), and some vinyl polymers) [Knop 2010; Moghimi 1991]. The conjugation of targeting ligands to the surface of PEGylated NPs has also been shown to affect their biodistribution [Takae 2005]. Although targeting ligands could improve the cell- or tissue-specific delivery of NPs, they may compromise the particle surface properties by masking the PEG layer and adversely affecting the NPs' macrophage uptake in vivo. A recent study on the effect of ligand density has also revealed a relatively narrow window of ligand density that could result in favorable tumor targeting, while minimizing NP accumulation in the liver and spleen [Gu 2008]. Thus, the successful development of targeted NP technology for efficient drug delivery strongly depends on striking a balance between cellular targeting and immune evasion.

2.6.1.5 Limitations of passive targeting

Passive targeting can be achieved by modulating the size, shape, and surface characteristics of the NP drug carriers. However, there remain significant barriers to transport that often result in insufficient drug concentrations at the tumor site and, consequently, little therapeutic efficacy [Brigger 2002b; Gu 2007]. Furthermore, passive targeting suffers from some of the same limitations of traditional chemotherapy such as an inability to actively distinguish healthy tissue from tumor tissue.

2.6.2 Active targeting

Despite their enormous potential for drug delivery, the translation of targeted NP systems has faced considerable challenges, and only a handful of candidates have made it to clinical trials. The reason targeted NPs have demonstrated limited success in

clinical development is complex and could be multifaceted [Farokhzad 2009]. Among others, an essential aspect for the successful development of targeted NPs relies on the choice of targeting ligands. Several variables that could be considered include ligand biocompatibility, cell specificity, binding affinity, and purity of the ligand [Allen 2002]. Other important factors that have to be taken into account are the size and charge of the ligand molecule, and their ease of modification and conjugation to the NPs. The choice of ligand, from a practical perspective, is also dependent on production cost, scalability, and stability (*e.g*, organic solvent and high temperature stability) in mass production.

Active targeting takes advantage of ligand-receptor, antigen–antibody and other forms of molecular recognition to deliver a particle or drug to a specific location [Haley and Frenkel 2008]. For cancer therapy, active targeting moieties are particularly beneficial because they reduce or eliminate the delivery of potentially toxic drugs to healthy tissue. Targeted NPs delivering chemotherapeutics are of interest because they can increase therapeutic effectiveness and reduce potential side effects [Gu 2007]. Active targeting takes advantage of the over-expression of receptors, such as folate and transferrin, on the tumor cell surface [Liechty and Peppas 2012]. These targeted nanodelivery devices have performed significantly better than their non-targeted counterparts resulting in an increased cytotoxicity to tumor cells and reduction of side effects [Phillips 2010]. This section will focus on the most widely utilized active targeting ligands for tumor therapy including folate, transferrin, aptamers, antibodies, and peptides.

2.6.2.1 Folate

Folate has been one of the most extensively utilized ligands for targeted drug delivery devices. The folate receptor [Haley and Frenkel], or the high affinity membrane folate binding protein, binds the folate molecule with extremely high affinity ($K_D \sim 10^{-9}$) [Gu 2007; Hilgenbrink 2005]. This receptor is also over-expressed in a variety of tumors such as ovarian carcinomas, choricarcinomas, meningiomas, uterine sarcomas, osteosarcomas, and non-Hodgkin's lymphomas [Sudimack 2000]. Particles conjugated with folate or folic acid and bound to a folate receptor are internalized by the cell and introduced to the cytoplasm (figure. 2.4A). The drug is then released by the NP in the cytoplasm of the tumor cell and proceed to interact with intracellular components [Haley and Frenkel 2008; Stella 2000].

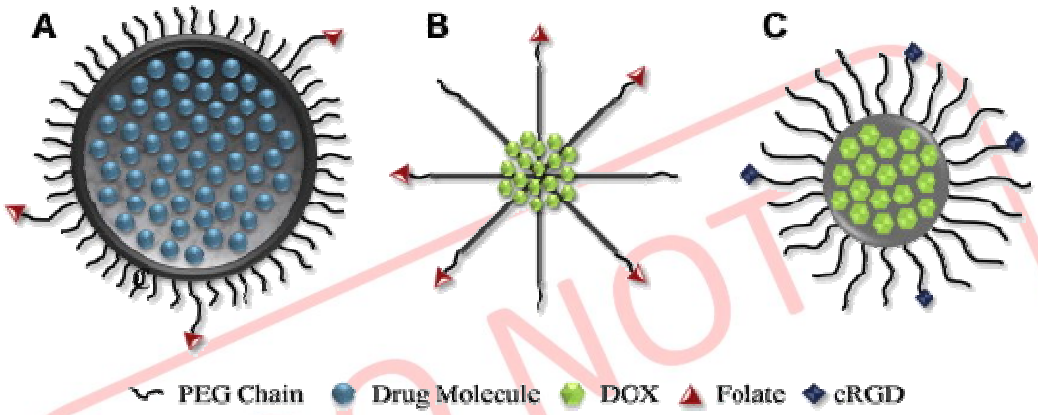

Figure 2.4 Targeted particles: (A) example of a folate receptor targeted particle. Liposome functionalized with PEG tethers to impart STEALTH characteristics and folate for tumor targeting, (B) folate-conjugated PLGA-PGA polymeric micelle loaded with encapsulated doxorubicin and (C) cRGD-functionalized PCL–PEG polymeric micelle containing encapsulated doxorubicin.

One such folate conjugated NP is a folate receptor targeted biodegradable polymeric micelle loaded with doxorubicin developed by Yoo and colleagues. Micelles were created from a copolymer of poly(D,L-lactic-co-glycolic acid) (PLGA) and poly(ethylene glycol). The PLGA allows the particle to biodegrade after delivery of its drug payload and the PEG increases the circulation time of the particles. Doxorubicin was conjugated via a chemical linkage to the PLGA while the folate was added to the PEG. The micelle (figure 2.4B and C) was tested for cytotoxicity and cardiotoxicity (a common side effect of DOX) compared to free DOX on folate-receptor-positive cell lines. It was determined that these particles exhibited increased cellular uptake, circulation time, and decreased cardiotoxicity [Yoo 2004]. The decrease of cardiotoxicity indicates that the targeting moiety was able to differentiate between healthy and tumor tissue with greater specificity than untargeted DOX. Furthermore, the increased cytotoxicity and cellular uptake shows that the folate-receptor actively internalized the conjugated particle into the cytoplasm [Yoo 2004].

2.6.2.2 Transferrin

Transferrin is another receptor-ligand pair that has been utilized for tumor targeting applications. Transferrin is a membrane glycoprotein that functions with its receptor, TfR, to aid in uptake of iron by the cell [Ponka 1999; Yoo 2004]. Much like folate, when transferrin binds to its receptor it initiates endocytosis and is internalized into the

cellular cytoplasm [Ponka 1999]. The transferrin receptor is overexpressed by as much as 10-fold on tumor cells making it an attractive option for targeted delivery of chemotherapeutics via NP carriers [Sahoo 2004]. Sahoo and colleagues have focused a great deal of attention on developing transferrin-conjugated paclitaxel-loaded NPs. The NPs were made using copolymerized PLGA and poly(vinyl alcohol) (PVA), both well-studied and defined materials for drug delivery. Transferrin was conjugated to the NP surface and loaded with paclitaxel. The conjugated and loaded NPs were introduced to a human prostate cancer cell line. These particles were compared to a simple solution of paclitaxel and loaded particles without transferrin. The transferrin-conjugated particles exhibited a sustained release profile and a cellular uptake three times greater than the unconjugated NPs. Furthermore, the conjugated NPs reduced cellular proliferation by 70%, while the unconjugated NPs only reduced it by 35%. The free paclitaxel, by comparison, only reduced proliferation by 20% [Sahoo 2004]. Transferrin-conjugated NPs have been shown to inhibit cellular proliferation and tumor growth while participating in sustained release profiles and increased cellular uptake. The effectiveness of the conjugated NPs is most likely due to their ability to be taken up by receptor-mediated endocytosis, which enhances the amount of drug delivered to tumor cells and limiting the amount delivered to healthy cells [Sahoo 2005; Sahoo 2004].

2.6.2.3 Aptamers

Aptamers are short oligonucleotides of RNA or DNA that can fold into various conformations and engage in ligand binding [Gu 2007]. However, finding such sequences is akin to finding a needle in a haystack, with only one in 10^{10} random RNA sequences folding into a configuration able to participate in ligand binding [Wilson 1999]. Systematic evolution of ligands by exponential amplification, is a process by which researchers can comb through vast populations of RNA and DNA sequences to find new aptamers to act as targeting ligands. Benefits of aptamers include their small size (~15 kD), lack of immunogenicity, and the potential to readily penetrate and target tumor cells. It has been shown that, much like folate and transferrin, aptamers result in increased targeting specificity and more efficient drug delivery to tumor cells [Gu 2007]. An aptamer-conjugated NP has been created for the delivery of cisplatin to prostate cancer cells [Dhar 2008]. The selected target is a prostate-specific membrane antigen (PSMA) that is highly overexpressed in prostate cancer cells and can be readily targeted by a PSMA aptamer. A traditional NP carrier composed of poly(D,L-lactic-co-glycolic

acid) and poly(ethylene glycol) tethers was used to encapsulate cisplatin. Cisplatin is a platinum-based chemotherapeutic that functions by interfering with DNA transcription but is normally ineffective against prostate cancer cells when administered systemically. It is thought that targeted delivery of cisplatin could increase its therapeutic effectiveness. In fact, when compared to free cisplatin the PSMA aptamer-targeted Pt(IV)-encapsulated PLGA-b-PEG NPs are 80 times more toxic to prostate cancer cells expressing PSMA. Aptamer-conjugated NPs have significant potential as cancer-drug-delivery vehicles.

2.6.2.4 Antibodies (monoclonal antibodies)

Antibodies and antibody fragments form an important class of targeting ligands with a high degree of specificity for cellular receptors and a wide range of binding affinities and have been extensively investigated in targeted drug delivery [Torchilin 2008]. Over the past 2 decades, the feasibility of antibody-based tissue targeting has been clinically demonstrated with several different monoclonal antibodies (mAbs) approved by the FDA [Gabizon 2001]. The recent advances in hybridoma technology have led to the development of chimeric, humanized, and fully human mAbs to reduce their immunogenicity. The ability of engineered mAbs to target disease processes has been demonstrated by the success of several monoclonal antibody therapeutics, including cetuximab rituximab, trastuzumab, and bevacizumab [Wang 2008]. mAbs have been used to direct the NP carriers in a site-specific manner. For example, mAb-conjugated PLA NPs exhibited a sixfold increase in the rate of particle uptake compared with nontargeted particles [Nobs 2004]. Additionally, J591, a mAb against PSMA, was conjugated to G5-PAMAM dendrimers and showed enhanced binding affinity for LNCaP cells, as compared to nontarget PC3 cells [Patri 2004]. Nevertheless, mAb conjugated NPs encounter considerable challenges and limitations for drug delivery, since mAb are complex and large (~150 kDa) molecules and require significant engineering at the molecular level to be effective [Brennan 2004].

Compared to mAbs, antibody fragments have demonstrated higher potential for the engineering of targeted NPs as they are smaller in size and lack the complement activation region of mAbs, while retaining the antigen binding specificity [Carter 2001]. Recent advances in protein engineering have led to the development of antibody fragments such as scFv (single-chain variable fragments), Fab (fragments of antigen binding), their dimers (F(ab') and diabody), and recombinant products [Pavlinkova

2001]. Some pioneering examples of antibody fragment-targeted liposomes (immunoliposomes) in clinical trials include MCC-465 that uses F(ab')2 for the targeted delivery of doxorubicin [Sankhala 2009] and SGT-53 that uses scFv to deliver tumor suppressor gene, p53.

Like aptamers, antibodies attached to the surfaces of NPs target specific antigens present on the cell membrane. The use of antibodies as targeting moieties has been extensively investigated over the past decade and has resulted in numerous available treatments (Table 2.1) [Adams 2005; Brannon-Peppas 2004; Gu 2007; Weber 2007]. Unconjugated antibodies have been shown to have antitumor effects on lymphomas, breast cancers, non-Hodgkin's lymphomas, colorectal cancers and chronic lymphocytic leukemias [Mehren 2003; Weiner 2000]. Antibody-based treatments function by recognizing specific antigens located on the surface of cancer cells. Once an antibody–antigen interaction occurs it can induce antitumor affects by multiple mechanisms including interfering with ligand-receptor binding or suppression of protein expression [Mehren 2003].

Table 2.1 Available antibody-based cancer treatments [Adams 2005; Brannon-Peppas 2004; Weber 2007].

Drug	Antigen target	Cancer	Release date
Alemtuzumab	CD52	Chronic lymphocytic leukemia	2001
Bevacizumab	VEGF	Colorectal, lung cancer	2004
Cetuximab	EGF receptor	Colorectal cancer	2004
Gefinitib	EGFR	Advanced NSCLC	2003
Gemtuzumab	CD33	Acute meylogenous leukemia	2000
Ibritumomab tiuxetan	CD20	Non-hodgkins lymphoma	2002
Ipilimumab	CTLA-4	Advanced melanoma	2011
Ofatumumab	CD20	Chronic lymphocytic leukemia	2010
Panitumumab	EGFR	Colorectal cancer	2008
Rituximab	CD20	Lymphoma	1997
Tostiumomab	CD20	Lymphoma	2003
Trastuzumab	HER2	Breast cancer	1998

Although utilized for multiple successful treatments, antibody-based targeting had several early limitations. The antibodies for human use were often derived from mice and, in some individuals, resulted in an immune response that limited the duration and effectiveness of treatment. Another limitation was the lack of specificity and adequate targeting of the antibodies to their antigen-binding sites [Brissette 2006]. Current technology has overcome some of these early limitations. Antibodies derived from murine proteins can now be manipulated into humanized versions that will provoke little to no immune response. Furthermore, the specific binding regions can be molecularly modified to specifically target a wide variety of receptors [Brissette 2006]. The IgG molecule is extensively used for this purpose, as it contains a binding region that recognizes antigens and can be readily modified to specifically distinguish a variety of targets [Brissette 2006].

One such target is the epidermal growth factor receptor (EGFR), which is over-expressed in many cancers, and will bind to two separate ligands: epidermal growth factor and transforming growth factor-alpha [Mendelsohn 1997]. When either ligand binds to the EGFR it stimulates growth of cells and is responsible for the rapid proliferation of cells in a variety of cancers. By blocking this ligand–receptor interaction via antibody-interference, the proliferative behavior of the cell is either reduced or stopped [Mendelsohn 1997]. Hoffman and colleagues have determined that combining anti-EGFR antibodies with cisplatin and doxorubicin increases the cytotoxic effects of the drugs and, in some cancers, entirely eradicates the tumor [Hoffmann 1997]. Monoclonal antibodies have also been examined as targets for conjugated-NP drug-delivery vehicles. The Alléman group tested two different biodegradable PLA NP formulations. The first formulation was conjugated with the trastuzumab mAb (HER2 antigen) and the second with rituximab mAb (CD20 antigen). The conjugated-NPs bound to cells expressing the respective antigens at a frequency 10 times higher than non-targeted NPs [Nobs 2005].

The specificity of antibodies lends particularly well to the active targeting of a variety of tumor types due to their ability to distinguish between healthy and cancerous cells and even amongst cancer cell types. In colorectal cancers, for example, over 95% of cases express the A33 antigen which can be targeted via a humanized A33 monoclonal antibody (huA33 mAb). A number of clinical studies have shown that huA33 mAb is capable of localizing specifically to colorectal cancer cells expressing the A33 antigen

[Johnston 2012]. Recently, Johnston and colleagues, have reported on the development of a polymeric NP system composed of a silica core followed by a layer-by-layer deposition of alkyne-modified poly(*N*-vinylpyrrolidone) (PVPONAlk) and poly(methacrylic acid) [Tang et al.]. To this particle, the A33 monoclonal antibody was conjugated to the surface via click chemistry and imparted targeting characteristics to the system. Upon incubating the huA33 mAb-conjugated particles with L1M1899 colorectal cancer cells expressing the A33 antigen, it was observed that extensive internalization of the particles occurred as compared to the particles conjugated with a negative control, IgG. The antibody-conjugated particles not only preferentially interacted with the cancerous cells but were also phagocytosed, which is ideal for the delivery of chemotherapeutic agents [Johnston 2012].

While antibody-based cancer therapeutics have shown promise there are several remaining limitations that must be considered in the future. The development and modification of antibodies is a complex and expensive process that is difficult to scale-up to large-scale manufacture [Brissette 2006]. Even with fully humanized antibodies an immune response is a potential road block to treatment. Tumor penetration has also been an issue, with observed non-uniform uptake into the tumor mass [Weiner 2000]. This lack of tumor penetration has been attributed to the increased size of NPs due to the hydrodynamic radius of antibodies (~20 nm) and an uneven distribution of antigens [Gu 2007; Weiner 2000]. Antibody fragments have been posed as a solution, as they are smaller, induce a lesser immune response, and can still selectively target antigen receptors on the surface of tumor cells [Gu 2007].

2.6.2.5 Peptides

Peptides have also been proposed as a potential targeting moiety for delivering chemotherapeutics. Peptides, much like antibodies, can be used to disrupt ligand–receptor interactions on tumor cells and lead to cessation of cellular proliferation. They have the added benefit of being much less expensive and complex to manufacture than antibodies [Brissette 2006]. Screening of potential protein ligands is typically completed using a combinatorial phage library. This technique results in ligands that range from 10–15 amino acids in length and are able to selectively bind to tumor targets with high affinity [Brissette 2006; Gu 2007; Krag 2006]. One such tumor target is the $\alpha_v\beta_3$ integrin, which is present at elevated levels on tumor cells and is an essential component of angiogenesis [Brooks 1994]. This integrin is recognized by the arginine–

glycine–aspartic acid (RGD) peptidic sequence [Byrne 2008]. The affinity of the RGD sequence to the $\alpha_v\beta_3$ integrin has potential to be exploited for drug delivery devices. Nasongkla and colleagues have functionalized the surface of polymeric micelles with a cyclic peptide containing the RGD sequence to deliver doxorubicin to Kaposi's sarcoma cells. The polymer micelle was composed of poly(ε-caprolactone)–poly(ethylene glycol) (PCL–PEG) imparting both biodegradable and long-circulating characteristics to the structure. The doxorubicin (DOX) was loaded into the polymeric micelle and preferentially located into the center of the structure. The polymer ends were then functionalized with a cyclic pentapeptide c(Arg-Gly-Asp-D-Phe-Lys) c(RGD) containing the RGD sequence to allow for selective targeting to the $\alpha_v\beta_3$ integrin. When introduced to Kaposi's sarcoma derived cells (displaying an overexpression of the $\alpha_v\beta_3$ integrin) a 30-fold increase in cellular uptake was observed between the cRGD-containing and non-functionalized micelles.

Another peptidic sequence capable of targeting behavior is Angiopep-2, the complementary ligand to the low-density lipoprotein receptor-related protein (LRP). The LRP is highly overexpressed both on the blood–brain barrier and on glioblastoma multiforme (GBM), or glioma, a tumor of the pituitary gland which is typically inoperable. The combined targeting effects of Angiopep-2 has the potential to allow a therapeutic to pass through the blood–brain barrier at sufficient concentration to then target the glioma within the brain. Xin et al., have conjugated Angiopep-2 to the surface of poly(ethylene glycol)–co-poly(-caprolactone) NPs to engage in dual-targeting of gliomas. After observing increased cellular uptake of Ang-targeted U87 MG glioma cells as compared to blank controls, the *in vivo* targeting effects were measured.

2.6.2.6 Limitations of active targeting

Active targeting moieties are capable of reducing off-target effects and improving the bioavailability of the chemotherapeutic agent. In addition, the inclusion of imaging modalities within these nanostructures yield particles that can, theoretically, be used to target and image the tumor, while simultaneously releasing a therapeutic payload. However, there are a number of limitations with active targeting that bear some discussion. The incorporation of active targeting ligands is designed to improve and enhance NP accumulation at the tumor site. What remains to be seen is whether the increased concentration of carriers and their respective payloads have any bearing upon the delivery of the therapeutic into the interior of the cell. Even if the NP carriers

are capable of preferentially collecting in the tumor site, their efficacy is wholly dependent on their ability to deliver the payload [Phillips 2010]. The harnessing of receptor-mediated endocytosis is coupled with the added challenge of encouraging endosomal-escape once the carrier or therapeutic is entrapped. Additionally, the replacement of stealth polymers, such as PEG, with the active targeting moieties can drastically affect opsonization and clearance of the carrier. In order for the active targeting ligands to perform their function they must encounter tumor cells expressing the motifs of interest. If the carriers are rapidly cleared from the bloodstream, accumulation in the liver, spleen and other RES organs will be observed, while the tumor will amass a lesser amount of the targeted carriers [Phillips 2010]. While active targeting ligands overcame a number of limitations seen with their passive targeted counterparts, additional work must be completed to enhance overall biodistribution and therapeutic efficacy of these actively targeted nanoparticulate carriers.

2.7 Poly lactic-co-glycolic acid (PLGA)

Recently, nano-sized drug delivery systems (DDS) especially biocompatible and biodegradable polymer NPs have attracted considerable interest since they can offer a suitable means of delivering small molecular weight drugs, proteins or genes to a targeted tissue or organ [Moghimi 2001; Zweers 2003]. NPs are colloidal systems that have size typically in the range of 10-1000 nm in diameter, and drug can be entrapped in, adsorbed or chemically coupled onto the polymer NP matrix [Labhasetwar 1997]. On the other hand, a number of polymers have been investigated for formulating biodegradable NPs, such as polylactide, polycaprolactone (PCL) and poly(lactide-co-glycolide) (PLGA). They are biocompatible and biodegradable polymers approved by FDA and have been studied extensively [Berton 1999; Rouzes 2000].

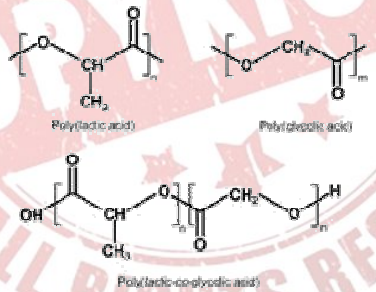

Figure 2.5 Molecular structure of lactide and glycolide based biodegradable polymer

PLGA is synthesized by means of random ring-opening co-polymerization of two different monomers, the cyclic dimers (1,4-dioxane-2,5-diones) of glycolic acid and lactic acid. Common catalysts used in the preparation of this polymer include tin(II) 2-ethylhexanoate, tin(II) alkoxides, or aluminum isopropoxide. During polymerization, successive monomeric units (of glycolic or lactic acid) are linked together in PLGA by ester linkages, thus yielding linear, aliphatic polyester as a product (figure 2.5)[Astete 2006].

Depending on the ratio of lactide to glycolide used for the polymerization, different forms of PLGA can be obtained: these are usually identified in regard to the monomers' ratio used (e.g. PLGA 75:25 identifies a copolymer whose composition is 75% lactic acid and 25% glycolic acid). All PLGAs are amorphous rather than crystalline and show a glass transition temperature in the range of 40-60 °C. Unlike the homopolymers of lactic acid (polylactide) and glycolic acid (polyglycolide) which show poor solubilities, PLGA can be dissolved by a wide range of common solvents, including chlorinated solvents, tetrahydrofuran, acetone or ethyl acetate.

PLGA degrades by hydrolysis of its ester linkages in the presence of water. It has been shown that the time required for degradation of PLGA is related to the monomers' ratio used in production: the higher the content of glycolide units, the lower the time required for degradation. An exception to this rule is the copolymer with 50:50 monomers' ratio which exhibits the faster degradation (about two months). In addition, polymers that are end-capped with esters (as opposed to the free carboxylic acid) demonstrate longer degradation half-lives.

PLGA is one of the most successfully used biodegradable nanosystem for the development of nanomedicines because it undergoes hydrolysis in the body to produce the biodegradable metabolite monomers, lactic acid and glycolic acid. Since the body effectively deals with these two monomers, there is very minimal systemic toxicity associated by using PLGA for drug delivery or biomaterial applications. PLGA NPs have been mostly prepared by emulsification–diffusion [Sahana et al. 2008], solvent emulsion–evaporation [Zambaux et al. 1999], interfacial deposition [Pinto Reis et al. 2006] and nanoprecipitation method [Barichello et al. 1999] (figure 2.6). Generally in emulsification–diffusion method, the PLGA polymers are dissolved in organic solvent, poured and separated in aqueous phase having stabilizer and subsequently emulsified by homogenizer. In solvent evaporation method, the polymers are dissolved in volatile

organic solvent and poured into continuously stirring aqueous phase with or without emulsifier/stabilizer and sonicated. Interfacial deposition methods have been used for the formation of both nanocapsule and nanospheres. The NPs are synthesized in the interfacial layer of water and organic solvent (water miscible) and finally the NPs are separated by centrifugations [Pinto Reis et al. 2006]. Most commonly used method for the preparation of PLGA NPs is nanoprecipitation. Polymer dissolved in acetone is added drop-wise into continuously stirring aqueous phase with or without emulsifier/stabilizer and consequently organic phase is evaporated under reduced pressure.

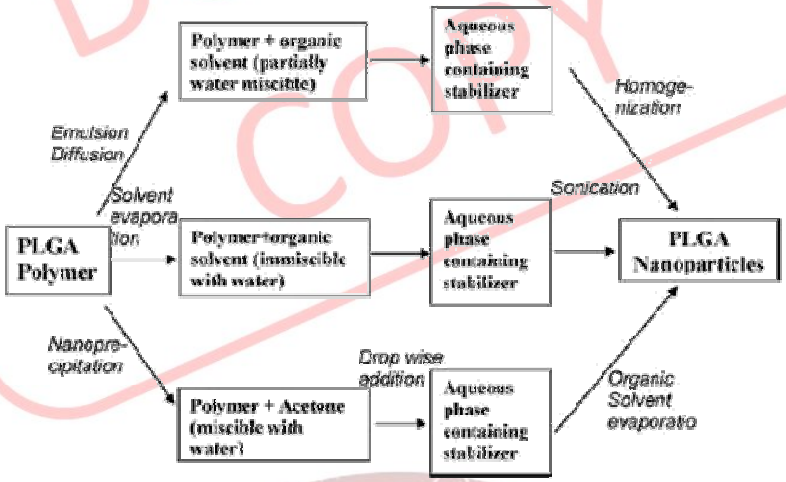

Figure 2.6 Different methods for preparation of PLGA NPs.

PLGA NPs have been used to develop the proteins and peptides nanomedicine, nano-vaccines, NPs based gene delivery system, nano-antigen and growth factor, etc. [Carrasquillo et al. 2001; Soppimath et al. 2001]. Surface modification of PLGA, drug encapsulation methods and particle size, additives added during formulation, molecular weight of drug, ratio of lactide to glycolide moieties has strong influence on the release and effective response of formulated nanomedicines [Mittal et al. 2007]. The acidic nature of PLGA monomers is not suitable for some sensitive drugs or bioactive molecules [Kumar et al. 2004]. However, the approaches to overcome these problems have been developed. PLGA nanomedicine formulations are blended with alginate, chitosan, pectin [Liu et al. 2004], poly(propylenefumarate) [Hedberg et al. 2005], polyvinylacohol [Patil et al. 2004], poly(orthoester), etc. [Wang et al. 2004]. The approval of PLGA has been granted by US Food and Drug Administration (USFDA) for human use and nanomedicines [Di Toro et al. 2004]. Various methods have been

optimized for formulations of PLGA NPs incorporating numerous anti cancer drugs [Chaudhari et al. 2012; Snehalatha et al. 2008; Yadav and Sawant 2010]. These loaded NPs protect poorly soluble and unstable payloads from the biological milieu and are small enough for capillary penetrations, cellular internalization and endosomal escape [Soppimath et al. 2001]. Furthermore, their surface is modified for targeted delivery of molecules to tumor or other tissues [Nobs et al. 2004]. The larger size of PLGA NPs is advantageous as multifunctional imaging and probes which incorporate encapsulated cancer drug, release, imaging, and targeting in a single NPs platform [Torchilin 2006].

The properties of NPs as precursor of good nanomedicine are particle size, size distribution, surface morphology, surface chemistry, surface charge, surface adhesion, surface erosion, interior porosity, drug diffusivity, drug encapsulation efficiency, drug stability and drug release kinetics. The surface charge of the NPs is important for the cellular internalization of the NPs, clustering in blood flow, adherence, and interaction with oppositely charged cells membrane [Feng 2004]. PLGA NPs are frequently used for the encapsulation of various cancer related drugs and their successful delivery in vivo. The cancer related drug paclitaxel, doxorubicin, docetaxel, 5-fluorouracil, 9-nitrocamptothecin, cisplatin, triptorelin, dexamethasone, xanthone, etc., have been successfully encapsulated on PLGA NPs [Chaudhari et al. 2012; Derakhshandeh et al. 2010; Fonseca et al. 2002; Snehalatha et al. 2008]. The mechanism of action of these drugs, encapsulation mechanism, encapsulation efficiency, peculiar characteristic for encapsulation and drug release mechanisms are studied.

2.8 Polycaprolactone

Polycaprolactone (PCL) is one of the earliest polymers synthesized by the Carothers group in the early 1930s [Van Natta 1934]. It became commercially available following efforts to identify synthetic polymers that could be degraded by microorganisms [Huang 1985]. PCL can be prepared by either ring opening polymerization of Ɛ-caprolactone using a variety of anionic, cationic and co-ordination catalysts or via free radical ring-opening polymerization of 2-methylene-1-3-dioxepane [Pitt 1990]. PCL is a hydrophobic, semi-crystalline polymer; its crystallinity tends to decrease with increasing molecular weight. The good solubility of PCL, its low melting point (59–64 ^{o}C) and exceptional blend-compatibility has stimulated extensive research into its potential application in the biomedical field [Chandra 1998; Nair 2007; Okada 2002].

Consequently, during the resorbable-polymer-boom of the 1970s and 1980s, PCL and its copolymers were used in a number of drug-delivery devices. Attention was drawn to these biopolymers owing to their numerous advantages over other biopolymers in use at that time. These included tailorable degradation kinetics and mechanical properties, ease of shaping and manufacture enabling appropriate pore sizes conducive to tissue in-growth, and the controlled delivery of drugs contained within their matrix. Functional groups could also be added to render the polymer more hydrophilic, adhesive, or biocompatible which enabled favourable cell responses.

Synthesis and physicochemical properties of PCL

PCL is prepared by the ring-opening polymerization of the cyclic monomer ε-caprolactone and was studied as early as the 1930s [Van Natta 1934]. Catalysts such as stannous octoate are used to catalyze the polymerization and low molecular weight alcohols can be used to control the molecular weight of the polymer [Storey 1996]. There are various mechanisms which affect the polymerization of PCL and these are anionic, cationic, co-ordination and radical. Each method affects the resulting molecular weight, molecular weight distribution, end group composition and chemical structure of the copolymers [Okada 2002]. PCL is a semi-crystalline polymer having a glass transition temperature of −60 ^{o}C and melting point ranging between 59 and 64 ^{o}C, dictated by the crystalline nature of PCL which enables easy formability at relatively low temperatures. The number average molecular weight of PCL samples may generally vary from 3000 to 80,000 g/mol and can be graded according to the molecular weight [Hayashi 1994]. PCL is soluble in chloroform, dichloromethane, carbon tetrachloride, benzene, toluene, cyclohexanone and 2-nitropropane at room temperature. It has a low solubility in acetone, 2-butanone, ethyl acetate, dimethylformamide and acetonitrile and is insoluble in alcohol, petroleum ether and diethyl ether [Coulembier 2006].

Biodegradation

Biodegradation occurs when water penetrates the entire polymer bulk, causing hydrolysis throughout the entire polymer matrix (figure 2.7a and b). Random hydrolytic chain scission would take place and produce an overall reduction in molecular weight. If water molecules can diffuse into the polymer bulk, hydrolyse the chains enabling the monomers or oligomers to diffuse out, erosion will occur gradually and equilibrium for this diffusion–reaction phenomenon would be achieved. If this equilibrium is disturbed, the degradation mechanism could provoke internal autocatalysis, via the carboxyl and

hydroxyl end group by-products. Whereas surface oligomers and carboxyl groups may freely diffuse into the surroundings (surface erosion situation), in the case of bulk degradation the internal concentration of autocatalysis products can produce an acidic gradient as the newly generated carboxyl end group formed during ester bond cleavage accumulate. This in turn accelerates the internal degradation compared to the surface, leaving an outer layer of higher molecular weight skin with a lower molecular weight, degraded, interior (figure 2.7c). The degradation mechanism thus becomes defined by bimodal molecular weight distribution. When the inner oligomers become small enough, they diffuse rapidly through the outer layer and this is accompanied by an onset of weight loss and a decrease in the rate of chain scission producing a higher molecular weight hollowed out structure. The rapid release of these oligomers and acid by-products can result in inflammatory reactions in vivo, as reported in the bioresorbable device literature [Bergsma 1995]. Furthermore, if the surrounding tissue is unable to buffer the pH change due to poor vascularization or low metabolic activity then local, temporary disturbances may arise – an example of this has been observed from fiber-reinforced PGA pins used during orthopedic surgery which led to increased osmotic pressure through local fluid accumulation at the time of rapid degradation [Bostman 1990].

PCL is suitable for controlled drug delivery due to a high permeability to many drugs excellent biocompatibility and its ability to be fully excreted from the body once bioresorbed. Biodegradation of PCL is slow in comparison to other polymers, so it is most suitable for long-term delivery extending over a period of more than 1 year. PCL also has the ability to form compatible blends with other polymers, which can affect the degradation kinetics, facilitating tailoring to fulfill desired release profiles [Freiberg 2004; Merkli 1998; Sinha 2004].

Drug release rates from PCL depends on type of formulation, method of preparation, PCL content, size and percent of drug loaded in the microcapsules. Due to a higher permeability of PCL it is blended with other polymers to improve stress, crack resistance, dyeability and control over release rate of drugs. Within the last decades, PCL polymers have been major area of interest to develop controlled delivery systems especially for peptides and proteins [Sinha 2004]. PCL nanospheres are colloidal drug-delivery systems, which act as transport carrier compartments for drugs or other active

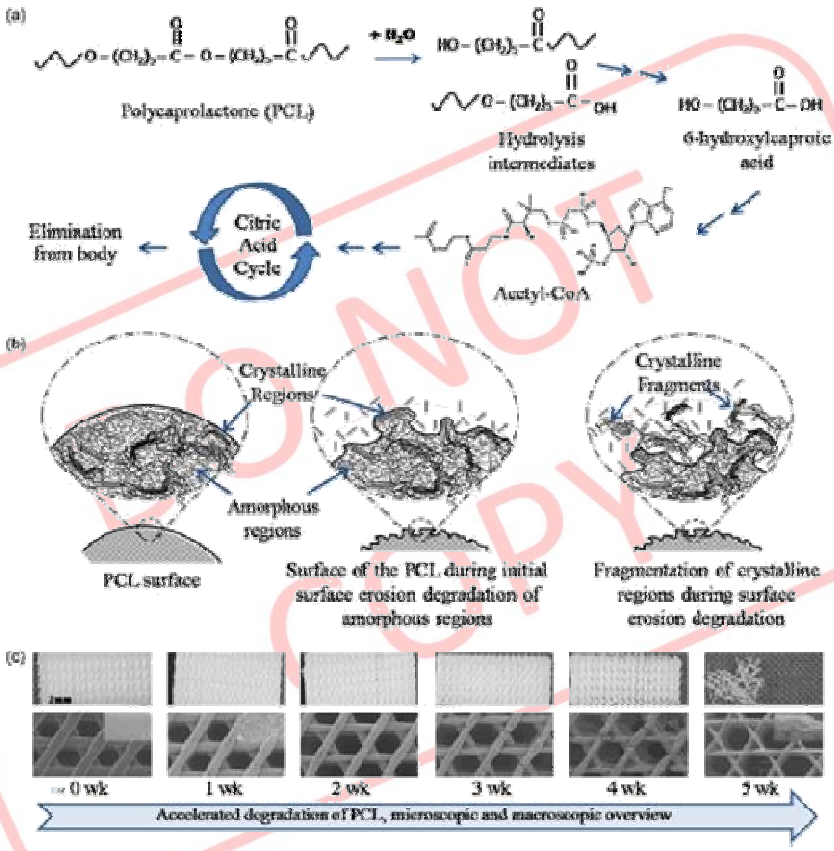

Figure 2.7 Degradation of polycaprolactone.

molecules, with a size range 10–1000 nm. Drug particles may be encapsulated, dispersed or absorbed in the nanospheres. They may also be termed as NPs or nanocapsules depending upon whether the drug is in a polymeric matrix or encapsulated in the shell. Nanospheres and nanocapsules can be prepared by the same methods as those described for microparticles, except that manufacturing parameters are adjusted to obtain nanometer size droplets. This can be obtained by using a relatively small ratio of the dispersed phase to the dispersion medium, and a substantially higher stirring speed [Zhang 2009]. Nanospheres can be used for selective targeting via the reticuloendothelial system to the liver and to cells that are phagocytically active. The size of nanospheres allows them to be administered intravenously via injection, unlike many other colloidal systems, which occlude both needles and capillaries. Injectable nanoparticulate carriers have good applicability for specific drug delivery and medical imaging, but they cannot generally be used due to their elimination by the reticuloendothelial system within seconds after intravenous injection. To overcome this limitation, monodisperse biodegradable nanospheres have

been developed from amphiphilic copolymers. These nanospheres were shown to exhibit increased blood circulation time and reduced drug accumulation in the liver of mice [Zhang 2009]. The efficacy of these colloidal particles as drug carriers is closely related to their interaction with proteins and enzymes in different body fluids. The interaction phenomenon between lysozyme, a positively charged enzyme that is highly concentrated in mucosa and two different drug carriers: nanocapsules made of an oily core coated by PCL and NPs made solely of PCL were studied. Results showed that the interaction of lysozyme with these colloidal drug carriers was highly affected by their surface charge [Calvo 1996]. Gref et al. analyzed plasma protein adsorption, zeta potential and the particle uptake by polymorphonuclear cells by biodegradable PEG-coated PLA, PLGA and PCL NPs. The influence of the PEG corona thickness and density, as well as the influence of the nature of the core was studied [Gref 2000]. The conditions to stabilize PLGA and the PCL NPs by freeze drying with several cryoprotective agents were identified. Studies indicated the necessity of adding sucrose, glucose, trehalose or gelatin to preserve the properties of NPs regardless of the freezing procedure [Saez 2000].

2.9 Anastrozole

Category: Non steroidal aromatase inhibitor

CAS Number: 120511-73-1

Proprietary name: Arimidex

Molecular formula: $C_{17}H_{19}N_5$

Molecular Weight: 293.4

Structural Formula and Chemical Name:

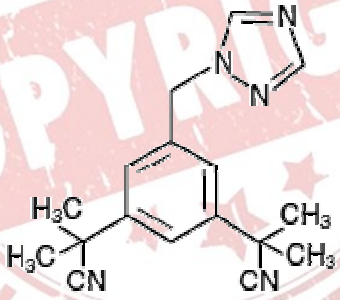

1,3-Benzenediacetonitrile, α, α, α', α'-tetramethyl-5-(1H-1,2,4-triazol-1-ylmethyl)

$C_{17}H_{19}N_5$

Physicochemical Properties:

Appearance and colour: An off-white powder.

Solubility: Anastrozole has moderate aqueous solubility (0.5 mg/ml at 25 °C); solubility is independent of pH in the physiological range. Anastrozole is freely soluble in methanol, acetone, ethanol, and tetrahydrofuran, and very soluble in acetonitrile.

Melting point: 81 to 82 °C.

Mechanism of action: The growth of many cancers of the breast is stimulated or maintained by estrogens. Treatment of breast cancer thought to be hormonally responsive (i.e., estrogen and/or progesterone receptor positive or receptor unknown) has included a variety of efforts to decrease estrogen levels (ovariectomy, adrenalectomy, hypophysectomy) or inhibit estrogen effects (antiestrogens and progestational agents). These interventions lead to decreased tumor mass or delayed progression of tumor growth in some women.

In postmenopausal women, estrogens are mainly derived from the action of the aromatase enzyme, which converts adrenal androgens primarily androstenedione and testosterone) to estrone and estradiol. The suppression of estrogen biosynthesis in peripheral tissues and in the cancer tissue itself can therefore be achieved by specifically inhibiting the aromatase enzyme. Anastrozole is a potent and selective non-steroidal aromatase inhibitor. It significantly lowers serum estradiol concentrations and has no detectable effect on formation of adrenal corticosteroids or aldosterone.

Pharmacokinetics

Absorption

Inhibition of aromatase activity is primarily due to anastrozole, the parent drug. Absorption of anastrozole is rapid and maximum plasma concentrations typically occur within 2 hours of dosing under fasted conditions. Studies with radiolabeled drug have demonstrated that orally administered anastrozole is well absorbed into the systemic circulation. Food reduces the rate but not the overall extent of anastrozole absorption. The mean Cmax of anastrozole decreased by 16% and the median Tmax was delayed from 2 to 5 h when anastrozole was administered 30 minutes after food. The pharmacokinetics of anastrozole are linear over the dose range of 1 to 20 mg, and do not change with repeated dosing. The pharmacokinetics of anastrozole was similar in patients and healthy volunteers.

Distribution

Steady-state plasma levels are approximately 3 to 4 fold higher than levels observed after a single dose of ARIMIDEX (anastrozole). Plasma concentrations approach steady-state levels at about 7 days of once daily dosing. Anastrozole is 40% bound to plasma proteins in the therapeutic range.

Metabolism

Metabolism of anastrozole occurs by N-dealkylation, hydroxylation and glucuronidation. Three metabolites of anastrozole (triazole, a glucuronide conjugate of hydroxy-anastrozole, and a glucuronide conjugate of anastrozole itself) have been identified in human plasma and urine. The major circulating metabolite of anastrozole, triazole, lacks pharmacologic activity.

Anastrozole inhibited reactions catalyzed by cytochrome P450 1A2, 2C8/9, and 3A4 in vitro with Ki values which were approximately 30 times higher than the mean steady-state Cmax values observed following a 1 mg daily dose. Anastrozole had no inhibitory effect on reactions catalyzed by cytochrome P450 2A6 or 2D6 in vitro. Administration of a single 30 mg/kg or multiple 10 mg/kg doses of anastrozole to healthy subjects had no effect on the clearance of antipyrine or urinary recovery of antipyrine metabolites.

Excretion

Eighty-five percent of radiolabeled anastrozole was recovered in feces and urine. Hepatic metabolism accounts for approximately 85% of anastrozole elimination. Renal elimination accounts for approximately 10% of total clearance. The mean elimination half-life of anastrozole is 50 h.

Indications: Advanced breast cancer in postmenopausal women with progression following tamoxifen therapy; first-line treatment of postmenopausal women with hormone receptor positive or hormone receptor unknown locally advanced or metastatic breast cancer.

Dosage and administration: The recommended dose of anastrozole is one tablet of 1 mg administered orally.

Adverse reactions:

Cardiovascular: Hypertension; thrombophlebitis; edema; vasodilation; chest pain.

CNS: Asthenia; headache; paresthesias; somnolence; confusion; insomnia; anxiety; dizziness; depression; hypertonia; lethargy; paresthesia.

Dermatologic: Alopecia; pruritus; rash; sweating.

GI: Low to moderate potential for nausea and vomiting; diarrhea; constipation; anorexia; increased LFTs (GGT, AST, ALT); GI disturbances; abdominal pain; dry mouth.
Genitourinary: UTIs; vaginal dryness; menstrual bleeding; sexual inactivity; atrophy of the female reproductive organs; pregnancy loss; pelvic pain.
Respiratory: Dyspnea; sinusitis; bronchitis; cough increased; pharyngitis.
Miscellaneous: Myalgia; arthralgia; breast pain; hot flashes; pain; back pain; peripheral edema; bone pain; flu-syndrome; tumor flare; weight gain; leukorrhea; edema.
The risk of bone fractures is a major drawback of oral anastrozole therapy.
To overcome these side effects and targeting of anastrozole for cancer treatment, different formulations like stealth NPs [Sarkar K. 2008] and microparticles [Zidan 2006] are already studied by researchers. Zidan et al. developed sustained release PLGA based anastrozole microparticles using emulsion/extraction method for treatment of breast cancer. Sarkar et al. formulated dendrimer-based stealth NPs composed of a PAMAM dendrimers core and PEG layer encapsulating anastrozole with a target to improve its water solubility.

2.10 Exemestane

Category: Irreversible steroidal aromatase inhibitor
CAS Number: 107868-30-4
Proprietary name: Aromasin
Molecular formula: $C_{20}H_{24}O_2$
Molecular Weight: 296.41
Structural Formula and Chemical Name:

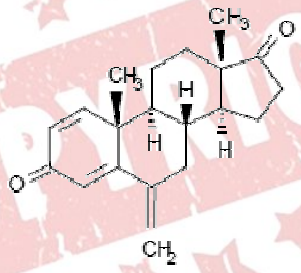

6-methylenandrosta-1,4-diene-3,17-dione

Physicochemical Properties:
Appearance and colour: A white to slightly yellow crystalline powder.

Solubility: Freely soluble in N, N-dimethylformamide, soluble in methanol, and practically insoluble in water.

Melting point: 180 to 182 °C.

Mechanism of action:

Breast cancer cell growth may be estrogen-dependent. Aromatase is the principal enzyme that converts androgens to estrogens both in pre- and postmenopausal women. While the main source of estrogen (primarily estradiol) is the ovary in premenopausal women, the principal source of circulating estrogens in postmenopausal women is from conversion of adrenal and ovarian androgens (androstenedione and testosterone) to estrogens (estrone and estradiol) by the aromatase enzyme in peripheral tissues. Estrogen deprivation through aromatase inhibition is an effective and selective treatment for some postmenopausal patients with hormone-dependent breast cancer.

Exemestane is an irreversible, steroidal aromatase inactivator, structurally related to the natural substrate androstenedione. It acts as a false substrate for the aromatase enzyme, and is processed to an intermediate that binds irreversibly to the active site of the enzyme, causing its inactivation, an effect also known as "suicide inhibition." Exemestane significantly lowers circulating estrogen concentrations in postmenopausal women, but has no detectable effect on adrenal biosynthesis of corticosteroids or aldosterone. Exemestane has no effect on other enzymes involved in the steroidogenic pathway up to a concentration at least 600 times higher than that inhibiting the aromatase enzyme.

Pharmacokinetics

Following oral administration to healthy postmenopausal women, exemestane is rapidly absorbed. After maximum plasma concentration is reached, levels decline polyexponentially with a mean terminal half-life of about 24 h. Exemestane is extensively distributed and is cleared from the systemic circulation primarily by metabolism. The pharmacokinetics of exemestane is dose proportional after single (10 to 200 mg) or repeated oral doses (0.5 to 50 mg). Following repeated daily doses of exemestane 25 mg, plasma concentrations of unchanged drug are similar to levels measured after a single dose.

Pharmacokinetic parameters in postmenopausal women with advanced breast cancer following single or repeated doses have been compared with those in healthy, postmenopausal women. Exemestane appeared to be more rapidly absorbed in the

women with breast cancer than in the healthy women, with a mean tmax of 1.2 h in the women with breast cancer and 2.9 h in the healthy women. After repeated dosing, the average oral clearance in women with advanced breast cancer was 45% lower than the oral clearance in healthy postmenopausal women, with corresponding higher systemic exposure. Mean AUC values following repeated doses in women with breast cancer (75.4 ng·h/ml) were about twice those in healthy women (41.4 ng·h/ml).

Absorption

Following oral administration of radiolabeled exemestane, at least 42% of radioactivity was absorbed from the gastrointestinal tract. Exemestane plasma levels increased by approximately 40% after a high-fat breakfast.

Distribution

Exemestane is distributed extensively into tissues. Exemestane is 90% bound to plasma proteins and the fraction bound is independent of the total concentration. Albumin and $\alpha_1$1-acid glycoprotein both contribute to the binding. The distribution of exemestane and its metabolites into blood cells is negligible.

Metabolism/Elimination

Following administration of radiolabeled exemestane to healthy postmenopausal women, the cumulative amounts of radioactivity excreted in urine and feces were similar (42 ± 3% in urine and 42 ± 6% in feces over a 1week collection period). The amount of drug excreted unchanged in urine was less than 1% of the dose. Exemestane is extensively metabolized, with levels of the unchanged drug in plasma accounting for less than 10% of the total radioactivity. The initial steps in the metabolism of exemestane are oxidation of the methylene group in position 6 and reduction of the 17-keto group with subsequent formation of many secondary metabolites. Each metabolite accounts only for a limited amount of drug-related material. The metabolites are inactive or inhibit aromatase with decreased potency compared with the parent drug. One metabolite may have androgenic activity (see). Studies using human liver preparations indicate that cytochrome P 450 3A4 (CYP 3A4) is the principal isoenzyme involved in the oxidation of exemestane. Exemestane is metabolized by cytochrome P 450 3A4 (CYP 3A4) and aldoketoreductases. It does not inhibit any of the major CYP isoenzymes, including CYP 1A2, 2C9, 2D6, 2E1, and 3A4.

Indications: Advanced breast cancer in postmenopausal women with progression following tamoxifen therapy; first-line treatment of postmenopausal women with

hormone receptor positive or hormone receptor unknown locally advanced or metastatic breast cancer.

Dosage and administration: The recommended dose of exemestane is one tablet of 25 mg administered orally.

Adverse reactions:

Cardiovascular: Chest pain, hypertension, peripheral edema.

CNS: Fatigue, depression, insomnia, anxiety, headache, dizziness.

Dermatologic: Rash, increased sweating, androgenic effects reported including hypertrichosis, hair loss and acne.

Endocrine: Hot flushes, weight gain.

GI: Low potential for nausea and vomiting, anorexia, constipation, diarrhea and increased appetite.

Hematologic: Lymphopenia.

Musculoskeletal: Musculoskeletal pain, anthralgia.

Respiratory: Dyspnea, coughing.

Miscellaneous: Flu like symptoms with fever, hoarseness.

Major drawbacks of orally delivered exemestane are musculoskeletal side effects including arthralgia (14.6 to 28.8%), pain in limb (9%), osteoarthritis (5.9%), myalgia (5.5%), back pain, pathological fracture, and skeletal pain.

To overcome these side effects and targeting of exemestane for cancer treatment, different formulations like SMEDDS [Singh 2008], powdered proliposomes [Hiremath 2009], PLGA NPs [Li 2013] and proliposomes [Jukanti 2011] are already studied by researchers. Singh et al. prepared and characterized SMEDDS containing exemestane and reported enhanced dissolution of the drug [Singh 2008]. Hiremath et al. developed proliposomal powder formulations using different ratios of drug (exemestane), distearoyl-phosphatidylcholine (DSPC), cholesterol and dimyristoyl-phosphatidylglycerol (DMPG) by solvent evaporation method to enhance the oral bioavailability of exemestane by improving solubility, dissolution and/or intestinal permeability [Hiremath 2009]. The in vitro transport studies in rat intestine, PAMPA and Caco-2 models revealed that the proliposomes were successful in enhancing the permeation of exemestane. These proliposomal formulations of exemestane could provide improved oral bioavailability due to enhanced solubility, permeability and hence absorption. Li et al. formulated PLGA and PLGA/MMT by a modified solvent

extraction/evaporation technology with vitamin E succinated polyethylene glycol 1000 (TPGS) as emulsifier for oral delivery. Exemestane formulated as NPs showed enhanced cytotoxicity than drug solution [Li 2013]. Jukanti et al. prepared proliposomes with the objective of improved and sustained transdermal delivery of exemestane. Proliposome gel showed significant improvement in bioavailability (2.4 folds) compared to oral suspension [Jukanti 2011].

2.11 References

Adams GP, Weiner, LM. 2005. Monoclonal antibody therapy of cancer. Nat. Biotechnol. 23:1147-1157.

Alexis F, Pridgen E, Molnar LK, Farokhzad OC. 2008. Factors affecting the clearance and biodistribution of polymeric nanoparticles. Mol. Pharmac. 5:505- 515.

Allen TM. 2002. Ligand-targeted therapeutics in anticancer therapy. Nat. Rev. Cancer 2(10):750-763.

Allen TM, Cullis PR. 2004. Drug delivery systems: entering the mainstream. Science 303:1818-1822.

Anand P, Kunnumakkara, AB, Kunnumakara AB, Sundaram C, Harikumar KB, Tharakan ST, Lai OS, Sung B, Aggarwal BB. 2008. Cancer is a preventable disease that requires major lifestyle changes. Pharm. Res. 25(9):2097-2116.

Arpino G, Weiss H, Lee AV, Schiff R, De Placido S, Osborne CK, Elledge RM. 2005. Estrogen receptor–positive, progesterone receptor–negative breast cancer: Association with growth factor receptor expression and tamoxifen resistance. J. Nat. Cancer Inst. 97(17):1254-1261.

Asperen J, van Tellingen O, van der Valk MA, Rozenhart M, Beijnen JH. 1998. Enhanced oral absorption and decreased elimination of paclitaxel in mice cotreated with cyclosporin A. Clin. Cancer Res. 4:2293-2297.

Astete CE, Sabliov CM. 2006. Synthesis and characterization of PLGA nanoparticles. J. Biomat. Sci. - Polymer Ed. 17(3):247-289.

Baban DF, Seymour LW. 1998. Control of tumour vascular permeability. Adv. Drug Deliv. Rev. 34:109-119.

Barichello JM, Morishita M, Takayama K, Nagai T. 1999. Encapsulation of hydrophilic and lipophilic drugs in PLGA nanoparticles by the nanoprecipitation method. Drug Dev. Ind. Pharm. 25(4):471-476.

Baum M, Budzar AU, Cuzick J, Forbes J, Houghton JH, Klijn JG, Sahmoud T. 2002. Anastrozole alone or in combination with tamoxifen versus tamoxifen alone for adjuvant treatment of postmenopausal women with early breast cancer: first results of the ATAC randomised trial. Lancet 359(9324):2131-2139.

Bergsma JE, de Bruijn WC, Rozema FR, Bos RRM, Boering G. 1995. Late degradation tissue response to poly(-lactide) bone plates and screws. Biomaterials 16:25-31.

Berton M, Allemann E, Stein CA, Gurny R. 1999. Highly loaded nanoparticulate carrier using an hydrophobic antisense oligonucleotide complex. Eur. J. Pharm. Biopharm 9:163-170.

Bhardwaj V, Ankola D, Gupta S, Schneider M, Lehr CM, Kumar MNVR. 2009. PLGA nanoparticles stabilized with cationic surfactant: safety studies and application in oral delivery of paclitaxel to treat chemical-induced breast cancer in rat. Pharm. Res. 26:2495 -2503.

Bonneterre J, Buzdar A, Nabholtz JM, Robertson JF, Thürlimann B, von Euler M, Sahmoud T, Webster A, Steinberg M. 2001. Anastrozole is superior to tamoxifen as first-line therapy in hormone receptor positive advanced breast carcinoma. Cancer 92:2247-2258.

Bosanquet AG, Gilby ED. 1982. Pharmacokinetics of oral and intravenous melphalan during routine treatment of multiple myeloma. Eur. J. Cancer Clin. Oncol. 18:355-362.

Bostman O, Hirvensalo E, Makinen J, Rokkanen P. 1990. Foreign-body reactions to fracture fixation implants of biodegradable synthetic polymers. J. Bone Joint Surg. Br. 72-B:592–596.

Boulikas T, Vougiouka M. 2003. Cisplatin and platinum drugs at the molecular level. (Review). Oncol. Rep. 10:1663-1682.

Brannon-Peppas L, Blanchette JO. 2004. Nanoparticle and targeted systems for cancer therapy. Adv. Drug Deliv. Rev. 56:1649-1659.

Brennan FR, Shaw L, Wing MG, Robinson C. 2004. Preclinical safety testing of biotechnology derived pharmaceuticals: understanding the issues and addressing the challenges. Mol. Biotechnol. 27(1):59-74.

Brigger I, Dubernet C, Couvreur P. 2002. Nanoparticles in cancer therapy and diagnosis. Adv. Drug Deliv. Rev. 54(5):631-651.

Brissette R, Prendergast J, Goldstein N. 2006. Identification of cancer targets and therapeutics using phage display. Curr. Opin. Drug Discov. Devel. 9:363-369.

Brooks PC, Montgomery AMP, Rosenfeld M, Reisfeld RA, Hu T, Klier G, Cheresh DA. 1994. Integrin $\alpha_v\beta_3$ antagonists promote tumor regression by inducing apoptosis of angiogenic blood vessels. Cell 79:1157-1164.

Brown JM, Giaccia AJ. 1998. The unique physiology of solid tumors: opportunities (and problems) for cancer therapy. Cancer Res. 58:1408-1416.

Buchholz TA. 2009. Radiation therapy for early-stage breast cancer after breast-conserving surgery. N. Engl. J. Med. 360(1):63-70.

Buzdar A, Jonat W, Howell A, Jones SE, Blomqvist C, Vogel CL, Eiermann W, Wolter JM, Azab M, Webster A and others. 1996. Anastrozole, a potent and selective aromatase inhibitor, versus megestrol acetate in postmenopausal women with advanced breast cancer: results of overview analysis of two phase III trials. Arimidex Study Group. J. Clin. Oncol. 14(7):2000-2011.

Byrne JD, Betancourt T, Brannon-Peppas L. 2008. Active targeting schemes for nanoparticle systems in cancer therapeutics. Adv. Drug Deliv. Rev. 60:1615-1626.

Cai W, Chen X. 2007. Nanoplatforms for targeted molecular imaging in living subjects. Small 3(11):1840-1854.

Caldorera-Moore M, Peppas NA. 2009. Micro- and nanotechnologies for intelligent and responsive biomaterial-based medical systems. Adv. Drug Deliv. Rev. 61:1391-1401.

Calvo P, VilaJato JL, Alonso MJ. 1996. Comparative in vitro evaluation of several colloidal systems, nanoparticles, nanocapsules, and nanoemulsions, as ocular drug carriers. J. Pharm. Sci. 85:530-536.

Campbell RA, Bhat-Nakshatri P, Patel NM, Constantinidou D, Ali S, Nakshatri H. 2001. Phosphatidylinositol 3-Kinase/AKT-mediated Activation of Estrogen Receptor α: a new model for anti-estrogen resistance. J. Biol. Chem. 276(13):9817-9824.

Carrasquillo KG, Stanley AM, Aponte-Carro JC, De Jesus P, Costantino HR, Bosques CJ, Griebenow K. 2001. Non-aqueous encapsulation of excipient-stabilized spray-freeze dried BSA into poly(lactide-co-glycolide) microspheres results in release of native protein. J. Controlled Rel. 76(3):199-208.

Carter P. 2001. Improving the efficacy of antibody-based cancer therapies. Nat. Rev. Cancer 1(2):118-129.

Causes of death in India Srs. 2009. Registrar general of India and centre for global health research. New Delhi: Government of India.

Champion JA, Katare YK, Mitragotri S. 2007. Making polymeric micro- and nanoparticles of complex shapes. Proc. Natl. Acad. Sci. USA 104:11901-11904.

Chan CM, Martin LA, Johnston SR, Ali S, Dowsett M. 2002. Molecular changes associated with the acquisition of oestrogen hypersensitivity in MCF-7 breast cancer cells on long-term oestrogen deprivation. J. Steroid Biochem. Mol. Biol. 81:333-341.

Chan JM, Valencia PM, Zhang L, Langer R, Farokhzad OC. 2010. Polymeric nanoparticles for drug delivery. Methods Mol. Biol. 624:163-175.

Chandra R, Rustgi R. 1998. Biodegradable polymers. Progr. Polym. Sci. 23:1273-1335.

Chaudhari KR, Kumar A, Khandelwal VKM, Ukawala M, Manjappa AS, Mishra AK, Monkkonen J, Murthy RSR. 2012. Bone metastasis targeting: A novel approach to reach bone using Zoledronate anchored PLGA nanoparticle as carrier system loaded with Docetaxel. J. Controlled Rel. 158(3):470-478.

Chithrani BD, Chan WCW. 2007. Elucidating the mechanism of cellular uptake and removal of protein-coated gold nanoparticles of different sizes and shapes. Nano Lett. 7:1542-1550.

Cole MP, Jones CT, Todd ID. 1971. A new anti-oestrogenic agent in late breast cancer. An early clinical appraisal of ICI46474. Br. J. Cancer 25(2):270-275.

Coombes RC, Kilburn LS, Snowdon CF, Paridaens R, Coleman RE, Jones SE, Jassem J, Van de Velde CJ, Delozier T, Alvarez I, Del Mastro L, Ortmann O, Diedrich K, Coates AS, Bajetta E, Holmberg SB, Dodwell D, Mickiewicz E, Andersen J, Lonning PE, Cocconi G, Forbes J, Castiglione M, Stuart N, Stewart A, Fallowfield LJ, Bertelli G, Hall E, Bogle RG, Carpentieri M, Colajori E, Subar M, Ireland E, Bliss JM. 2007. Survival and safety of exemestane versus tamoxifen after 2 to 3 years tamoxifen treatment (Intergroup Exemestane Study): a randomized controlled trial. Lancet 369(9561):559-570.

Coulembier O, Degee P, Hedrick JL, Dubois P. 2006. From controlled ring-opening polymerization to biodegradable aliphatic polyester: especially poly(beta-malic acid) derivatives. Progr. Polym. Sci. 31:723-747.

Davis ME. 2009. The first targeted delivery of siRNA in humans via a self-assembling, cyclodextrin polymer-based nanoparticle: from concept to clinic. Mol. Pharm. 6(3):659-668.

Davis ME, Chen Z, Shin DM. 2008. Nanoparticle therapeutics: an emerging treatment modality for cancer. Nat. Rev. Drug Discov. 7:771-782.

De Laurentiis M, Arpino G, Massarelli E, Ruggiero A, Carlomagno C, Ciardiello F, Tortora G, D'Agostino D, Caputo F, Cancello G, Montagna E, Malorni L, Zinno L, Lauria R, Bianco AR, De Placido S. 2005. A meta-analysis on the interaction between HER-2 expression and response to endocrine treatment in advanced breast cancer. Clin. Cancer Res. 11(13):4741-4748.

Dellian M, Witwer BP, Salehi HA, Yuan F, Jain RK. 1996. Quantitation and physiological characterization of angiogenic vessels in mice. Effect of basic fibroblast growth factor, vascular endothelial growth factor/vascular permeability factor, and host microenvironment. Am. J. Pathol. 149:59-71.

Derakhshandeh K, Soheili M, Dadashzadeh S, Saghiri R. 2010. Preparation and in vitro characterization of 9-nitrocamptothecin-loaded long circulating nanoparticles for delivery in cancer patients. Int. J. Nanomed. 5:463-471.

Dhar S, Gu FX, Langer R, Farokhzad OC, Lippard SJ. 2008. Targeted delivery of cisplatin to prostate cancer cells by aptamer functionalized Pt(IV) prodrug PLGA-PEG nanoparticles. Proc. Natl. Acad. Sci. USA 105:17356-17361.

Dhar S, Kolishetti N, Lippard SJ, Farokhzad OC. 2011. Targeted delivery of a cisplatin prodrug for safer and more effective prostate cancer therapy in vivo. Proc. Natl. Acad. Sci. USA 108(5):1850-1855.

Di Toro R, Betti V, Spampinato S. 2004. Biocompatibility and integrin-mediated adhesion of human osteoblasts to poly(DL-lactide-co-glycolide) copolymers. Eur. J. Pharm. Sci. 21(2-3):161-169.

Dikshit R, Gupta PC, Ramasundarahettige C, Gajalakshmi V, Aleksandrowicz L, Badwe R, Kumar R, Roy S, Suraweera W, Bray F and others. 2012. Cancer mortality in India: a nationally representative survey. Lancet 379(9828):1807-1816.

Dombernowsky P, Smith I, Falkson G, Leonard R, Panasci L, Bellmunt J, Bezwoda W, Gardin G, Gudgeon A, Morgan M and others. 1998. Letrozole, a new oral aromatase inhibitor for advanced breast cancer: double-blind randomized trial

showing a dose effect and improved efficacy and tolerability compared with megestrol acetate. J. Clin. Oncol. 16(2):453-461.

Dowsett M, Allred C, Knox J, Quinn E, Salter J, Wale C, Cuzick J, Houghton J, Williams N, Mallon E, Bishop H, Ellis I, Larsimont D, Sasano H, Carder P, Cussac AL, Knox F, Speirs V, Forbes J, Buzdar A. 2008. Relationship between quantitative estrogen and progesterone receptor expression and human epidermal growth factor receptor 2 (HER-2) status with recurrence in the Arimidex, Tamoxifen, Alone or in Combination trial. J. Clin. Oncol. 26(7):1059-1065.

Dowsett M, Cuzick J, Wale C, Howell T, Houghton J, Baum M. 2005. Retrospective analysis of time to recurrence in the ATAC trial according to hormone receptor status: an hypothesis-generating study. J. Clin. Oncol. 23(30):7512-7517.

Dreher MR, Liu W, Michelich CR, Dewhirst MW, Yuan F, Chilkoti A. 2006. Tumor vascular permeability, accumulation, and penetration of macromolecular drug carriers. J. Natl. Cancer Inst. 98:335-344.

Duncan R. 2003. The dawning era of polymer therapeutics. Nat. Rev. Drug Discov. 2:347-360.

Eisenstein M. 2006. Protein arrays: growing pains. Nature 444:959-962.

Ellis MJ, Tao Y, Young O, White S, Proia AD, Murray J, Renshaw L, Faratian D, Thomas J, Dowsett M, Krause A, Evans DB, Miller WR, Dixon JM. 2006. Estrogen-independent proliferation is present in estrogen-receptor HER2-positive primary breast cancer after neoadjuvant letrozole. J. Clin. Oncol. 24(19):3019-3025.

Fang C, Shi B, Pei YY, Hong MH, Wu J, Chen HZ. 2006b. In vivo tumor targeting of tumor necrosis factor-α-loaded stealth nanoparticles: effect of mPEG molecular weight and particle size. Eur. J. Pharm. Sci. 27(1):27-36.

Farokhzad OC, Jon S, Khademhosseini A, Tran TN, Lavan DA, Langer R. 2004. Nanoparticle-aptamer bioconjugates: a new approach for targeting prostate cancer cells. Cancer Res. 64(21):7668-7672.

Farokhzad OC, Langer R. 2009. Impact of nanotechnology on drug delivery. ACS Nano 3(1):16-20.

Farokhzad OC, Langer R. 2006. Nanomedicine: developing smarter therapeutic and diagnostic modalities. Adv. Drug Deliv. Rev. 58(14):1456-1459.

Feng SS. 2004. Nanoparticles of biodegradable polymers for new-concept chemotherapy. Exp. Rev. Med. Devices 1(1):115-125.

Feng SS, Chien S. 2003. Chemotherapeutic engineering: application and further development of chemical engineering principles for chemotherapy of cancer and other diseases. Chem. Eng. Sci. 58:4087-4114.

Ferlay J, Shin HR, Bray F, Forman D, Mathers C, Parkin DM. 2010. Estimates of worldwide burden of cancer in 2008: GLOBOCAN 2008. Int. J. Cancer 127(12):2893-2917.

Fisher B, Costantino JP, Redmond CK, Fisher ER, Wickerham DL, Cronin WM. 1994. Endometrial cancer in tamoxifen-treated breast cancer patients: findings from the National Surgical Adjuvant Breast and Bowel Project (NSABP) B-14. J. Natl. Cancer Inst. 86(7):527-537.

Fisher B, Redmond C, Brown A, Fisher ER, Wolmark N, Bowman D, Plotkin D, Wolter J, Bornstein R, Legault-Poisson S and others. 1986. Adjuvant chemotherapy with and without tamoxifen in the treatment of primary breast cancer: 5-year results from the National surgical adjuvant breast and bowel project trial. J. Clin. Oncol. 4(4):459-471.

Fonseca C, Simoes S, Gaspar R. 2002. Paclitaxel-loaded PLGA nanoparticles: preparation, physicochemical characterization and in vitro anti-tumoral activity. J. Controlled Rel. 83(2):273-286.

Freiberg S, Zhu, X. 2004. Polymer microspheres for controlled drug release. Int. J. Pharm. 282:1-18.

Gabizon AA. 2001. Pegylated liposomal doxorubicin: metamorphosis of an old drug into a new form of chemotherapy. Cancer Invest. 19(4):424-436.

Gabriel N, Hortobagyi MD. 2005. Trastuzumab in the treatment of breast cancer. N. Engl. J. Med. 353:1734-1736.

Ganta S, Devalapally H, Shahiwala A, Amiji M. 2008. A review of stimuli-responsive nanocarriers for drug and gene delivery. J. Controlled Rel. 126(3):187-204.

Gao W, Chan JM, Farokhzad OC. 2010. pH-responsive nanoparticles for drug delivery. Mol. Pharm. 7(6):1913-1920.

Glangchai LC, Caldorera-Moore M, Shi L, Roy K. 2008. Nanoimprint lithography based fabrication of shape-specific, enzymatically-triggered smart nanoparticles. J. Controlled Rel. 125:263-272.

Gore M, Oza A, Rustin G, Malfetano J, Calvert H, Clarke-Pearson D, Carmichael J, Ross G, Beckman R, Fields S. 2002. A randomised trial of oral versus intravenous

topotecan in patients with relapsed epithelial ovarian cancer. Eur. J. Cancer 38:57-63.

Gottardis MM, Robinson SP, Satyaswaroop PG, Jordan VC. 1988. Contrasting actions of tamoxifen on endometrial and breast tumor growth in the athymic mouse. Cancer Res. 48(4):812-815.

Gratton SEA, Ropp PA, Pohlhaus PD, Luft JC, Madden VJ, Napier ME, DeSimone JM. 2008. The effect of particle design on cellular internalization pathways. Proc. Natl. Acad. Sci. USA 105:11613-11618.

Greco F, Vicent MJ. 2009. Combination therapy: opportunities and challenges for polymerdrug conjugates as anticancer nanomedicines. Adv. Drug Deliv. Rev. 61(13):1203-1213.

Gref R, Lück M, Quellec P, Marchand M, Dellacherie E, Harnisch S, Blunk T, Muller RH. 2000. 'Stealth' corona-core nanoparticles surface modified by polyethylene glycol (PEG): influences of the corona (PEG chain length and surface density) and of the core composition on phagocytic uptake and plasma protein adsorption. Colloids Surf. B: Biointerface 18:301-313.

Grefa R, Lück M, Quellec P, Marchand M, Dellacherie E, Harnisch S, Blunke T, Müller RH. 2000. 'Stealth' corona-core nanoparticles surface modified by polyethylene glycol (PEG): influences of the corona (PEG chain length and surface density) and of the core composition on phagocytic uptake and plasma protein adsorption. Colloids Surf. B Biointerfaces 18(3-4):301-313.

Gu F, Zhang L, Teply BA, Mann N, Wang A, Radovic-Moreno AF, Langer R, Farokhzad OC. 2008. Precise engineering of targeted nanoparticles by using self-assembled biointegrated block copolymers. Proc. Natl. Acad. Sci. USA 105(7):2586-2591.

Gu FX, Karnik R, Wang AZ, Alexis F, Levy-Nissenbaum E, Hong S, Langer RS, Farokhzad OC. 2007. Targeted nanoparticles for cancer therapy. Nano Today 2:14-21.

Haley B, Frenkel E. 2008. Nanoparticles for drug delivery in cancer treatment. Urol. Oncol. 26:57-64.

Hamaguchi T, Doi T, Eguchi-Nakajima T, Kato K, Yamada Y, Shimada Y, Fuse N, Ohtsu A, Matsumoto S, Takanashi M, Matsumura Y. 2010. Phase I study of NK012, a novel SN-38-incorporating micellar nanoparticle, in adult patients with solid tumors. 16(20):5 Clin. Cancer Res. 16(20):5058-5066.

Hamaguchi T, Matsumura Y, Suzuki M, Shimizu K, Goda R, Nakamura I, Nakatomi I, Yokoyama M, Kataoka K, Kakizoe T. 2005. NK105, a paclitaxel-incorporating micellar nanoparticle formulation, can extend in vivo antitumour activity and reduce the neurotoxicity of paclitaxel. Br. J. Cancer 92(7):1240-1246.

Hayashi T. 1994. Biodegradable polymers for biomedical uses. Progr. Polym. Sci. 19:663-702.

Heath T, Fraley R, Papahdjopoulos D. 1980. Antibody targeting of liposomes: cell specificity obtained by conjugation of F(ab')2 to vesicle surface. Science 210:539-541.

Hedberg EL, Kroese-Deutman HC, Shih CK, Crowther RS, Carney DH, Mikos AG, Jansen JA. 2005. In vivo degradation of porous poly(propylene fumarate)/poly(DL-lactic-co-glycolic acid) composite scaffolds. Biomaterials 26(22):4616-4623.

Hendrick RE. 2010. Radiation doses and cancer risks from breast imaging studies. Radiology 257(1):246-253.

Hilgenbrink AR, Low PS. 2005. Folate receptor-mediated drug targeting: from therapeutics to diagnostics. J. Pharm. Sci. 94:2135-2146.

Hiremath PS, Soppimath KS, Betageri GV. 2009. Proliposomes of exemestane for improved oral delivery: formulation and in vitro evaluation using PAMPA, Caco-2 and rat intestine. Int. J. Pharm. 380(1-2):96-104.

Hoffmann T, Hafner D, Ballo H, Haas I, Bier H. 1997. Antitumor activity of antiepidermal growth factor receptor monoclonal antibodies and cisplatin in ten human head and neck squamous cell carcinoma lines. Anticancer Res. 17:4419 - 4425.

Holmberg K, Bergstrom K, Brink C, Österberg E, Tiberg F, Harris JM. 1993. Effects on protein adsorption, bacterial adhesion and contact angle of grafting PEG chains to polystyrene. J. Adhesive Sci. Technol. 7:503-517.

Hori K, Suzuki M, Tanda S, Saito S. 1991. Characterization of heterogeneous distribution of tumor blood flow in the rat. Cancer Sci. 82:109-117.

Huang S. 1985. Biodegradable polymers. Mark F, Bikales, N.,Overberger, C., Menges, G., Kroshwitz, J., editor. New York: John Wiley and Sons.

Hughes GA. 2005. Nanostructure-mediated drug delivery. Nanomedicine 1:22-30.

Hurley LH. 2002. DNA and its associated processes as targets for cancer therapy. Nat. Rev. Cancer 2:188-200.

Jain RK. 1987. Transport of molecules in the tumor interstitium: a review. Cancer Res. 47:3039-3051.

Jain RK. 1998. Delivery of molecular and cellular medicine to solid tumors. J. Controlled Rel. 53:49-67.

Jang SH, Wientjes MG, Lu D, Au JL. 2003. Drug delivery and transport to solid tumors. Pharm. Res. 20:1337-1350.

Jeanneret LA, Schneider MP, Troxler S, Bugnon O, Luthi F. 2011. Therapeutic adherence to oral cancer therapy and interdisciplinary management. Rev. Med. Suisse 7:1154-1158.

Jemal A, Bray F, Center MM, Ferlay J, Ward E, Forman D. 2011. Global cancer statistics. CA: a cancer journal for clinicians 61(2):69-90.

Jeng MH, Yue W, Eischeid A, Wang JP, Santen RJ. 2000. Role of MAP kinase in the enhanced cell proliferation of long term estrogen deprived human breast cancer cells. Breast Cancer Res. Treat. 62(3):167-175.

Jensen EV, Jacobson HI. 1962. Basic guides to the mechanism of estrogen action. Recent Prog. Horm. Res. 18:387-414.

Jha P. 2009. Avoidable global cancer deaths and total deaths from smoking. Nat Rev Cancer 9(9):655-664.

Johnston APR, Kamphuis MMJ, Such GK, Scott AM, Nice EC, Heath JK, Caruso F. 2012. Targeting cancer cells: controlling the binding and internalization of antibody-functionalized capsules. ACS Nano. 6(8):6667-6674.

Johnston SR, Dowsett M. 2003. Aromatase inhibitors for breast cancer: lessons from the laboratory. Nat. Rev. Cancer 3:821-831.

Johnston SR, Head J, Pancholi S, Detre S, Martin LA, Smith IE, Dowsett M. 2003. Integration of signal transduction inhibitors with endocrine therapy: an approach to overcoming hormone resistance in breast cancer. Clin Cancer Res 9(1 Pt 2):524S-532S.

Jones A, Harris AL. 1998. New developments in angiogenesis: a major mechanism for tumor growth and target for therapy. Cancer J. Sci. Am. 4:209-217.

Jordan VC, Dowse LJ. 1976. Tamoxifen as an anti-tumour agent: effect on oestrogen binding. J. Endocrinol. 68(02):297-303.

Jukanti R, Sheela S, Bandari S, Veerareddy PR. 2011. Enhanced bioavailability of exemestane via proliposomes based transdermal delivery. J. Pharm. Sci. 100(8):3208-3222.

Kale AA, Torchilin VP. 2010. Environment-responsive multifunctional liposomes. Methods Mol. Biol. 605:213-242.

Kao YC, Cam LL, Laughton CA, Zhou D, Chen S. 1996. Binding characteristics of seven inhibitors of human aromatase: a site-directed mutagenesis study. Cancer Res. 56(15):3451-3460.

Kataoka K. 1994. Design of nanoscopic vehicles for drug targeting based on micellization of amphiphilic block copolymers. J. Macromol. Sci. Pure Apl. Chem. A31:1759-1769.

Kataoka K, Kwon GS, Yokoyama M, Okano T, Sakurai Y. 1993. Block co polymer micelles as vehicles for drug delivery. J. Controlled Rel. 24:119-132.

Kaufmann M, Jonat W, Hilfrich J, Eidtmann H, Gademann G, Zuna I, von Minckwitz G. 2007. Improved overall survival in postmenopausal women with early breast cancer after anastrozole initiated after treatment with tamoxifen compared with continued tamoxifen: the ARNO 95 study. J. Clin. Oncol. 25:2664-2670.

Kim TY, Kim DW, Chung JY, Shin SG, Kim SC, Heo DS, Kim NK, Bang YJ. 2004. Phase I and pharmacokinetic study of Genexol-PM, a cremophor-free, polymeric micelle-formulated paclitaxel, in patients with advanced malignancies. Clin. Cancer Res. 10(11):3708-3716.

Klijn JG, Look MP, Portengen H, Alexieva-Figusch J, van Putten WL, Foekens JA. 1994. The prognostic value of epidermal growth factor receptor (EGF-R) in primary breast cancer: results of a 10 year follow-up study. Breast Cancer Res Treat 29:73-83.

Knop K, Hoogenboom R, Fischer D, Schubert US. 2010. Poly(ethylene glycol) in drug delivery: pros and cons as well as potential alternatives. Angew. Chem. Int. Ed. 49(36):6288-6308.

Kong G, Braun RD, Dewhirst MW. 2000. Hyperthermia enables tumor-specific nanoparticle delivery: effect of particle size. Cancer Res. 60(16):4440-4445.

Krag DN, Shukla GS, Shen GP, Pero S, Ashikaga T, Fuller S, Weaver DL, Burdette-Radoux S, Thomas C. 2006. Selection of tumor-binding ligands in cancer patients with phage display libraries. Cancer Res. 66:7724-7733.

Kumar MN, Mohapatra SS, Kong X, Jena PK, Bakowsky U, Lehr CM. 2004. Cationic poly(lactide-co-glycolide) nanoparticles as efficient in vivo gene transfection agents. J. Nanosci. Nanotechnol. 4(8):990-994.

Kuppens I, Bosch TM, van Maanen MJ, Rosing H, Fitzpatrick A, Beijnen JH, Schellens JHM. 2005. Oral bioavailability of docetaxel in combination with OC144-093 (ONT-093). Cancer Chemother. Pharmacol. 55:72-78.

Kurokawa H, Arteaga CL. 2003. ErbB (HER) receptors can abrogate antiestrogen action in human breast cancer by multiple signaling mechanisms. Clin. Cancer Res. 9(1 Pt 2):511S-515S.

Kurokawa H, Lenferink AE, Simpson JF, Pisacane PI, Sliwkowski MX, Forbes JT, Arteaga CL. 2000. Inhibition of HER2/neu (erbB-2) and mitogen-activated protein kinases enhances tamoxifen action against HER2-overexpressing, tamoxifen-resistant breast cancer cells. Cancer Res. 60:5887-5894.

Kwon GS, Kataoka K. 1995. Block copolymer micelles as long-circulating drug vehicles. Adv. Drug Deliv. Rev. 16:295-309.

Labhasetwar V. 1997. Nanoparticles for drug delivery. Pharm. News 4:28-31.

Lasic DD. 1998. Novel applications of liposomes. Trends Biotechnol. 16:307-321.

Lavasanifar A, Samuel J, Kwon GS. 2002. Poly(ethylene oxide)-block-poly(l-amino acid) micelles for drug delivery. Adv. Drug Deliv. Rev. 54:169-190.

Lee KS, Chung HC, Im SA, Park YH, Kim CS, Kim SB, Rha SY, Lee MY, Ro J. 2008. Multicenter phase II study of a cremophor-free polymeric micelleformulated paclitaxel in patients with metastatic breast cancer (MBC). Breast Cancer Res. Treat. 108(2):241-250.

Leserman LD, Barbet J, Kourilsky F, Weinstein JN. 1980. Targeting to cells of fluorescent liposomes covalently coupled with monoclonal antibody or protein A. Nature 288:602-604.

Li Z, Liu K, Sun P, Mei L, Hao T, Tian Y, Tang Z, Li L, Chen D. 2013. Poly(D, L-lactide-co-glycolide)/montmorillonite nanoparticles for improved oral delivery of exemestane. J. Microencapsul. 30(5):432-440.

Liechty WB, Peppas NA. 2012. Expert opinion: responsive polymer nanoparticles in cancer therapy. Eur. J. Pharm. Biopharm. 80:241-246.

Liechty WB, Peppas NA. 2012. Expert opinion: responsive polymer nanoparticles in cancer therapy. Eur. J. Pharm. Biopharm. 80:241-246.

Liu L, Won YJ, Cooke PH, Coffin DR, Fishman ML, Hicks KB, Ma PX. 2004. Pectin/poly(lactide-co-glycolide) composite matrices for biomedical applications. Biomaterials 25(16):3201-3210.

Maeda H. 2001. The enhanced permeability and retention (EPR) effect in tumor vasculature: the key role of tumor-selective macromolecular drug targeting. Adv. Biol. Regul. 41:189-207.

Majoros InJ, Myc A, Thomas T, Mehta CB, Baker JR. 2006. PAMAM dendrimer based multifunctional conjugate for cancer therapy: synthesis, characterization, and functionality. Biomacromolecules 7:572-579.

Manegold C, Drings P, Pawinski A, Lentz MA, van Glabbeke M, van Zandwijk N, Bachmann P, Schnaa rs Y, Zatloukal P, Dolensky J. 1996. Oral ifosfamide/ mesna versus intravenous ifosfamide/mesna in non-small- cell lung cancer: a randomized phase II trial of the EORTC lung cancer cooperative group. Ann. Oncol. 7:637-639.

Martin LA, Farmer I, Johnston SRD, Ali S, Marshall C, Dowsett M. 2003. Enhanced estrogen receptor (ER) α, ERBB2, and MAPK signal transduction pathways operate during the adaptation of MCF-7 cells to long term estrogen deprivation. J. Bio. Chem. 278(33):30458-30468.

Masamura S, Santner SJ, Heitjan DF, Santen RJ. 1995. Estrogen deprivation causes estradiol hypersensitivity in human breast cancer cells. J. Clin. Endocrinol. Metab. 80:2918-2925.

Matsumura Y. 2004. Phase I Clinical trial and pharmacokinetic evaluation of NK911, a micelle-encapsulated doxorubicin. Br. J. Cancer 91:1775-1781.

Matsumura Y, Kataoka K. 2009. Preclinical and clinical studies of anticancer agentincorporating polymer micelles. Cancer Sci. 100(4):572-579.

Matsumura Y, Kimura M, Yamamoto T, Maeda H. 1988. Involvement of the Kinin-generating cascade in enhanced vascular permeability in tumor tissue. Cancer Sci. 79:1327-1334.

Mehren Mv, Adams GP, Weiner LM. 2003. Monoclonal antibody therapy for cancer. Annu. Rev. Med. 54:343-369.

Mendelsohn J. 1997. Epidermal growth factor receptor inhibition by a monoclonal antibody as anticancer therapy. Clin. Cancer Res. 3:2703-2707.

Merkli A, Tabatabay C, Gurny R, Heller J. 1998. Biodegradable polymers for the controlled release of ocular drugs. Progr. Polym. Sci. 23:563-580.

Minotti G, Menna P, Salvatorelli E, Cairo G, Gianni L. 2004. Anthracyclines: molecular advances and pharmacologic developments in antitumor activity and cardiotoxicity. Pharmacol. Rev. 56:185-229.

Mittal G, Sahana DK, Bhardwaj V, Ravi Kumar MN. 2007. Estradiol loaded PLGA nanoparticles for oral administration: effect of polymer molecular weight and copolymer composition on release behavior in vitro and in vivo. J. Controlled Rel. 119(1):77-85.

Moghimi SM, Hedeman H, Christy NM, Illum L, Davis SS. 1993. Enhanced hepatic clearance of intravenously administered sterically stabilized microspheres in zymosan-stimulated rats. J. Leukocyte Biol. 54:513-517.

Moghimi SM, Hunter AC, Murray JC. 2001. Long-circulating and target specific nanoparticles: theory to practice. Pharmacol. Rev. 53:283-318.

Moghimi SM, Hunter AC, Murray JC. 2005. Nanomedicine: current status and future prospects. FASEB J. 19(3):311-330.

Moghimi SM, Porter CJH, Illum L, Davis SS. 1991. The effect of Poloxamer-407 on liposome stability and targeting to bone marrow: comparison with polystyrene microspheres. Int. J. Pharm. 68(1-3):121-126.

Moghimi SM, Szebeni J. 2003. Stealth liposomes and long circulating nanoparticles: critical issues in pharmacokinetics, opsonization and protein-binding properties. Prog. Lipid Res. 42(6):463-478.

Mouridsen H, Gershanovich M, Sun Y, Pérez-Carrión R, Boni C, Monnier A, Apffelstaedt J, Smith R, Sleeboom HP, Jänicke F, Pluzanska A, Dank M, Becquart D, Bapsy PP, Salminen E, Snyder R, Lassus M, Verbeek JA, Staffler B, Chaudri-Ross HA, Dugan M. 2001. Superior efficacy of letrozole versus tamoxifen as first-line therapy for postmenopausal women with advanced breast cancer: results of a phase III study of the international letrozole breast cancer group. J. Clin. Oncol. 19:2596-2606.

Nagayama S, Ogawara K, Fukuoka Y, Higaki K, Kimura T. 2007. Time-dependent changes in opsonin amount associated on nanoparticles alter their hepatic uptake characteristics. Int. J. Pharm. 342(1-2):215-221.

Nahta R, Hortobagyi GN, Esteva FJ. 2003. Growth factor receptors in breast cancer: potential for therapeutic intervention. Oncol. 8:5-17.

Nahta R, Hortobagyi GN, Esteva FJ. 2003. Growth factor receptors in breast cancer: potential for therapeutic intervention. Oncol. 8:5-17.

Nair LS, Laurencin CT. 2007. Biodegradable polymers as biomaterials. Progr. Polym. Sci. 32:762-798.

Napier ME, DeSimone JM. 2007. Nanoparticle drug delivery platform. Polym. Rev. 47(3):321-327.

Nobs L, Buchegger F, Gurny R, Allemann E. 2004. Poly(lactic acid) nanoparticles labeled with biologically active Neutravidin for active targeting. Eur. J. Pharm. Biopharm. 58(3):483-490.

Nobs L, Buchegger F, Gurny R, Allemann E. 2005. Biodegradable nanoparticles for direct or two-step tumor immunotargeting. Bioconjugate Chem. 17:139 - 145.

O'Neill VJ, Twelves CJ. 2002. Oral cancer treatment: developments in chemotherapy and beyond. Br. J. Cancer 87:933-937.

Oh KT, Yin H, Lee ES, Bae YH. 2007. Polymeric nanovehicles for anticancer drugs with triggering release mechanisms. J. Mater. Chem. 17(38):3987-4001.

Okada M. 2002. Chemical syntheses of biodegradable polymers. Progr. Polym. Sci. 27:87-133.

Ostuni E, Chapman RG, Holmlin RE, Takayama S, Whitesides GM. 2001. A survey of structure-property relationships of surfaces that resist the adsorption of protein. Langmuir 17(18):5605-5620.

Owens DE, Peppas NA. 2006a. Opsonization, biodistribution, and pharmacokinetics of polymeric nanoparticles. Int. J. Pharm. 307:93-102.

Paridaens R, Dirix L, Lohrisch C, Beex L, Nooij M, Cameron D, Biganzoli L, Cufer T, Duchateau L, Hamilton A, Lobelle JP, Piccart M. 2003. Mature results of a randomized phase II multicenter study of exemestane versus tamoxifen as first-line hormone therapy for postmenopausal women with metastatic breast cancer. Ann. Oncol. 14:1391-1398.

Partridge AH, Avorn J, Wang PS, Winer EP. 2002. Adherence to therapy with oral antineoplastic agents. J. Natl. Cancer Inst. 94:652-661.

Patil SD, Papadimitrakopoulos F, Burgess DJ. 2004. Dexamethasone-loaded poly(lactic-co-glycolic) acid microspheres/poly(vinyl alcohol) hydrogel composite coatings for inflammation control. Diabetes Technol. Ther. 6(6):887-897.

Patri AK, Myc A, Beals J, Thomas TP, Bander NH, Baker JR Jr. 2004. Synthesis and in vitro testing of J591 antibody-dendrimer conjugates for targeted prostate cancer therapy. Bioconjug. Chem. 15(6):1174-1181.

Pavlinkova G, Colcher D, Booth BJ, Goel A, Wittel UA, Batra SK. 2001. Effects of humanization and gene shuffling on immunogenicity and antigen binding of anti-TAG-72 single-chain Fvs. Int. J. Cancer 94(5):717-726.

Peltier S, Oger JM, Lagarce F, Couet W, Benoît JP. 2006. Enhanced oral paclitaxel bioavailability after administrati on of paclitaxel-loaded lipid nanocapsules. Pharm. Res. 23:1243-1250.

Petit T, Dufour P, Tannock I. 2011. A critical evaluation of the role of aromatase inhibitors as adjuvant therapy for postmenopausal women with breast cancer. Endocr. Relat. Cancer 18(3):79-89.

Petros RA, DeSimone JM. 2010. Strategies in the design of nanoparticles for therapeutic applications. Nat. Rev. Drug Discov. 9(8):615-627.

Phillips MA, Gran ML, Peppas NA. 2010. Targeted nanodelivery of drugs and diagnostics. Nano Today 5:143-159.

Pinto Reis C, Neufeld RJ, Ribeiro AJ, Veiga F. 2006. Nanoencapsulation I. Methods for preparation of drug-loaded polymeric nanoparticles. Nanomedicine 2(1):8-21.

Pitt CG. 1990. Poly-ε-caprolactone and its copolymers. Chasin M, Langer, R., editor. New York: Marcel Dekker.

Ponka P, Lok CN. 1999. The transferrin receptor: role in health and disease. Int. J. Biochem. Cell Biol. 31:1111-1137.

Roberts WG, Palade GE. 1995. Increased microvascular permeability and endothelial fenestration induced by vascular endothelial growth factor. J. Cell Sci. 108:2369-2379.

Rolland JP, Maynor BW, Euliss LE, Exner AE, Denison GM, DeSimone JM. 2005. Direct fabrication and harvesting of monodisperse, shape-specific nanobiomaterials. J. Am. Chem. Soc. 127:10096-10100.

Roser M, Fischer D, Kissel T. 1998. Surface-modified biodegradable albumin nano- and microspheres. II: effect of surface charges on in vitro phagocytosis and biodistribution in rats. Eur. J. Pharm. Biopharm. 46(3):255-263.

Rothenfluh DA, Bermudez H, O'Neil CP, Hubbell JA. 2008. Biofunctional polymer nanoparticles for intra-articular targeting and retention in cartilage. Nat. Mater. 7(3):248-254.

Rouzes C, Gref R, Leonard M, De Sousa Delgado A, Dellacherie E. 2000. Surface modification of poly(lactic acid) nanospheres using hydrophobically modified dextrans as stabilizers in an o/w emulsion/evaporation technique. J. Biomed. Mater. Res. 50:557-565.

Rowinsky M, Eric K. 1997. The development and clinical utility of the taxane class of antimicrotubule chemotherapy agents. Annu. Rev. Med. 48:353-374.

Ruddy K, Mayer E, Partridge A. 2009. Patient adherence and persistence with oral anticancer treatment. CA Cancer J. Clin. 59:56-66.

Saez A, Guzman M, Molpeceres J, Aberturas MR. 2000. Freeze-drying of polycaprolactone and poly(d ,l -lactic-glycolic) nanoparticles induce minor particle size changes affecting the oral pharmacokinetics of loaded drugs. Eur. J. Pharm. Biopharm. 50:379-387.

Sahana DK, Mittal G, Bhardwaj V, Kumar MN. 2008. PLGA nanoparticles for oral delivery of hydrophobic drugs: influence of organic solvent on nanoparticle formation and release behavior in vitro and in vivo using estradiol as a model drug. J. Pharm. Sci. 97(4):1530-1542.

Sahoo SK, Labhasetwar V. 2005. Enhanced antiproliferative activity of transferrin conjugated paclitaxel-loaded nanoparticles is mediated via sustained intracellular drug retention. Mol. Pharmac. 2:373-383.

Sahoo SK, Ma W, Labhasetwar V. 2004. Efficacy of transferrin-conjugated paclitaxel-loaded nanoparticles in a murine model of prostate cancer. Int. J. Cancer 112:335-340.

Salvador-Morales C, Zhang L, Langer R, Farokhzad OC. 2009. Immunocompatibility properties of lipid-polymer hybrid nanoparticles with heterogeneous surface functional groups. Biomaterials 30(12):2231-2240.

Sankhala KK, Mita AC, Adinin R, Wood L, Beeram M, Bullock S, Yamagata N, Matsuno K, Fujisawa T, Phan AT. 2009. A phase I pharmacokinetic (PK) study of MBP-426, a novel liposome encapsulated oxaliplatin. J. Clin. Oncol. 27(15S):2535.

Santen R, Jeng MH, Wang JP, Song R, Masamura S, McPherson R, Santner S, Yue W, Shim WS. 2001. Adaptive hypersensitivity to estradiol: potential mechanism for

secondary hormonal responses in breast cancer patients. J. Steroid Biochem. Mol. Biol. 79(1-5):115-125.

Sariego J. 2010. Breast cancer in the young patient. The American surgeon 76(12):1397-1401.

Sarkar K, Yang H. 2008. Encapsulation and extended release of anti-cancer anastrozole by stealth nanoparticles. Drug Deliv. 15(5):343-346.

Schoener CA, Hutson HN, Peppas NA. 2012. pH-responsive hydrogels with dispersed hydrophobic nanoparticles for the delivery of hydrophobic therapeutic agents. Polym. Int. 61:874-879.

Schwendener RA, Lagocki PA, Rahman YE. 1984. The effects of charge and size on the interaction of unilamellar liposomes with macrophages. Biochim. Biophys. Acta (BBA) - Biomembranes 772(1):93-101.

Service RF. 2010. Nanoparticle trojan horses gallop from the lab into the clinic. Science 330:314-315.

Shi J, Votruba AR, Farokhzad OC, Langer R. 2010. Nanotechnology in drug delivery and tissue engineering: from discovery to applications. Nano Lett. 10(9):3223-3230.

Singh AK, Chaurasiya A, Singh M, Upadhyay SC, Mukherjee R, Khar RK. 2008. Exemestane loaded self-microemulsifying drug delivery system (SMEDDS): Development and optimization. AAPS PharmSciTech 9(2):628-634.

Sinha VR, Bansal K, Kaushik R, Kumria R, Trehan A. 2004. Poly-epsiloncaprolactone microspheres and nanospheres: an overview. Int. J. Pharm. 278:1-23.

Slamon DJ, Leyland-Jones B, Shak S, Fuchs H, Paton V, Bajamonde A, Fleming T, Eiermann W, Wolter J, Pegram M, Baselga J, Norton L. 2001. Use of chemotherapy plus a monoclonal antibody against HER2 for metastatic breast cancer that overexpresses HER2. N Engl. J. Med. 344:783-792.

Smith IE, Dowsett M, Ebbs SR, Dixon JM, Skene A, Blohmer JU, Ashley SE, Francis S, Boeddinghaus I, Walsh G. 2005. Neoadjuvant treatment of postmenopausal breast cancer with anastrozole, tamoxifen, or both in combination: the Immediate Preoperative Anastrozole, Tamoxifen, or Combined with Tamoxifen (IMPACT) multicenter double-blind randomized trial. J. Clin. Oncol. 23(22):5108-5116.

Snehalatha M, Venugopal K, Saha RN, Babbar AK, Sharma RK. 2008. Etoposide loaded PLGA and PCL nanoparticles II: biodistribution and pharmacokinetics after radiolabeling with Tc-99m. Drug Deliv. 15(5):277-287.

Soppimath KS, Aminabhavi TM, Kulkarni AR, Rudzinski WE. 2001. Biodegradable polymeric nanoparticles as drug delivery devices. J. Controlled Rel. 70(1-2):1-20.

Sourdaine P, Parker MG, Telford J, Miller WR. 1994. Analysis of the aromatase cytochrome P450 gene in human breast cancers. J. Mol. Endocrinol. 13(3):331-337.

Spigel DR, Burstein HJ. 2002. HER2 overexpressing metastatic breast cancer. Curr. Treat. Options Oncol. 3:163-174.

Stella B, Arpicco S, Peracchia MT, Desmaële D, Hoebeke J, Renoir M, D'Angelo J, Cattel L, Couvreur P. 2000. Design of folic acid-conjugated nanoparticles for drug targeting. J. Pharm. Sci. 89:1452-1464.

Storey RF, Taylor AE. 1996. Effect of stannous octoate concentration on the ethylene glycol-initiated polymerization of epsilon-caprolactone. Abstr. Pap. Am. Chem. Soc. 211:114-120.

Storm G, Belliot SO, Daemen T, Lasic DD. 1995. Surface modification of nanoparticles to oppose uptake by the mononuclear phagocyte system. Adv. Drug Deliv. Rev. 17:31-48.

Struck RF, Alberts DS, Horne K, Phillips JG, Peng YM, Roe DJ. 1987. Plasma pharmacokinetics of cyclophosphamide and its cytotoxic metabolites after intravenous versus oral administration in a randomized, crossover trial. Cancer Res. 47:2723-2726.

Sudimack J, Lee RJ. 2000. Targeted drug delivery via the folate receptor. Adv. Drug Deliv. Rev. 41:147-162.

Sutton D, Nasongkla N, Blanco E, Gao J. 2007. Functionalized micellar systems for cancer targeted drug delivery. Pharm. Res. 24(6):1029-1046.

Takae S, Akiyama Y, Otsuka H, Nakamura T, Nagasaki Y, Kataoka K. 2005. Ligand density effect on biorecognition by PEGylated gold nanoparticles: regulated interaction of RCA120 lectin with lactose installed to the distal end of tethered PEG strands on gold surface. Biomacromolecules 6(2):818-824.

Tang CK, Gong XQ, Moscatello DK, Wong AJ, Lippman ME. 2000. Epidermal growth factor receptor vIII enhances tumorigenicity in human breast cancer. Cancer Res. 60(11):3081-3087.

Thun MJ, DeLancey JO, Center MM, Jemal A, Ward EM. 2010. The global burden of cancer: priorities for prevention. Carcinogenesis 31(1):100-110.

Thürlimann B, Keshaviah A, Coates AS, Mouridsen H, Mauriac L, Forbes JF, Paridaens R, Castiglione-Gertsch M, Gelber RD, Rabaglio M, Smith I, Wardley A, Price KN, Goldhirsch A. 2005. A comparison of letrozole and tamoxifen in postmenopausal women with early breast cancer. N. Engl. J. Med. 353(26):2747-2757.

Torchilin VP. 2006. Multifunctional nanocarriers. Adv. Drug. Deliv. Rev. 58(14):1532-1555.

Torchilin VP. 2008. Antibody-modified liposomes for cancer chemotherapy. Expert Opin. Drug Deliv. 5:1003-1025.

Troutman MD, Thakker DR. 2003. Novel experimental parameters to quantify the modulation of absorptive and secretory transport of compounds by P-glycoprotein in cell culture models of intestinal epithelium. Pharm. Res. 20:1210-1224.

Urien S, Brain E, Bugat R, Pivot X, Lochon I, van MLV, Vauzelle F, Lokiec F. 2005. Pharmacokinetics of platinum after oral or intravenous cisplatin: a phase 1study in 32 adult patients. Cancer Chemother. Pharmacol. 55:55-60.

Van Natta FJ, Hill JW, Carruthers WH. 1934. Polymerization and ring formation, ε-caprolactone and its polymers. J. Am. Chem. Soc. 56:455-459.

Venturoli D, Rippe B. 2005. Ficoll and dextran vs. globular proteins as probes for testing glomerular permselectivity: effects of molecular size, shape, charge, and deformability. Am. J. Physiol. Renal Physiol. 288:F605-F613.

Viale G, Regan MM, Maiorano E, Mastropasqua MG, Dell'Orto P, Rasmussen BB, Raffoul J, Neven P, Orosz Z, Braye S, Ohlschlegel C, Thürlimann B, Gelber RD, Castiglione-Gertsch M, Price KN, Goldhirsch A, Gusterson BA, Coates AS. 2007. Prognostic and predictive value of centrally reviewed expression of estrogen and progesterone receptors in a randomized trial comparing letrozole and tamoxifen adjuvant therapy for postmenopausal early breast cancer: BIG 1-98. J. Clin. Oncol. 25(25):3846-3852.

Vogel CL, Cobleigh MA, Tripathy D, Gutheil JC, Harris LN, Fehrenbacher L, Slamon DJ, Murphy M, Novotny WF, Burchmore M, Shak S, Stewart SJ, Press M. 2002. Efficacy and safety of trastuzumab as a single agent in first-line treatment of HER2-overexpressing metastatic breast cancer. J. Clin. Oncol. 20(3):719-726.

von Pawel J, Gatz emeier U, Pujol JL, Moreau L, Bildat S, Ranson M, Richardson G, Steppert C, Rivière A, Camlett I. 2001. Phase II comparator study of oral versus intravenous topotecan in patients with chemosensitive small-cell lung cancer. J. Clin. Oncol. 19:1743-1749.

Vonarbourg A, Passirani C, Saulnier P, Benoit JP. 2006. Parameters influencing the stealthiness of colloidal drug delivery systems. Biomaterials 27(24):4356-4373.

Wagner V, Dullaart A, Bock AK, Zweck A. 2006. The emerging nanomedicine landscape. Nat. Biotechnol. 24(10):1211-1217.

Wang AZ, Gu F, Zhang L, Chan JM, Radovic-Moreno A, Shaikh MR, Farokhzad OC. 2008. Biofunctionalized targeted nanoparticles for therapeutic applications. Expert Opin. Biol. Ther. 8(8):1063-1070.

Wang L, Chaw CS, Yang YY, Moochhala SM, Zhao B, Ng S, Heller J. 2004. Preparation, characterization, and in vitro evaluation of physostigmine-loaded poly(ortho ester) and poly(ortho ester)/poly(D,L-lactide-co-glycolide) blend microspheres fabricated by spray drying. Biomaterials 25(16):3275-3282.

Weber J. 2007. Review: AntiCTLA-4 antibody ipilimumab: case studies of clinical response and immune-related adverse events. Oncologist 12:864-872.

Weiner LM, Adams GP. 2000. New approaches to antibody therapy. Oncogene 19:6144-6151.

Weiss RB. 1992. The anthracyclines: will we ever find a better doxorubicin? Semin. Oncol. 19:670-686.

Wilson DS, Szostak JW. 1999. In vitro selection of functional nucleic acids. Annu. Rev. Biochem. 68:611-647.

Wilson RHP, Adam R, Eatock J, Boddy MM, Griffin AV, Miller MR, Matsumura Y, Shimizu T, Calvert V. 2008. Phase I and pharmacokinetic study of NC-6004, a new platinum entity of cisplatin-conjugated polymer forming micelles. J. Clin. Oncol. (Meeting Abstracts) 26:2573.

Wu J, Akaike T, Maeda H. 1998. Modulation of enhanced vascular permeability in tumors by a Bradykinin antagonist, a cyclooxygenase inhibitor, and a nitric oxide scavenger. Cancer Res. 58:159-165.

Yadav KS, Sawant KK. 2010. Modified nanoprecipitation method for preparation of cytarabine-loaded PLGA nanoparticles. AAPS Pharmscitech 11(3):1456-1465.

Yarden Y. 2001a. Biology of HER2 and its importance in breast cancer. Oncology 61 Suppl 2:1-13.

Yarden Y. 2001b. The EGFR family and its ligands in human cancer signalling mechanisms and therapeutic opportunities. Eur. J. Cancer 37 Suppl 4:S3-8.

Yarden Y, Sliwkowski MX. 2001. Untangling the ErbB signalling network. Nat. Rev. Mol. Cell. Biol. 2(2):127-137.

Yokoyama M, Okano T, Sakurai Y, Ekimoto H, Shibazaki C, Kataoka K. 1991. Toxicity and antitumor activity against solid tumors of micelle-forming polymeric anticancer drug and its extremely long circulation in blood. Cancer Res. 51:3229-3236.

Yoo HS, Park TG. 2004. Folate receptor targeted biodegradable polymeric doxorubicin micelles. J. Controlled Rel. 96:273-283.

Yuan F, Dellian M, Fukumura D, Leunig M, Berk DA, Torchilin VP, Jain RK. 1995. Vascular permeability in a human tumor xenograft: molecular size dependence and cutoff size. Cancer Res. 55(17):3752-3756.

Zambaux MF, Bonneaux F, Gref R, Dellacherie E, Vigneron C. 1999. Preparation and characterization of protein C-loaded PLA nanoparticles. J. Controlled Rel. 60(2-3):179-188.

Zhang S, Uludag H. 2009. Nanoparticulate systems for growth factor delivery. Pharm. Res. 26:1561-1580.

Zidan AS, Sammour OA, Hammad MA, Megrab NA, Hussain MD, Khan MA, Habib MJ. 2006. Formulation of anastrozole microparticles as biodegradable anticancer drug carriers. AAPS PharmSciTech 7(3):E38-E46.

Zweers MLT, Grijpma DW, Engbers GHM, Feijen J. 2003. The preparation of monodisperse biodegradable polyester nanoparticles with a controlled size. J. Biomed. Mater. Res. Part B: Appl. Biomater. 66B:559-566.

Chapter 3

ANALYTICAL METHODS

3.1 Materials

Anastrozole and Exemestane were received as gift samples from Sun Pharma Advance Research Centre, Vadodara, India. Monobasic potassium phosphate, tri ethyl amine (TEA), sodium hydroxide, hydrochloric acid and acetonitrile were of HPLC grade and procured from S.D. Fine Chemicals, Vadodara, India. Double distilled water (DDW) was purified by passing through 0.45µ Millipore filters (Millipore, Bangalore, India).

3.2 Estimation method for anastrozole

3.2.1 High Performance Liquid Chromatography (HPLC)

Quantitative estimation of anastrozole (ATZ) was done by HPLC as described by Mendes et al. with slight modifications [Mendes et al. 2007]. The HPLC system (Shimadzu, Japan) composed of a UV-visible spectrophotometric detector. The separation was performed on a reversed phase C-18 HPLC column (Lichro Cart – RP8, 250 mm × 4.6 mm, 5 µ). Column temperature was maintained at 25 °C throughout the experiment using column oven. A filtered and degassed mixture of buffer (phosphate buffer, 2 g monobasic potassium phosphate in 1000 ml of double distilled water and pH adjusted to 6.0 with TEA) and acetonitrile (60:40) was used as mobile phase. The run time was 10 min and the retention time was 5.2 min. The mobile phase was delivered at a flow rate of 1.5 ml/min, the injection volume was 20 µl and the effluent was monitored at ultraviolet detection at 215 nm. Data processing was done using Spinchrom CFR (Spinchotech, Japan).

3.2.2 Preparation of standard stock solutions

Stock solution of ATZ was prepared in acetonitrile by accurately weighing 10 mg of ATZ in 10 ml (1000 µg/ml) acetonitrile. Further dilution was performed using mobile phase.

3.2.3 Preparation of calibration curve

Suitable aliquots of standard stock solution were accurately measured and transferred to the 10 ml volumetric flask to prepare a working stock solution of ATZ (100 µg/ml). Suitable aliquots of working stock solution were accurately measured and transferred to 10 ml volumetric flasks. The final volume was made up to 10 ml with the mobile phase to give final concentrations of 8, 16, 24, 32 and 40 µg/ml. Standards were analyzed by RP HPLC at UV detection wavelength 215 nm and mobile phase flow rate 1.5 ml/min. After 10 min elution, results were processed using data processing software Spinchrom CFR. The above procedure was repeated three times and results recorded in

the table 3.1 and shown in figure 3.1 and 3.2. All the estimations were carried out at 25 °C, and care was taken to prevent solvent evaporation at every stage of estimation. Calibration plot was constructed for the measured area against drug concentration. Accuracy and precision of the method was determined by performing recovery studies after addition of known concentration of ATZ.

Table 3.1 Calibration curve of ATZ by HPLC at 215 nm, Data presented as Mean ± SD, n=3.

Concentration (µg/ml)	Retention time (min)	Area (mV.s)
8	5.17	117.58 ± 4.97
16	5.17	244.27 ± 8.86
24	5.16	396.70 ± 7.93
32	5.17	519.24 ± 7.80
40	5.18	640.81 ± 10.52

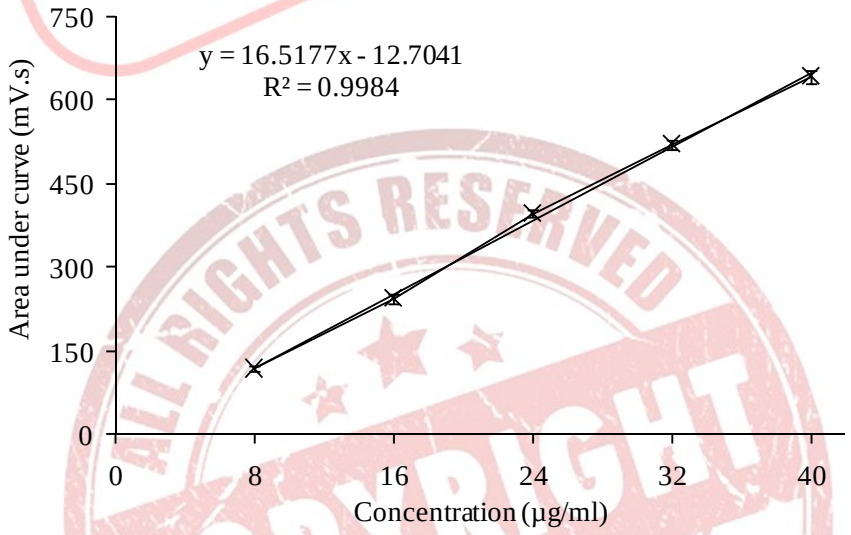

Figure 3.1 Regressed calibration curve of ATZ by HPLC at 215 nm. Data presented as Mean ± SD, n=3 (some error bars are too small to be shown).

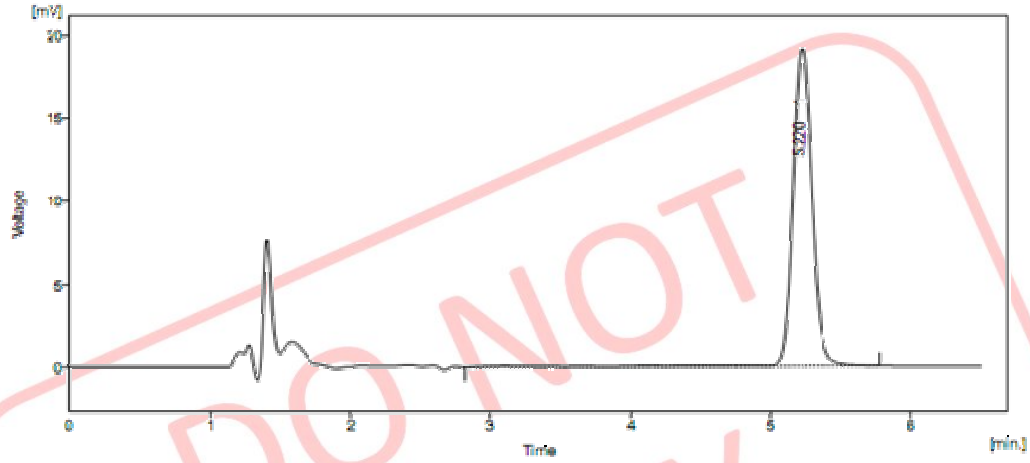

Figure 3.2 Chromatogram of ATZ solution by HPLC at 215 nm.

3.2.4 Analytical method validation

The method was validated for accuracy, precision and linearity.

3.2.4.1 Linearity

The linearity of an analytical method is its ability to elicit, test results that are directly or by a well defined mathematical transformation proportional to the concentration of analyte in samples with a given range (Rifino 2003). A calibration curve is prepared by plotting a dependent variable (AUC, Y) as a function of an independent variable (concentration, X). For evaluation of the linearity of the HPLC method of ATZ, the standard solutions were prepared at 8, 16, 24, 32 and 40 µg/ml concentrations (n = 3) and AUC was calculated. The method was said to be linear for estimation of ATZ if it R^2 was near to 1. Least square regression method was used to determine the regression coefficient, r and the equation for the best fitting line.

This relation if found with a series of measurements, which in practice is often linear one.

$$Y = mX + C$$

Where,

m is a slope of line and C is the intercept on the Y axis.

Linearity of an analytical method for ATZ in mobile phase was established by the regression coefficient.

3.2.4.2 Accuracy

Accuracy of an analytical method is the closeness of test results obtained by that method to true value (The United States Pharmacopoeia 27 NF 22, 2004). Accuracy is

calculated from the test results as the % analyte recovered by assay. Accuracy was calculated by analysis of three replicate samples for the above described methods. The observed concentrations of the drug were then back calculated using the equation of standard calibration curve and compared with actual concentrations.

3.2.4.3 Precision

Precision of an analytical method is the degree of agreement among individual test results when the procedure is applied repeatedly to multiple sampling of homogenous sample (The United States Pharmacopoeia 27 NF 22, 2004). Precision may be measure of either the degree of reproducibility or of repeatability of the analytical method under normal operating conditions. The precision of an analytical method is usually expressed as the standard deviation or confidence limit. The standard deviation is calculated from following formula (Rifino 2003).

$SD = [\Sigma(X-x)/ n-1]^{½}$

Where, X – an individual measurement in a set.

x – Arithmetic mean of the set.

n – Total number of replicated measurement taken in set.

Precision between different samples can be compared with RSD as follows:

% RSD = [SD/ Mean]* 100

The intra- and inter day precision of the assay were calculated by replicate analysis of the solutions of known concentrations of ATZ at three quality control concentration (Low quality control concentration [LQC], Medium quality control concentration [MQC] and High quality control concentration [HQC] levels). The observed concentrations of the drug were then back calculated (from AUC) using the equation of standard calibration curve. The variations between the observed concentrations were determined by calculating the % RSD (Rifino 2003).

In order to determine the accuracy and precision of the developed method, known amounts of ATZ at low, medium and high concentration (12, 24 and 36 µg/ml) were subjected to recovery studies as per the procedure described earlier. All standard samples were also performed for intraday and interday variability. The results obtained are tabulated in table 3.2 and 3.3.

Intraday precision of the assay

Primary stock solutions were appropriately diluted using suitable solvent to obtain final concentration of 12 (LQC), 24 (MQC) and 36 µg/ml (HQC). Three different sets of

primary stock solutions were prepared and diluted in the similar manner. The AUC was calculated three times on the same day. The solutions were prepared freshly each time. The % relative error was calculated and the results recorded.

The % relative error was calculated using the formula, (Rifino 2003)

$$\% \text{ Relative error} = \frac{[\text{Observed value} - \text{True value}]}{\text{True value}} * 100$$

Interday precision of the assay

Primary stock solutions were appropriately diluted using suitable solvent to obtain final concentration of 12 (LQC), 24 (MQC) and 36 µg/ml (HQC). Three different sets of primary stock solutions were prepared and diluted in the similar manner and AUC was calculated on three consecutive days. The solutions were prepared freshly on each time. The % relative error was calculated and the results recorded.

Table 3.2 Accuracy of ATZ measurement using mobile phase at 215 nm.

Conc. of ATZ (µg/ml)	RT	Area (mV.s)	Conc. of ATZ obtained (µg/ml)	Accuracy	Precision (RSD %)
12	5.12	196.82 ± 6.64	12.68	99.23	0.769
24	5.11	398.64 ± 7.79	24.90	100.49	0.489
36	5.15	599.80 ± 3.75	37.08	100.79	0.799

Table 3.3 Precision of ATZ measurement using mobile phase at 215 nm, Data presented as Mean, n=3.

Conc. (µg/ml)	Measured conc. (µg/ml)		Accuracy (%)	
	Intra day	Inter day	Intra day	Inter day
12	12.68	12.71	99.23	100.22
24	24.90	25.01	100.49	100.40
36	37.08	36.88	100.79	99.45

3.2.5 Estimation of ATZ in nanoparticulate formulations

Nanoparticulate formulations (PLGA, PLGA PEG, PCL and PCL PEG NPs) were dissolved in required amount of acetonitrile to obtain the final concentration of ATZ ranging

between 8 to 40 µg/ml. The contents were gently mixed to ensure uniform mixing and kept aside for 30 min at room temperature. The samples were filtered using 0.2 µ membrane filter and the filtrate was collected and estimated by RP HPLC at UV detection wavelength 215 nm and mobile phase flow rate 1.5 ml/min. Results were processed using data processing software Spinchrom CFR.

3.3 Estimation method for Exemestane

3.3.1 High Performance Liquid Chromatography (HPLC)

Quantitative estimation of exemestane (EXE) was done by HPLC as reported by Breda et al. with slight modifications [Breda et al. 1993]. The HPLC system (Shimadzu, Japan) composed of a UV-visible spectrophotometric detector. The separation was performed on a reversed phase C-18 HPLC column (Lichro Cart – RP8, 250 mm × 4.6 mm, 5 µ). Column temperature was maintained at 25 °C throughout the experiment using column oven. A filtered and degassed mixture of acetonitrile:0.02M phosphate buffer (pH 4.0) (75:25) was used as mobile phase. The run time was 10 min and the retention time of EXE was 5.0 min. The mobile phase was delivered at a flow rate of 1.0 ml/min, the injection volume was 20 µl and the effluent was monitored at ultraviolet detection at 247 nm. Data processing was done using Spinchrom CFR (Spinchotech, Japan).

3.3.2 Preparation of standard stock solutions

Stock solution of EXE was prepared in acetonitrile by accurately weighing 10 mg of EXE in 10 ml (1000 µg/ml) acetonitrile. Further dilution was performed using mobile phase.

3.3.3 Preparation of calibration curve

Suitable aliquots of standard stock solution were accurately measured and transferred to the 10 ml volumetric flask to prepare a working stock solution of EXE (100 µg/ml). Suitable aliquots of working stock solution were accurately measured and transferred to 10 ml volumetric flasks. The final volume was made up to 10 ml with the mobile phase to give final concentrations of 8, 16, 24, 32 and 40 µg/ml. Standards were analyzed by RP HPLC at UV detection wavelength 247 nm and mobile phase flow rate 1.0 ml/min. After 10 min elution, results were processed using data processing software Spinchrom CFR. The above procedure was repeated three times and results recorded in the table 3.4 and shown in figure 3.3 and 3.4. All the estimations were carried out at 25 °C, and care was taken to prevent solvent evaporation at every stage of estimation. Calibration plot was constructed for the measured area against drug concentration.

Accuracy and precision of the method was determined by performing recovery studies after addition of known concentration of EXE.

Table 3.4 Calibration curve of EXE by HPLC at 247 nm, Data presented as Mean ± SD, n=3.

Concentration (µg/ml)	Retention time (min)	Area (mV.s)
8	5.02	174.34 ± 7.52
16	5.01	344.44 ± 6.74
24	5.03	532.47 ± 7.51
32	5.02	708.61 ± 9.23
40	5.01	917.14 ± 10.06

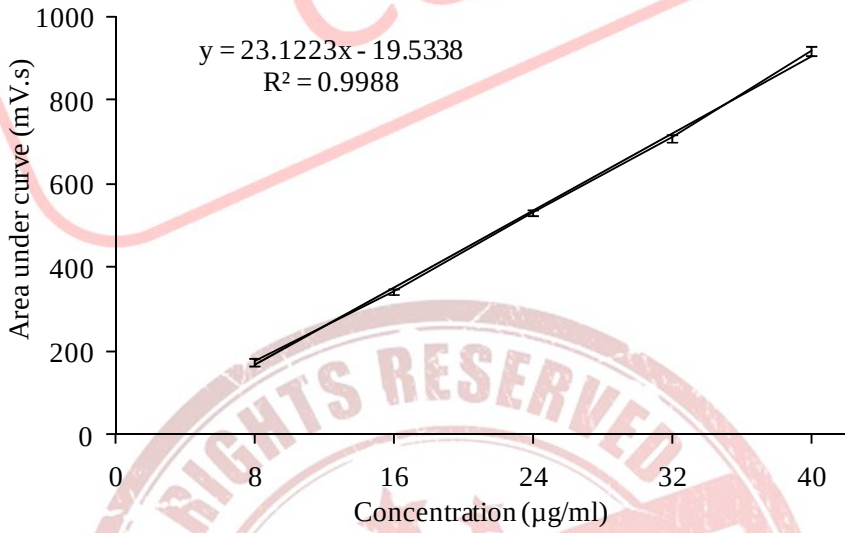

Figure 3.3 Regressed calibration curve of EXE by HPLC at 247 nm. Data presented as Mean ± SD, n = 3 (some error bars are too small to be shown).

3.3.4 Accuracy and Precision

In order to determine the accuracy and precision of the developed method, known amounts of EXE were subjected to recovery studies at low medium and high concentration (12, 24, and 36 µg/ml) as per the procedure described earlier. All standard samples were also performed for intraday and interday variability. The results obtained are tabulated in table 3.5 and 3.6.

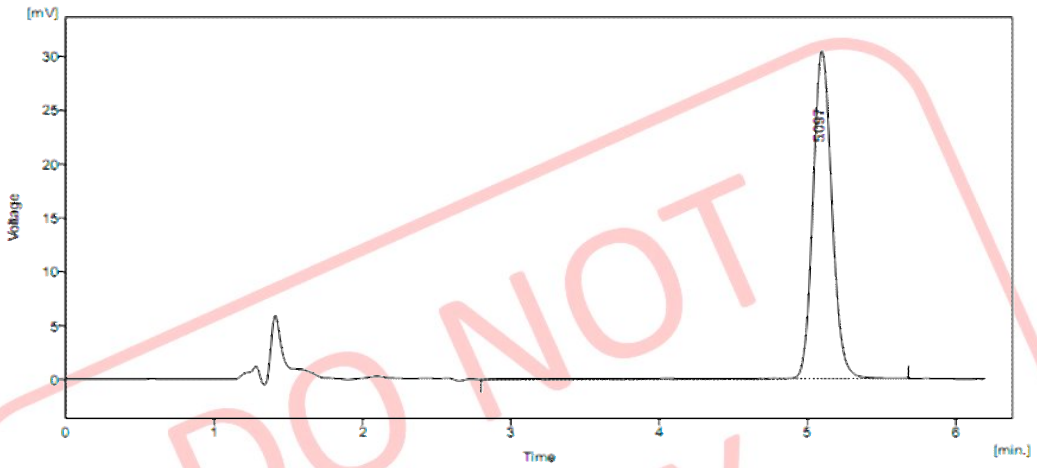

Figure 3.4 Chromatogram of EXE solution by HPLC at 247 nm.

Table 3.5 Accuracy of EXE measurement using mobile phase at 247 nm.

Conc. of EXE (µg/ml)	RT	Area (mV.s)	Conc. of EXE obtained (µg/ml)	Accuracy	Precision (RSD %)
12	5.02	264.55 ± 3.17	12.28	99.37	0.633
24	5.02	536.43 ± 5.51	24.04	100.74	0.744
36	5.01	796.99 ± 7.24	35.31	99.78	0.214

Table 3.6 Precision of EXE measurement using mobile phase at 247 nm, Data presented as Mean, n=3.

Conc (µg/ml)	Measured conc (µg/ml)		Accuracy (%)	
	Intra day	Inter day	Intra day	Inter day
12	12.28	12.30178	99.37	100.1376
24	24.04	23.87716	100.74	99.27881
36	35.31	35.17743	99.78	99.60535

3.3.5 Estimation of EXE in nanoparticulate formulations

Nanoparticulate formulations (PLGA, PLGA PEG, PCL and PCL PEG NPs) were dissolved in required amount of acetonitrile to obtain the final concentration of ATZ ranging between 8 to 40 µg/ml. The contents were gently mixed to ensure uniform mixing and

kept aside for 30 min at room temperature. The samples were filtered and the filtrate was collected and estimated by RP HPLC at UV detection wavelength 247 nm and mobile phase flow rate 1.0 ml/min. Results were processed using data processing software Spinchrom CFR.

3.4 References

Rifino CB. 2003. Pharmaceutical Process Validation. In: Robert AN, Wachter AH (Eds.) Process Validation and Quality Assurance. Switzerland: Marcel Dekker, Inc., 1-43.

The United States Pharmacopoeia 27, NF 22, United States Pharmacopoeial convention, Rockville, MD, 2004.

Mendes GD, Hamamoto D, Ilha J, Pereira Ados S, De Nucci G. 2007. Anastrozole quantification in human plasma by high-performance liquid chromatography coupled to photospray tandem mass spectrometry applied to pharmacokinetic studies. J. Chromatogr. B Analyt. Technol. Biomed. Life Sci. 850(1-2): 553-559.

Breda M, Pianezzola E, Benedetti MS. 1993. Determination of exemestane, a new aromatase inhibitor, in plasma by high-performance liquid chromatography with ultraviolet detection. J. Chromatogr. 620: 225-231.

Chapter 4

FORMULATION, OPTIMIZATION AND CHARACTERIZATION OF NANOPARTICULATE FORMULATIONS

4.1 Introduction

Breast cancer is the leading cause of death among women, with one million new cases in the world each year [McPherson et al. 2000], out of which one-third are reported to be hormone-dependent [Henderson and Canellos 1980; Theobald 2000]. Growth of breast cancer cells is often estrogen-dependent. Continuous estrogen suppression in patients with hormone sensitive breast cancer prevents proliferation of tumor. Aromatase is the key enzyme that converts androgens to estrogens both in pre- and post-menopausal women [Lonning 1998; Strassmer-Weippl and Goss 2003]. Treatment of breast cancer has included efforts to decrease estrogen levels by the use of antiestrogen and progestational agents [Chowdhury and Ellis 2005]. Anastrozole (ATZ) is a nonsteroidal aromatase inhibitor. The problems associated with oral delivery of ATZ are low aqueous solubility, short half-life and uncontrolled release [Sarkar and Yang 2008]. Exemestane (EXE) is a third generation, potent irreversible Type I steroidal aromatase inhibitor approved by the Food and Drug Administration (FDA) for the treatment of breast cancer [Johannessen et al. 1997]. It acts as a false substrate for the aromatase enzyme, and is processed to an intermediate that binds irreversibly to the active site of the enzyme causing its inactivation, an effect also known as suicide inhibition [Dowsett 1998]. Although treatment with orally administered EXE has been shown to be well tolerated by patients, the most common adverse events consist of hot flashes, nausea, fatigue, dizziness, increased sweating, headache, body weight change, vaginal dryness, arthralgias, and myalgias [Clemett and Lamb 2000; Scott and Wiseman 1999]. The problem with the oral delivery of EXE is its inability to target the tumor site. This problem can be overcome by employing delivery systems capable of providing targeted drug delivery.

One of the technological resources to improve the availability of drugs at the site of action is by colloidal carriers like nanoparticles (NPs) prepared using biodegradable polymers like poly(d,l-lactic-co-glycolic acid) (PLGA) and poly caprolactone (PCL) [De Jong and Borm 2008]. PLGA has been studied extensively as a polymeric carrier for NPs. PLGA nanoparticles (NPs) are already reported to provide passive targeting of anticancer drugs to tumor site [Fonseca et al. 2002; Yallapu et al. 2010]. A wide variety of drugs ranging from small molecular-weight therapeutic agents to peptide hormones, antibiotics, and chemotherapeutic drugs have been formulated using PLGA [Tuncay et

al. 2000]. PLGA NPs have proven to be successful targeted drug delivery systems for different classes of drugs, such as anticancer drugs like etoposide [Snehalatha et al. 2008] and rapamycin [Acharya et al. 2009], proteins and peptides like insulin [Shi et al. 2009] and steroidal hormones like estrogen [Kwon et al. 2001]. PCL is biodegradable polyester and is prepared by ring opening polymerization of ε-caprolactone. PCL is degraded by hydrolysis of its ester linkages in physiological conditions and has therefore received a great deal of attention for use as a biomaterial for sustained release drug delivery systems [Aberturas et al. 2011; Lam et al. 2008]. Different methods reported for preparing NPs using biodegradable polymers include monomer polymerization, interfacial deposition, salting out, nanoprecipitation, emulsification solvent evaporation, etc. [Quintanar-Guerrero et al. 1998]. Interfacial deposition of preformed polymer technique is based upon interfacial deposition of a polymer followed by diffusion of a semi polar and miscible solvent in aqueous medium containing surfactant [Barichello et al. 1999; Fessi et al. 1989]. Moraes et al. used this method for preparation of PLGA nanocapsules with particle size of 123 nm and 69% drug loading [Moraes et al. 2009]. Formulation of NPs by this method involves many important factors which contribute to the outcome of experiment in terms of drug entrapment and particle size. Different process variables include stirring speed, temperature, rate of addition of organic phase to aqueous phase, etc. Different formulation variables include drug:polymer ratio, concentration of polymer in organic phase, surfactants, surfactant concentration, volume of aqueous and organic phase, organic solvents, etc.

Optimization of any pharmaceutical process begins with the objectives to find out and evaluate independent variables that affect formulation response, determine them and establish their best response values. However, considering the cost of the drugs and polymers, it is desirable to optimize the formulation development with minimum batches with maximum desired characteristics. While developing formulations, various formulations as well as process variables related to effectiveness, safety and usefulness should be simultaneously optimized. Polynomial non-linear regression analysis are widely used for establishing approximate mathematical models in which the variables are screened by stepwise selection method according to statistical significance [Miller 1984; Wagner and Shimshak 2007] and final model would be used to predict the

relationship between different variables and their levels. But such predictions are often limited to low levels, resulting in poor estimation of optimum formulation [Levison et al. 1994; Shirakura et al. 1991]. Therefore, it is important to understand the complexity of pharmaceutical formulations by using established statistical tools such as multiple regression analysis (MRA), Box Behnken design (BBD), etc. Optimization by changing one-variable-at-a-time is a complex method to evaluate the effects of different variables on an experimental outcome. This approach assesses one variable at a time instead of all simultaneously. The method is time-consuming, expensive and often leads to misinterpretation of results when interactions between different components are present. Another approach is to accurately evaluate the impact of the independent variables on the dependent variables by varying all the important factors simultaneously in a systematic manner. This approach is known as response surface methodology (RSM). RSM is a statistical technique which can address the present scenario and can be used to establish relationships between several independent variables and one or more dependent variables [Myer and Montogomery 2002; Ray et al. 2009]. RSM optimizes multiple variables by systematic variation of all variables in a well-designed experiment with a minimum number of experiments. The RSM optimization process involves the following steps: performing statistically designed experiments; estimating the coefficients of a mathematical model using regression analysis technique; and predicting the response and checking the adequacy of the model. Among the available statistical design methods, a full factorial design (FFD) involves a large number of experiments for accurately predicting the response. At the same time, it is often considered unpractical due to its requirement of more number of experiment as compared to other designs [Box et al. 1978; Myer et al. 1989]. Fractional factorial design lacks the ability to accurately predict all positions of the factor space that are equidistant from the centre (rotatability). Based upon the desirable features of orthogonality and rotatability, Central Composite design (CCD) and BBD are commonly chosen for the purpose of response optimization [Bae and Shoda 2005; Ray 2006]. BBD is successfully used by Rahman et al. for optimization of risperidone loaded solid lipid nanoparticles [Rahman et al. 2010]. The BBD requires fewer runs than 3-factor, 3-level FFD and CCD when three or more variables are involved. This cubic design is characterized by a set of points lying at the midpoint of each edge and a replicate centre

point of the multidimensional cube [George Box 1960]. The BBD technique is a three-level design based upon the combination of two-level factorial designs and incomplete block designs. BBD is a spherical design with excellent predictability within the spherical design space. Compared to the CCD method, the BBD technique is considered as the most suitable for evaluating quadratic response surfaces particularly in cases when prediction of response at the extreme level is not the goal of the model. In addition, the BBD technique is rotatable or nearly rotatable regardless of the number of factors under consideration [Bae and Shoda 2005; Myer and Montogomery 2002; Ray 2006]. Also, it is very time consuming method. Hence, deriving a quantitative mathematical relationship between the variables to evaluate its effect on dependent variables is of utmost importance [Mehta et al. 2007; Seth and Misra 2002].

The number of formulations required for such studies is dependent on the number of independent variables selected after preliminary experiments. The dependent response is measured for each trial and then either simple linear equation (equation 1), or interactive equation (equation 2) or quadratic model (equation 3) is fitted by carrying out MRA and F-statistic to identify statistically significant terms.

$$Y = b_0 + b_1X_1 + b_2X_2 + b_3X_3 \quad (1)$$

$$Y = b_0 + b_1X_1 + b_2X_2 + b_3X_3 + b_{12}X_1X_2 + b_{13}X_1X_3 + b_{23}X_2X_3 + b_{123}X_1X_2X_3 \quad (2)$$

$$Y = b_0 + b_1X_1 + b_2X_2 + b_3X_3 + b_{12}X_1X_2 + b_{13}X_1X_3 + b_{23}X_2X_3 + b_1^2X_{11} + b_2^2X_{22} + b_3^2X_{33} + b_{123}X_1X_2X_3 \quad (3)$$

where, Y is estimated response; b_0 is constant; b_1, b_2, b_3 are linear coefficients; b_{12}, b_{23}, b_{13} are interaction coefficients; and b_1^2, b_2^2, b_3^2 are quadratic coefficients.

Based on the results obtained in preliminary experiments, variables which are found to be influencing majorly to dependent variables were selected to find the optimized condition required for higher PDE and lower PS using MRA. In developing the regression equation, the test factors were coded according to the equation 4.

$$x_i = (X_i - X_i^X) / \Delta X_i \quad (4)$$

where, x_i is the coded value of the i^{th} independent variable, X_i is the natural value of the i^{th} independent variable, X_i^X is the natural value of the i^{th} independent variable at the center point and ΔX_i is the step change value.

Equation for quadratic model (equation 3) can be summarized as,

$$Y = b_0 + \sum_i b_iX_i + \sum_i \sum_j b_{ij}X_iX_j + \sum b_{ii}X_i^2 \quad (5)$$

where Y is the measured response, b_0 is the intercept term, b_i, b_{ij} and b_{ii} are, respectively the measures of the variables X_i, X_iX_j and X_i^2. The variable X_iX_j represents the first order interactions between X_i and X_j ($i < j$). A full model (FM) was established after putting the values of regression coefficients in equation 5.

4.2 Materials

Anastrozole and Exemestane were received as gift sample from Sun Pharma Advanced Research Centre, Vadodara, India. Poly (D, L Lactide-co-Glycolide) (PLGA 50:50, inherent viscosity 0.2 dl/g) was received as gift sample from PURAC Biomaterials, Gorinchem, Netherlands. Poloxamer 188 was obtained as gift sample from BASF, Ludwigshafen, Germany. Capric/caprylic triglyceride (Capmul MCM, C8) was obtained as gift sample from Abitec Corporation, Janesville, USA. Caprolactone monomer and Sulpho-NHS were purchased from Sigma-Aldrich, Mumbai, India. All other chemicals were of analytical reagent grade and obtained commercially.

4.3 Synthesis of polymer and conjugates

4.3.1 Synthesis of PLGA-PEG conjugate

PLGA-PEG conjugate was synthesized using N-Hydroxysuccinimide (NHS) and 1-ethyl-3-(3-dimethylaminopropyl) carbodiimide hydrochloride (EDC) as an activator [Chaudhari et al. 2012]. Carboxylic group of PLGA (1.7 g) was activated by addition of NHS (240 mg) and EDC (384 mg) in dichloromethane (DCM) (free from moisture) to form PLGA-NHS. The reaction mixture was stirred in tightly closed flask under nitrogen blanket for 12 h. PLGA-NHS was then precipitated with addition of ice cold methanol. Reaction mixture was centrifuged at 50,000×g for 5 min to collect activated PLGA. Precipitation process was repeated again to remove excess EDC and NHS by dissolving it in small quantity of acetone and again precipitated in ice cold methanol. Residual methanol was then evaporated using rotary flask evaporator. Activated PLGA was dissolved in DCM followed by addition of amine-PEG-carboxylic acid (600 mg) which was allowed to react for 12 h. Reaction mixture was precipitated in double distilled water and centrifuged at 50,000×g for 5 min to collect PLGA-PEG. Precipitation process was repeated twice to remove un-reacted PEG and the product was lyophilized (Heto Drywinner, Allerod, Denmark). Lyophilized product was stored under refrigeration till

further use. Each reaction step as well as purification step were monitored by TLC using 100% ethyl acetate as a mobile phase and iodine as a spotting reagent. Characterization of conjugate was done by FTIR, NMR and GPC.

4.3.2 Synthesis of cPCL

Synthesis of carboxylated PCL was carried out by ring opening polymerization of caprolactone monomer in presence of succinic acid as reported by Zhang et al. with some modifications [Zhang et al. 1994]. Reaction was carried out at room temperature in presence of tertiary butoxide (4 g) for 24 h instead of heating reaction mixture at 225 °C for 3 h. Polymerization was carried out in a flask sealed with a ball filled with nitrogen. The reactant mixture of succinic acid (23.5 mg) and caprolactone (3.65 g) was added to about 15 ml of dichloromethane in the flask for initiation of polymerization reaction. The reaction was catalyzed using tertiary butoxide (4 g). The reaction was allowed to continue for 24 h. The reaction mixture was precipitated in ice cold water and precipitates were dissolved in acetone for re-precipitation and purification to remove excess succinic acid. Each reaction step as well as purification step was monitored by TLC using 100% ethyl acetate as a mobile phase and iodine as a spotting reagent. The reaction was considered to be complete when there was absence of spots for caprolactone monomer and succinic acid from the reaction mixture.

4.3.3 Synthesis of PCL-PEG conjugate

Caprolactone containing carboxylic acid groups was polymerized as per previous reported method [Kumar and Sawant 2013]. PCL-PEG conjugate was synthesized using NHS and EDC as an activator [Chaudhari et al. 2012]. Carboxylic group of PCL (1.75 g) was activated by addition of NHS (240 mg) and EDC (384 mg) in DCM (free from moisture) to form PCL-NHS. The reaction mixture was stirred in tightly closed flask under nitrogen blanket for 12 h. PCL-NHS was then precipitated with addition of ice cold methanol. Reaction mixture was centrifuged at 50,000×g for 5 min to collect activated PCL. Precipitation process was repeated again to remove excess EDC and NHS by dissolving it in small quantity of acetone and again precipitated in ice cold methanol. Residual methanol was then evaporated using rotary flask evaporator. Activated PCL was dissolved in DCM followed by addition of amine-PEG-carboxylic acid (600 mg) which was allowed to react for 12 h. Reaction mixture was precipitated in double distilled water and centrifuged at 50,000×g for 5 min to collect PCL-PEG. Precipitation

process was repeated twice to remove un-reacted PEG and the product was lyophilized (HetoDry, Germany). Lyophilized product was stored under refrigeration till further use. Each reaction step as well as purification step were monitored by TLC using 100% ethyl acetate as a mobile phase and iodine as a spotting reagent. Characterization of PCL and PCL-PEG conjugate was done by FTIR, NMR and GPC.

4.4 Characterization of polymer and conjugates

4.4.1 FTIR spectroscopy

The sample (2 mg) was finely grounded with purified potassium bromide (200 mg) (to remove scattering effects from large crystals). This powder mixture was then pressed in a mechanical die press to form a pellet. These pellets were scanned and spectra were recorded on FTIR (Bruker Corporation, USA). The scanning range was 400 - 4000 cm^{-1} with the resolution of 2 cm^{-1}.

4.4.2 NMR spectroscopy

The proton NMR spectrum of the conjugate was recorded to confirm formation of amide bond. Sample was dissolved in DMSO (deuterated, Merck Germany) and transferred to a 5 mm NMR tube. NMR tube containing sample was placed in 5 mm broad band probe head and pulse programming was performed using Brucker 300MHz (Switzerland) and the NMR spectra was recorded.

4.4.3 Molecular weight determination

Gel permeation chromatography (GPC) was carried out to determine the molecular weight of the formed polymer [Behan et al. 2001]. The molecular weight of PCL-PEG polymer was determined by GPC equipped with a Waters 510 pump, 50, 10–3, and 10–4 ºA Phenogel columns serially set (Phenomenex, USA) and a Waters 410 differential refractometer. The mobile phase was tetrahydrofuran at a flow rate of 1.0 ml/min. 50 µl of a 2% polymer solution in THF was injected into the system, and size exclusion chromatogram was recorded.

4.5 Formulation and optimization of ATZ loaded PLGA NPs

4.5.1 Preparation of ATZ loaded PLGA NPs

ATZ loaded PLGA NPs were prepared using solvent diffusion (nanoprecipitation) method [Fessi et al. 1989; Seju et al. 2011]. The optimized formulation was prepared by

dissolving PLGA (100 mg) and ATZ (5 mg) in 5 ml of acetone. This organic phase was added at the rate of 0.5 ml/min into 10 ml of aqueous phase containing 0.25% w/v Poloxamer 188 with continuous stirring on magnetic stirrer at room temperature. Stirring was continued for 3-4 h to allow complete evaporation of organic solvent. The NPs suspension was centrifuged at 50,000×g for 30 min at 4 °C (3K30, Sigma Centrifuge, Osterode, Germany), supernatant was alienated and free drug present in supernatant was measured using HPLC [Mendes et al. 2007]. Based on preliminary experiments, variables like drug:polymer ratio (X_1), polymer concentration in organic phase (X_2) and surfactant concentration in aqueous phase (X_3) were selected as independent variables and percentage drug entrapment (PDE) and particle size (PS) were taken as dependent variables. Effect of independent variables on dependent variables was studied using 3^3 factorial design.

4.5.2 Drug content and percentage drug entrapment

The drug content in the NPs was determined by dissolving 10 mg of lyophilized NPs in 10 ml of acetonitrile. The solution was then filtered through 0.22 µ, appropriately diluted with mobile phase and drug content in the NPs was determined by HPLC.

Drug loading was calculated as follows,

Percentage drug loading = A/B × 100

Where A is the drug content in the NPs and B is the weight of NPs.

PDE was estimated by calculating amount of drug entrapped in NPs with respect to total drug added during preparation of formulation.

The PDE was calculated according to following formula:

PDE (%) = (TD-FD/TD) × 100

where, TD is total amount of drug added and FD is amount of drug in supernatant

4.5.3 Particle size

The PS and polydispersity index (PDI) of the NPs were determined using a Malvern Zetasizer (Nano ZS, Malvern Instrument, Worcestershire, UK). Each sample was diluted ten times with filtered distilled water to avoid multi-scattering phenomena and placed in disposable sizing cuvette. PDI was studied to determine the narrowness of the particle size distribution. The size analysis of a sample consisted of 3 measurements, and the results are expressed as mean size ± SD.

4.5.4 Preliminary optimization of ATZ loaded PLGA NPs

Different formulation parameters were optimized based on their effect on response parameters like PDE and PS. Some of the formulation parameters like organic solvent, volume of organic solvent and type of surfactant were optimized in preliminary stages, while drug:polymer ratio, polymer concentration in organic phase and surfactant concentration in aqueous phase were optimized by 3^3 full factorial design. All the experiments were performed in triplicate. Formulation parameters optimized in preliminary stages were selection of organic solvent, volume of organic solvent and type of surfactant.

4.5.4.1 Selection of organic solvent

Three different organic solvents (acetone, acetonitrile and tetrahydrofuran) were used for preparation of PLGA NPs. Volume of organic phase (4 ml) and ratio of organic phase and aqueous phase (1:2.5) were kept constant. All other parameters were also kept constant in all three experiments.

4.5.4.2 Selection of volume of organic solvent

Acetone was used as organic solvent. Three different volumes of organic phase were selected (3, 4 and 5 ml) and their effect of different volume of organic phase was observed on PDE and PS. Volume of aqueous phase (10 ml) was kept constant along with other formulation and process variables.

4.5.4.3 Selection of surfactant

Three different surfactants were initially used for formulation development, namely Pluronic F-68®, Pluronic F-127® and Poly vinyl alcohol (PVA). Out of these, better one was selected based on resultant PDE and PS. Concentration of surfactants were kept constant (0.5%) for all three surfactants. All other parameters were also kept constant in all three formulations.

4.5.5 Optimization

4.5.5.1 Experimental design for optimization of key formulation variables

Twenty seven batches of different combinations were prepared using 3^3 factorial design by taking values of X_1, X_2 and X_3 at different levels and evaluated for PDE and PS. Mathematical modeling was carried out by using equation 3 to obtain a second order polynomial equation [Armstrong and James 1996]. A FM equation was established after putting the values of regression coefficients of PDE and PS in equation 3. The predicted

values were calculated by using the mathematical model based on the coefficients of the model and the predicted values along with their observed values were recorded along with percentage of error obtained when predicted value and observed values were compared. Neglecting non-significant ($p<0.05$) terms from the FM, a reduced model (RM) was established to facilitate the optimization technique by plotting contour plots and response surface plots by keeping least significant independent variable constant and varying other two independent variables, to establish the relationship between independent and dependent variables. F-Statistic was applied on the results of analysis of variance (ANOVA) of FM and RM to check whether the non-significant terms can be omitted or not from the FM [Bolton 1997]. Design Expert 8.0.3 and Microsoft Excel 2007 were used for the statistical optimization.

4.5.5.2 Contour plots

Contour plots are diagrammatic representation of the values of the responses that help in explaining the relationship between independent and dependent variables. Two dimensional contour plots were established between X_1 and X_2 at different levels (-1, 0, 1) of X_3 for PDE and PS.

4.5.5.3 Response surface plots

To understand the main and the interaction effects of two variables, response surface plots were used as a function of two factors at a time maintaining all other factors at fixed levels [Box 1951; Mak 1995]. These plots were obtained by calculating the values taken by one factor where the second varies (from -1 to 1 for instance) with constraint of a given Y value. The yield values for different levels of variables can also be predicted from the respective response surface plots.

4.5.5.4 Check point analysis

A check point analysis was performed to confirm the utility of the established contour plots and reduced polynomial equation in the preparation of NPs. Values of independent variables (X_1 and X_2) were taken from three check points on contour plots plotted at fixed levels of -1, 0 and 1 of X_3 and the values of PDE (Y_1) and PS (Y_2) were calculated by substituting the values in the reduced polynomial equation. ATZ loaded NPs were prepared experimentally by taking the amounts of the independent variables (X_1 and X_2). Each batch was prepared three times and mean values were determined. Difference

in the predicted and mean values of experimentally obtained PDE and PS was compared by using student's 't' test.

4.5.5.5 Desirability criteria

For simultaneous optimization of PDE and PS, desirability function (multi-response optimization technique) was applied and total desirability was calculated using Design Expert software (version 8.0.3). The desirability lies between 0 and 1 and it represents the closeness of a response to its ideal value (equation 6). The total desirability is defined as a geometric mean of the individual desirability for PDE and PS [Derringer and Suich 1980].

$$D = (d_{PDE} \times d_{PS})^{1/2} \quad (6)$$

Where, D is the total desirability, d_{PDE} and d_{PS} are individual desirability for PDE and PS. If both the quality characteristics reach their ideal values, the individual desirability is 1 for both. Consequently, the total desirability is also 1. Our optimization criteria included maximum PDE and PS of less than 200 nm.

4.5.5.6 Normalized error determination

The quantitative relationship established by MRA was confirmed by evaluating experimentally prepared ATZ loaded NPs. PDE and PS predicted from the MRA were compared with those generated from prepared batches of check point analysis using normalized error (NE). The equation of NE (equation 7) is expressed as follows:

$$NE = [\Sigma\{(Pre - Obs)/Obs\}^2]^{1/2} \quad (7)$$

where, Pre and Obs represents predicted and observed response, respectively.

4.5.6 Lyophilization and optimization of cryoprotectant

In the present study, trehalose, sucrose and mannitol were investigated in different ratios and change in particle size upon re-dispersion was observed. Nanoparticulate suspension (2 ml) was dispensed in 10 ml semi-stoppered vials with rubber closures and frozen for 24 h at -60 °C. Thereafter, the vials are lyophilized (Heto Drywinner, Allerod, Denmark) using different cryoprotectants like trehalose, sucrose and mannitol in different concentrations (1:1, 1:2, 1:3 and 1:4). Finally, glass vials were sealed under anhydrous conditions and stored until being re-hydrated. Lyophilized NPs were re-dispersed in exactly the same volume of distilled water as before lyophilization. NP suspension was subjected to particle size measurement as described earlier. Ratio of

final particle size (S_f) and initial particle size (S_i) was calculated to finalize the suitable cryoprotectant based upon lowest S_f/S_i ratio.

4.6 Formulation and optimization of ATZ loaded cPCL NPs

4.6.1 Preparation of ATZ loaded cPCL NPs

ATZ loaded cPCL NPs were prepared using solvent diffusion (nanoprecipitation) method [Fessi et al. 1989; Seju et al. 2011]. The optimized formulation was prepared by dissolving cPCL (100 mg) and ATZ (5 mg) in 5 ml of acetone. This organic phase was added at the rate of 0.5 ml/min into 10 ml of aqueous phase containing 0.25% w/v Poloxamer 188 with continuous stirring on magnetic stirrer at room temperature. Stirring was continued for 3-4 h to allow complete evaporation of organic solvent. The NPs suspension was centrifuged at 50,000×g for 30 min at 4 °C (3K30, Sigma Centrifuge, Osterode, Germany), supernatant was alienated and free drug present in supernatant was measured using HPLC [Mendes et al. 2007]. Based on preliminary experiments, variables like drug:polymer ratio (X_1), polymer concentration in organic phase (X_2) and surfactant concentration in aqueous phase (X_3) were selected as independent variables and percentage drug entrapment (PDE) and particle size (PS) were taken as dependent variables. Effect of independent variables on dependent variables was studied using 3^3 factorial design.

4.6.2 Drug content and percentage drug entrapment

The drug content in the NPs was determined by dissolving 10 mg of lyophilized NPs in 10 ml of acetonitrile. The solution was then filtered through 0.22 µ, appropriately diluted with mobile phase and drug content in the NPs was determined by HPLC.

Drug loading was calculated as follows,

Percentage drug loading = A/B × 100

Where A is the drug content in the NPs and B is the weight of NPs.

PDE was estimated by calculating amount of drug entrapped in NPs with respect to total drug added during preparation of formulation.

The PDE was calculated according to following formula:

PDE (%) = (TD-FD/TD) × 100

where, TD is total amount of drug added and FD is amount of drug in supernatant

4.6.3 Particle size

The PS and PDI of the NPs were determined using a Malvern Zetasizer (Nano ZS, Malvern Instrument, Worcestershire, UK). Each sample was diluted ten times with filtered distilled water to avoid multi-scattering phenomena and placed in disposable sizing cuvette. PDI was studied to determine the narrowness of the particle size distribution. The size analysis of a sample consisted of 3 measurements, and the results are expressed as mean size ± SD.

4.6.4 Preliminary optimization of ATZ loaded cPCL NPs

Different formulation parameters were optimized based on their effect on response parameters like PDE and PS. Some of the formulation parameters like organic solvent, volume of organic solvent and type of surfactant were optimized in preliminary stages, while drug:polymer ratio, polymer concentration in organic phase and surfactant concentration in aqueous phase were optimized by 3^3 full factorial design. All the experiments were performed in triplicate. Formulation parameters optimized in preliminary stages were selection of organic solvent, volume of organic solvent and type of surfactant.

4.6.4.1 Selection of organic solvent

Three different organic solvents (acetone, acetonitrile and tetrahydrofuran) were used for preparation of cPCL NPs. Volume of organic phase (4 ml) and ratio of organic phase and aqueous phase (1:2.5) were kept constant. All other parameters were also kept constant in all three experiments.

4.6.4.2 Selection of volume of organic solvent

Acetone was used as organic solvent. Three different volumes of organic phase were selected (3, 4 and 5 ml) and the effect of different volume of organic phase was observed on PDE and PS. Volume of aqueous phase (10 ml) was kept constant along with other formulation and process variables.

4.6.4.3 Selection of surfactant

Three different surfactants were initially used for formulation development namely Pluronic F-68®, Pluronic F-127® and Poly vinyl alcohol (PVA). Out of these, better one is selected based on resultant PDE and PS. Concentration of surfactants were kept constant (0.5%) for all three surfactants. All other parameters were also kept constant in all three formulations.

4.6.5 Optimization

4.6.5.1 Experimental design for optimization of key formulation variables

Twenty seven batches of different combinations were prepared using 3^3 factorial design by taking values of X_1, X_2 and X_3 at different levels as shown in table 1 and evaluated for PDE and PS. Mathematical modeling was carried out by using equation 3 to obtain a second order polynomial equation [Armstrong and James 1996]. A FM equation was established after putting the values of regression coefficients of PDE and PS in equation 3. The predicted values were calculated by using the mathematical model based on the coefficients of the model and the predicted values along with their observed values were recorded along with percentage of error obtained when predicted value and observed values were compared. Neglecting non-significant ($p<0.05$) terms from the FM, RM was established to facilitate the optimization technique by plotting contour plots and response surface plots by keeping least significant independent variable constant and varying other two independent variables, to establish the relationship between independent and dependent variables. F-Statistic was applied on the results of analysis of variance (ANOVA) of FM and RM to check whether the non-significant terms can be omitted or not from the FM [Bolton 1997]. Design Expert 8.0.3 and Microsoft Excel 2007 were used for the statistical optimization.

4.6.5.2 Contour plots

Contour plots are diagrammatic representation of the values of the responses that help in explaining the relationship between independent and dependent variables. Two dimensional contour plots were established between X_1 and X_2 at different levels (-1, 0, 1) of X_3 for PDE and PS.

4.6.5.3 Response surface plots

To understand the main and the interaction effects of two variables, response surface plots were used as a function of two factors at a time maintaining all other factors at fixed levels [Box 1951; Mak 1995]. These plots were obtained by calculating the values taken by one factor where the second varies (from -1 to 1 for instance) with constraint of a given Y value. The yield values for different levels of variables can also be predicted from the respective response surface plots.

4.6.5.4 Check point analysis

A check point analysis was performed to confirm the utility of the established contour plots and reduced polynomial equation in the preparation of NPs. Values of independent variables (X_1 and X_2) were taken from three check points on contour plots plotted at fixed levels of -1, 0 and 1 of X_3 and the values of PDE (Y_1) and PS (Y_2) were calculated by substituting the values in the reduced polynomial equation. ATZ loaded NPs were prepared experimentally by taking the amounts of the independent variables (X_1 and X_2). Each batch was prepared three times and mean values were determined. Difference in the predicted and mean values of experimentally obtained PDE and PS was compared by using student's 't' test.

4.6.5.5 Desirability criteria

For simultaneous optimization of PDE and PS, desirability function (multi-response optimization technique) was applied and total desirability was calculated using Design Expert software (version 8.0.3). The desirability lies between 0 and 1 and it represents the closeness of a response to its ideal value (equation 6). The total desirability is defined as a geometric mean of the individual desirability for PDE and PS [Derringer and Suich 1980].

$$D = (d_{PDE} \times d_{PS})^{1/2} \quad (6)$$

Where, D is the total desirability, d_{PDE} and d_{PS} are individual desirability for PDE and PS. If both the quality characteristics reach their ideal values, the individual desirability is 1 for both. Consequently, the total desirability is also 1. Our optimization criteria included maximum PDE and PS of less than 200 nm.

4.6.5.6 Normalized error determination

The quantitative relationship established by MRA was confirmed by evaluating experimentally prepared ATZ loaded NPs. PDE and PS predicted from the MRA were compared with those generated from prepared batches of check point analysis using normalized error (NE). The equation of NE (equation 7) is expressed as follows:

$$NE = [\Sigma\{(Pre - Obs)/Obs\}^2]^{1/2} \quad (7)$$

where, Pre and Obs represents predicted and observed response, respectively.

4.6.6 Lyophilization and optimization of cryoprotectant

In the present study, trehalose, sucrose and mannitol were investigated in different ratios and change in particle size upon re-dispersion was observed. Nanoparticulate

suspension (2 ml) was dispensed in 10 ml semi-stoppered vials with rubber closures and frozen for 24 h at -60 °C. Thereafter, the vials are lyophilized (Heto Drywinner, Allerod, Denmark) using different cryoprotectants like trehalose, sucrose and mannitol in different concentrations (1:1, 1:2, 1:3 and 1:4). Finally, glass vials were sealed under anhydrous conditions and stored until being re-hydrated. Lyophilized NPs were re-dispersed in exactly the same volume of distilled water as before lyophilization. NP suspension was subjected to particle size measurement as described earlier. Ratio of final particle size (S_f) and initial particle size (S_i) was calculated to finalize the suitable cryoprotectant based upon lowest S_f/S_i ratio.

4.7 Formulation and optimization of EXE loaded PLGA NPs

4.7.1 Preparation of EXE loaded PLGA NPs

PLGA NPs loaded with EXE were prepared by interfacial deposition of preformed polymer [Fessi et al. 1989]. EXE (5 mg) was dissolved in oil (400 µl capric/caprylic triglyceride mixture) and added to acetone (8 ml) in which PLGA (100 mg) was dissolved along with sorbitan monooleate (Span 60, 0.05 ml), under moderate magnetic stirring. This solution was then added to an aqueous phase (40 ml distilled water) containing Poloxamer 188 (0.5%) with continuous stirring on magnetic stirrer at room temperature. Stirring was continued for 3-4 h to allow complete evaporation of organic solvent. The NPs suspension was centrifuged at 50,000×g for 30 min at 4 °C (3K30, Sigma Centrifuge, Osterode, Germany), supernatant was alienated and free drug present in supernatant was measured using modified HPLC method [Breda et al. 1993]. Nanoparticulate pellet was redispersed in water (10 ml) and lyophilized (Heto Drywinner, Allerod, Denmark) using sucrose as cryoprotectant [NPs (1 part) and cryoprotectant (2 parts)]. Empty NPs were prepared by the method described above with the exception of adding EXE. Based on preliminary experiments, variables like drug:polymer ratio (X_1), amount of polymer (X_2) and volume of organic phase (X_3) were selected as independent variables and PDE and PS were taken as dependent variables. Effect of independent variables on dependent variables was studied using 3×3 BBD.

4.7.2 Drug content and percentage drug entrapment

The drug content in the NPs was determined by dissolving 10 mg of lyophilized NPs in 10 ml of acetonitrile. The solution was then measured by HPLC after filtration through

0.22 μ and appropriate dilution with mobile phase and the amount of drug entrapped in the NPs was determined.

Drug loading was calculated as follows,

Percentage drug loading = A/B × 100

Where A is the drug content in the NPs and B is the weight of NPs.

PDE was estimated by calculating amount of drug entrapped in NPs with respect to total drug added during preparation of formulation.

The PDE was calculated according to following formula:

PDE (%) = (TD-FD/TD) × 100

where, TD is total amount of drug added and FD is amount of drug in supernatant

4.7.3 Particle size

The PS and PDI of the NPs were determined using a Malvern Zetasizer Nano ZS (Malvern Instrument, Worcestershire, UK). Each sample was diluted ten times with filtered distilled water to avoid multi-scattering phenomena and placed in disposable sizing cuvette. Polydispersity index was noted to determine the narrowness of the particle size distribution. The size analysis was performed in triplicate and the results were expressed as mean size ± SD.

4.7.4 Preliminary optimization of EXE loaded PLGA NPs

Different formulation parameters were optimized based on their effect on response parameters like PDE and PS. Some of the formulation parameters like type of organic solvent, type of surfactant and concentration of surfactant were optimized in preliminary stages, while drug:polymer ratio, amount of polymer in organic phase and volume of organic phase were optimized using 3×3 BBD. All the experiments were performed in triplicate.

4.7.4.1 Type of organic solvent

Three different organic solvents (acetone, acetonitrile and tetrahydrofuran) were used for preparation of EXE loaded PLGA NPs. Volume of organic phase (10 ml) and ratio of organic phase and aqueous phase (1:4) were kept constant. All other parameters were also kept constant in all three experiments.

4.7.4.2 Selection of surfactant

Three different surfactants were initially used for formulation development namely Pluronic F-68®, Pluronic F-127® and Poly vinyl alcohol (PVA). Out of these, better one is

selected based on resultant PDE and PS. Concentration of surfactants were kept constant (0.5%) for all three surfactants. All other parameters were also kept constant in all three formulations.

4.7.4.3 Concentration of surfactant

Different concentration (0.5, 1.0 and 1.5%) of surfactant (Pluronic F-68®) were used for the preparation of EXE loaded PLGA NPs. Others parameters were kept constant in all the three formulations.

4.7.5 Optimization

4.7.5.1 Experimental design for optimization of key formulation variables

A 3-factor, 3-level Box-Behnken statistical design was employed to optimize the process and formulation parameters in preparation of EXE loaded PLGA NPs and evaluate main effects, interaction effects and quadratic effects of the process parameters on the percentage drug entrapment (PDE) and particle size (PS). The independent variables selected were ratio of drug:polymer ratio (X_1), amount of PLGA (X_2), and volume of organic phase (X_3). A design matrix comprising of 13 experimental runs was constructed. The design was used to explore quadratic response surfaces and constructing second order polynomial models and construct contour plots to predict responses with Design Expert (Version 8.0.3, Stat-Ease Inc., Minneapolis, MN, USA).

4.7.5.2 Contour plots

Contour plots are diagrammatic representation of the values of the response. They are helpful in explaining the relationship between independent and dependent variables. The reduced models were used to plot two dimension contour plots. Two contour plots for PDE and PS were established between X_2 and X_3 at fixed levels (-1, 0 and 1) of X_1.

4.7.5.3 Response surface plots

To understand the main and the interaction effects of two variables, response surface plots were used as a function of two factors at a time, maintaining the third factor at fixed level [Mak et al. 1995]. These plots were obtained by calculating the values obtained by one factor where the second varied (from -1 to 1 for instance) with constraint of a given Y value.

4.7.5.4 Check point analysis

A check point analysis was performed to confirm the utility of the established contour plots and reduced polynomial equation in the preparation of NPs. Values of independent

variables (X_2 and X_3) were taken from three check points on contour plots plotted at fixed levels of -1, 0 and 1 of X_1 and the values of PDE (Y_1) and PS (Y_2) were calculated by substituting the values in the reduced polynomial equation. EXE loaded NPs were prepared experimentally by taking the amounts of the independent variables (X_1 and X_2). Each batch was prepared three times and mean values were determined. Difference in the predicted and mean values of experimentally obtained PDE and PS was compared by using student's 't' test.

4.7.5.5 Desirability Criteria

For simultaneous optimization of PDE and PS, desirability function (multi-response optimization technique) was applied and total desirability was calculated using Design Expert software. The desirability lies between 0 and 1 and it represents the closeness of a response to its ideal value. The total desirability is defined as a geometric mean of the individual desirability for PDE and PS [Derringer and Suich 1980].

$$D = (d_{PDE}\ X\ d_{PS})^{1/2} \quad (6)$$

where, D is the total desirability, d_{PDE} and d_{PS} are individual desirability for PDE and PS. If both the quality characteristics reach their ideal values, the individual desirability is 1 for both. Consequently, the total desirability is also 1. Our criteria included highest possible PDE and PS of less than 200 nm.

4.7.5.6 Normalized error determination

The quantitative relationship established by BBD was confirmed by evaluating experimentally prepared EXE loaded NPs. PDE and PS predicted from the BBD were compared with those generated from prepared batches of check point analysis using normalized error (NE). The equation of NE (equation 7) is expressed as follows:

$$NE = [\Sigma\{(Pre - Obs)/Obs\}^2]^{1/2} \quad (7)$$

where, Pre and Obs represents predicted and observed response, respectively.

4.7.6 Lyophilization and optimization of cryoprotectant

Lyophilization is the process in which freeze-drying is done to remove solvent from the formulation and therefore improve its stability upon storage. The process of freeze drying is stressful and hence a cryoprotectant is added in the process, which also helps in re-dispersibility of the freeze-dried NPs in a suitable solvent [Chacon et al. 1999]. One of the main challenges during the freeze-drying process is preserving or rather increasing the re-dispersibility of the NPs upon reconstitution with distilled water or

buffered saline. Cryoprotectants are generally added to the NPs prior to the drying step and also act as re-dispersants. Cryoprotectants such as trehalose, sucrose, mannitol can be used to increase the physical stability of NPs during freeze-drying [Paolicelli et al. 2010]. In the present study, trehalose, sucrose and mannitol were investigated in different ratios (1:1, 1:2, 1:3 and 1:4) and change in particle size upon re-dispersion was observed. Nanoparticulate suspension (2 ml) was dispensed in 10 ml semi-stoppered glass vials with rubber closures and frozen for 24 h at -60 °C. Thereafter, the vials were lyophilized (Heto Drywinner, Allerod, Denmark) using different cryoprotectants like trehalose, sucrose and mannitol in different concentrations. Finally, vials were sealed under anhydrous conditions and stored until being re-hydrated. Lyophilized NPs were re-dispersed in exactly the same volume of distilled water as before lyophilization. NP suspension was subjected to particle size measurement as described earlier. Ratio of final particle size (S_f) and initial particle size (S_i) was calculated to finalize the suitable cryoprotectant based on lowest S_f/S_i ratio [Kashi et al. 2012].

4.8 Formulation and optimization of EXE loaded cPCL NPs

4.8.1 Preparation of EXE loaded cPCL NPs

cPCL NPs loaded with EXE were prepared by interfacial deposition of preformed polymer [Fessi et al. 1989]. EXE (5 mg) was dissolved in oil (400 µl capric/caprylic triglyceride mixture) and added to acetone (8 ml) in which PCL (100 mg) was dissolved along with sorbitan monooleate (Span 60, 0.05 ml), under moderate magnetic stirring. This solution was then added to an aqueous phase (40 ml distilled water) containing Poloxamer 188 (0.5%) with continuous stirring on magnetic stirrer at room temperature. Stirring was continued for 3-4 h to allow complete evaporation of organic solvent. The NPs suspension was centrifuged at 50,000×g for 30 min at 4 °C (3K30, Sigma Centrifuge, Osterode, Germany), supernatant was alienated and nanoparticulate pellet was re-dispersed in water (10 ml) and lyophilized (Heto Drywinner, Allerod, Denmark) using sucrose as cryoprotectant [NPs (1 part) and cryoprotectant (2 parts)]. Empty NPs were prepared by the method described above with the exception of adding EXE. Based on preliminary experiments, variables like drug:polymer ratio (X_1), amount of polymer (X_2) and volume of organic phase (X_3) were selected as independent

variables and PDE and PS were taken as dependent variables. Effect of independent variables on dependent variables was studied using 3×3 BBD.

4.8.2 Drug content and percentage drug entrapment

The drug content in the NPs was determined by dissolving 10 mg of lyophilized NPs in 10 ml of acetonitrile analyzing by HPLC after filtration through 0.22 µ and appropriate dilution with mobile phase. Drug loading was calculated as follows,

Percentage drug loading = A/B × 100

Where A is the drug content in the NPs and B is the weight of NPs.

PDE was estimated by calculating amount of drug entrapped in NPs with respect to total drug added during preparation of formulation.

The PDE was calculated according to following formula:

PDE (%) = (TD-FD/TD) × 100

where, TD is total amount of drug added and FD is amount of drug in supernatant

4.8.3 Particle size

The size analysis and polydispersity index of the NPs were determined using a Malvern Zetasizer Nano ZS (Malvern Instrument, Worcestershire, UK). Each sample was diluted ten times with filtered distilled water to avoid multi-scattering phenomena and placed in disposable sizing cuvette. Polydispersity index was noted to determine the narrowness of the particle size distribution. The size analysis was performed in triplicate and the results were expressed as mean size ± SD.

4.8.4 Preliminary optimization of EXE loaded cPCL NPs

Different formulation parameters were optimized based on their effect on response parameters like PDE and PS. Some of the formulation parameters like type of organic solvent, type of surfactant and concentration of surfactant were optimized in preliminary stages, while drug:polymer ratio, amount of polymer in organic phase and volume of organic phase were optimized using 3×3 BBD. All the experiments were performed in triplicate.

4.8.4.1 Type of organic solvent

Three different organic solvents (acetone, acetonitrile and tetrahydrofuran) were used for preparation of EXE loaded cPCL NPs. Volume of organic phase (10 ml) and ratio of organic phase and aqueous phase (1:4) were kept constant. All other parameters were also kept constant in all three experiments.

4.8.4.2 Selection of surfactant

Three different surfactants were initially used for formulation development namely Pluronic F-68®, Pluronic F-127® and Poly vinyl alcohol (PVA). Out of these, better one is selected based on resultant PDE and PS. Concentration of surfactants were kept constant (0.5%) for all three surfactants. All other parameters were also kept constant in all three formulations.

4.8.4.3 Concentration of surfactant

Different concentration (0.5, 1.0 and 1.5%) of surfactant (Pluronic F-68®) were used for the preparation of EXE loaded cPCL NPs. Others parameters were kept constant in all the three formulations.

4.8.5 Optimization

4.8.5.1 Experimental design for optimization of key formulation variables

A 3-factor, 3-level Box-Behnken statistical design was employed to optimize the process and formulation parameters in preparation of EXE loaded cPCL NPs and evaluate main effects, interaction effects and quadratic effects of the process parameters on the percentage drug entrapment (PDE) and particle size (PS). The independent variables selected were ratio of drug:polymer ratio (X_1), amount of cPCL (X_2), and volume of organic phase (X_3). A design matrix comprising of 13 experimental runs was constructed. The design was used to explore quadratic response surfaces and constructing second order polynomial models and construct contour plots to predict responses with Design Expert (Version 8.0.3, Stat-Ease Inc., Minneapolis, MN, USA).

4.8.5.2 Contour plots

Contour plots are diagrammatic representation of the values of the response. They are helpful in explaining the relationship between independent and dependent variables. The reduced models were used to plot two dimension contour plots. Two contour plots for PDE and PS were established between X_2 and X_3 at fixed levels (-1, 0 and 1) of X_1.

4.8.5.3 Response surface plots

To understand the main and the interaction effects of two variables, response surface plots were used as a function of two factors at a time, maintaining the third factor at fixed level [Mak et al. 1995]. These plots were obtained by calculating the values obtained by one factor where the second varied (from -1 to 1 for instance) with constraint of a given Y value.

4.8.5.4 Check point analysis

A check point analysis was performed to confirm the utility of the established contour plots and reduced polynomial equation in the preparation of NPs. Values of independent variables (X_2 and X_3) were taken from three check points on contour plots plotted at fixed levels of -1, 0 and 1 of X_1 and the values of PDE (Y_1) and PS (Y_2) were calculated by substituting the values in the reduced polynomial equation. EXE loaded NPs were prepared experimentally by taking the amounts of the independent variables (X_1 and X_2). Each batch was prepared three times and mean values were determined. Difference in the predicted and mean values of experimentally obtained PDE and PS was compared by using student's 't' test.

4.8.5.5 Desirability criteria

For simultaneous optimization of PDE and PS, desirability function (multi-response optimization technique) was applied and total desirability was calculated using Design Expert software. The desirability lies between 0 and 1 and it represents the closeness of a response to its ideal value. The total desirability is defined as a geometric mean of the individual desirability for PDE and PS [Derringer and Suich 1980].

$$D = (d_{PDE}\ X\ d_{PS})^{1/2} \quad (6)$$

where, D is the total desirability, d_{PDE} and d_{PS} are individual desirability for PDE and PS. If both the quality characteristics reach their ideal values, the individual desirability is 1 for both. Consequently, the total desirability is also 1. Our criteria included highest possible PDE and PS of less than 200 nm.

4.8.5.6 Normalized error determination

The quantitative relationship established by BBD was confirmed by evaluating experimentally prepared EXE loaded NPs. PDE and PS predicted from the BBD were compared with those generated from prepared batches of check point analysis using normalized error (NE). The equation of NE (equation 1) is expressed as follows:

$$NE = [\Sigma\{(Pre - Obs)/Obs\}^2]^{1/2} \quad (7)$$

where, Pre and Obs represents predicted and observed response, respectively.

4.8.6 Lyophilization and optimization of cryoprotectant

Lyophilization is the process in which freeze-drying is done to remove solvent from the formulation and therefore improve its stability upon storage. The process of freeze drying is stressful and hence a cryoprotectant is added in the process, which also helps

in re-dispersibility of the freeze-dried NPs in a suitable solvent [Chacon et al. 1999]. One of the main challenges during the freeze-drying process is preserving or rather increasing the re-dispersibility of the NPs upon reconstitution with distilled water or buffered saline. Cryoprotectants are generally added to the NPs prior to the drying step and also act as re-dispersants. Cryoprotectants such as trehalose, sucrose, mannitol can be used to increase the physical stability of NPs during freeze-drying [Paolicelli et al. 2010]. In the present study, trehalose, sucrose and mannitol were investigated in different ratios (1:1, 1:2, 1:3 and 1:4) and change in particle size upon re-dispersion was observed. Nanoparticulate suspension (2 ml) was dispensed in 10 ml semi-stoppered glass vials with rubber closures and frozen for 24 h at -60 °C. Thereafter, the vials were lyophilized (Heto Drywinner, Allerod, Denmark) using different cryoprotectants like trehalose, sucrose and mannitol in different concentrations. Finally, vials were sealed under anhydrous conditions and stored until being re-hydrated. Lyophilized NPs were re-dispersed in exactly the same volume of distilled water as before lyophilization. NP suspension was subjected to particle size measurement as described earlier. Ratio of final particle size (S_f) and initial particle size (S_i) was calculated to finalize the suitable cryoprotectant based on lowest S_f/S_i ratio.

4.9 Characterization of optimized nanoparticulate formulation

4.9.1 Zeta potential

Zeta potential distribution was also measured using a Zetasizer (Nano ZS, Malvern instrument, Worcestershire, UK). Each sample was suitably diluted 10 times with filtered distilled water and placed in a disposable zeta cell. Zeta limits ranged from -200 to +200 mV. The electrophoretic mobility (µm/sec) was converted to zeta potential by in-built software using Helmholtz-Smoluchowski equation. Average of 3 measurements of each sample was used to derive average zeta potential.

4.9.2 Transmission electron microscope (TEM) studies

A sample of NPs (0.5 mg/ml) was suspended in water and bath sonicated for 30 s. 2 µl of this suspension was placed over a formvar coated copper TEM grid (150 mesh) and negatively stained with 2 µl uranyl acetate (1%) for 10 min, allowed to dry and the images were visualized at 80 kV under TEM (FEI Tecnai G2 Spirit Twin, Czech Republic) and captured using Gatan Digital Micrograph software.

4.9.3 Differential scanning calorimetric (DSC) studies

All the samples were dried in desiccators for 24 h before thermal analysis. DSC studies on pure drug, polymer, physical mixtures of drug and polymer and drug loaded NPs were performed in order to characterize the physical state of drug in the NPs. Thermograms were obtained using DSC model 2910 (TA Instruments, New Castle, USA). Dry nitrogen gas was used as the purge gas through the DSC cell at a flow rate of 40 ml/min. Samples (4 - 8 mg) were sealed in standard aluminum pans with lids and heated at a rate of 10 °C /min from 20 to 300 °C. Data was analyzed using TA Universal Analysis 2000 software (TA Instruments, New Castle, USA).

4.9.4 In vitro drug release studies

In vitro release of drug from non-pegylated NPs and pegylated NPs were evaluated by the dialysis bag diffusion technique in phosphate buffered saline (PBS) (pH 7.4) [Yang et al. 1999]. The aqueous nanoparticulate dispersion equivalent to 2 mg of drug was placed in a dialysis bag (cut-off 12,000 Da; Himedia, Mumbai, India), which was previously soaked overnight in water, cleaned next morning and sealed at both ends. The dialysis bag was immersed in the receptor compartment containing 50 ml of PBS (pH 7.4), which was stirred at 100 rpm and maintained at 37 ± 2 ^{o}C. The receptor compartment was covered to prevent the evaporation of release medium. Samples (2 ml) were withdrawn at regular time intervals, the same volume was replaced by fresh release medium and measured for amount of drug released using previously described HPLC method [Breda et al. 1993; Mendes et al. 2007]. All the experiments were performed in triplicate, and the average values were taken. Drug suspension prepared in PBS (pH 7.4) was used as a control. The kinetic analysis of the release data was done using Korsmeyer and Peppas equation or the Power law equation [Peppas 1985]:

$M_t/M_\infty = kt^n$

$\text{Log } (M_t/M_\infty) = \log k + n \log t$ (8)

Where, M_t/M_∞ is the fractional amount of drug released, k is the release constant, n is the release exponent and t is the time of release.

4.9.5 Stability studies

Stability studies were conducted using the optimized batch of lyophilized NPs. The NPs were stored at ambient temperature and at refrigerated temperature (2-8 ^{o}C). At

different time points, samples were withdrawn and subjected to drug content and particle size analysis as described previously.

4.10 Results and discussion

4.10.1 Characterization of PLGA-PEG conjugate

The infra red spectra of polymers are presented in figure 4.1 (A: PLGA; B: PEG and C: PLGA-PEG). The peak at 1760 cm^{-1} was observed corresponding to amide bond formation between PLGA and PEG. Peak due to N-H stretching observed in PEG at 3450 cm^{-1} was retained in PLGA-PEG. PLGA-PEG also retained all other peaks present in PEG confirming conjugation of PEG with PLGA. The NMR spectrum (figure 4.2) showed some distinct peaks confirming successful conjugation of PEG with PLGA as reported by other authors [Song et al. 2011]. The major peaks present at δ values 1.55 and 5.21 ppm showed presence of methyl (CH_3) and methine (CH) protons of lactic acid. The peaks of methene protons in CH_2 group of PEG and in terminal CH_2 group of PEG were around 3.65 and 4.32 ppm, respectively. The peak at 4.81 corresponds to methane in glycolic acid. Peak at 7.2 ppm is due to protons in amide linkage. Hence, we could conclude the successful formation of PLGA-PEG from the combined results of FTIR and NMR. The

Figure 4.1 FTIR spectra of polymers, A: PLGA; B: PEG and C: PLGA-PEG.

Figure 4.2 NMR spectra of pegylated PLGA.

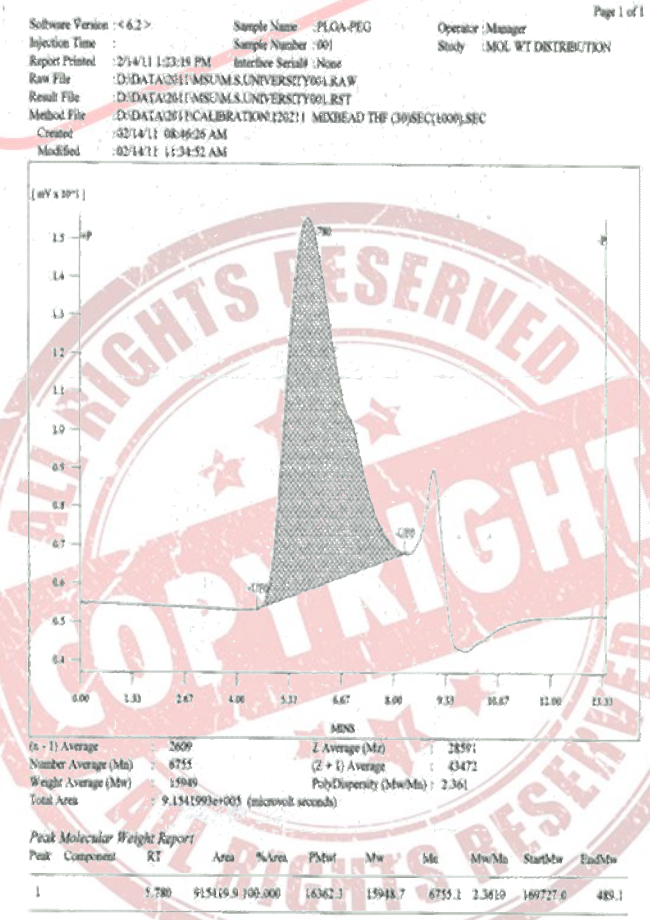

Page 1 of 1

Software Version : < 6.2 >
Sample Name : PLGA-PEG
Operator : Manager
Injection Time :
Sample Number : 001
Study : MOL WT DISTRIBUTION
Report Printed : 2/14/11 1:23:19 PM
Interface Serial# : None
Raw File : D:\DATA\2011\MSUM.S.UNIVERSITY00\1.RAW
Result File : D:\DATA\2011\MSUM.S.UNIVERSITY00\1.RST
Method File : D:\DATA\2011\CALIBRATION\120211 MIXBEAD THF (30)SEC(1000).SEC
Created : 02/14/11 08:46:26 AM
Modified : 02/14/11 11:34:52 AM

[mV x 10^3]

MINS

(n - 1) Average : 2609
Z Average (Mz) : 28597
Number Average (Mn) : 6755
(Z + 1) Average : 43472
Weight Average (Mw) : 15949
PolyDispersity (Mw/Mn) : 2.361
Total Area : 9.1341993e+005 (microvolt seconds)

Peak Molecular Weight Report

Peak	Component	RT	Area	%Area	PMwt	Mw	Mn	Mw/Mn	StartMw	EndMw
1		5.780	915419.9	100.000	16362.3	15948.7	6755.1	2.3610	169727.0	489.1

Figure 4.3 Gel permeation chromatogram of pegylated PLGA.

molecular weight of pegylated PLGA was determined using GPC. Chromatogram of copolymer is shown in figure 4.3. The Mw (Weight-average molecular weight) of PLGA-PEG was 15949 ± 683 Da) which was found to be close to theoretically predicted molecular weight (17000 Da). These results confirmed that PEG reacted with PLGA and as a result, PLGA-PEG was produced.

4.10.2 Characterization of cPCL

Successful polymerization of caprolactone to cPCL was confirmed by FTIR spectra of polymer (figure 4.4). The peak at 1727.81 cm^{-1} corresponding to carboxylic group and 3441 cm^{-1} for OH stretching of COOH group confirmed the conversion of caprolactone to cPCL [Zhang et al. 1994]. Molecular weight of cPCL was found to be 17487 ± 276 Da using GPC (figure 4.5) which was found to be close to theoretically predicted molecular weight (17814 Da).

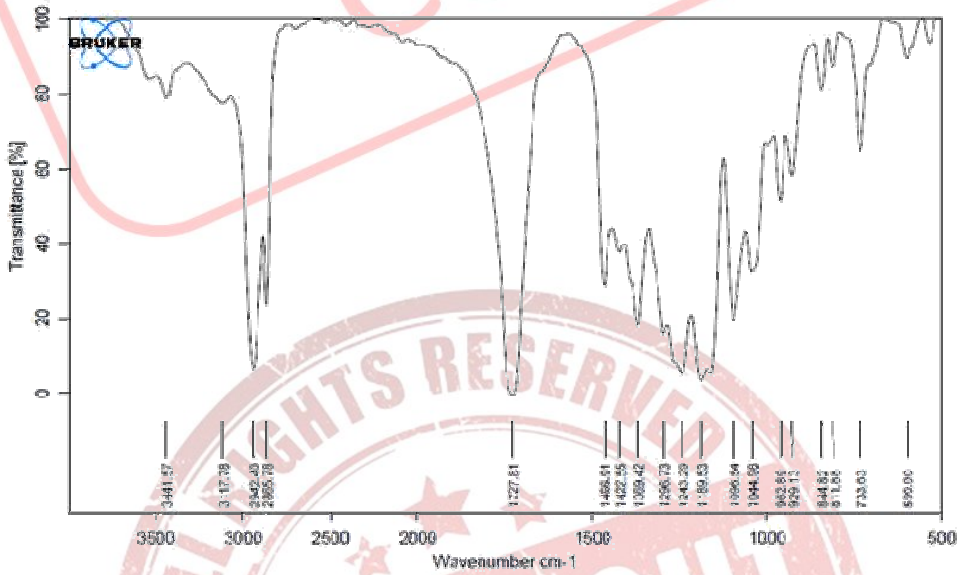

Figure 4.4 FTIR spectra of cPCL

4.10.3 Characterization of PCL-PEG conjugate

FTIR, NMR and GPC

The infra red spectra of polymers were presented in figure 4.6 (A: PCL; B: PEG and C: PCL-PEG). The peak at 1642 cm^{-1} was observed corresponding to C=O str. of amide bond between PCL and PEG. Peak at 3444 cm^{-1} due to N-H str. observed in PEG is retained in PCL-PEG. PCL-PEG also retained all other peaks present in PEG. These results confirmed

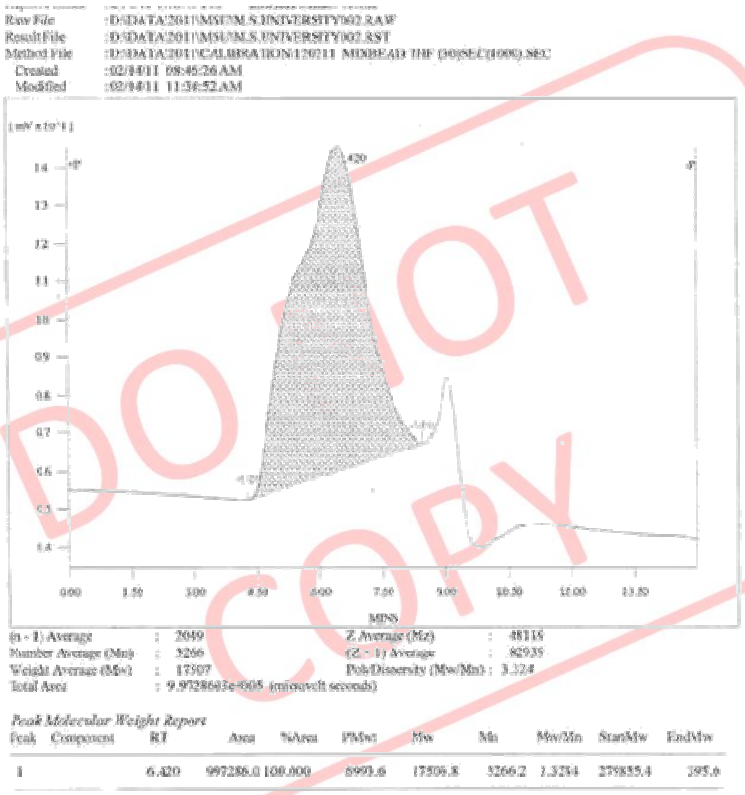

Figure 4.5 Gel permeation chromatogram of cPCL.

that PEG reacted with PCL and as a result, PCL-PEG was produced. The NMR spectrum (figure 4.7) showed some distinct peaks in PCL-PEG as reported by other researchers [Darbandy et al. 2011]. The major peaks are at δ values 1.3 and 1.6 ppm showed presence of methene (CH_2) protons of caprolactone. The peak of methene protons in terminal CH_2 group of caprolactone polymer chain was around 2.3 ppm. The peaks of methene protons in CH_2 group of PEG and in terminal CH_2 group of PEG were around 3.65 and 4.1 ppm, respectively. Peak at 7.2 ppm corresponds to protons in amide linkage. The molecular weight of pegylated PCL was determined using GPC method. Chromatogram of copolymer was shown in figure 4.8. The Mw (Weight-average molecular weight) of PCL-PEG was 22374 ± 779 Da which was found to be close to theoretically predicted molecular weight (22500 Da).

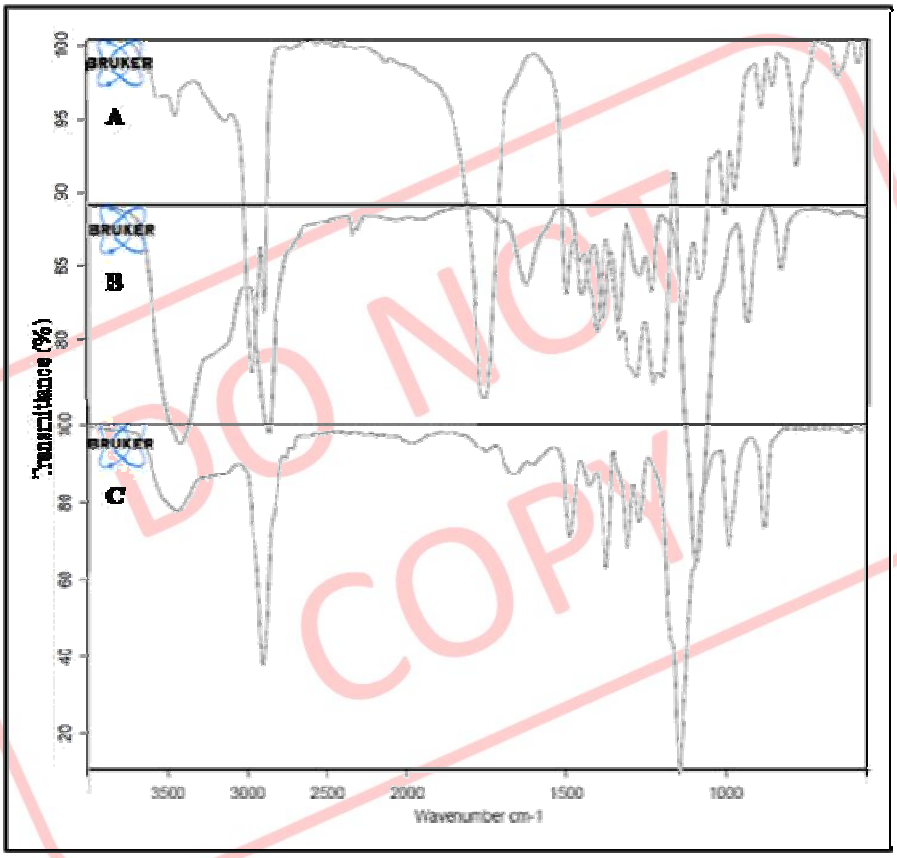

Figure 4.6 FTIR spectra of polymers, A: cPCL; B: PEG and C: PCL-PEG.

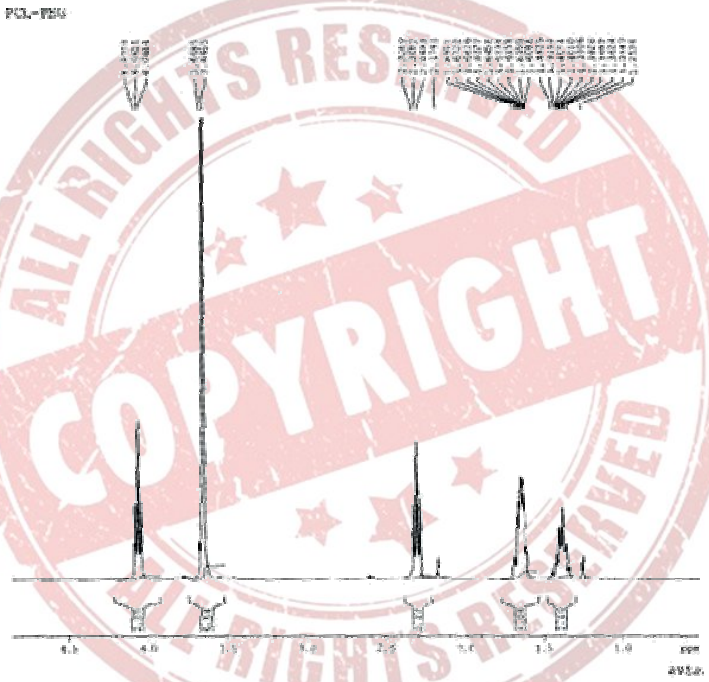

Figure 4.7 NMR spectra of pegylated PCL.

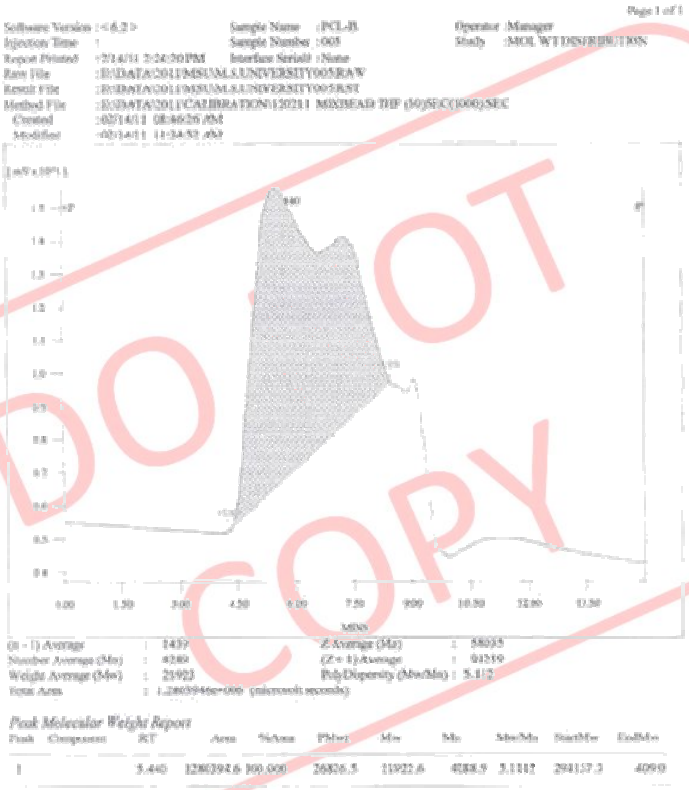

Figure 4.8 Gel permeation chromatogram of pegylated PCL.

4.11Formulation and optimization of ATZ loaded PLGA NPs

4.11.1 Preliminary optimization of ATZ loaded PLGA NPs

4.11.1.1 Selection of organic solvent

Three different organic solvents (acetone, acetonitrile and tetrahydrofuran) were used for preparation of PLGA NPs (table 4.1). NPs formulated using acetone showed PDE of 41.21 ± 0.85% with PS of 136.2 ± 5.3 nm while NPs formulated using acetonitrile were of low PDE and PS. PDE was again decreased when tetrahydrofuran was used as solvent with no significant change in PS. Hence, acetone was selected for further studies.

Table 4.1 Selection of organic phase in preliminary optimization of ATZ loaded PLGA NPs

Solvents	PDE (%)	PS (nm)
Acetone	41.21 ± 0.85	136.2 ± 5.3
Acetonitrile	35.79 ± 1.16	125.3 ± 3.9
Tetra hydro furan	33.61 ± 0.91	131.2 ± 4.1

4.11.1.2 Selection of volume of organic solvent

Different volumes of organic solvent (acetone) were used to dissolve polymer (50 mg) and results are represented in table 4.2. It was observed that as the volume of organic solvent was increased, PS decreases significantly with no major change in PDE. This was possibly due to decreased viscosity of organic phase with increase in volume of organic solvent which can easily dispersed in aqueous phase containing surfactant. Hence, 5 ml of acetone was selected as organic phase.

Table 4.2 Selection of volume of organic solvent in preliminary optimization of ATZ loaded PLGA NPs

Volume of organic solvent	PDE (%)	PS (nm)
3 ml	55.63 ± 0.91	230.1 ± 5.5
4 ml	53.32 ± 0.64	202.5 ± 7.2
5 ml	54.32 ± 1.81	180.1 ± 6.8

4.11.1.3 Selection of surfactant

Three different surfactants were initially used for formulation development namely Pluronic F-68® (P188), Pluronic F-127® (P127) and Poly vinyl alcohol (PVA) (table 4.3). Out of these, better one is selected based on resultant PDE and PS. With constant level of surfactant concentration (0.5%) for all three surfactants, PDE was found to be highest when PVA was used, but at the same time PS was found to be of larger size (332.4 ± 7.6 nm). No significant difference in PS was observed when P188 or P127 was used, but PDE was higher when P188 was used as surfactant. Hence, P188 was used in further studies.

Table 4.3 Selection of surfactant in preliminary optimization of ATZ loaded PLGA NPs

Surfactant	PDE (%)	PS (nm)
P188	45.99 ± 1.07	154.6 ± 6.8
P127	42.37 ± 0.89	148.2 ± 3.6
PVA	47.37 ± 1.07	332.4 ± 7.6

4.11.2 Optimization of ATZ loaded PLGA NPs using 3^3 factorial design

Twenty seven batches of ATZ loaded PLGA NPs were prepared by using 3^3 factorial design varying three independent variables, drug:polymer ratio (X_1), polymer

concentration in organic phase (X_2) and surfactant concentration in aqueous phase (X_3) (table 4.4). The PDE and PS were taken as dependent variables and the results were recorded (table 4.5). The main effects of X_1, X_2 and X_3 represent the average result of changing one variable at a time from its low to high value. The interactions (X_1X_2, X_1X_3, X_2X_3 and $X_1X_2X_3$) show how the PDE and PS changes when two or more variables were simultaneously changed. The values for the twenty seven batches showed a wide variation from 36.66 to 61.65% and 117.8 to 180.15 nm for PDE and PS respectively (table 4.5). This is reflected by the wide range of coefficients of the terms of equation 3 representing the individual and combined variables.

Table 4.4 Coded values of the formulation parameters of ATZ loaded PLGA NPs

Coded values	Actual values of dependent variables		
	X_1	X_2	X_3
-1	1 : 10	0.50 %	0.25 %
0	1 : 15	0.75 %	0.50 %
1	1 : 20	1.0 %	0.75 %

X_1 Drug:polymer ratio
X_2 Polymer concentration (% w/v)
X_3 Surfactant concentration (% w/v)

$$Y_1 = 51.08 + 0.69\,X_1 + 8.12\,X_2 - 0.87\,X_3 + 0.64\,X_1X_2 - 0.32\,X_1X_3 - 0.67\,X_2X_3 - 2.32\,X_1^2 - 0.86\,X_2^2 + 0.444\,X_3^2 - 1.51\,X_1X_2X_3 \quad (9)$$

$$Y_2 = 137.62 + 1.53\,X_1 + 10.22\,X_2 + 10.41\,X_3 - 1.46\,X_1X_2 + 2.05\,X_1X_3 + 1.05\,X_2X_3 + 15.37\,X_1^2 + 3.91\,X_2^2 - 0.74\,X_3^2 + 1.01\,X_1X_2X_3 \quad (10)$$

$$Y_1 = 50.8011 + 8.115\,X_2 - 2.3188\,X_1^2 \quad (11)$$

$$Y_2 = 137.1293 + 10.2183\,X_2 + 10.41\,X_3 + 15.3727\,X_1^2 + 3.906\,X_2^2 \quad (12)$$

The significance of each coefficient of equation 9 and 10 were determined by student's 't' test and p-value, which are listed in table 4.6 and 4.7 respectively. The larger the magnitude of the 't' value and the smaller the p-value, the more significant is the corresponding coefficient [Adinarayana and Ellaiah 2002; Akhnazarova 1982]. Small values of the coefficients of the terms X_1, X_3, X_2^2, X_3^2, X_1X_2, X_2X_3, X_1X_3, and $X_1X_2X_3$ in equation 9 and X_1, X_3^2, X_1X_2, X_2X_3, X_1X_3, and $X_1X_2X_3$ in equation 10 for PDE and PS respectively implied that all these terms were least contributing in the preparation of

Table 4.5 Layout of 3^3 full factorial design for ATZ loaded PLGA NPs

Sr. No.	X_1	X_2	X_3	Y_1* (PDE, in %)	Y_2* (PS, in nm)
1	-1	-1	-1	41.21 ± 0.8	136.3 ± 5.3
2	-1	-1	0	37.61 ± 0.6	145.2 ± 3.8
3	-1	-1	1	39.55 ± 0.9	153.3 ± 4.9
4	-1	0	-1	50.53 ± 0.9	139.5 ± 5.5
5	-1	0	0	45.99 ± 1.1	154.6 ± 6.8
6	-1	0	1	47.87 ± 0.9	158.1 ± 4.7
7	-1	1	-1	56.75 ± 1.9	158.7 ± 6.3
8	-1	1	0	53.26 ± 1.2	161.7 ± 4.4
9	-1	1	1	57.38 ±1.8	174.9 ± 6.6
10	0	-1	-1	43.29 ± 0.9	117.8 ± 3.3
11	0	-1	0	44.66 ± 1.2	129.2 ± 5.4
12	0	-1	1	42.42 ± 1.3	131.4 ± 5.2
13	0	0	-1	54.82 ± 0.9	127.0 ± 3.3
14	0	0	0	48.66 ± 1.3	140.7 ± 4.1
15	0	0	1	52.66 ± 1.8	152.7 ± 4.0
16	0	1	-1	58.52 ± 2.0	141.4 ± 3.3
17	0	1	0	55.04 ± 1.3	156.3 ± 3.7
18	0	1	1	57.14 ± 2.2	161.2 ± 7.0
19	1	-1	-1	36.66 ± 1.2	143.7 ± 3.8
20	1	-1	0	43.18 ± 1.0	149.4 ± 4.1
21	1	-1	1	39.11 ± 1.1	163.4 ± 5.2
22	1	0	-1	49.03 ± 2.7	136.4 ± 3.5
23	1	0	0	52.53 ± 2.3	151.5 ± 4.1
24	1	0	1	46.35 ± 1.0	166.3 ± 6.1
25	1	1	-1	61.65 ± 2.6	153.7 ± 4.4
26	1	1	0	59.7 ± 1.7	165.9 ± 3.5
27	1	1	1	54.32 ± 1.8	180.1 ± 6.8

*values are represented as mean ± s.d.

equations (equation 11 and 12, for PDE and PS respectively) were obtained following MRA of PDE and PS. Based on their p-value, it implied that the quadratic main effects of

Table 4.6 Model coefficients estimated by multiple regression analysis for PDE of ATZ loaded PLGA NPs

Factor	Coefficients	t Stat	p-value
Intercept	51.08	38.9531	< 0.0001*
X_1	0.69	1.1331	0.2731
X_2	8.11	13.3695	< 0.0001*
X_3	-0.87	-1.4716	0.1703
X_1X_2	0.64	0.8632	0.4000
X_1X_3	-0.32	-0.3639	0.6697
X_2X_3	-0.67	-0.8968	0.3823
X_1^2	-2.32	-2.2057	0.0421*
X_2^2	-0.86	-0.8154	0.4260
X_3^2	0.44	0.4227	0.6776
$X_1X_2X_3$	-1.51	-1.6571	0.1164

* Significant at $p < 0.05$

Table 4.7 Model coefficients estimated by multiple regression analysis for PS of ATZ loaded PLGA NPs

Factor	Coefficients	t Stat	p-value
Intercept	137.62	60.5771	< 0.0001*
X_1	1.53	1.4585	0.1477
X_2	10.22	9.7162	< 0.0001*
X_3	10.41	9.9540	< 0.0001*
X_1X_2	-1.46	-1.1367	0.2530
X_1X_3	2.05	1.1145	0.1159
X_2X_3	1.05	0.8120	0.4095
X_1^2	15.37	8.4394	< 0.0001*
X_2^2	3.91	2.1444	0.0399*
X_3^2	-0.74	-0.4075	0.6765
$X_1X_2X_3$	1.01	0.6379	0.5153

* Significant at $p < 0.05$

the ATZ loaded PLGA NPs by nanoprecipitation method. The small values of coefficients were not-significant ($p>0.05$) and hence neglected from the FM. Reduced polynomial

polymer concentration in organic phase (X_2) was significant for both PDE and PS, and surfactant concentration in aqueous phase (X_3) for PS only. The second order main effects of drug:polymer ratio (X_1) for PDE, and drug:polymer ratio (X_1) and polymer concentration in organic phase (X_2) for PS were found to be significant, as is evident from their p-values. The interactions between X_1X_2, X_2X_3, X_1X_3 and $X_1X_2X_3$ were not found to be significant for both PDE and PS from their p-values (table 4.6 and 4.7). The results of ANOVA of the second order polynomial equation of PDE and PS are given in table 4.8 and 4.9 respectively. Since the calculated F value was less than the tabulated F value for PDE and for PS [Bolton 1997], it was concluded that the neglected terms did not significantly contribute in the prediction of PDE and PS. Hence, F-Statistic of the results of ANOVA of full and reduced model justified the omission of non-significant terms of equation 9 and 10.

Table 4.8 ANOVA of full and reduced models for PDE of ATZ loaded PLGA NPs

		df	SS	MS	F	R	R^2	Adjusted R^2
Regression	FM	10	1274.7	127.5	19.22	0.9608	0.9231	0.8751
	RM	2	1217.6	608.8	89.53	0.9390	0.8818	0.8719
Residual	FM	16	106.1	6.6				
	RM	24	163.2	6.8				

SSE2 - SSE1 =163.201 - 106.106 = 57.0958

No. of parameters omitted = 8

MS of error (full model) = 6.6316

F calculated = (SSE2 - SSE1 / No. of parameters omitted) / MS of error (FM)

= (57.0958 / 8) / 6.6318 = 1.0761

F tabulated = 2.59

Table 4.9 ANOVA of full and reduced models for PS of ATZ loaded PLGA NPs

		df	SS	MS	F	R	R^2	Adjusted R^2
Regression	FM	10	5456.9	545.7	27.41	0.9720	0.9448	0.9104
	RM	4	5339.6	1334.9	67.38	0.9615	0.9245	0.9108
Residual	FM	16	318.5	19.9				
	RM	22	435.9	19.8				

SSE2 - SSE1 = 435.872 - 318.535 = 117.337

No. of parameters omitted = 6

MS of error (full model) = 19.908

F calculated = (SSE2 - SSE1 / No. of parameters omitted) / MS of error (FM)

= (117.337 / 6) / 19.908 = 0.9823

F tabulated = 2.74

When the coefficients of the three independent variables in equation 9 and 10 were compared, the value for the variable X_2 (b_1 = 8.12 for PDE and b_1 = 10.22 for PS) was found to be maximum and hence X_2 was considered to be a major contributing variable affecting the PDE and PS of the NPs. The Fisher F test with a very low probability value (P_{model} > F = 0.000001) demonstrated a very high significance for the regression model. The goodness of fit of the model was checked by the determination coefficient (R^2). In this case, the values of the determination coefficients (R^2 = 0.9232 and 0.9448 for FM and 0.8818 and 0.9245 for RM for PDE and PS respectively) indicated that over 88% of the total variations were explained by the model. High R^2 values of FM as compared to RM were due to the large number of factors included. More the number of factors more is the R^2 value [Montgomery 2004]. The values of adjusted R^2 (0.8751 and 0.9104 for FM and 0.8719 and 0.9108 for RM for PDE and PS respectively) were similar for FM and RM for both PDE and PS, indicating the suitability of reducing the model. Moreover, the high values of correlation coefficients (R = 0.9608 and 0.9720 for FM and 0.9390 and 0.9615 for RM for PDE and PS respectively) signifies an excellent correlation between the independent variables [Box et al. 1978]. All the above considerations indicated an excellent adequacy of the developed regression model [Adinarayana and Ellaiah 2002; Akhnazarova 1982; Box et al. 1978; Yee and Blanch 1993].

4.11.2.1 Contour plots

Contour plots were established between X_1 vs X_2, X_1 vs X_3 and X_2 vs X_3 at fixed level (- 1) of third variable as shown in figure 4.9 and 4.10 for each PDE and PS respectively. The plots showed that PDE was greatly dependent on drug:polymer ratio and polymer concentration (figure 4.9A). When both these variables were at their maximum levels, PDE was found to be maximum. However, the contour of drug:polymer ratio vs surfactant concentration (figure 4.9B) showed PDE between 40 to 42.5% in the whole range (-1 to 1) of both variables indicating negligible interaction between them. PDE was found to increase linearly with increase in polymer concentration (figure 4.9C). Also, the parallel lines of the contour plot with respect to X_1 implies that the surfactant

concentration in aqueous phase has negligible influence on PDE at constant levels of X_2 and X_3.Lowest PS of about 120 nm was observed at -1 level of polymer and surfactant concentration and 0 level of drug:polymer ratio (figure 4.10A). Relationship between drug:polymer ratio vs surfactant concentration was found to be non-linear (figure 4.10B). PS was found to show maximum variation at low level (-1) of drug:polymer ratio. It increased from 135 to 175 nm linearly with increase in both the variables i.e., polymer and surfactant concentration (figure 4.10C). It was concluded from the contours that low concentration of surfactant but high concentration of PLGA and high drug:polymer ratio was required for highest PDE and lowest PS in preparation of ATZ loaded PLGA NPs.

4.11.2.2 Response surface plots

Response surface plots, which are very helpful in learning about both the main and interaction effects of the independent variables, were plotted between X_1 vs X_2, X_1 vs X_3 and X_2 vs X_3 at fixed level (- 1) of third variable as shown in figure 4.11 and 4.12 for each PDE and PS respectively. PDE was not significantly affected when drug:polymer ratio was varied alone, but was increased upon simultaneous increase in drug:polymer ratio with polymer concentration (figure 4.11A). However, PDE was unaffected by simultaneous variation of X_1 and X_3. This may be because, increase in PDE due to increase in drug:polymer ratio was negated by increase in surfactant concentration (figure 4.11B). PDE was found to increase linearly with increase in polymer concentration, but no significant change was observed when surfactant concentration was varied. When both the variables were increased from -1 to 1 level, PDE increased linearly (figure 4.11C).

Response surface plot of drug:polymer ratio vs polymer concentration showed non-linear behaviour (figure 4.12A). With decrease in drug:polymer ratio from 1 to 0 level, PS first decreased and then increased. Response surface plot between drug:polymer ratio and surfactant concentration showed almost similar trends as observed in surface plot between drug:polymer ratio vs polymer concentration (figure 4.12B). Plot between polymer concentration and surfactant concentration showed linear relationship, with both the variables showing positive effect on PS, as simultaneous increase in levels of both the variables resulted into increase in PS (figure 4.12C).

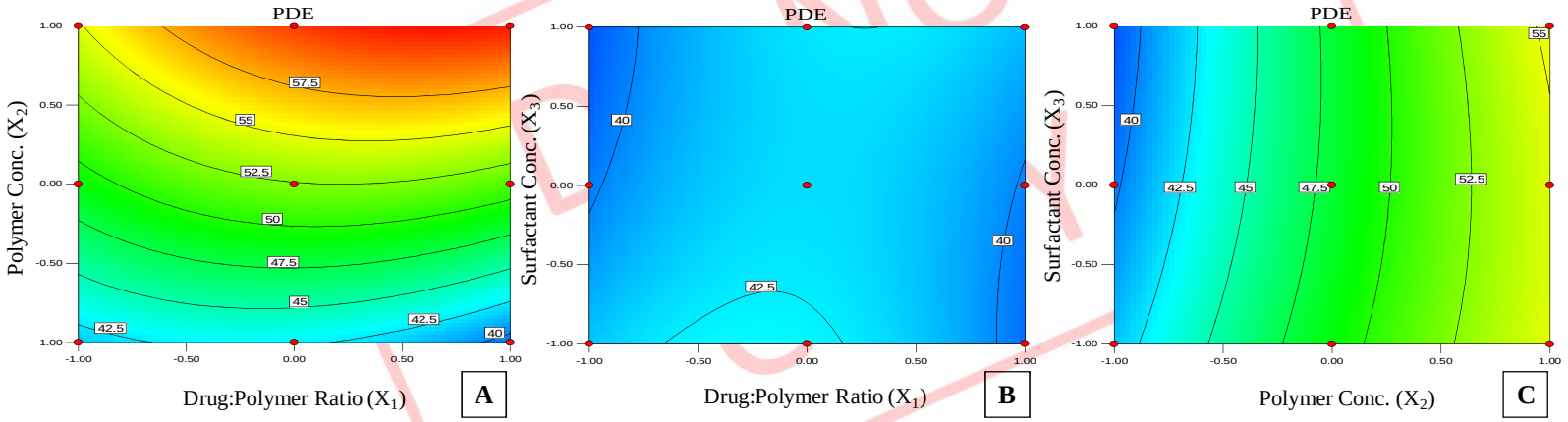

Figure 4.9 Contour plots showing effect of (A) X_1 vs X_2 (at -1 level of X_3), (B) X_1 vs X_3 (at -1 level of X_2) and (C) X_2 vs X_3 (at -1 level of X_1) on PDE of ATZ loaded PLGA NPs.

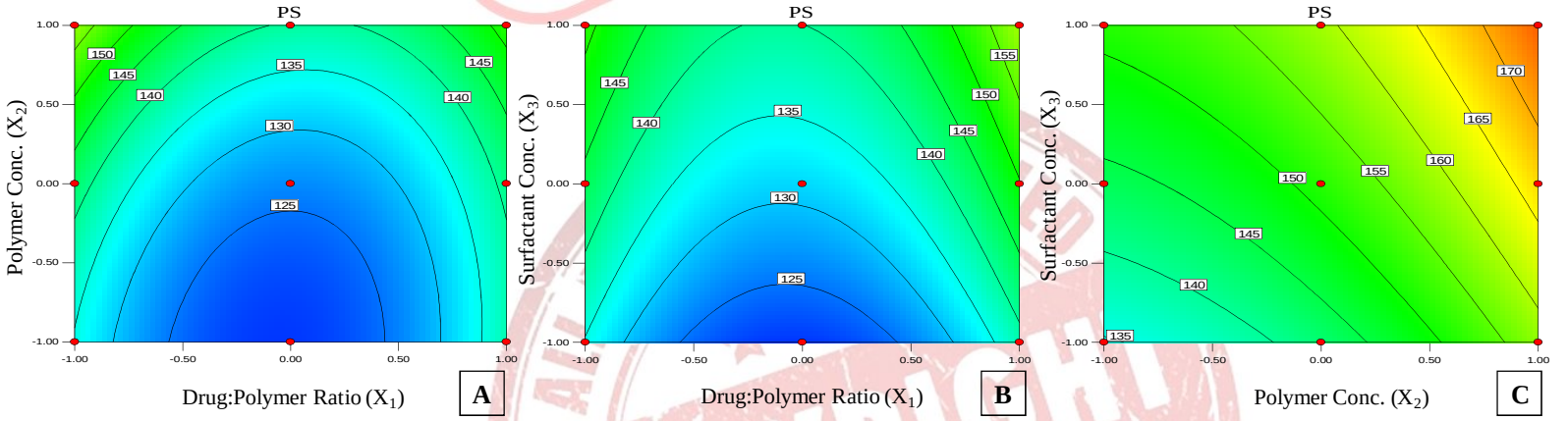

Figure 4.10 Contour plots showing effect of (A) X_1 vs X_2 (at -1 level of X_3), (B) X_1 vs X_3 (at -1 level of X_2) and (C) X_2 vs X_3 (at -1 level of X_1) on PS of ATZ loaded PLGA NPs.

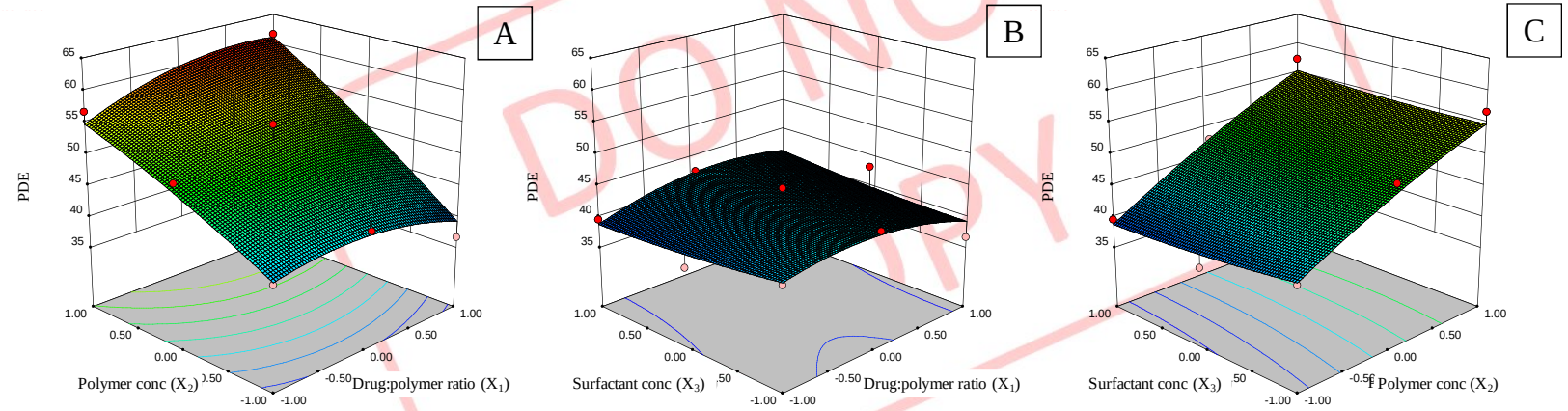

Figure 4.11 Response surface plot showing effect of (A) X_1 vs X_2 (at -1 level of X_3), (B) X_1 vs X_3 (at -1 level of X_2) and (C) X_2 vs X_3 (at -1 level of X_1) on PDE of ATZ loaded PLGA NPs.

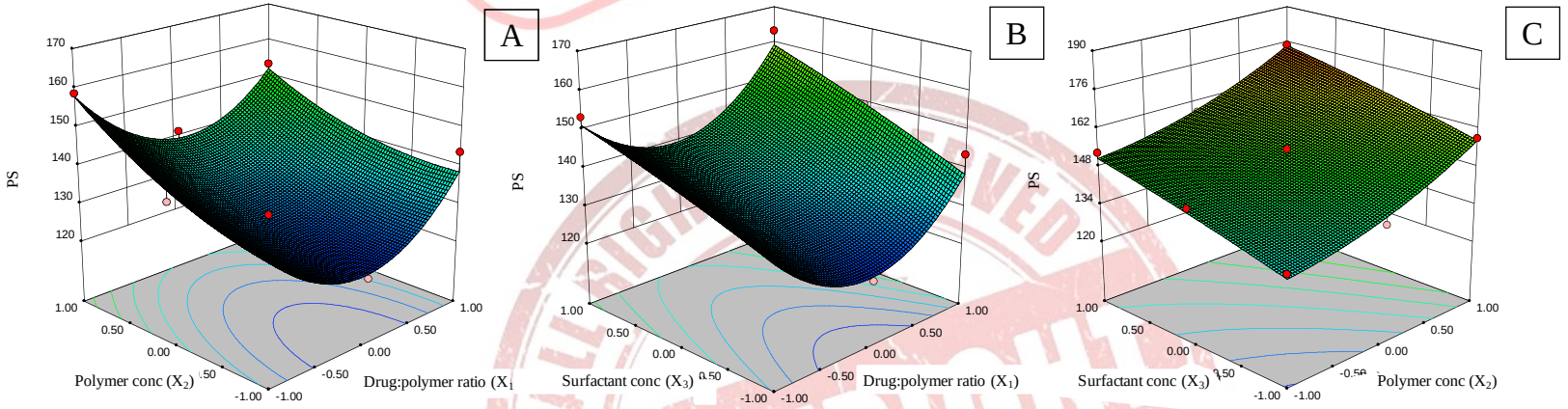

Figure 4.12 Response surface plot showing effect of (A) X_1 vs X_2 (at -1 level of X_3), (B) X_1 vs X_3 (at -1 level of X_2) and (C) X_2 vs X_3 (at -1 level of X_1) on PS of ATZ loaded PLGA NPs.

4.11.2.3 Desirability criteria

From the results, the optimum levels of independent variables were screened by multiple regression analysis. Since PDE and PS were taken into consideration simultaneously, the batch with smallest PS of 120 nm exhibited only 42.5% PDE (at X_1 = 0, X_2 = -0.6 to -1.0, X_3 = -0.6 to -1.0) while that with highest PDE of 60% produced particle size of 155 nm (at X_1 = 1, X_2 = 0.6 to 1.0, X_3 = -0.4 to -1.0). Hence, desirability criteria obtained using Design Expert software (version 8.0.3) was used to find out optimized formulation parameters. Our criteria included maximum PDE and PS not more than 200 nm. The optimum formulation offered by the software based on desirability was found at 0.68, 1, and -1 level of X_1, X_2 and X_3 respectively. The results of dependent variables from the software were found to be 61.39% for PDE and 144.68 nm for PS (figure 4.13) at these levels which is as per our desired criteria. The calculated desirability factor for offered formulations was 0.990, which was near to 1 and indicates suitability of the designed factorial model.

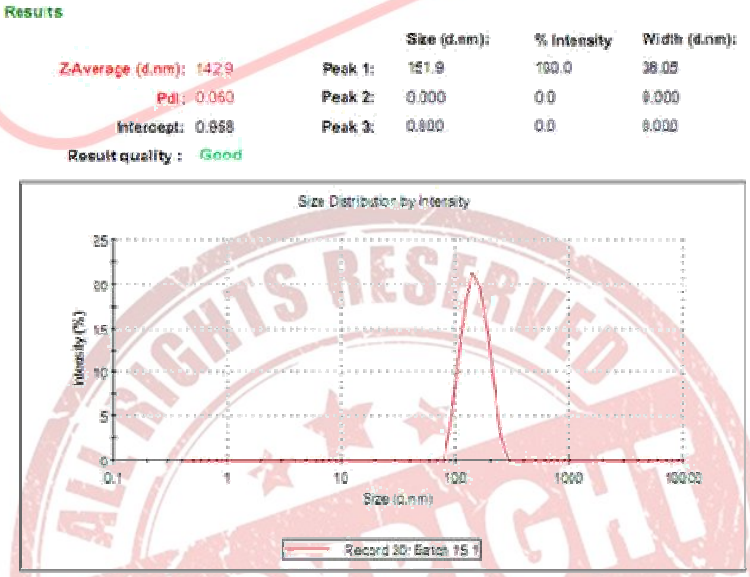

Figure 4.13 Particle size distribution of ATZ loaded PLGA NPs

4.11.2.4 Checkpoint analysis and normalized error

Three batches were prepared for check point analysis and results of both PDE and PS (table 4.10) indicated that the measured response was more accurately predicted by regression analysis which was proven by lower NE value of regression analysis (0.07022 for PDE and 0.04754 for PS). Data analysis using student's t test revealed that

there was no statistically significant difference ($p<0.05$) between experimentally obtained values and predicted values by MRA.

Table 4.10 Check point analysis, t test analysis and normalized error determination

Checkpoint batches with their predicted and measured values of PDE and PS							
Batch No.	X_1	X_2	X_3	PDE		PS	
				Observed	Predicted	Observed	Predicted
1	-1 (1:10)	0.7 (92.5 mg)	0.1 (52.5 mg)	52.74	54.163	161.4	162.609
2	0 (1:15)	-0.8 (55 mg)	0.8 (70 mg)	42.88	44.309	134.6	139.782
3	1 (1:20)	-0.3 (67.5 mg)	-0.5 (37.5 mg)	48.76	46.048	140.8	144.583
$t_{calculated}$				0.97608		0.10031	
$t_{tabulated}$				2.9199		2.9199	
Normalized Error				0.070229		0.04754	

4.11.3 Lyophilization and optimization of cryoprotectants

In this study, different cryoprotectants (trehalose, sucrose and mannitol) were used in different ratios (1:1, 1:2, 1:3, 1:4) and PS was recorded as shown in table 4.11. Initial PS

Table 4.11 Effect of cryoprotectants and their concentration on PS of lyophilized NPs after re-dispersion in distilled water

Cryoprotectant	Ratio	Final Avg. PS (nm)	S_f/S_i
Trehalose	1:1	252.8	1.57*
	1:2	243.3	1.51*
	1:3	260.1	1.62*
	1:4	355.7	2.21
Sucrose	1:1	216.8	1.35*
	1:2	213.9	1.33*
	1:3	233.3	1.45*
	1:4	250.3	1.56
Mannitol	1:1	239.1	1.49
	1:2	304.7	1.89
	1:3	278	1.73
	1:4	277.1	1.72

*indicates good re-dispersibility

of NPs was found to be 160.9 nm. The ratio of PS (after lyophilization, S_f and before lyophilization, S_i) was found to be lowest (1.33) for sucrose in 1:2 ratio. Trehalose also showed less increase in PS after re-dispersion (S_f/S_i ratio of 1.51). Batches prepared with trehalose and sucrose at 1:1, 1:2 and 1:3 ratio showed good re-dispersibility with PDI less than 0.2. PDI is a measure of dispersion homogeneity and usually ranges from 0 to 1. Values close to 0 indicate a homogeneous dispersion while those greater than 0.3 indicate high heterogeneity [Ahlin et al. 2002].

4.12Formulation and optimization of ATZ loaded cPCL NPs

4.12.1 Preliminary optimization of ATZ loaded cPCL NPs

4.12.1.1 Selection of organic solvent

Three different organic solvents (acetone, acetonitrile and tetrahydrofuran) were used for preparation of cPCL NPs (table 4.12). NPs formulated using acetone showed PDE of 49.63 ± 1.15% with PS of 138.2 ± 4.9 nm while NPs formulated using acetonitrile were of low PDE and PS. PDE was again decreased when tetrahydrofuran was used as solvent with no significant change in PS. Hence, acetone was selected for further studies.

Table 4.12 Selection of organic phase in preliminary optimization of ATZ loaded cPCL NPs

Solvents	PDE (%)	PS (nm)
Acetone	49.63 ± 1.15	138.2 ± 4.9
Acetonitrile	43.45 ± 1.64	130.6 ± 4.6
Tetra hydro furan	44.67 ± 1.12	150.6 ± 6.7

4.12.1.2 Selection of volume of organic solvent

Different volumes of organic solvent (acetone) were used to dissolve polymer (50 mg) and results are represented in table 4.13. It was observed that as the volume of organic

Table 4.13 Selection of volume of organic solvent in preliminary optimization of ATZ loaded cPCL NPs

Volume of organic solvent	PDE (%)	PS (nm)
3 ml	56.35 ± 1.82	235.2 ± 7.1
4 ml	53.68 ± 1.12	205.4 ± 4.7
5 ml	55.38 ± 2.23	190.6 ± 5.1

solvent was increased, PS decreases significantly with no major change in PDE. This was possibly due to decreased viscosity of organic phase with increase in volume of organic solvent which can easily dispersed in aqueous phase containing surfactant. Hence, 5 ml of acetone was selected as organic phase.

4.12.1.3 Selection of surfactant

Three different surfactants were initially used for formulation development namely Pluronic F-68® (P188), Pluronic F-127® (P127) and Poly vinyl alcohol (PVA) (table 4.14). Out of these, better one is selected based on resultant PDE and PS. With constant level of surfactant concentration (0.5%) for all three surfactants, PDE was found to be highest when PVA was used, but at the same time PS was found to be of larger size (332.4 ± 7.6 nm). No significant difference in PS was observed when P188 or P127 was used, but PDE was higher when P188 was used. Hence, P188 was used in further studies.

Table 4.14 Selection of surfactant in preliminary optimization of ATZ loaded cPCL NPs

Surfactant	PDE (%)	PS (nm)
P188	52.45 ± 0.42	175.9 ± 2.4
P127	50.6 ± 0.96	170.1 ± 3.9
PVA	54.36 ± 1.05	404.1 ± 8.63

4.12.2 Optimization of ATZ loaded cPCL NPs using 3^3 factorial design

Twenty seven batches of ATZ loaded cPCL NPs were prepared by using 3^3 factorial design varying three independent variables, drug:polymer ratio (X_1), polymer concentration in organic phase (X_2) and surfactant concentration in aqueous phase (X_3) (Table 4.15). The PDE and PS were taken as dependent variables and the results were recorded (Table 4.16). The main effects of X_1, X_2 and X_3 represent the average result of changing one variable at a time from its low to high value. The interactions (X_1X_2, X_1X_3, X_2X_3 and $X_1X_2X_3$) show how the PDE and PS changes when two or more variables were simultaneously changed. The values for the twenty seven batches showed a wide variation from 39.4 ± 1.9 to 72.5 ± 1.7% and 138.2 ± 4.9 to 241.6 ± 3.1 nm for PDE and PS respectively (Table 4.16). This is reflected by the wide range of coefficients of the terms of equation 3 representing the individual and combined variables.

Table 4.15 Coded values of the formulation parameters of ATZ loaded cPCL NPs

Coded Values	Actual values of dependent variables		
	X_1	X_2	X_3
-1	1 : 10	0.50 %	0.25 %
0	1 : 15	0.75 %	0.50 %
1	1 : 20	1.0 %	0.75 %

X_1 Drug:polymer ratio
X_2 Polymer concentration (% w/v)
X_3 Surfactant concentration (% w/v)

$$Y_1 = 55.92 + 6.23\ X_1 + 4.34\ X_2 - 4.33\ X_3 - 0.53\ X_1X_2 + 0.04\ X_1X_3 - 0.34\ X_2X_3 + 0.70\ X_1^2 - 0.32\ X_2^2 + 0.25\ X_3^2 - 0.44\ X_1X_2X_3 \quad (13)$$

$$Y_2 = 192.82 + 17.29\ X_1 + 16.31\ X_2 + 17.69\ X_3 - 0.7\ X_1X_2 + 0.32\ X_1X_3 + 0.50\ X_2X_3 + 1.03\ X_1^2 + 2.02\ X_2^2 - 4.19\ X_3^2 + 1.11\ X_1X_2X_3 \quad (14)$$

$$Y_1 = 56.34 + 6.23\ X_1 + 4.34\ X_2 - 4.33\ X_3 \quad (15)$$

$$Y_2 = 194.86 + 17.29\ X_1 + 16.31\ X_2 + 17.65\ X_3 - 4.19\ X_3^2 \quad (16)$$

The significance of each coefficient of equation 13 and 14 were determined by student's 't' test and p-value, which are listed in table 4.17 and 4.18 respectively. The larger the magnitude of the 't' value and the smaller the p-value, the more significant is the corresponding coefficient [Adinarayana and Ellaiah 2002; Akhnazarova 1982]. Small values of the coefficients of the terms X_1^2, X_2^2, X_3^2, X_1X_2, X_2X_3, X_1X_3, and $X_1X_2X_3$ in equation 13 and X_1^2, X_2^2, X_1X_2, X_2X_3, X_1X_3, and $X_1X_2X_3$ in equation 14 for PDE and PS respectively implied that all these terms were least contributing in the preparation of the ATZ loaded cPCL NPs.

The small values of coefficients were not-significant ($p>0.05$) and hence neglected from the FM. Reduced polynomial equations (equation 15 and 16, for PDE and PS resp.) were obtained following MRA of PDE and PS. Based on their p-value, it implied that the second order effects of drug:polymer ratio (X_1) and polymer concentration in organic phase (X_2) were not found to be significant for both PDE and PS. The interactions between X_1X_2, X_2X_3, X_1X_3 and $X_1X_2X_3$ were also not found to be significant for both PDE and PS as evident from their p-values (p-values>0.05 in all cases) (table 4.17 and 4.18).

Table 4.16 Layout of 3^3 full factorial design for ATZ loaded cPCL NPs

Sr. No.	X_1	X_2	X_3	Y_1* (PDE, in %)	Y_2* (PS, in nm)
1	-1	-1	-1	49.6 ± 1.15	138.2 ± 4.9
2	-1	-1	0	44.2 ± 1.87	164.6 ± 6.6
3	-1	-1	1	39.4 ± 1.89	178.0 ± 3.6
4	-1	0	-1	55.3 ± 1.18	157.1 ± 1.9
5	-1	0	0	52.5 ± 0.42	175.9 ± 2.4
6	-1	0	1	47.7 ± 1.76	187.9 ± 2.5
7	-1	1	-1	59.4 ± 0.6	174.8 ± 2.5
8	-1	1	0	54.3 ± 1.43	191.7 ± 4.7
9	-1	1	1	50.8 ± 0.96	207.8 ± 2.9
10	0	-1	-1	56.2 ± 2.35	156.3 ± 4.6
11	0	-1	0	51.9 ± 1.8	175.1 ± 4.3
12	0	-1	1	48.34 ± 1.72	188.6 ± 4.5
13	0	0	-1	60.7 ± 0.92	170.3 ± 1.2
14	0	0	0	5.1.4 ± 2.2	190.6 ± 5.1
15	0	0	1	52. ± 2.3	206.3 ± 5.7
16	0	1	-1	65.63 ± 2.08	188.5 ± 2.8
17	0	1	0	58.82 ± 0.79	215.2 ± 3.6
18	0	1	1	53.99 ± 1.28	231.5 ± 3.8
19	1	-1	-1	62.94 ± 2.10	175.9 ± 2.9
20	1	-1	0	59.3 ± 1.68	200.3 ± 5.9
21	1	-1	1	55.17 ± 1.78	210.7 ± 3.9
22	1	0	-1	64.72 ± 3.10	191.1 ± 6.7
23	1	0	0	62.31 ± 3.07	214.8 ± 4.4
24	1	0	1	58.53 ± 3.45	222.5 ± 2.7
25	1	1	-1	72.49 ± 1.71	204.8 ± 4.3
26	1	1	0	66.88 ± 1.45	225.5 ± 2.7
27	1	1	1	62.85 ± 0.51	241.6 ± 3.1

*values are represented as mean ± s.d.

The results of ANOVA of the second order polynomial equation of PDE and PS are given in table 4.19 and 4.20 respectively. Since the calculated F value was less than the

Table 4.17 Model coefficients estimated by multiple regression analysis for PDE of ATZ loaded cPCL NPs.

Factor	Coefficients	t Stat	p-value
Intercept	55.92	83.798	< 0.0001*
X_1	6.23	20.165	< 0.0001*
X_2	4.34	14.042	< 0.0001*
X_3	-4.33	-13.863	< 0.0001*
X_1^2	0.70	1.306	0.2098
X_2^2	-0.32	-0.608	0.5519
X_3^2	0.25	0.469	0.6449
X_1X_2	-0.53	-1.408	0.1782
X_1X_3	0.04	0.089	0.9302
X_2X_3	-0.34	-0.892	0.3855
$X_1X_2X_3$	-0.44	-0.946	0.3580

* Significant at $p < 0.05$

Table 4.18 Model coefficients estimated by multiple regression analysis for PS of ATZ loaded cPCL NPs

Factor	Coefficients	t Stat	p-value
Intercept	192.82	115.068	< 0.0001*
X_1	17.29	22.293	< 0.0001*
X_2	16.31	21.025	< 0.0001*
X_3	17.69	22.547	< 0.0001*
X_1^2	1.03	0.769	0.453
X_2^2	2.02	1.501	0.153
X_3^2	-4.19	-3.118	0.0066*
X_1X_2	-0.7	-0.737	0.472
X_1X_3	0.32	0.305	0.764
X_2X_3	0.49	0.523	0.608
$X_1X_2X_3$	1.11	0.956	0.353

* Significant at $p < 0.05$

tabulated F value for PDE and for PS [Bolton 1997], it was concluded that the neglected terms did not significantly contribute in the prediction of PDE and PS. Hence, F-Statistic

of the results of ANOVA of full and reduced model justified the omission of non-significant terms of equation 9 and 10.

Table 4.19 ANOVA of full and reduced models for PDE of ATZ loaded cPCL NPs

		df	SS	MS	F	R	R^2	Adjusted R^2
Regression	FM	10	1385.7	138.6	80.7	0.9902	0.9805	0.9684
	RM	3	1375.4	458.5	279.3	0.9865	0.9733	0.9698
Residual	FM	16	27.5	1.71				
	RM	23	37.8	1.64				

SSE2 - SSE1 = 37.8 - 27.5 = 10.3

No. of parameters omitted = 7

MS of error (full model) = 1.71

F calculated = (SSE2 - SSE1 / No. of parameters omitted) / MS of error (FM)

= (10.3 / 7) / 1.71

= 0.8605

F tabulated = 2.6572

Table 4.20 ANOVA of full and reduced models for PS of ATZ loaded cPCL NPs

		df	SS	MS	F	R	R^2	Adjusted R^2
Regression	FM	10	15934.9	1593.5	147.1	0.9946	0.9892	0.9825
	RM	4	15884.3	3971.1	390.3	0.9930	0.9861	0.9836
Residual	FM	16	173.3	10.83				
	RM	22	223.9	10.18				

SSE2 - SSE1 = 223.9 - 173.3 = 50.6

No. of parameters omitted = 6

MS of error (full model) = 10.83

F calculated = (SSE2 - SSE1 / No. of parameters omitted) / MS of error (FM)

= (50.6 / 6) / 10.83

= 0.7787

F tabulated = 2.7413

When the coefficients of the three independent variables in equation 13 and 14 were compared, the value for the variable X_1 (b_1 = 6.23) for PDE and X_3 (b_3 = 17.69) for PS was considered to be a major contributing variable affecting the PDE and PS of the NPs. The Fisher F test with a very low probability value ($P_{model} > F = 0.000001$) demonstrated

a very high significance for the regression model. The goodness of fit of the model was checked by the determination coefficient (R^2). In this case, the values of the determination coefficients (R^2 = 0.9805 and 0.9892 for FM and 0.9733 and 0.9861 for RM for PDE and PS respectively) indicated that over 97% of the total variations were explained by the model. High R^2 values of FM as compared to RM were due to the large number of factors included. R^2 value is more if the number of factors are more [Montgomery 2004]. The values of adjusted R^2 (0.9684 and 0.9825 for FM and 0.9698 and 0.9836 for RM for PDE and PS respectively) were similar for FM and RM for both PDE and PS, indicating the suitability of reducing the model. Moreover, the high values of correlation coefficients (R = 0.9902 and 0.9946 for FM and 0.9865 and 0.9930 for RM for PDE and PS respectively) signifies an excellent correlation between the independent variables [Box et al. 1978]. All the above considerations indicated an excellent adequacy of the developed regression model [Adinarayana and Ellaiah 2002; Akhnazarova 1982; Box et al. 1978; Yee and Blanch 1993].

4.12.2.1 Contour plots

Contour plots were established between X_1 vs X_2, X_1 vs X_3 and X_2 vs X_3 at fixed level (-1) of third variable as shown in figure 4.14 and 4.15 for PDE and PS respectively. The plots showed that PDE was greatly dependent on drug:polymer ratio and polymer concentration (figure 4.14A). When both these variables were at their maximum levels, PDE was found to be maximum (>65%). However, the contour of drug:polymer ratio vs surfactant concentration (figure 4.14B) showed increase in PDE with increase in drug:polymer ratio and decrease in surfactant conc. PDE was found to increase linearly with increase in polymer concentration and simultaneous decrease in surfactant conc. (figure 4.14C). Also, the parallel lines in all the three contour plots implies the linear increase or decrease in PDE with change in any two independent variables at constant level of third variable. PS was found to increase with increase in both drug:polymer ratio and polymer conc. (figure 4.15A) and was maximum at +1 level of X_1 and X_2 at 0 level of X_3. Similar observations were observed when counter of drug:polymer ratio was plotted with surfactant conc. at fixed level (-1) of polymer conc. PS was found to increase with simultaneous increase in both the variables (figure 4.15B). Lowest PS of about 160 nm was observed at -1 level of polymer and surfactant concentration and 0 level of drug:polymer ratio (figure 4.15C). PS was found to be maximum at high level

(+1) of polymer conc. and high level of surfactant conc. It increased from 160 to 220 nm linearly with increase in both the variables i.e., polymer and surfactant concentration (figure 4.15C). It was concluded from the contours that NPs with smallest PS can be prepared at low levels (-1) of all the three variables.

4.12.2.2 Response surface plots

Three dimensional response surface plots are very helpful in learning about both the main and interaction effects of the independent variables. These were plotted between X_1 vs X_2, X_1 vs X_3 and X_2 vs X_3 at fixed level (-1) of third variable as shown in figure 4.16 and 4.17 for each PDE and PS respectively. PDE was not significantly affected when polymer conc. was varied alone, but was increased upon simultaneous increase in drug:polymer ratio with polymer concentration showing interactive effect between the two variables (figure 4.16A). However, PDE was found to increase with decrease in surfactant conc. and increase in drug:polymer ratio and found to be highest at -1 level of X_3 and +1 level of X_1 (figure 4.16B). Similar trend was observed in response surface plot of polymer conc. and surfactant conc. (figure 4.16C). It can be concluded from the response surface plots that increase in drug:polymer ratio and polymer conc. increases PDE, whereas increase in surfactant conc. causes decrease in PDE. Response surface plot of drug:polymer ratio vs polymer concentration showed increase in PS with increase in drug:polymer ratio and increase in polymer conc. possibly due to increased viscosity of organic phase with increase in polymer conc. (figure 4.17A). Response surface plot of drug:polymer ratio and surfactant conc. also showed similar trends and NPs of the PS more than 220 nm was formed at +1 level of both the variables at 0 level of polymer conc. (figure 4.17B). Interaction effect of polymer conc. and surfactant conc. showed increase in PS with increase in both the variables (figure 4.17C).

4.12.2.3 Desirability criteria

From the results, the optimum levels of independent variables were screened by multiple regression analysis. Since PDE and PS were taken into consideration simultaneously, the batch with smallest particle size of 138.2 ± 4.9 nm exhibited only 49.63 ± 1.15% PDE while that with highest PDE of 72.49 ± 1.71% produced particle size of 204.8 ± 4.3 nm (at X_1 = 1, X_2 = 0.6 to 1.0, X_3 = -0.4 to -1.0). Hence, desirability criteria obtained using Design Expert software (version 8.0.3) was used to find out optimized formulation parameters. Our criteria included maximum PDE and PS not more

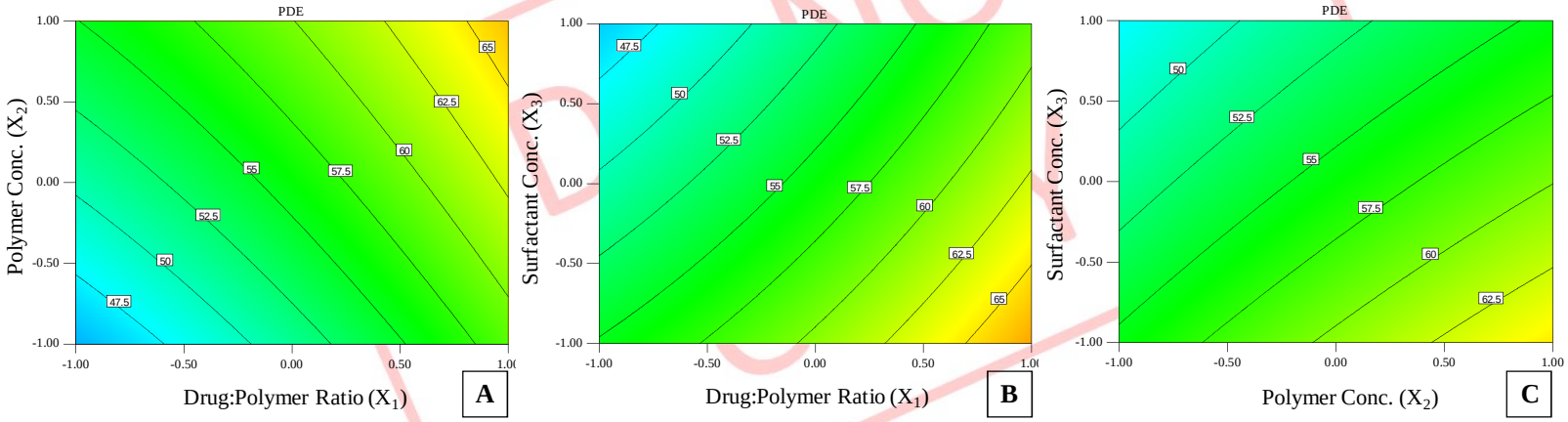

Figure 4.14 Contour plots showing effect of (A) X_1 vs X_2 (at -1 level of X_3), (B) X_1 vs X_3 (at -1 level of X_2) and (C) X_2 vs X_3 (at -1 level of X_1) on PDE of ATZ loaded cPCL NPs.

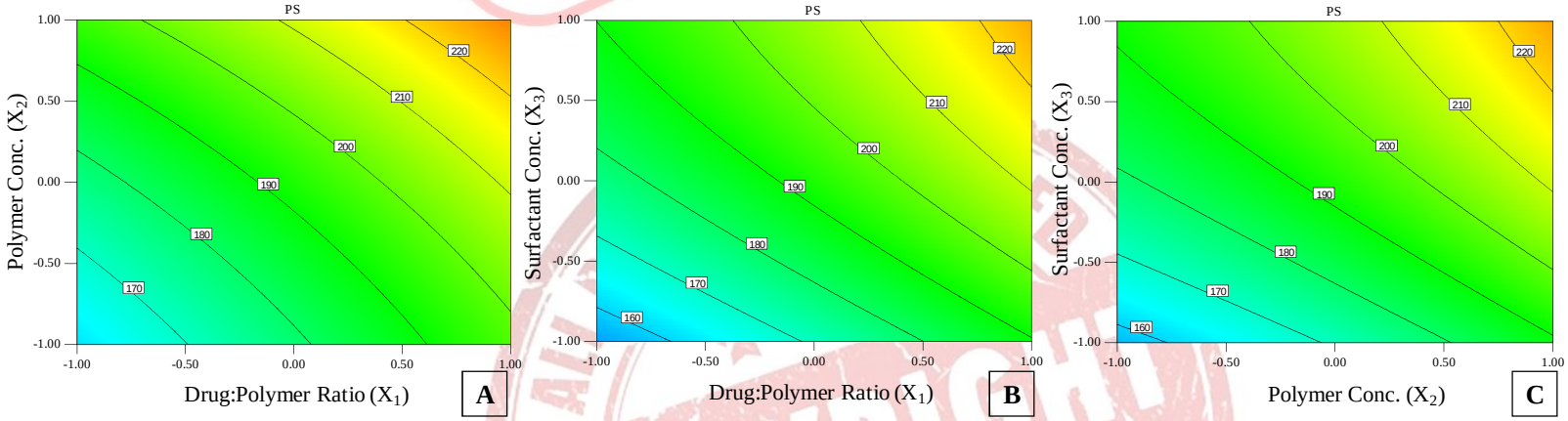

Figure 4.15 Contour plots showing effect of (A) X_1 vs X_2 (at -1 level of X_3), (B) X_1 vs X_3 (at -1 level of X_2) and (C) X_2 vs X_3 (at -1 level of X_1) on PS of ATZ loaded cPCL NPs.

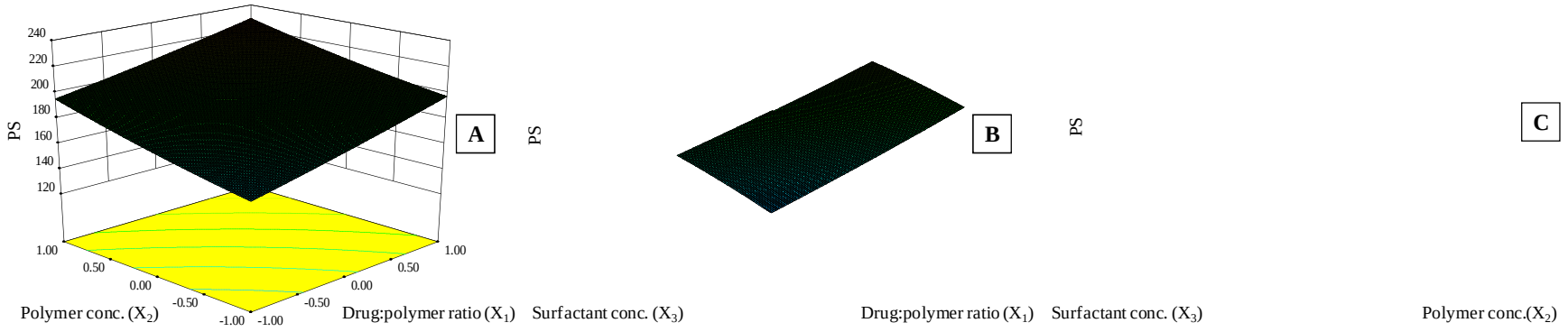

Figure 4.17 Response surface plot showing effect of (A) X_1 vs X_2 (at -1 level of X_3), (B) X_1 vs X_3 (at -1 level of X_2) and (C) X_2 vs X_3 (at -1 level of X_1) on PS of ATZ loaded cPCL NPs.

than 200 nm. The optimum formulation offered by the software based on desirability was found at 1.0, 0.69, and -1.0 level of X_1, X_2 and X_3 respectively. The results of dependent variables from the software were found to be 70.21% for PDE and 200 nm for PS (figure 4.18) at these levels which is as per our desired criteria. The calculated desirability factor for offered formulations was 0.965, which was near to 1 and indicates suitability of the designed factorial model.

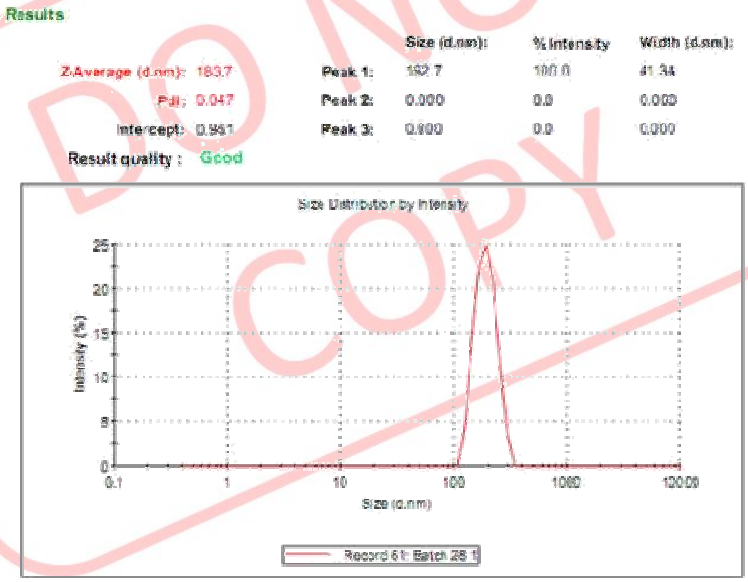

Figure 4.18 Particle size distribution of ATZ loaded cPCL NPs

4.12.2.4 Checkpoint analysis and normalized error

Table 4.21 Check point analysis, t test analysis and normalized error determination

Checkpoint batches with their predicted and measured values of PDE and PS							
Batch No.	X_1	X_2	X_3	PDE		PS	
				Observed (avg.)	Predicted	Observed (avg.)	Predicted
1	-1 (1:10)	-0.2 (92.5 mg)	0.1 (52.5 mg)	47.93	48.81	173.8	176.02
2	0 (1:15)	0.7 (55 mg)	-0.8 (70 mg)	63.51	62.84	192.9	189.47
3	1 (1:20)	-0.8 (67.5 mg)	-0.3 (37.5 mg)	59.58	60.39	195.4	193.43
		$t_{calculated}$		0.5681		0.024	
		$t_{tabulated}$		2.9199		2.9199	
		Normalized Error		0.0252		0.0431	

Three batches were prepared for check point analysis and results of both PDE and PS (table 4.21) indicated that the measured response was more accurately predicted by regression analysis which was proven by lower NE value of regression analysis (0.0252 for PDE and 0.0431 for PS). Data analysis using student's t test revealed that there was no statistically significant difference ($p<0.05$) between experimentally obtained values and predicted values by MRA.

4.12.3 Lyophilization and optimization of cryoprotectants

In this study, different cryoprotectants (trehalose, sucrose and mannitol) were used in different ratios (1:1, 1:2, 1:3, 1:4) and PS was recorded as shown in table 4.22. Initial PS of NPs was found to be 194.7 nm. The ratio of PS (after lyophilization, S_f and before lyophilization, S_i) was found to be lowest (1.24) for sucrose in 1:2 ratio. Trehalose also showed less increase in PS after re-dispersion (S_f/S_i ratio of 1.41). Batches prepared with trehalose and sucrose at 1:1 and 1:2 ratio showed good re-dispersibility with PDI less than 0.2. PDI is a measure of dispersion homogeneity and usually ranges from 0 to 1. Values close to 0 indicate a homogeneous dispersion while those greater than 0.3 indicate high heterogeneity [Ahlin et al. 2002].

Table 4.22 Effect of cryoprotectants and their concentration on PS of lyophilized NPs after re-dispersion in distilled water

Cryoprotectant	Ratio	Final Avg. PS (nm)	S_f/S_i
Trehalose	1:1	280.3	1.44*
	1:2	275.1	1.41*
	1:3	297.1	1.53
	1:4	342.1	1.76
Sucrose	1:1	254.9	1.31*
	1:2	241.5	1.24*
	1:3	272	1.40*
	1:4	302.3	1.55
Mannitol	1:1	282.9	1.45*
	1:2	326.1	1.67
	1:3	341.2	1.75
	1:4	332.8	1.71

*indicates good re-dispersibility

4.13 Formulation and optimization of EXE loaded PLGA NPs

4.13.1 Preliminary optimization of EXE loaded PLGA NPs

4.13.1.1 Selection of organic solvent

Three different organic solvents (acetone, acetonitrile and tetrahydrofuran) were used for preparation of PLGA NPs (table 4.23). NPs formulated using acetone showed PDE of 73.2 ± 2.0% with PS of 195.1 ± 3.6 nm while NPs formulated using acetonitrile were of low PDE and high PS. No significant change in PDE was observed when tetrahydrofuran was used as solvent with increase in PS. Hence, acetone was selected for further studies.

Table 4.23 Selection of organic phase in preliminary optimization of EXE loaded PLGA NPs

Solvents	PDE (%)	PS (nm)
Acetone	73.2 ± 2.0	195.1 ± 3.6
Acetonitrile	71.6 ± 1.3	211.3 ± 4.1
Tetra hydro furan	72.7 ± 1.1	245.7 ± 4.1

4.13.1.2 Selection of surfactant phase

Three different surfactants were initially used for formulation development namely Pluronic F-68® (P188), Pluronic F-127® (P127) and Poly vinyl alcohol (PVA) (table 4.24). Out of these, better one is selected based on resultant PDE and PS. With constant level of surfactant concentration (0.5%) for all three surfactants, no significant change in PDE was observed, but at the same time PS was found to be of larger size (229.8 ± 4.2 nm) using PVA as surfactant. No significant difference in PS was observed when P188 or P127 was used, but PDE was higher when P188 was used as surfactant. Hence, P188 was used in further studies.

Table 4.24 Selection of surfactant phase in preliminary optimization of EXE loaded PLGA NPs

Surfactant	PDE (%)	PS (nm)
P188	51.2 ± 2.0	203.7 ± 2.7
P127	50.7 ± 1.1	217.6 ± 5.4
PVA	51.6 ± 1.8	229.8 ± 4.2

4.13.1.3 Selection of surfactant concentration

Different concentrations (0.5, 1.0, 1.5%) of surfactant (P188) were used in aqueous phase and results are represented in table 4.25. It was observed that as the

concentration was increased, PS increases significantly with no major change in PDE (50.8 – 52.4%). This was possibly due to coating of surfactant on NPs after precipitation. Hence, 0.5% of P188 was selected as surfactant concentration.

Table 4.25 Selection of surfactant concentration in preliminary optimization of EXE loaded PLGA NPs

Surfactant concentration	PDE (%)	PS (nm)
0.5%	51.2 ± 2.0	203.7 ± 2.7
1.0%	50.8 ± 1.4	218.6 ± 4.1
1.5%	52.4 ± 1.5	240.1 ± 3.9

4.13.2 Optimization of EXE loaded PLGA NPs using BBD

Using BBD, thirteen batches of EXE loaded PLGA NPs were prepared with drug:polymer ratio (X_1), amount of polymer (X_2) and volume of organic phase (X_3) as three independent variables. Coded values and actual values of the three independent variables are represented in table 4.26. Batches prepared using BBD were evaluated for PDE and PS as the dependent variables and recorded in table 4.27.

Table 4.26 Coded values of the formulation parameters of EXE loaded PLGA NPs

Coded values	Actual values		
	X_1	X_2	X_3
-1	1 : 15	50 mg	6 ml
0	1 : 20	100 mg	8 ml
1	1 : 25	150 mg	10 ml

X_1 Drug:polymer ratio
X_2 Amount of polymer (mg)
X_3 Volume of organic phase

The obtained PDE and PS were subjected to multiple regression to yield second order polynomial equations (equation 17 and 18, for PDE and PS respectively). Linear coefficients (b_1, b_2 and b_3 of X_1, X_2 and X_3, respectively) represent extent of effect by changing individual variable. Positive or negative sign in equation against different coefficients indicate increase or decrease in individual dependent response. The value of coefficients against interactions terms (X_1X_2, X_1X_3 and X_2X_3) shows how the PDE and

Table 4.27 Box Behnken experimental design with measured responses for EXE loaded PLGA NPs

Sr. No.	Box Behnken experimental design with measured responses				
	X_1	X_2	X_3	Y_1* (PDE ± SD)	Y_2* (PS ± SD)
1	0	-1	-1	51.2 ± 2.0	203.7 ± 2.7
2	0	-1	1	66.7 ± 1.7	150.7 ± 4.9
3	0	1	-1	21.8 ± 2.5	239.7 ± 6.8
4	0	1	1	66.3 ± 0.8	187.5 ± 8.1
5	-1	0	-1	52.7 ± 0.1	258.9 ± 5.8
6	-1	0	1	58.8 ± 1.7	192.5 ± 2.7
7	1	0	-1	44.3 ± 2.1	293.3 ± 0.6
8	1	0	1	73.2 ± 2.0	195.1 ± 3.6
9	-1	-1	0	64.5 ± 0.6	169.1 ± 3.8
10	-1	1	0	49.9 ± 1.8	345.9 ± 22.1
11	1	-1	0	68.1 ± 2.2	214.4 ± 7.1
12	1	1	0	62.7 ± 0.9	384.1 ± 10.9
13	0	0	0	75.49	188.55
14	0	0	0	76.15	190.4
15	0	0	0	73.84	186.7

*values are represented as mean ± s.d.

$$Y_1 = 75.16 + 2.79\ X_1 - 6.22\ X_2 + 11.88\ X_3 + 2.28\ X_1X_2 + 5.69\ X_1X_3 + 7.25\ X_2X_3 - 4.06\ X_1^2 - 9.81\ X_2^2 - 13.87\ X_3^2 \quad (17)$$

$$Y_2 = 188.55 + 13.81\ X_1 + 52.4\ X_2 - 33.98\ X_3 - 1.78\ X_1X_2 - 8.46\ X_1X_3 + 0.2\ X_2X_3 + 64.39\ X_1^2 + 25.38\ X_2^2 - 18.51\ X_3^2 \quad (18)$$

$$Y_1 = 72.66 - 6.22\ X_2 + 11.88\ X_3 + 7.25\ X_2X_3 - 9.49\ X_2^2 - 13.56\ X_3^2 \quad (19)$$

$$Y_2 = 192.48 + 52.4\ X_2 + 63.9\ X_1^2 \quad (20)$$

PS changes when two variables were simultaneously changed. The values of all the 13 batches showed wide variation of 21.8 ± 2.5 to 76.2 ± 1.2% and 150.7 ± 4.9 to 384.1 ± 10.9 nm for PDE and PS, respectively as shown in table 4.27. This variation is reflected by the wide range of coefficients of the terms representing the individual and combined variables.

Table 4.28 Model coefficients estimated by multiple regression analysis for PDE of EXE loaded PLGA NPs

Factor	Coefficients	t Stat	P-value
Intercept	75.16	28.21	1.05E-06*
X_1	2.79	1.71	0.1477
X_2	-6.22	-3.81	0.0125*
X_3	11.88	7.28	0.0008*
X_1X_2	2.28	0.99	0.3687
X_1X_3	7.25	2.46	0.0569
X_2X_3	5.69	3.14	0.0256*
X_1^2	-4.06	-1.69	0.1519
X_2^2	-9.81	-4.08	0.0095*
X_3^2	-13.87	-5.77	0.0021*

* Significant at $p < 0.05$

Table 4.29 Model coefficients estimated by multiple regression analysis for PS of EXE loaded PLGA NPs

Factor	Coefficients	t Stat	P-value
Intercept	188.55	7.25	0.0008*
X_1	14.81	0.93	0.3952
X_2	52.40	3.29	0.0217*
X_3	-33.98	-2.13	0.0860
X_1X_2	-1.78	-0.08	0.9402
X_1X_3	-8.46	-0.38	0.7225
X_2X_3	0.20	0.01	0.9933
X_1^2	64.39	2.75	0.0405*
X_2^2	25.38	1.08	0.3283
X_3^2	-18.51	-0.79	0.4656

* Significant at $p < 0.05$

The significance of each coefficient of equations 17 and 18 were determined by student's 't' test and p-value, which are listed in table 4.28 and 4.29 respectively. The larger the magnitude of the 't' value and the smaller the p-value, the more significant is the corresponding coefficient [Adinarayana and Ellaiah 2002; Akhnazarova 1982]. Small

values of the coefficients of the terms X_1, X_1X_2, X_1X_3 and X_1^2 in equation 17 and X_1, X_3, X_1X_2, X_1X_3, X_2X_3, X_2^2 and X_3^2 in equation 18 implied that all these terms were least contributing in the preparation of EXE loaded PLGA NPs. These small values of coefficients had $p>0.05$. Hence, these terms were neglected from the FM considering non-significance and reduced polynomial equations (equation 19 and 20, for PDE and PS respectively) were obtained following regression analysis of PDE and PS. From RM, it was evident that drug:polymer ratio did not affect any of the dependent variables significantly ($p>0.05$). For PDE, the quadratic effect of drug:polymer ratio and interaction effects of X_1X_2 and X_1X_3 were found to be non-significant ($p>0.05$). For PS, all factors other than linear effect of amount of polymer and quadratic effect of drug:polymer ratio were found to be non-significant ($p>0.05$) (table 4.28 and 4.29).

The results of ANOVA of the second order polynomial equation of PDE and PS are given in table 4.30 and 4.31 respectively. Since the calculated F value (3.2077) is less than the tabulated F value (5.1922) ($\alpha = 0.05$, $V_1 = 4$ and $V_2 = 5$) [Bolton 1997] for PDE, and calculated F value (1.0719) is less than the tabulated F value (4.8759) ($\alpha = 0.05$, $V_1 = 7$ and $V_2 = 5$) [Bolton 1997] for PS, it was concluded that the neglected terms did not significantly contribute in the prediction of PDE and PS. Thus, the results of ANOVA of full and reduced model justified the omission of non-significant terms of equation 17 and 18. When the coefficients of the three independent variables in equation 17 and 18 were compared, the values for the variables X_3 (11.88) for PDE and X_2 (52.4) for PS were

Table 4.30 ANOVA of full and reduced models for PDE of EXE loaded PLGA NPs

		df	SS	MS	F	R	R^2	Adjusted R^2
Regression	FM	10	2876.2	287.6	15.01	0.9820	0.9643	0.7000
	RM	6	2602.9	433.8	12.34	0.9342	0.8727	0.6908
Residual	FM	5	106.5	21.3				
	RM	9	379.8	42.2				

SSE2 - SSE1 = 379.8 – 106.5 = 273.3

No. of parameters omitted = 4

MS of error (full model) = 21.3

F calculated = (SSE2 - SSE1 / No. of parameters omitted) / MS of error (FM)

= (273.3 / 4) / 21.3

= 3.2077

found to be maximum and hence these variables were considered to be major contributing variables affecting the PDE and PS of the NPs. The Fisher F test with a very low probability value ($P_{model} > F = 0.000001$) demonstrated a very high significance for the derived regression model.

Table 4.31 ANOVA of full and reduced models for PS of EXE loaded PLGA NPs

		df	SS	MS	F	R	R^2	Adjusted R^2
Regression	FM	10	52435.4	5243.5	2.87	0.9154	0.8379	0.3461
	RM	3	37211.3	12403.8	8.80	0.7711	0.5946	0.4437
Residual	FM	5	10144.3	2028.9				
	RM	12	25368.4	2114.0				

SSE2 - SSE1 = 25368.4 – 10144.3 = 15224.1

No. of parameters omitted = 7

MS of error (full model) = 2028.9

F calculated = (SSE2 - SSE1 / No. of parameters omitted) / MS of error (FM)

= (15224.1 / 7) / 2028.9

= 1.0719

4.13.2.1 Contour plots

Values of X_1, X_2 and X_3 were computed for PDE and PS and contour plots were established between X_1 vs X_2, X_1 vs X_3 and X_2 vs X_3 at fixed level (+1) of third variable as shown in figure 4.19 and 4.20 for each PDE and PS respectively. Contour plots showed that PDE was greatly dependent on drug:polymer ratio and amount of polymer (figure 4.19A). PDE was found to be more than 75% in the range of -0.25 to +0.75 for X_1 and -0.7 to 0 level of X_2 at +1 level of X_3. Contour plot of drug:polymer ratio vs volume of organic phase showed maximum PDE of more than 75% at -0.4 to +1.0 value of X_1 and 0.0 to +1.0 value of X_3 at +1 level of X_2 (figure 4.19B). PDE was found to be below 55% when formulations prepared at any level of X_1 (-1.0 to +1.0) and -0.75 to -1 level of X_3 at +1 level of X_2. Contour plot of amount of polymer vs volume of organic phase at +1 level of drug:polymer ratio indicated PDE of more than 75% when X_2 varied from -0.75 to 0.25 level and X_3 from 0 to +0.75 level (figure 4.19C). Lowest PS of about 180 nm was observed at -0.7 to 0.4 level of drug:polymer ratio, -0.4 to -1.0 level of amount of polymer and at +1 level of volume of organic phase (figure 4.20A). When drug:polymer ratio was varied with volume of organic phase, PS was first found to decrease and then

it increases as drug:polymer ratio increases. PS of less than 160 nm can be obtained at -0.5 to 0.5 level of X_1, 0.7 to 1.0 level of X_3 and 1.0 level of X_2 (figure 4.20B). From figure 4.20C, it can be concluded that PS increases as amount of polymer increases (from -1.0 to 1.0) and volume of organic solvent decreases. It was concluded from the contours that mid level of drug:polymer ratio, low amount of polymer and highest volume of organic phase are required for preparation of EXE NPs with highest PDE and lowest PS.

4.13.2.2 Response surface plots

Response surface plot is a very important tool when interaction effects of independent variables needs to be evaluated. Response surface plots were plotted between X_1 vs X_2, X_1 vs X_3 and X_2 vs X_3 at fixed level (+1) of third variable as shown in figure 4.21 and 4.22 for PDE and PS respectively. PDE was found to first increase with decrease in amount of polymer, and further decrease caused decrease in PDE (figure 4.21A). Drug:polymer ratio does not have significant effect on PDE, with increase in drug:polymer ratio, PDE first increases marginally and then decreases. No increase or decrease in PDE was observed when both the variables varied simultaneously. In response surface plot of drug:polymer ratio vs volume of organic phase, PDE increases with increase in volume of organic phase from -1.0 to 0.5 level and then decreases. Simultaneous increase in both the variable results into increase in PDE and was found to be maximum at 0.5 level of X_3 and 1.0 level of X_1 (figure 4.21B). In response surface plot of volume of organic phase vs amount of polymer, PDE was found to increase with increase in volume of organic phase and found to be maximum at mid level (0) of X_2 and 1.0 level of X_3 (figure 4.21C). Response surface plot of drug:polymer ratio vs amount of polymer showed increase in PS with increase in X_2. PS first decreases upto 0 level of $X_1$and then increases. Smallest particles were formed at 0 level of X_1 and -1 level of X_2 (figure 4.22A). In response surface plot of drug:polymer ratio vs volume of organic phase, PS was found to be maximum at high level of X_1 and low level of X_3 (figure 4.22B). Response surface plot of amount of polymer vs volume of organic phase depicts that as volume of organic phase increases and amount of polymer decreases, PS increases. Both the variables together showed interactive effect with decreases in PS as X_3 increases and X_2 decreases (figure 4.22C).

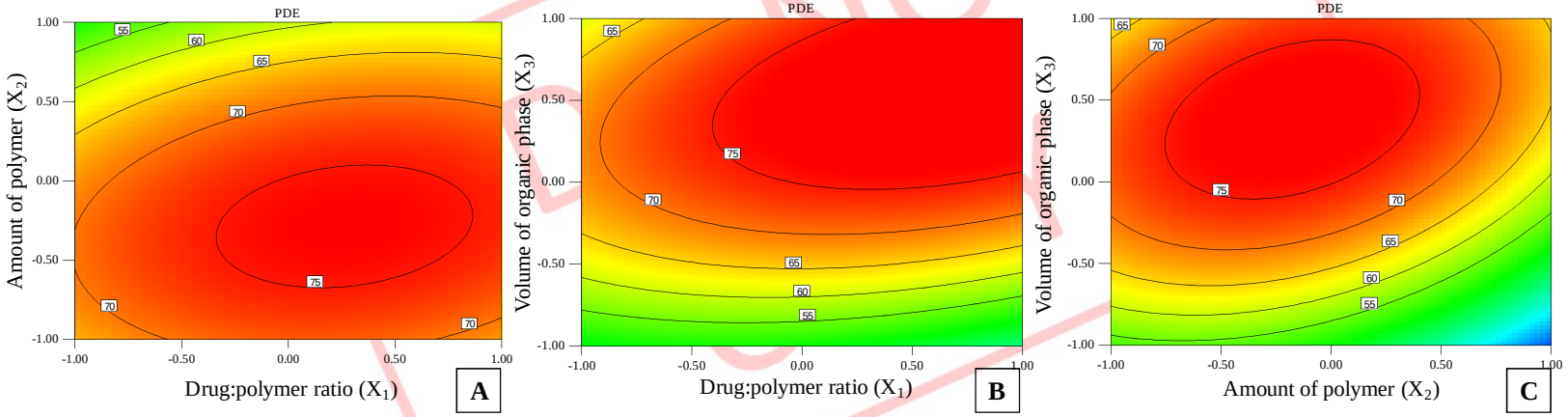

Figure 4.19 Contour plots showing effect of (A) X_1 vs X_2 (at -1 level of X_3), (B) X_1 vs X_3 (at -1 level of X_2) and (C) X_2 vs X_3 (at -1 level of X_1) on PDE of EXE loaded PLGA NPs.

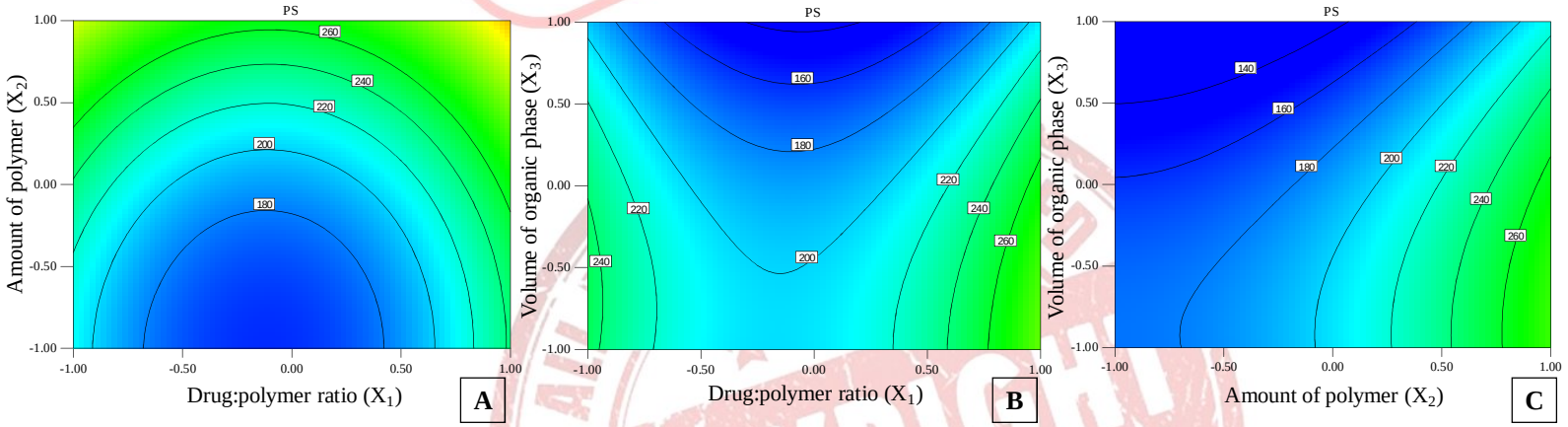

Figure 4.20 Contour plots showing effect of (A) X_1 vs X_2 (at -1 level of X_3), (B) X_1 vs X_3 (at -1 level of X_2) and (C) X_2 vs X_3 (at -1 level of X_1) on PS of EXE loaded PLGA NPs.

4.13.2.3 Desirability criteria

From the results of experiments performed as per Box-Behnken design, the optimum levels of independent variables were screened out by regression analysis. Formulation was optimized on the basis of PDE and PS and as both these dependent variables were taken into consideration simultaneously, the results were unable to attend both the dependent variables at a time. The batch with smallest particle size of 150.7 ± 4.9 nm exhibited only about 66.7 ± 1.7% while that with highest PDE of 73.2 ± 2.0% had particle size close to 200 nm. Hence, desirability criteria were used to find out formula with desired parameters. The desirability criteria were obtained using Design Expert software (version 8.0.3). Our criteria included maximum PDE and PS not more than 200 nm. The optimum formulation offered by the Design Expert 8.0.3 software based on desirability was found at 0.41, -0.09 and 0.75 levels of X_1, X_2 and X_3 respectively. The calculated desirability factor for offered formulations was 1, which indicated suitability of the designed factorial model. The results of dependent variables from the software were found to yield 78.37% PDE and 162.28 nm PS (figure 4.23) at these levels.

4.13.2.4 Checkpoint analysis and normalized error

Check point analysis was performed to check the predictability of the results from the generated algorithm. Three batches with random levels were prepared for check point analysis and evaluated for PDE and PS as shown in table 4.32. Results indicated that the measured response was more accurately predicted by reduced model of regression analysis which was proved by lower normalized error value of regression analysis

Table 4.32 Check point analysis, t test analysis and normalized error determination

Batch No.	X_1	X_2	X_3	PDE		PS	
				Observed	Predicted	Observed	Predicted
1	-1 (1:15)	- 0.3 (85 mg)	0.5 (9 ml)	56.91	57.53	305.2	298.3
2	0 (1:20)	0.2 (110 mg)	- 0.8 (6.4 ml)	75.26	74.62	204.1	199.76
3	1 (1:25)	- 0.7 (65 mg)	0.8 (9.6 ml)	52.72	53.46	242	239.51
			$t_{calculated}$		0.6411		0.0699
			$t_{tabulated}$		2.9199		2.9199
			Normalized Error		0.0197		0.0327

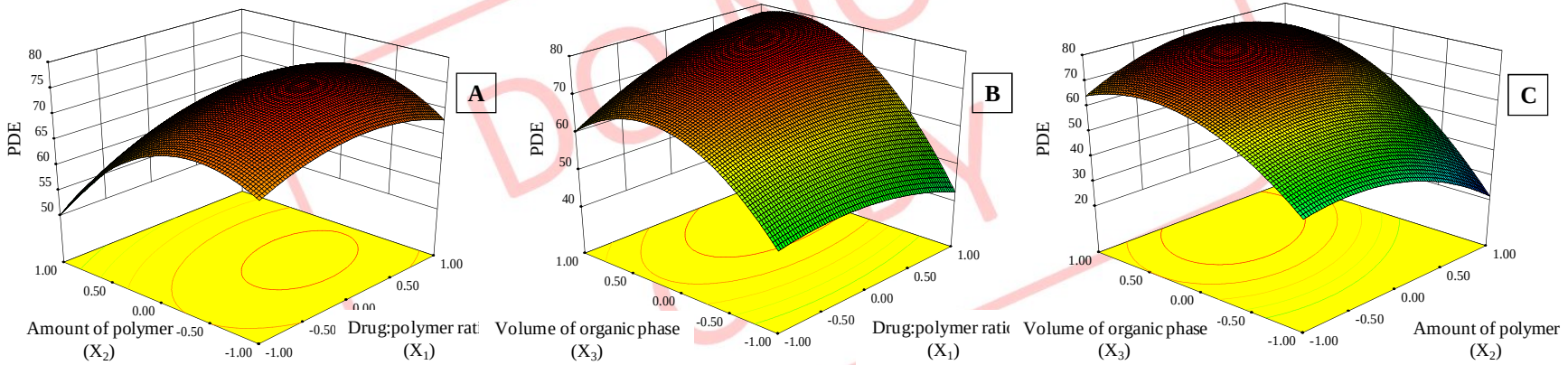

Figure 4.21 Response surface plot showing effect of (A) X_1 vs X_2 (at -1 level of X_3), (B) X_1 vs X_3 (at -1 level of X_2) and (C) X_2 vs X_3 (at -1 level of X_1) on PDE of EXE loaded PLGA NPs.

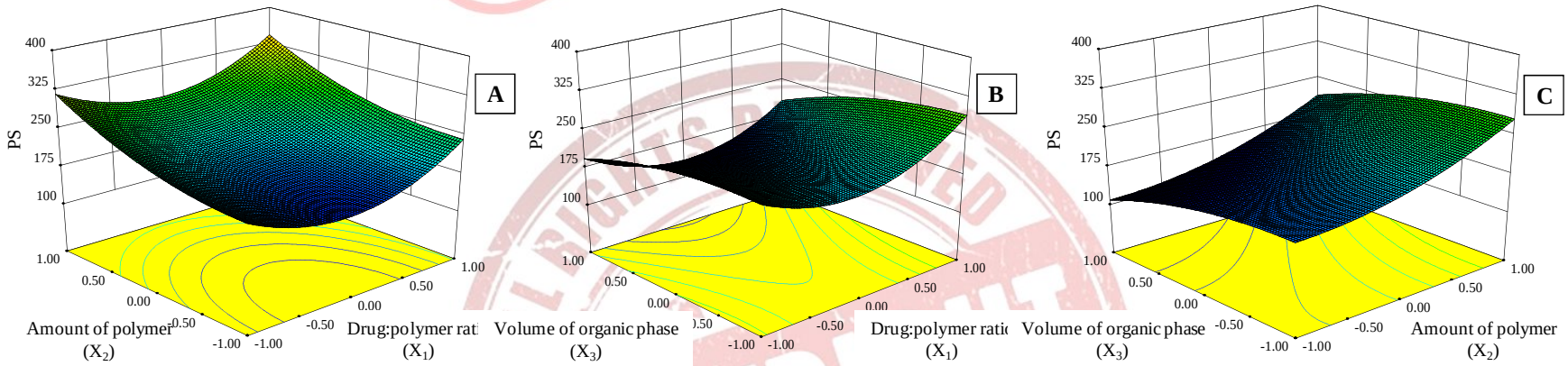

Figure 4.22 Response surface plot showing effect of (A) X_1 vs X_2 (at -1 level of X_3), (B) X_1 vs X_3 (at -1 level of X_2) and (C) X_2 vs X_3 (at -1 level of X_1) on PS of EXE loaded PLGA NPs.

(0.0197 for PDE and 0.0327 for PS). Data analysis using student's 't' test was performed to check the difference in the observed and predicted responses. Calculated t value ($t_{calculated}$) for PDE and PS was found to be 0.6411 and 0.0699, respectively which was less than the tabulated 't' value of 2.9199 which indicates that there was no statistically significant difference ($p<0.05$) between experimentally obtained values and predicted values by regression analysis and hence confirms the utility of the established contour plots and reduced polynomial equations in the preparation of NPs.

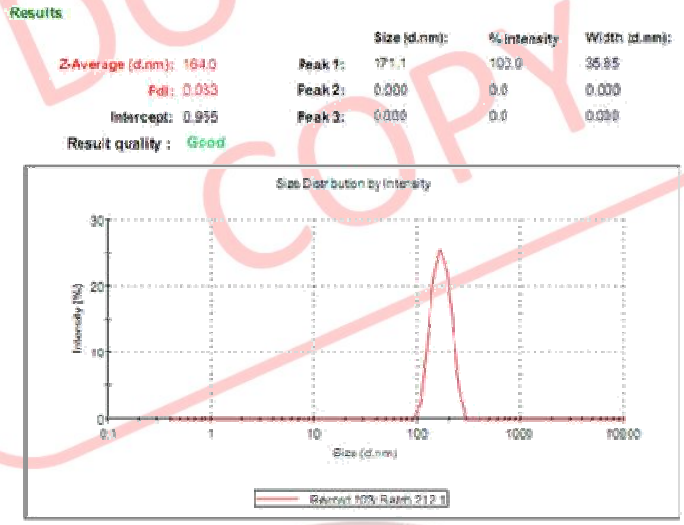

Figure 4.23 Particle size of EXE loaded PLGA NPs

4.13.3 Lyophilization and optimization of cryoprotectants

In this study, different cryoprotectants (trehalose, sucrose and mannitol) were used in different ratios (1:1, 1:2, 1:3, 1:4) and PS was recorded as shown in table 4.33. Initial PS of NPs was found to be 174.8 nm. The ratio of PS (after lyophilization, S_f and before lyophilization, S_i) was found to be lowest (1.25) for sucrose in 1:2 ratio. Trehalose also showed less increase in PS after re-dispersion (S_f/S_i ratio of 1.39). Trehalose at 1:2 and sucrose 1:1 and 1:2 ratio showed less S_f/S_i ratio indicating good re-dispersibility with PDI less than 0.2. PDI is a measure of dispersion homogeneity and usually ranges from 0 to 1. Values close to 0 indicate a homogeneous dispersion while those greater than 0.3 indicate high heterogeneity [Ahlin et al. 2002].

Table 4.33 Effect of cryoprotectants and their concentration on PS of lyophilized NPs after re-dispersion in distilled water

Cryoprotectant	Ratio	Final Avg. PS (nm)	S_f/S_i
Trehalose	1:1	252.5	1.44
	1:2	237.3	1.36*
	1:3	281.3	1.61
	1:4	324.3	1.86
Sucrose	1:1	229.6	1.31*
	1:2	218.2	1.25*
	1:3	260.2	1.49
	1:4	304.3	1.74
Mannitol	1:1	264.9	1.52
	1:2	289.9	1.66
	1:3	320.2	1.83
	1:4	332.8	1.90

*indicates good re-dispersibility

4.14Formulation and optimization of EXE loaded cPCL NPs

4.14.1 Preliminary optimization of EXE loaded cPCL NPs

4.14.1.1 Selection of organic solvent

Three different organic solvents (acetone, acetonitrile and tetrahydrofuran) were used for preparation of cPCL NPs (table 4.34). NPs formulated using acetone showed PDE of 82.0 ± 1.1% with PS of 212.4 ± 3.1 nm while NPs formulated using acetonitrile were of low PDE and high PS. No significant change in PDE was observed when tetrahydrofuran was used as solvent with significant increase in PS. Hence, acetone was selected for further studies.

Table 4.34 Selection of organic phase in preliminary optimization of EXE loaded cPCL NPs

Solvents	PDE (%)	PS (nm)
Acetone	82.0 ± 1.1	212.4 ± 3.1
Acetonitrile	80.6 ± 2.3	227.6 ± 5.2
Tetra hydro furan	82.3 ± 1.7	255.1 ± 4.7

4.14.1.2 Selection of surfactant

Three different surfactants were initially used for formulation development namely Pluronic F-68® (P188), Pluronic F-127® (P127) and Poly vinyl alcohol (PVA) (table 4.35). Out of these, better one is selected based on resultant PDE and PS. With constant level of surfactant concentration (0.5%) for all three surfactants, no significant change in PDE was observed, but at the same time PS was found to be of larger size (251.1 ± 5.3 nm) using PVA as surfactant. No significant difference in PS was observed when P188 or P127 was used, but PDE was higher when P188 was used as surfactant. Hence, P188 was used in further studies.

Table 4.35 Selection of surfactant in preliminary optimization of EXE loaded cPCL NPs

Surfactant	PDE (%)	PS (nm)
P188	56.32 ± 1.74	224.1 ± 7.2
P127	55.98 ± 2.12	214.6 ± 3.7
PVA	56.67 ± 1.89	251.1 ± 5.3

4.14.1.3 Selection of surfactant concentration

Different concentrations (0.5, 1.0, 1.5%) of surfactant (P188) were used in aqueous phase and results are represented in table 4.36. It was observed that as the concentration was increased, PS increases significantly with no major change in PDE (55.86 – 56.97%). This was possibly due to coating of surfactant on NPs after precipitation. Hence, 0.5% of P188 was selected as surfactant concentration.

Table 4.36 Selection of surfactant concentration in preliminary optimization of EXE loaded cPCL NPs

Surfactant concentration	PDE (%)	PS (nm)
0.5%	56.32 ± 1.74	224.1 ± 7.2
1.0%	55.86 ± 1.41	232.5 ± 2.9
1.5%	56.97 ± 1.64	258.1 ± 4.6

4.14.2 Optimization of EXE loaded cPCL NPs using BBD

Thirteen batches of EXE loaded cPCL NPs were prepared as per BBD changing three independent variables, drug:polymer ratio (X_1), amount of polymer (X_2) and volume of organic phase (X_3). Coded values and actual values of the three independent variables,

drug:polymer ratio (X_1), surfactant concentration (X_2) and volume of organic phase (X_3) are represented in table 4.37. Batches prepared using BBD were evaluated for PDE and PS as the dependent variables and recorded in table 4.38.

Table 4.37 Coded values of the formulation parameters of EXE loaded cPCL NPs

Coded Values	Actual values		
	X_1	X_2	X_3
-1	1 : 15	50 mg	6 ml
0	1 : 20	100 mg	8 ml
1	1 : 25	150 mg	10 ml

X_1 Drug:polymer ratio
X_2 Amount of polymer (mg)
X_3 Volume of organic phase (ml)

Table 4.38 Box Behnken experimental design with measured responses for EXE loaded cPCL NPs

Sr. No.	X_1	X_2	X_3	Y_1 (PDE, mean ± S.D.)	Y_2 (PS, mean ± S.D.)
1	0	-1	-1	56.32 ± 1.74	224.1 ± 7.2
2	0	-1	1	73.36 ± 2.08	115.0 ± 3.6
3	0	1	-1	23.94 ± 1.25	263.7 ± 4.5
4	0	1	1	72.89 ± 1.44	256.3 ± 5.4
5	-1	0	-1	57.93 ± 1.73	284.8 ± 4.9
6	-1	0	1	64.68 ± 1.92	185.0 ± 4.4
7	1	0	-1	48.71 ± 0.71	302.6 ± 2.9
8	1	0	1	82.00 ± 1.10	212.4 ± 3.1
9	-1	-1	0	70.91 ± 1.79	185.9 ± 3.5
10	-1	1	0	54.94 ± 1.81	340.4 ± 8.3
11	1	-1	0	74.89 ± 2.64	235.8 ± 6.8
12	1	1	0	68.95 ± 3.21	350.0 ± 7.2
13	0	0	0	82.67 ± 1.31	207.4 ± 2.0

*values are represented as mean ± s.d.

$Y_1 = 82.68 + 3.26\ X_1 - 6.84\ X_2 + 13.25\ X_3 + 2.51\ X_1X_2 + 6.63\ X_1X_3 + 7.98\ X_2X_3 - 4.27\ X_1^2 - 10.98\ X_2^2 - 15.07\ X_3^2$ (21)

$Y_2 = 207.41 + 13.08\ X_1 + 56.19\ X_2 - 38.32\ X_3 - 10.06\ X_1X_2 + 2.38\ X_1X_3 + 25.42\ X_2X_3 + 51.04\ X_1^2 + 19.61\ X_2^2 – 12.25\ X_3^2$ (22)

$Y_1 = 77.79 – 6.84\ X_2 + 13.25\ X_3 + 7.98\ X_2X_3 – 9.14\ X_2^2 – 13.23\ X_3^2$ (23)

$Y_2 = 213.29 + 56.19\ X_2 - 38.32\ X_3 + 25.42\ X_2X_3 + 48.83\ X_1^2$ (24)

The obtained PDE and PS were subjected to multiple regression to yield second order polynomial equations (equation 21 and 22, for PDE and PS respectively). Linear coefficients (b_1, b_2 and b_3 of X_1, X_2 and X_3, respectively) represents extent of effect by changing individual variable. Positive or negative sign in equation against different coefficients indicate increase or decrease in individual dependent response. The value of coefficients against interactions terms (X_1X_2, X_1X_3 and X_2X_3) shows how the PDE and PS changes when two variables were simultaneously changed. The values of all the 13 batches showed wide variation of 23.94 ± 1.25 to 82.68 ± 1.31% and 115.03 ± 3.60 to 350.03 ± 7.21 nm for PDE and PS, respectively as shown in table 4.38. This variation is reflected by the wide range of coefficients of the terms representing the individual and combined variables. The significance of each coefficient of equations 21 and 22 were determined by student's 't' test and p-value, which are listed in table 4.39 and 4.40 respectively. The larger the magnitude of the 't' value and the smaller the p-value, the more significant is the corresponding coefficient [Adinarayana and Ellaiah 2002; Akhnazarova 1982]. Small values of the coefficients of the terms X_1, X_1X_2, X_1X_3 and X_1^2 in equation 21 and X_1, X_1X_2, X_1X_3, X_2^2 and X_3^2 in equation 22 implied that all these terms were least contributing in the preparation of EXE loaded cPCL NPs. These small values of coefficients had $p>0.05$. Hence, these terms were neglected from the full model considering non-significance and reduced polynomial equations (equation 23 and 24, for PDE and PS respectively) were obtained following regression analysis of PDE and PS. From reduced model, it was evident that drug:polymer ratio did not affect any of the dependent variables significantly ($p>0.05$). The interaction effects of X_1X_2 and X_1X_3 was also found to be non-significant ($p>0.05$) for both PDE and PS. For PDE, the quadratic effect of drug:polymer ratio, while for PS the quadratic effect of amount of polymer and volume of organic phase were insignificant (table 4.39 and 4.40).

Table 4.39 Model coefficients estimated by multiple regression analysis for PDE of EXE loaded cPCL NPs

Factor	Coefficients	t Stat	P-value
Intercept	82.67	13.5711	0.0009*
X_1	3.2596	1.5135	0.2274
X_2	-6.8440	-3.1777	0.0482*
X_3	13.2531	6.1536	0.0086*
X_1X_2	2.5067	0.8230	0.4708
X_1X_3	6.6334	2.1779	0.1176
X_2X_3	7.9769	2.6190	0.0491*
X_1^2	-4.2709	-1.0600	0.3669
X_2^2	-10.9755	-2.7240	0.0423*
X_3^2	-15.0662	-3.7392	0.0334*

* Significant at $p < 0.05$

Table 4.40 Model coefficients estimated by multiple regression analysis for PS of EXE loaded cPCL NPs

Factor	Coefficients	t Stat	P-value
Intercept	207.4	8.7941	0.0031*
X_1	13.0775	1.5684	0.2148
X_2	56.1863	6.7384	0.0067*
X_3	-38.3225	-4.5960	0.0194*
X_1X_2	-10.0588	-0.8530	0.4563
X_1X_3	2.3788	0.2017	0.8530
X_2X_3	25.4188	2.1556	0.0301*
X_1^2	51.0381	3.2718	0.0467*
X_2^2	19.6131	1.2573	0.2976
X_3^2	-12.2444	-0.7849	0.4898

* Significant at $p < 0.05$

The results of ANOVA of the second order polynomial equation of PDE and PS are given in table 4.41 and 4.42 respectively. Since the calculated F value (1.3911) is less than the tabulated F value (9.0135) ($\alpha = 0.05$, $V_1 = 5$ and $V_2 = 3$) [Bolton 1997] for PDE, and calculated F value (2.2086) is less than the tabulated F value (9.1172) ($\alpha = 0.05$, $V_1 = 4$

and V_2 = 3) [Bolton 1997] for PS, it was concluded that the neglected terms did not significantly contribute in the prediction of PDE and PS. Thus, the results of ANOVA of full and reduced model justified the omission of non-significant terms of equation 21 and 22. When the coefficients of the three independent variables in equation 23 and 24 were compared, the values for the variables X_3 (13.25) for PDE and X_2 (56.19) for PS were found to be maximum and hence these variables were considered to be major contributing variables affecting the PDE and PS of the NPs. The Fisher F test with a very low probability value (P_{model} > F = 0.000001) demonstrated a very high significance for the derived regression model.

Table 4.41 ANOVA of full and reduced models for PDE of EXE loaded cPCL NPs

		df	SS	MS	F	R	R^2	Adjusted R^2
Regression	FM	9	50793.0	5643.7	10.1466	0.9839	0.9681	0.8727
	RM	4	46924.3	11731.1	16.9481	0.9457	0.8944	0.8416
Residual	FM	3	1668.6	556.2				
	RM	8	5537.4	692.2				

SSE2 - SSE1 =5537.387 – 1668.632 = 3868.755

No. of parameters omitted = 5

MS of error (full model) = 556.2107

F calculated = (SSE2 - SSE1 / No. of parameters omitted) / MS of error (FM)

= (3868.755 / 5) / 556.2107

= 1.3911

Table 4.42 ANOVA of full and reduced models for PS of EXE loaded cPCL NPs

		df	SS	MS	F	R	R^2	Adjusted R^2
Regression	FM	9	2935.15	326.13	8.7886	0.9815	0.9634	0.8538
	RM	5	2607.32	521.46	8.3118	0.9251	0.8558	0.7528
Residual	FM	3	111.32	37.11				
	RM	7	439.16	62.74				

SSE2 - SSE1 = 439.1605 - 111.3241 = 327.8364

No. of parameters omitted = 4

MS of error (full model) = 37.1080

F calculated = (SSE2 - SSE1 / No. of parameters omitted) / MS of error (FM)

= (327.8364 / 4) / 37.1080

= 2.2086

The goodness of fit of the model was checked by the determination coefficient (R^2). In this case, the values of the determination coefficients (R^2 = 0.9681 and 0.9634 for PDE and PS, respectively) indicated that over 96% of the total variations were explained by the model. After reducing the equation, the values of the determination coefficients (R^2 = 0.8944 and 0.8558 for PDE and PS, respectively) indicated that over 85% of the total variations were explained by the model. High R^2 values of full model as compared to reduced model is possibly due to the number of factors included. More the number of factors, more is the R^2 value, even if the factors are not significant [Montgomery 2004]. The values of adjusted determination coefficients (adj R^2 = 0.8727 and 0.8538 for PDE and PS respectively) were also very high (>85%) indicating high significance of the model. Moreover, the high values of correlation coefficients (R = 0.9839 and 0.9815 for PDE and PS, respectively) signify an excellent correlation between the independent variables [Box et al. 1978]. All the above considerations indicate an excellent adequacy of the derived regression model [Adinarayana and Ellaiah 2002; Akhnazarova 1982; Box et al. 1978; Yee and Blanch 1993].

4.14.2.1 Contour plots

Values of X_1, X_2 and X_3 were computed for PDE and PS and contour plots were established between X_1 vs X_2, X_1 vs X_3 and X_2vs X_3 at fixed level (+1) of third variable as shown in figure 4.24 and 4.25 for each PDE and PS respectively. Contour plots showed that PDE was greatly dependent on drug:polymer ratio and amount of polymer (figure 4.24A). PDE was found to be maximum at high level of X_1 and mid to high level of X_2. PDE was found to be more than 60% in the whole range of -1 to +1 for both X_1 and X_2 at +1 level of X_3. Contour plot of drug:polymer ratio vs volume of organic phase showed maximum PDE of more than 70% at 0 to +1 value of X_1 and +0.1 to +1.0 value of X_3 at +1 level of X_2 (figure 4.24B). PDE remained to be less than 80% in the whole range (-1 to +1) of both variables. Contour plot of amount of polymer vs volume of organic phase at +1 level of drug:polymer ratio indicated PDE of more than 80% when X_2 varied from -0.5 to 0.9 level and X_3 from 0 to +1.0 level (figure 4.24C). Lowest PS of about 175 nm was observed at -0.5 to 0 level of drug:polymer ratio, -0.8 to -1.0 level of amount of polymer at +1 level of volume of organic phase (figure 4.25A). When drug:polymer ratio was varied with volume of organic phase, PS was less than 275 nm at -0.5 to 0.5 level of X_1 and 0.5 to 1.0 level of X_3 at +1 level of X_2 (figure 4.25B). From figure 4.25C, it is

evident that at highest level of drug:polymer ratio (+1.0), PS increased as the amount of polymer increased (-1.0 to +1.0) and volume of organic phase decreased (+1.0 to -1.0), PS increases. It was concluded from the contours that high drug:polymer ratio, low amount of polymer and highest volume of organic phase were required for preparation of EXE NPs with highest PDE and lowest PS.

4.14.2.2 Response surface plots

Response surface plots are very important tools in learning both the main and interaction effects of the independent variables. Response surface plots were plotted between X_1 vs X_2, X_1 vs X_3 and X_2 vs X_3 at fixed level (+1) of third variable as shown in figure 4.26 and 4.27 for PDE and PS respectively. PDE was found to first increase with increase in amount of polymer, and further increase caused decrease in PDE. PDE was maximum at highest level of drug:polymer ratio and mid level of amount of polymer (figure 4.26A). The volume of organic phase had more significant effect on the outcome of PDE. PDE decreased sharply with decrease in volume of organic phase. However, PDE was not found to be much influenced by changing the drug:polymer ratio (figure 4.26B). PDE was found to decrease with increase in amount of polymer. Decrease in volume of organic phase and increase in amount of polymer resulted in overall decrease in PDE (figure 4.26C). Response surface plot of drug:polymer ratio vs amount of polymer showed non-linear behavior. With decrease in drug:polymer ratio, no significant change in PS was observed. Simultaneous increase in both drug:polymer ratio as well as polymer concentration showed increased PS. Increase in PS was more influenced by change in amount of polymer than drug:polymer ratio (figure 4.27A). Response surface plot between drug:polymer ratio and volume of organic phase showed no significant change in PS (figure 4.27B). Plot between amount of polymer and volume of organic phase showed increase in PS when amount of polymer increased and volume of organic phase decreased at the same time (figure 4.27C).

4.14.2.3 Desirability criteria

From the results, the optimum levels of independent variables were screened out by regression analysis. Since PDE and PS were taken into consideration simultaneously, the results were unable to attend both the dependent variables at a time. The batch with smallest particle size of less than 175 nm exhibited only about 69-71% PDE (at X_1 = -0.5 to 0, X_2 = -0.8 to -1.0, X_3 = +1.0) while that with highest PDE of more than 80% had

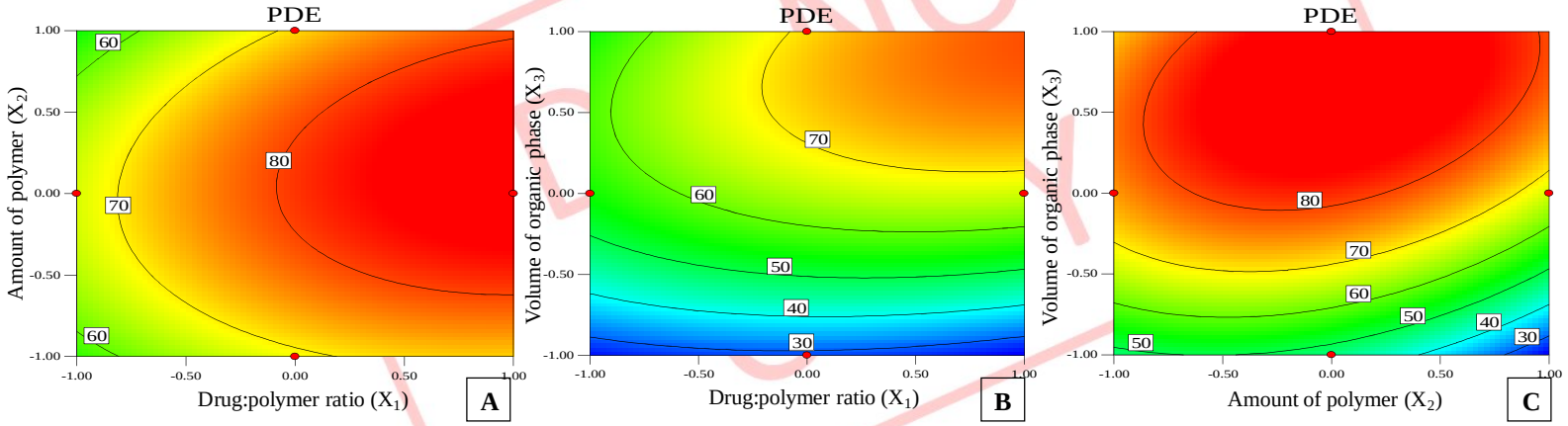

Figure 4.24 Contour plots showing effect of (A) X_1 vs X_2 (at -1 level of X_3), (B) X_1 vs X_3 (at -1 level of X_2) and (C) X_2 vs X_3 (at -1 level of X_1) on PDE of EXE loaded cPCL NPs.

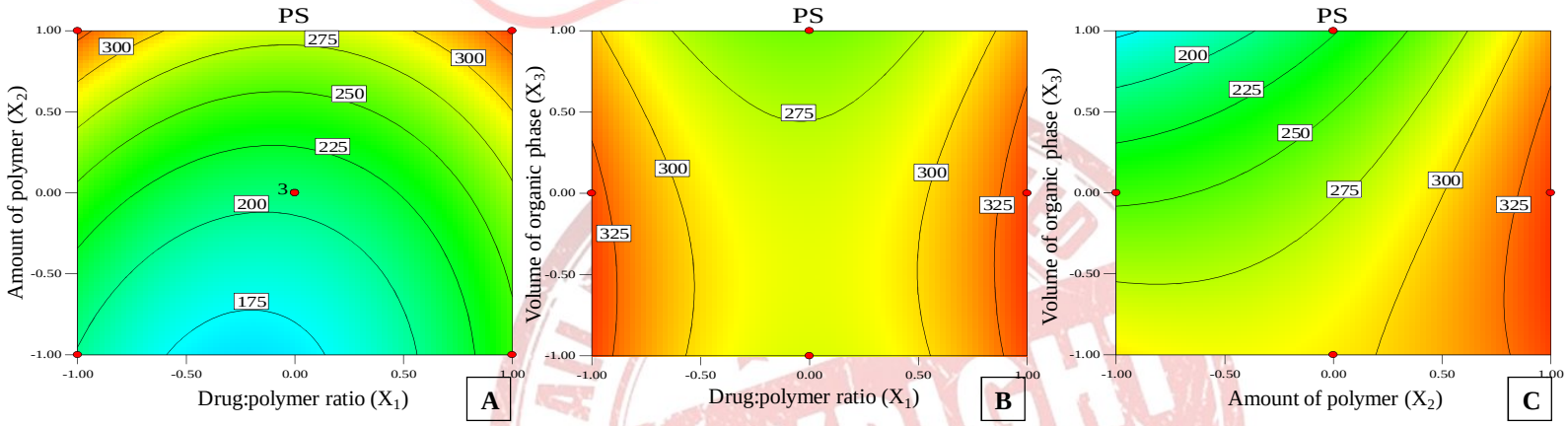

Figure 4.25 Contour plots showing effect of (A) X_1 vs X_2 (at -1 level of X_3), (B) X_1 vs X_3 (at -1 level of X_2) and (C) X_2 vs X_3 (at -1 level of X_1) on PS of EXE loaded cPCL NPs.

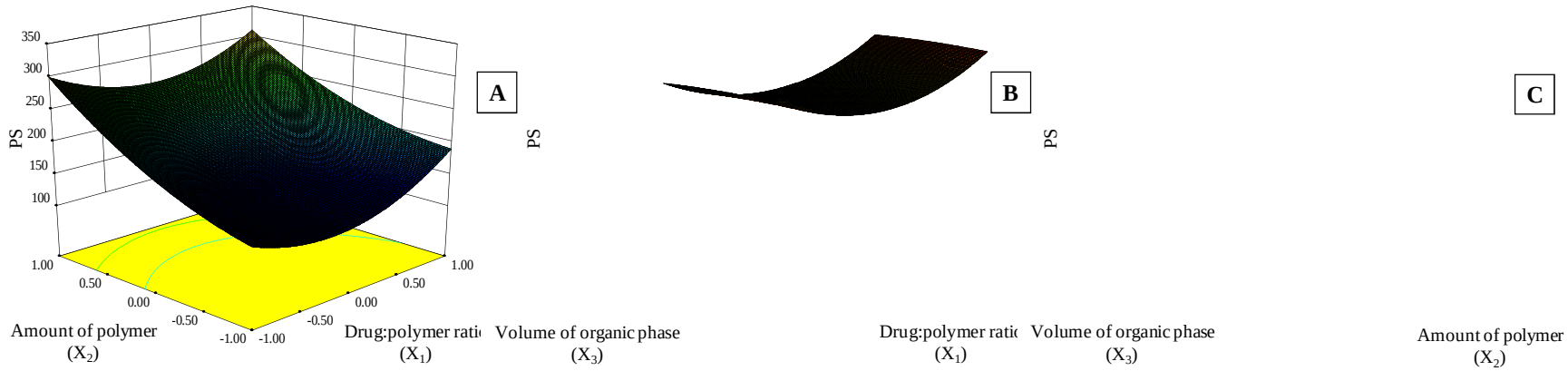

Figure 4.27 Response surface plot showing effect of (A) X_1 vs X_2 (at -1 level of X_3), (B) X_1 vs X_3 (at -1 level of X_2) and (C) X_2 vs X_3 (at -1 level of X_1) on PS of EXE loaded cPCL NPs.

PS of 210 to 300 nm (at X_1 = +1, X_2 = -0.5 to 0.9, X_3 = 0 to +1.0) (figure 4.23 and 4.24). Hence, desirability criteria were used to find out optimized formulation parameters. The desirability criteria were obtained using Design Expert software (version 8.0.3). Our criteria included maximum PDE and PS not more than 200 nm. The optimum formulation offered by the Design Expert 8.0.3 software based on desirability was found at 0.43, -0.68, and 0.27 level of X_1, X_2 and X_3 respectively. The calculated desirability factor for offered formulations was 1, which indicated suitability of the designed factorial model. The results of dependent variables from the software were found to yield 83.96% PDE and 180.51 nm PS (figure 4.28) at these levels.

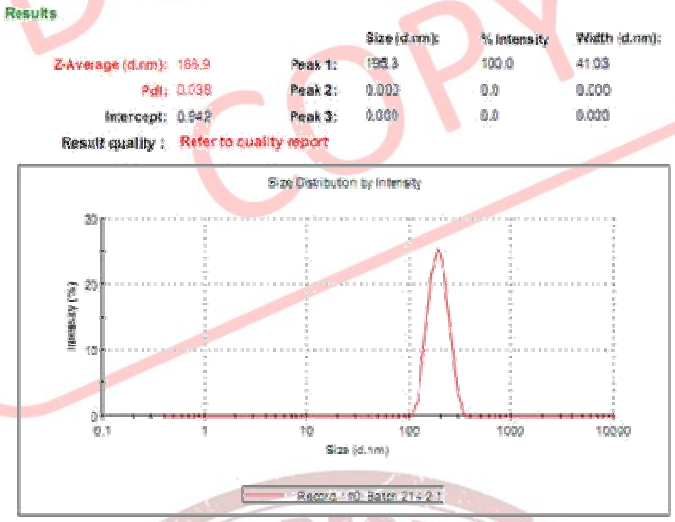

Figure 4.28 Particle size distribution of EXE loaded cPCL NPs

4.14.2.4 Checkpoint analysis and Normalized error

Three batches were prepared for check point analysis and evaluated for PDE and PS as shown in table 4.43. Results indicated that the measured response was more accurately predicted by regression analysis which was proved by lower normalized error value of regression analysis (0.04167 for PDE and 0.02591 for PS). Data analysis using student's 't' test revealed that there was no statistically significant difference ($p<0.05$) between experimentally obtained values and predicted values by regression analysis and hence, it confirms the utility of the established contour plots and reduced polynomial equation in the preparation of NPs.

Table 4.43 Check point analysis, t test analysis and normalized error determination

Batch No.	X_1	X_2	X_3	PDE		PS	
				Observed (avg.)	Predicted	Observed (avg.)	Predicted
1	-1 (1:15)	- 0.3 (85 mg)	0.5 (9 ml)	84.14	85.93	225.6	222.29
2	0 (1:20)	0.2 (110 mg)	- 0.8 (6.4 ml)	58.63	57.08	256.4	251.12
3	1 (1:25)	- 0.7 (65 mg)	0.8 (9.6 ml)	65.72	64.13	176.9	177.9
$t_{calculated}$				0.7267		0.3057	
$t_{tabulated}$				2.9199		2.9199	
Normalized Error				0.04167		0.02591	

4.14.3 Lyophilization and optimization of cryoprotectants

In this study, different cryoprotectants (trehalose, sucrose and mannitol) were used in different ratios (1:1, 1:2, 1:3, 1:4) and PS was recorded as shown in table 4.44. Initial PS of NPs was found to be 180.5 nm. The ratio of PS (after lyophilization, S_f and before

Table 4.44 Effect of cryoprotectants and their concentration on PS of lyophilized NPs after re-dispersion in distilled water

Cryoprotectant	Ratio	Final Avg. PS (nm)	S_f/S_i
Trehalose	1:1	254.0	1.41*
	1:2	250.6	1.39*
	1:3	288.4	1.60*
	1:4	315.9	1.75
Sucrose	1:1	232.4	1.29*
	1:2	220.7	1.22*
	1:3	273.5	1.52*
	1:4	298.1	1.65
Mannitol	1:1	275.9	1.53
	1:2	290.2	1.61
	1:3	318.0	1.76
	1:4	348.5	1.93

*indicates good re-dispersibility

lyophilization, S_i) was found to be lowest (1.22) for sucrose in 1:2 ratio. Trehalose also showed less increase in PS after re-dispersion (S_f/S_i ratio of 1.39). Trehalose and sucrose at 1:1, 1:2 and 1:3 ratio showed less S_f/S_i ratio indicating good re-dispersibility with PDI less than 0.2. PDI is a measure of dispersion homogeneity and usually ranges from 0 to 1. Values close to 0 indicate a homogeneous dispersion while those greater than 0.3 indicate high heterogeneity [Ahlin et al. 2002].

4.15 Characterization of ATZ loaded PLGA NPs

4.15.1 Zeta potential

Zeta potential gives information to predict the storage stability of colloidal dispersions [Thode et al. 2000]. The zeta potential values ranged between -21.5 to -34.4 mV for all 27 formulations. Highly negative values of the zeta potential indicate that the electrostatic repulsion between particles will prevent their aggregation and thereby stabilize the nanoparticulate dispersion [Feng and Huang 2001; Joshi et al. 2010]. The surfactant concentration affected the charge on the particle. It was seen that as the surfactant concentration was increased from 0.25 to 0.75%, there was a decrease in the zeta potential value. This is possibly because the surfactant is non- ionic and with increase in its concentration, total charge on the particle decreases due to increased surfactant coating which also results in increased PS [Redhead et al. 2001].

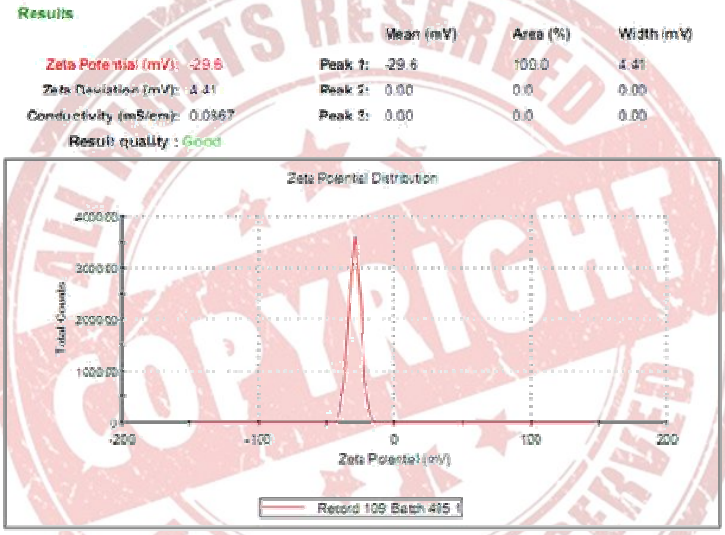

Figure 4.29 Zeta potential of ATZ loaded PLGA NPs

4.15.2 Transmission electron microscopy (TEM)

TEM image of ATZ loaded PLGA NPs is shown in figure 4.30 which reveals discrete, round and uniformly shaped NPs. The mean diameters of NPs were in the range of 80 - 100 nm. The higher hydrodynamic diameter of NPs achieved by DLS analysis as compared to the size obtained by TEM analysis may be contributed by the hydration of the surface associated Poloxamer [Das and Sahoo 2012; Misra and Sahoo 2010].

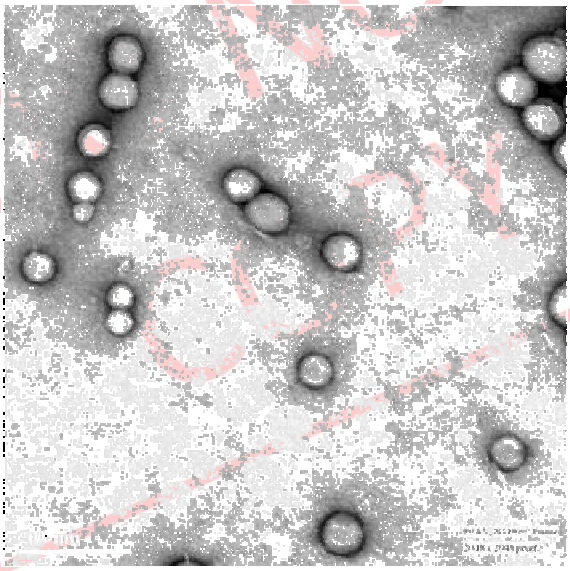

Figure 4.30 TEM image of ATZ loaded PLGA NPs

4.15.3 Differential scanning calorimetry (DSC)

In the absence of any interaction, the thermogram of a formulation will show patterns corresponding to those of the individual components. In the event that an interaction occurs, there may be disappearance of one or more peaks, the appearance of one or more new peaks corresponding to those of the components [Nanjwade et al. 2009] or shift in peaks [Jain and Ram 2011]. DSC thermograms of pure ATZ (A), PLGA polymer (B) and ATZ loaded PLGA NPs (C) are shown in figure 4.31. Pure ATZ showed an endothermic melting peak at 84.7 °C indicating its crystalline nature while PLGA showed endothermic peak at 51.99 °C corresponding to its glass transition temperature [Montgomery] [Chaudhari et al. 2010; Lacoulonche et al. 1999]. There was no peak of ATZ in the thermogram of NPs indicating that ATZ may be in an amorphous phase in the polymer matrix [Kashi et al. 2012].

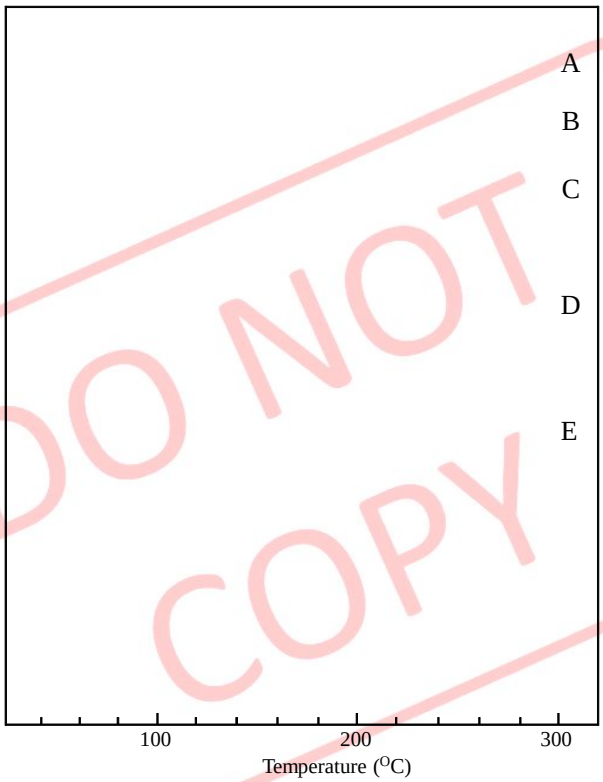

Figure 4.31 DSC thermogram of ATZ (A), ATZ loaded PLGA NPs (B), Sucrose (C), PLGA (D) and Physical mixture (E).

4.15.4 In vitro drug release studies

The in vitro drug release studies from different nanoparticulate formulations were performed in PBS pH 7.4. Pegylated NPs showed faster release as compared with non-pegylated NPs. In vitro release of ATZ from drug suspension and NPs is shown in figure 4.32. Within 3 h, 82.56 ± 0.623% drug release occurred from plain drug suspension, whereas only 24.14 ± 0.316% and 28.90 ± 1.03% drug released from PLGA and pegylated PLGA NPs, reaching 48.02 ± 0.566% and 60.29 ± 0.85% after 120 h and 64.9 ± 0.249% and 83.04 ± 0.55% after 240 h from PLGA and pegylated PLGA NPs, respectively indicative of sustained release. The drug release from NPs followed biphasic release model with an initial burst release for about 3 h followed by sustained release for more than 240 h. This biphasic release may be attributed to the drug molecules entrapped near particle surface causing initial burst release [Seju et al. 2011]. This initial fast release may also have been mediated by the presence of the surfactant molecules which are known to facilitate drug release. Also, particles of nano size range leads to a shorter

average diffusion path for the matrix entrapped drug molecules, thereby causing faster diffusion [Mainardes and Evangelista 2005; Shah et al. 2009]. After initial burst release, the release rate decreased, reflecting the release of drug entrapped in the strong polymer matrix. The release rate in the second phase is assumed to be controlled by diffusion rate of drug across the polymer matrix [Corrigan and Li 2009]. Pegylated PLGA NPs showed faster release of drug when compared to PLGA NPs as reported by Derakhshandeh et al. [Derakhshandeh et al. 2010].

The regression coefficient of the plot of log M_t/M_∞ versus log t for PLGA and pegylated PLGA NPs was found to be 0.948 and 0.956 with value of release exponent (n) as 0.255 and 0.264, respectively. The n value is the release exponent which characterizes the transport mechanism and if its value is less than 0.5, it indicates Fickian release. Hence, it can be concluded that the release of ATZ from NPs was by Fickian diffusion.

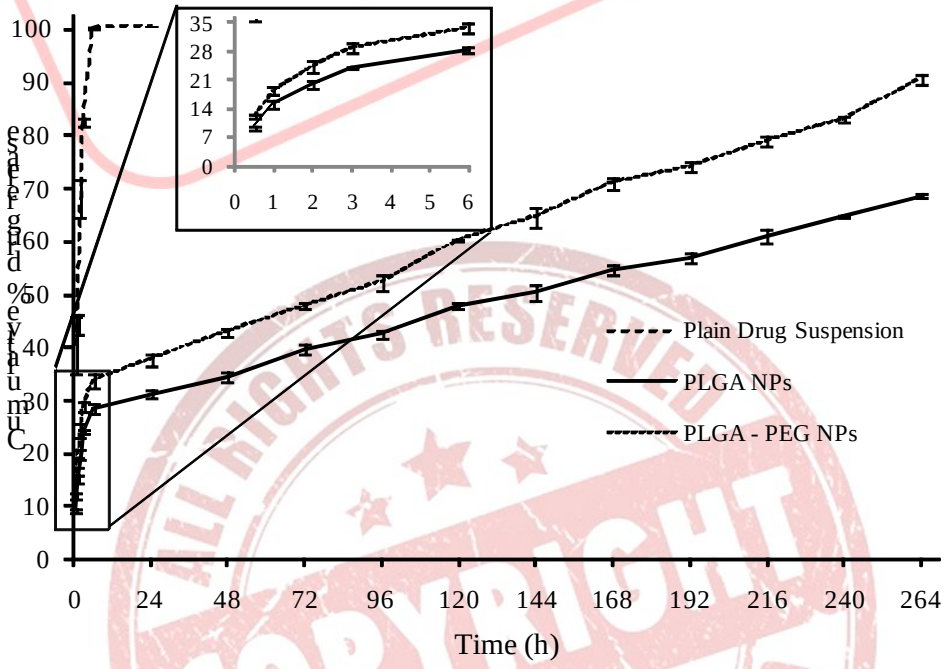

Figure 4.32 Drug release profile of ATZ from plain drug suspension, PLGA NPs and pegylated PLGA NPs across semi-permeable membrane using the dialysis bag diffusion technique in phosphate buffered saline (pH 7.4). The values represent mean ± S.D. of three batches.

4.15.5 Stability studies

Total drug content after different time intervals showed change in case of the NPs stored at room temperature to that of the NPs stored at refrigerator temperature. After different time intervals, increase in PS was observed for NPs stored at room temperature as compared to NPs stored at refrigerator temperature, which may attributed to the aggregation of polymeric particles (table 4.45). Also, drug content was found to decrease with increase in time as well as storage temperature (figure 4.33). Thus, it was concluded that the optimum temperature condition for storage of the ATZ loaded PLGA NPs would be refrigerated condition (2-8 °C).

Table 4.45 Stability data of ATZ loaded PLGA NPs stored at different temperature conditions

Storage time	% Drug content		Particle size (nm)	
	Room temp.	Refrigerator temp. (2–8 °C)	Room temp.	Refrigerator temp. (2–8 °C)
Initial	100	100	157.8 ± 2.3	157.8 ± 2.3
1 month	99.78 ± 0.29	99.85 ± 0.34	160.2 ± 1.4	159.7 ± 1.1
2 months	99.41 ± 0.58	99.57 ± 0.41	165.7 ± 2.9	160.2 ± 2.7
3 months	98.79 ± 0.61	99.14 ± 0.43	171.6 ± 3.8	165.9 ± 4.2

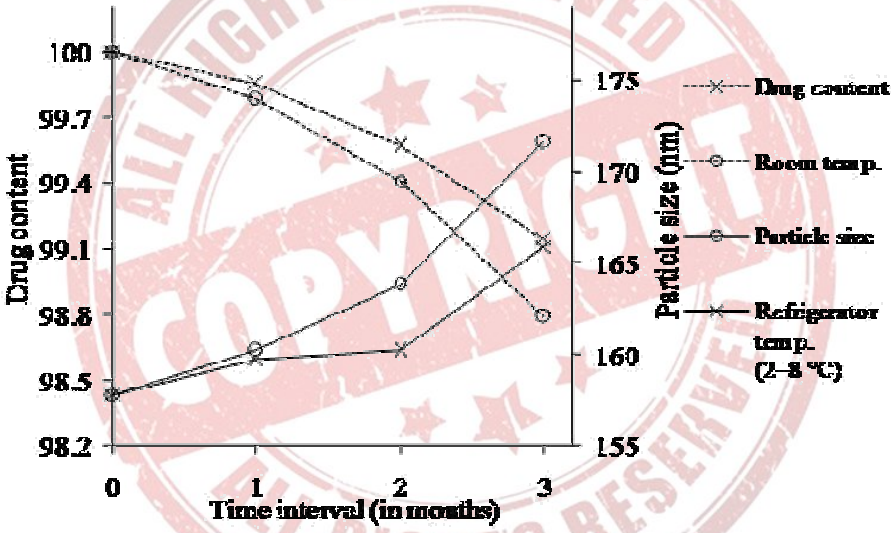

Figure 4.33 Effect of different storage conditions on drug content and PS of ATZ loaded PLGA NPs.

4.16 Characterization of ATZ loaded cPCL NPs

4.16.1 Zeta potential

Zeta potential gives information to predict the storage stability of colloidal dispersions [Thode et al. 2000]. The zeta potential values ranged between -23.7 to -35.1 mV for all 27 formulations. Highly negative values of the zeta potential indicate that the electrostatic repulsion between particles will prevent their aggregation and thereby stabilize the nanoparticulate dispersion [Feng and Huang 2001; Joshi et al. 2010]. Zeta potential was found to be affected by surfactant concentration, as the surfactant concentration was increased from 0.25 to 0.75%, the decrease in the zeta potential values were observed which is possibly because with increase in concentration of non-ionic surfactant, total charge on the particle decreases due to increased surfactant coating which also resulted into increased particle size [Redhead et al. 2001]. Polymer concentration had no significant effect on zeta potential values. The optimized batch of ATZ loaded cPCL NPs was found to have zeta potential of -32.1 ± 1.1 mV (figure 4.34). Zeta potential values in the -15 to -30 mV are common for well stabilized NPs [Musumeci et al. 2006]. Hence it was concluded that the NPs would remain physically stable.

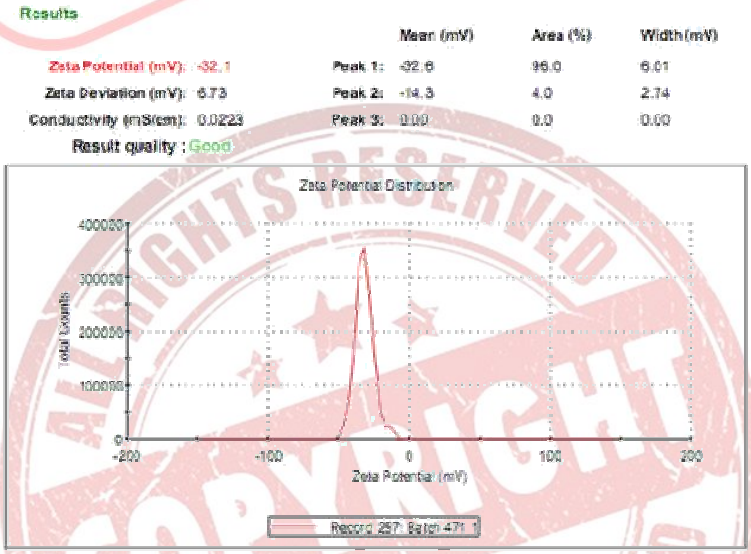

Figure 4.34 Zeta potential of ATZ loaded cPCL NPs

4.16.2 Transmission electron microscopy (TEM)

TEM image of ATZ loaded cPCL NPs is shown in figure 4.35 which reveals discrete, round and uniformly shaped NPs. The NPs were found with mean diameters in the

range of 80 - 100 nm. The higher hydrodynamic diameter of NPs observed by DLS analysis as compared to the size obtained by TEM analysis is possible due to the hydration of the surface associated Poloxamer [Das and Sahoo 2012; Misra and Sahoo 2010].

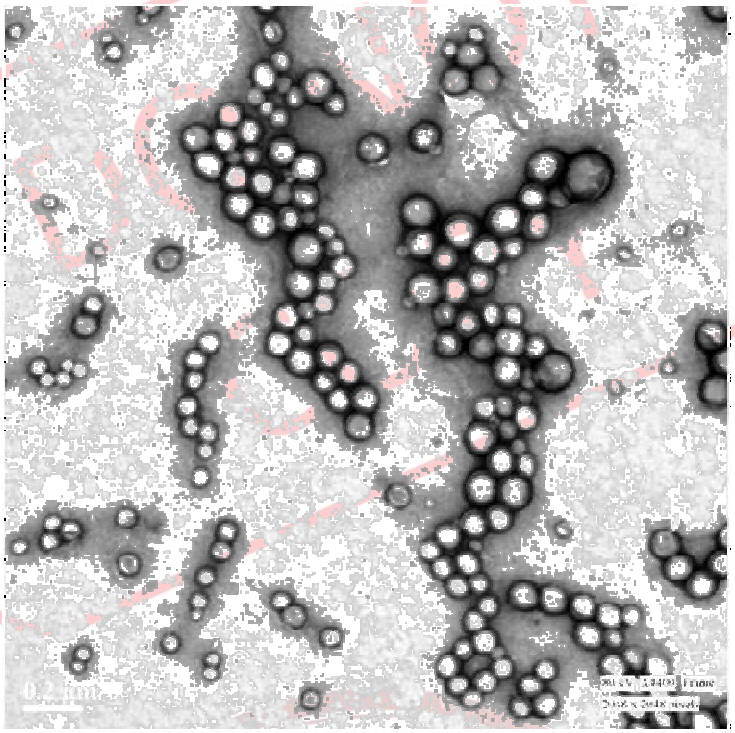

Figure 4.35 TEM image of ATZ loaded cPCL NPs

4.16.3 Differential scanning calorimetry (DSC)

In the absence of any interaction, the thermogram of a formulation will show patterns corresponding to those of the individual components. In the event that an interaction occurs, there may be disappearance of one or more peaks, the appearance of one or more new peaks corresponding to those of the components [Nanjwade et al. 2009] or shift in peaks [Jain and Ram 2011]. DSC thermograms of pure ATZ (A), cPCL polymer (B) and ATZ loaded cPCL NPs (C) are shown in figure 4.36. Pure ATZ showed an endothermic melting peak at 84.7 °C indicating its crystalline nature while cPCL showed endothermic peak at 47.65 °C corresponding to its melting temperature [Chaudhari et al. 2010; Lacoulonche et al. 1999]. There was no peak of ATZ in the thermogram of NPs

indicating that ATZ may be in an amorphous phase in the polymer matrix [Kashi et al. 2012].

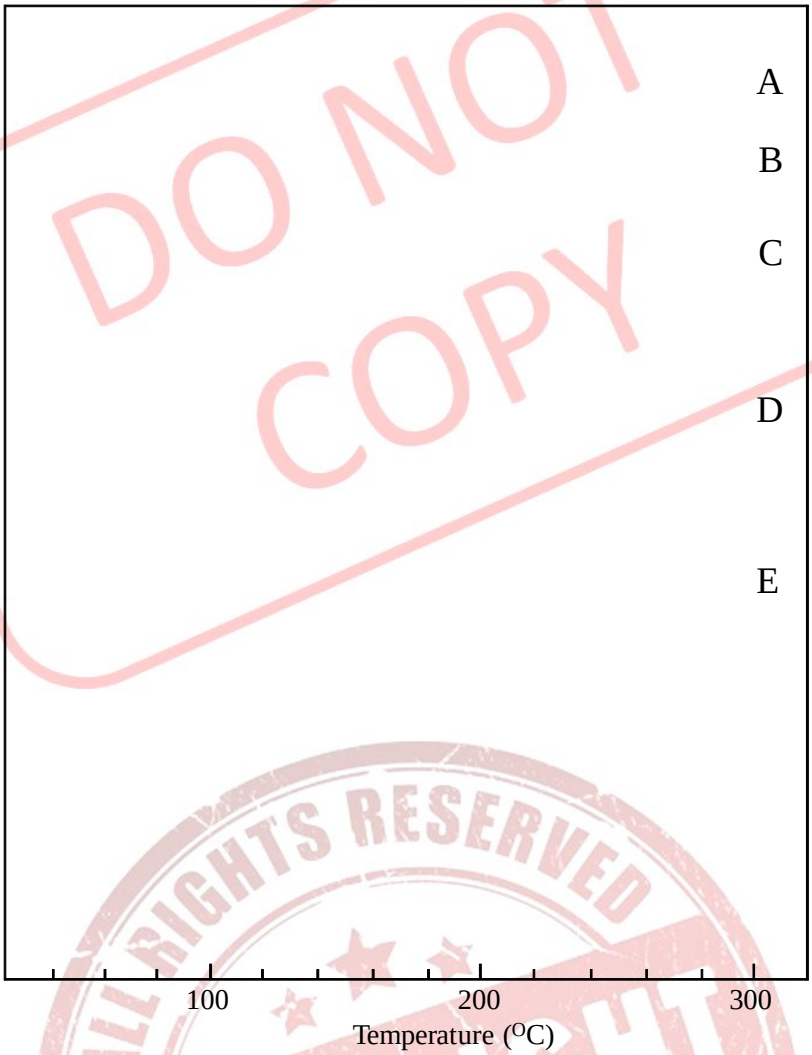

Figure 4.36 DSC thermogram of ATZ (A), ATZ loaded cPCL NPs (B), Sucrose (C), cPCL (D) and Physical mixture (E).

4.16.4 In vitro drug release studies

In vitro release of ATZ from plain drug suspension and NPs is shown in figure 4.37. In 3 h, 82.56 ± 0.62% drug released from plain drug suspension, whereas only 21.36 ± 0.41% and 26.57 ± 1.81% drug release occurred from cPCL NPs and pegylated PCL NPs, reaching 44.14 ± 0.69% and 56.71± 0.67% after 120 h and 58.22 ± 0.99% and 82.21 ±

0.74% after 240 h from cPCL and pegylated PCL NPs, respectively indicative of sustained release. The drug release from NPs followed biphasic release model with an initial burst release in about first 3 h followed by sustained release for more than 240 h. Pegylated nanoparticulated system is reported to release drug at a comparatively faster rate when compared to non-pegylated systems [Derakhshandeh et al. 2010]. In our study, pegylated PCL NPs showed comparatively faster release rate when compared to cPCL NPs. This biphasic release may be attributed to the drug molecules entrapped near particle surface causing initial burst release [Seju et al. 2011]. This initial fast release may also have been mediated by the presence of the surfactant molecules which are known to facilitate drug release. Also, particles of nano size range leads to a shorter average diffusion path for the matrix entrapped drug molecules, thereby causing faster diffusion [Mainardes and Evangelista 2005; Shah et al. 2009]. After initial burst release, the release rate decreased, reflecting the release of drug entrapped in the strong polymer matrix. The release rate in the second phase is assumed to be controlled by diffusion rate of drug across the polymer matrix [Corrigan and Li 2009].

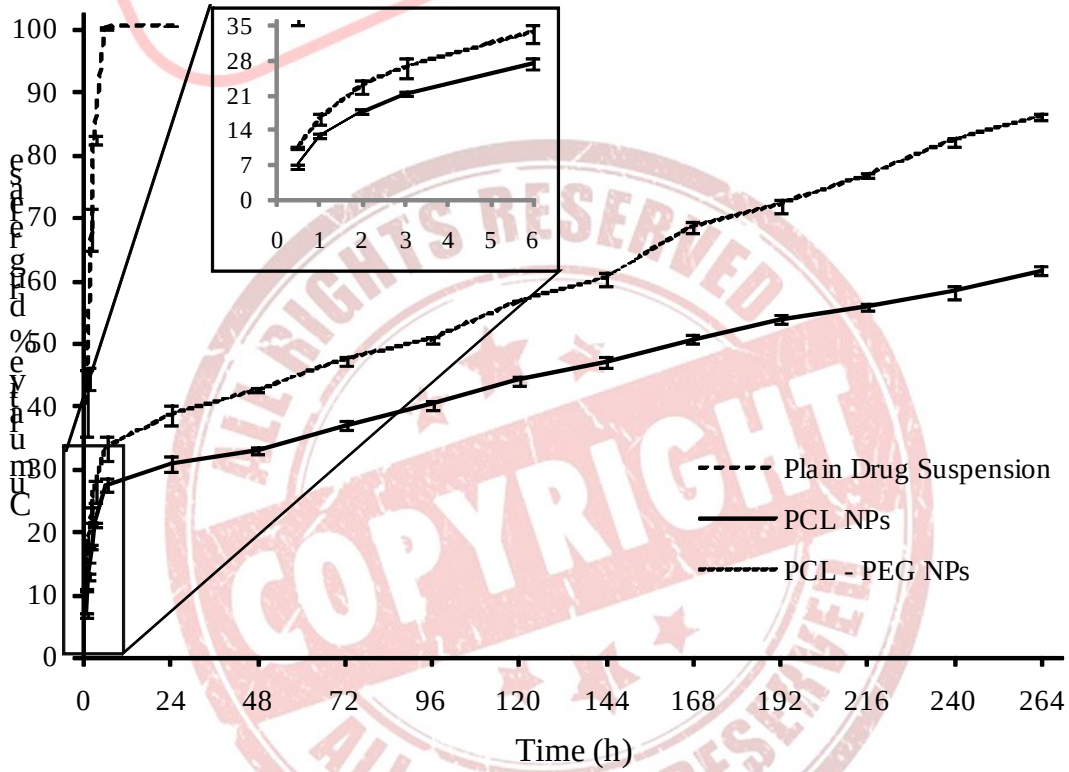

Figure 4.37 Drug release profile of ATZ from plain drug suspension, cPCL NPs and pegylated PCL NPs across semi-permeable membrane using the dialysis bag diffusion

technique in phosphate buffered saline (pH 7.4). The values represent mean ± S.D. of three batches.

4.16.5 Stability studies

Total drug content after different time intervals showed change in case of the NPs stored at room temperature to that of the NPs stored at refrigerator temperature. After different time intervals, increase in PS was observed for NPs stored at room temperature as compared to NPs stored at refrigerator temperature, which may attributed to the aggregation of polymeric particles (table 4.46). Also, drug content was found to decrease with increase in time as well as storage temperature (figure 4.38). Thus, it was concluded that the optimum temperature condition for storage of the ATZ loaded cPCL NPs would be refrigerated condition (2-8 °C).

Table 4.46 Stability data of ATZ loaded cPCL NPs stored at different temperature conditions

Storage time	% Drug content		Particle size (nm)	
	Room temp.	Refrigerator temp. (2–8 °C)	Room temp.	Refrigerator temp. (2–8 °C)
Initial	100	100	198.4 ± 3.7	198.4 ± 3.7
1 month	99.81 ± 0.25	99.91 ± 0.21	200.5 ± 2.2	200.1 ± 1.8
2 months	99.38 ± 0.64	99.62 ± 0.18	207.1 ± 4.1	204.5 ± 2.5
3 months	99.01 ± 0.49	99.24 ± 0.37	215.0 ± 3.8	211.2 ± 3.1

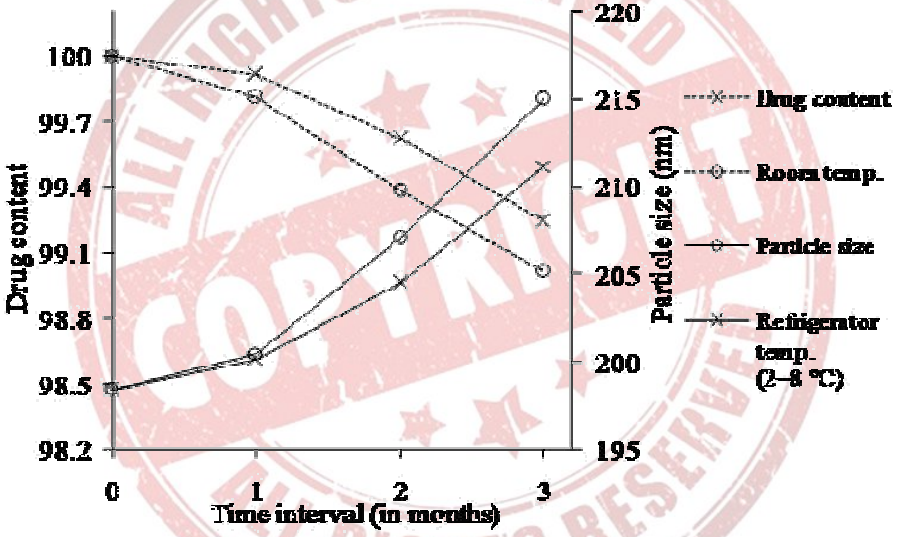

Figure 4.38 Effect of different storage conditions on drug content and PS of ATZ loaded cPCL NPs.

4.17 Characterization of EXE loaded PLGA NPs

4.17.1 Zeta potential

The zeta potential values ranged between -21.2 to -31.9 mV for all 13 formulations. The surfactant concentration affected the charge on the particle. It was seen that as the surfactant concentration was increased from 0.25 to 0.75%, there was a decrease in the zeta potential value. This is possibly because with increase in concentration of non-ionic surfactant, total charge on the particle decreases due to increased amount of surfactant coating which also resulted in increased particle size [Redhead et al. 2001]. However, change in polymer concentration had no effect on zeta potential values. The optimized batch of EXE loaded cPCL NPs was found to have zeta potential of -29.5 ± 1.4 mV (figure 4.39). Zeta potential values in the -15 mV to -30 mV are common for well stabilized NPs [Musumeci et al. 2006]. Hence it was concluded that the NPs would remain physically stable.

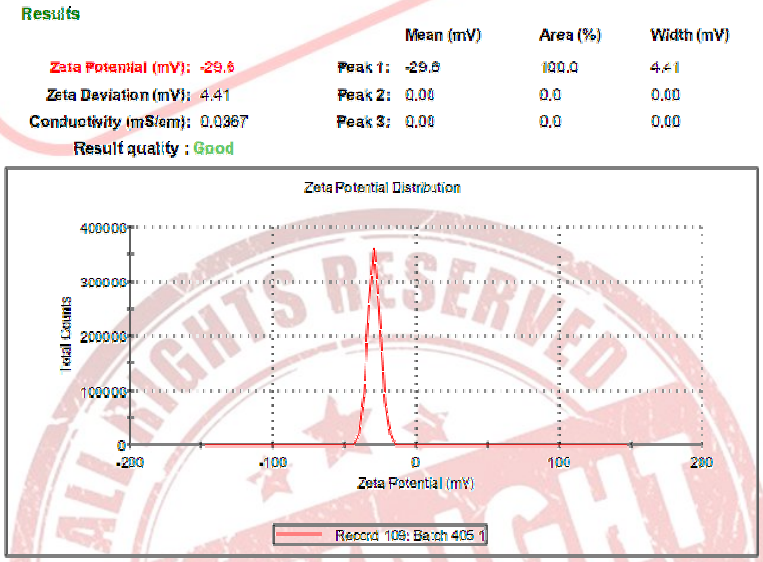

Figure 4.39 Zeta potential of EXE loaded PLGA NPs

4.17.2 Transmission electron microscopy (TEM)

TEM image of EXE loaded PLGA NPs is shown in figure 4.40. The image reveals that the particles were discrete, round and uniform in shape with diameters in the range of 80–100 nm. The higher hydrodynamic diameter of NPs achieved by DLS analysis as

compared to the size obtained by TEM analysis may be contributed by the hydration of the surface associated Poloxamer [Das and Sahoo 2012; Misra and Sahoo 2010].

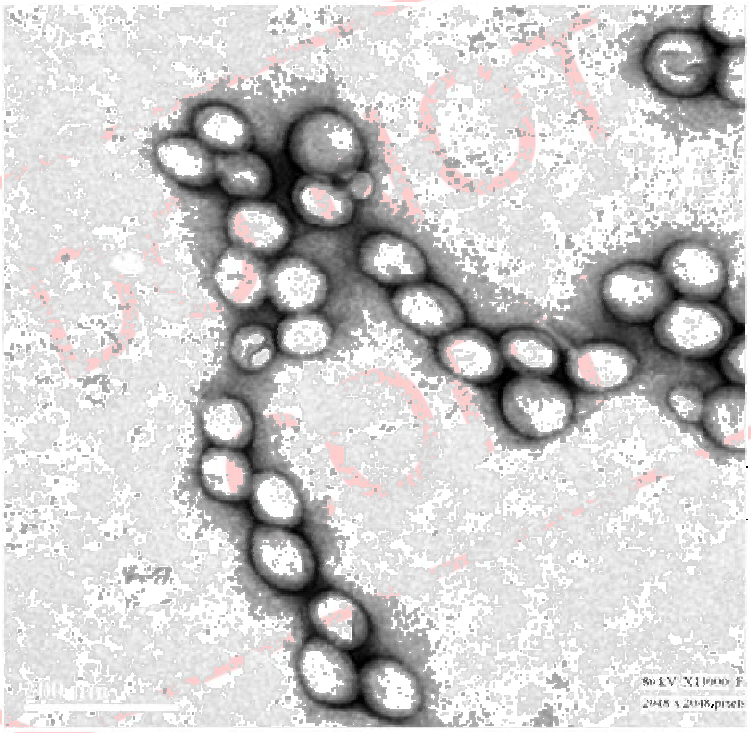

Figure 4.40 TEM image of EXE loaded PLGA NPs

4.17.3 Differential scanning calorimetry (DSC)

DSC thermograms of pure EXE, PLGA polymer, sucrose, physical mixture and EXE loaded PLGA NPs are shown in figure 4.41. Pure EXE showed an endothermic melting peak at 182.56 °C indicating its crystalline nature while PLGA showed endothermic peak at 51.9 °C corresponding to its glass transition temperature [Chaudhari et al. 2010; Lacoulonche et al. 1999]. In the absence of any interaction, the thermogram of a formulation will show patterns corresponding to those of the individual components. In the event that an interaction occurs, there may be disappearance of one or more peaks, the appearance of one or more new peaks corresponding to those of the components [Nanjwade et al. 2009] or shift in peaks [Jain and Ram 2011]. There was no peak of EXE in the thermogram of NPs indicating that EXE may be in an amorphous phase in the polymer matrix [Kashi et al. 2012].

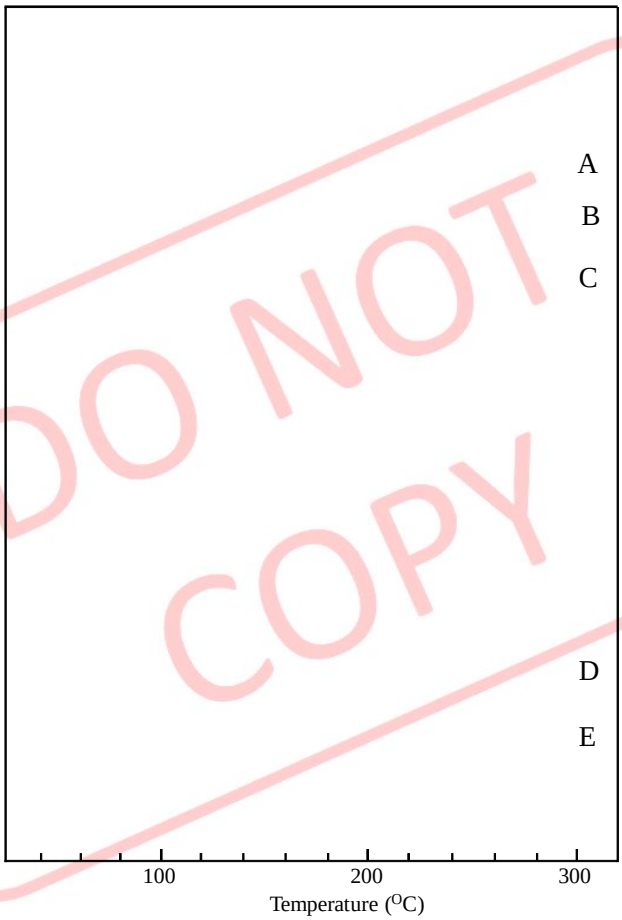

Figure 4.41 DSC thermogram of EXE loaded PLGA NPs (A), EXE (B), Sucrose (C), PLGA (D) and Physical mixture (E).

4.17.4 In vitro drug release studies

The in vitro drug release studies from different nanoparticulate formulations were performed in PBS pH 7.4. Pegylated PLGA NPs showed faster release as compared with non-pegylated NPs. In vitro release of EXE from drug suspension and NPs is shown in figure 4.42. Within 3 h, 71.36 ± 1.23% drug release occurred from plain drug suspension, whereas only 25.18 ± 0.56% and 20.21 ± 0.23% drug released from PLGA and pegylated PLGA NPs, reaching 48.05 ± 0.94% and 54.25 ± 0.23% after 120 h and 71.4 ± 1.23% and 73.9 ±0.86% after 240 h from PLGA and pegylated PLGA NPs, respectively indicative of sustained release. The drug release from NPs followed biphasic release model with an initial burst release for about 3 h followed by sustained release for more than 240 h. Pegylated PLGA NPs showed faster release when compared to PLGA NPs as reported by Derakhshandeh et al. [Derakhshandeh et al. 2010]. The

burst release may be attributed to the drug molecules associated near particle surface [Seju et al. 2011]. Also, particles of nano size range lead to a shorter average diffusion path for the matrix entrapped drug molecules, thereby causing faster diffusion [Mainardes and Evangelista 2005; Shah et al. 2009]. After initial burst release, the release rate decreased, reflecting the release of drug entrapped in the polymer matrix. The release rate in the second phase was assumed to be controlled by diffusion rate of drug across the polymer matrix [Corrigan and Li 2009]. The data obtained from *in vitro* drug release studies was fitted to Korsmeyer - Peppas model.

The regression coefficient of the plot of log M_t/M_∞ versus log t for PLGA and pegylated PLGA NPs was found to be 0.935 and 0.984 with value of release exponent (n) as 0.271 and 0.312, respectively. The n value is the release exponent which characterizes the transport mechanism and if its value is less than 0.5, it indicates Fickian release. Hence, it can be concluded that the release of EXE from NPs was by Fickian diffusion.

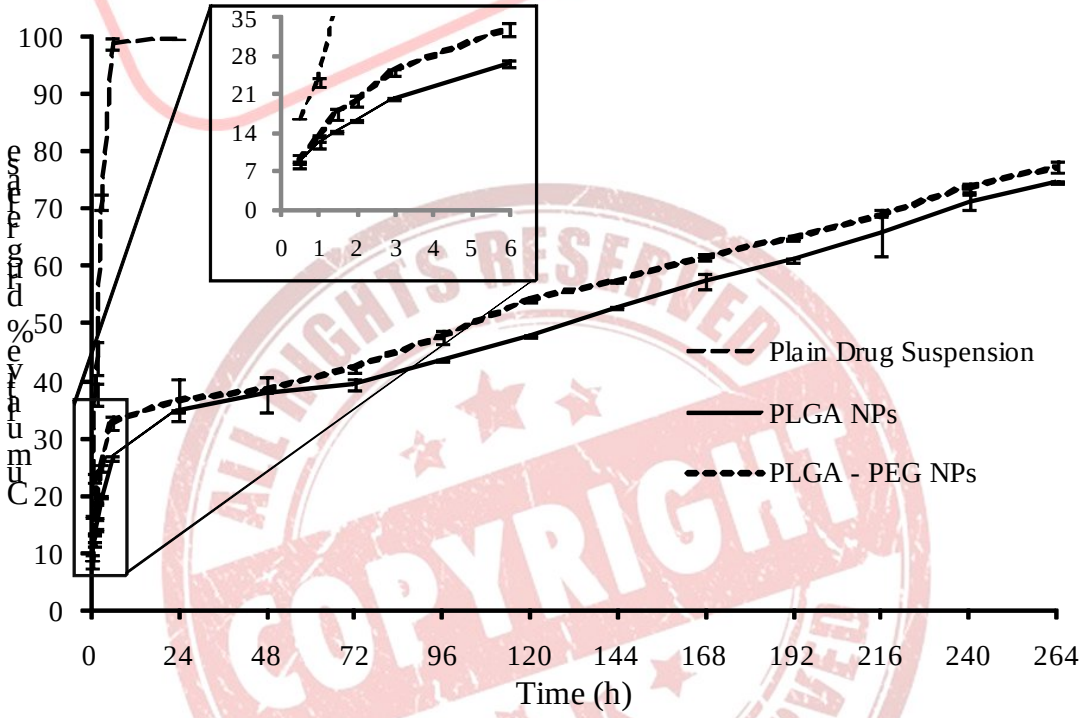

Figure 4.42 Drug release profile of EXE from plain drug suspension, PLGA NPs and pegylated PLGA NPs across semi-permeable membrane using the dialysis bag diffusion technique in phosphate buffered saline (pH 7.4). The values represent mean ± S.D. of three batches.

4.17.5 Stability studies

Total drug content after different time intervals showed change in case of the NPs stored at room temperature to that of the NPs stored at refrigerator temperature. After different time intervals, increase in PS was observed for NPs stored at room temperature as compared to NPs stored at refrigerator temperature, which may attributed to the aggregation of polymeric particles (table 4.47). Also, drug content was found to decrease with increase in time as well as storage temperature (figure 4.43). Thus, it was concluded that the optimum temperature condition for storage of the EXE loaded PLGA NPs would be refrigerated condition (2-8 °C).

Table 4.47 Stability data of EXE loaded PLGA NPs stored at different temperature conditions

Storage time	% Drug content		Particle size (nm)	
	Room temp.	Refrigerator temp. (2–8 °C)	Room temp.	Refrigerator temp. (2–8 °C)
Initial	100	100	179.8 ± 2.8	179.8 ± 2.8
1 month	99.54 ± 0.52	99.67 ± 0.38	181.3 ± 2.4	180.1 ± 3.4
2 months	99.09 ± 0.64	99.24 ± 0.41	186.7 ± 2.9	186.4 ± 1.7
3 months	98.79 ± 0.75	98.96 ± 0.66	195.4 ± 4.1	188.6 ± 2.3

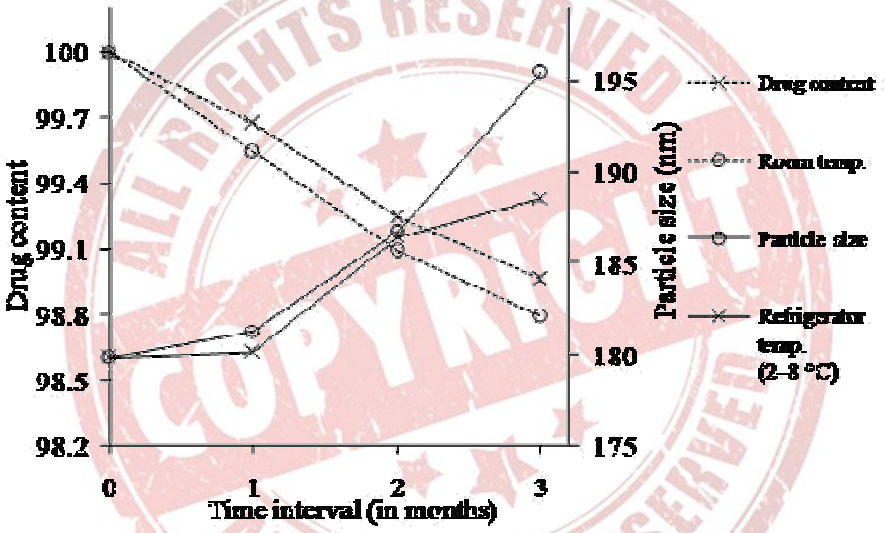

Figure 4.43 Effect of different storage conditions on drug content and PS of EXE loaded PLGA NPs.

4.18 Characterization of EXE loaded cPCL NPs

4.18.1 Zeta potential

The zeta potential values ranged between -19.6 to -34.0 mV for all 13 formulations. The surfactant concentration affected the charge on the particle. It was seen that as the surfactant concentration was increased from 0.25 to 0.75%, there was a decrease in the zeta potential value. This is possibly because with increase in concentration of non-ionic surfactant, total charge on the particle decreases due to increased amount of surfactant coating which also resulted in increased particle size [Redhead et al. 2001]. However, change in polymer concentration had no effect on zeta potential values. The optimized batch of EXE loaded cPCL NPs was found to have zeta potential of -33.8 ± 2.1 mV (figure 4.44). Zeta potential values in the -15 mV to -30 mV are common for well stabilized NPs [Musumeci et al. 2006]. Hence it was concluded that the NPs would remain physically stable.

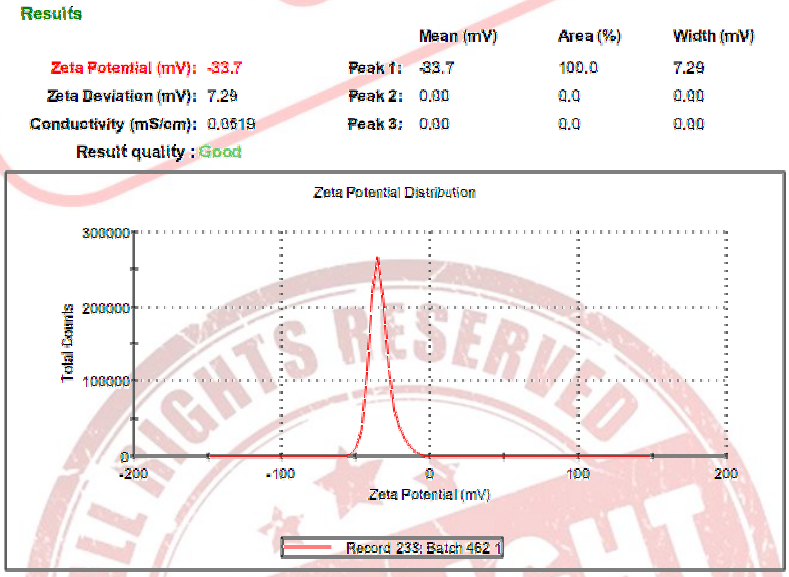

Figure 4.44 Zeta potential of EXE loaded cPCL NPs

4.18.2 Transmission electron microscopy (TEM)

TEM image of EXE loaded cPCL NPs is shown in figure 4.45. The image reveals that the particles were discrete, round and uniform in shape with diameters in the range of 80–100 nm. The higher hydrodynamic diameter of NPs achieved by DLS analysis as compared to the size obtained by TEM analysis may be contributed by the hydration of the surface associated Poloxamer [Das and Sahoo 2012; Misra and Sahoo 2010].

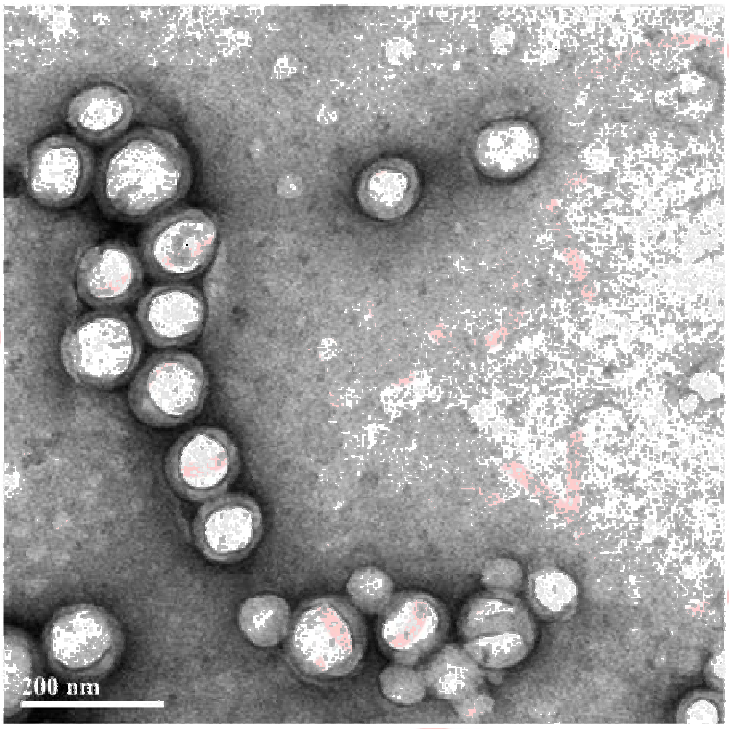

Figure 4.45 TEM image of EXE loaded cPCL NPs

4.18.3 Differential scanning calorimetry (DSC)

DSC thermograms of pure EXE, cPCL polymer, sucrose, physical mixture and EXE loaded cPCL NPs are shown in figure 4.46. Pure EXE showed an endothermic melting peak at 182.56 °C indicating its crystalline nature. cPCL showed endothermic peak at 47.65 °C, which was lower than the reported melting point of PCL (60 °C). It has been reported that modifications in polymer or polymer structure will change its melting point (Orozco-Castellanos et al. 2011). Thus, the lowering of melting point of PCL in cPCL can be taken as an indication of its carboxylation, which was also confirmed by FTIR and GPC. There was no peak of EXE in the thermogram of NPs indicating that EXE may be existing as a molecular dispersion or in an amorphous phase in the polymer matrix [Kashi et al. 2012]. It is reported that no detectable endotherm will be observed if the drug is present in a molecular dispersion or solid solution state in the polymeric NPs [Dubernet 1995]. However, as the drug is crystalline, total disappearance of its peak in the thermogram of the NPs indicate towards its existence as a molecular dispersion rather than amorphous form.

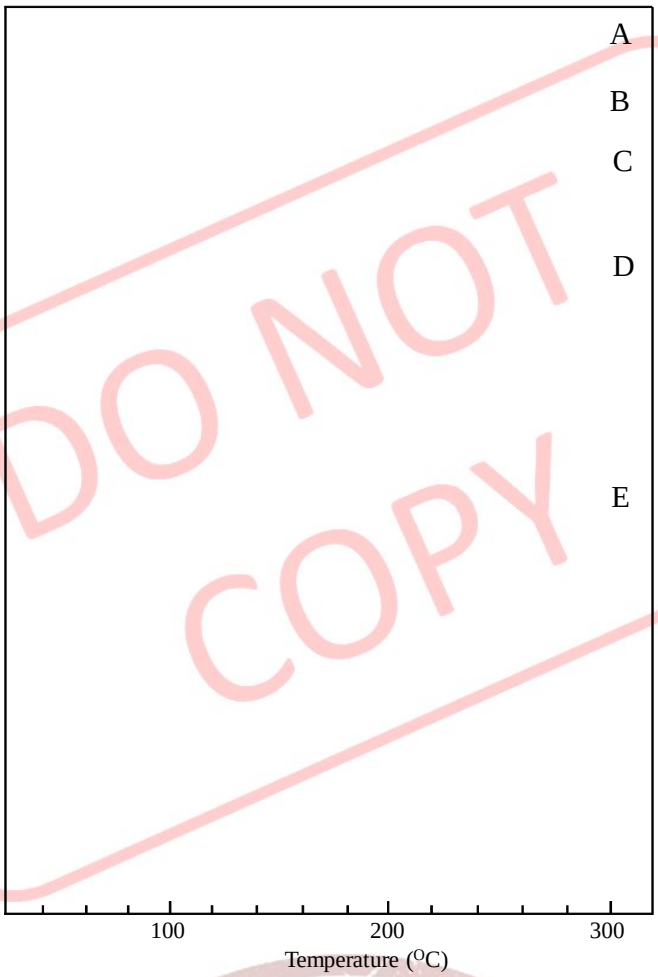

Figure 4.46 DSC thermogram of EXE loaded cPCL NPs (A), EXE (B), cPCL (C), Sucrose (D) and Physical mixture (E).

4.18.4 In vitro drug release studies

The in vitro drug release studies from different nanoparticulate formulations were performed in PBS pH 7.4. Pegylated PCL NPs showed faster release as compared with non-pegylated NPs. In vitro release of EXE from drug suspension and NPs is shown in figure 4.47. Within 3 h, 71.36 ± 1.23% drug release occurred from plain drug suspension, whereas only 20.06 ± 1.31% and 24.88 ± 1.13% drug released from cPCL and pegylated PCL NPs, reaching 44.89 ± 1.3% and 52.22 ± 3.1% after 120 h and 70.67 ± 1.76% and 83.26 ± 0.85% after 240 h from cPCL and pegylated PCL NPs, respectively indicative of sustained release. The drug release from NPs followed biphasic release model with an initial burst release for about 3 h followed by sustained release for more than 240 h. Pegylated PCL NPs showed faster release when compared to cPCL NPs as reported by Derakhshandeh et al. [Derakhshandeh et al. 2010]. The burst release may

be attributed to the drug molecules associated near particle surface [Seju et al. 2011]. Also, particles of nano size range lead to a shorter average diffusion path for the matrix entrapped drug molecules, thereby causing faster diffusion [Mainardes and Evangelista 2005; Shah et al. 2009]. After initial burst release, the release rate decreased, reflecting the release of drug entrapped in the polymer matrix. The release rate in the second phase was assumed to be controlled by diffusion rate of drug across the polymer matrix [Corrigan and Li 2009]. The data obtained from *in vitro* drug release studies was fitted to Korsmeyer - Peppas model. The regression coefficient of the plot of log M_t/M_∞ versus log t for cPCL and pegylated PCL NPs was found to be 0.942 and 0.952 with value of release exponent (n) as 0.303 and 0.306, respectively. The n value is the release exponent which characterizes the transport mechanism and if its value is less than 0.5, it indicates Fickian release. Hence, it can be concluded that the release of EXE from NPs was by Fickian diffusion.

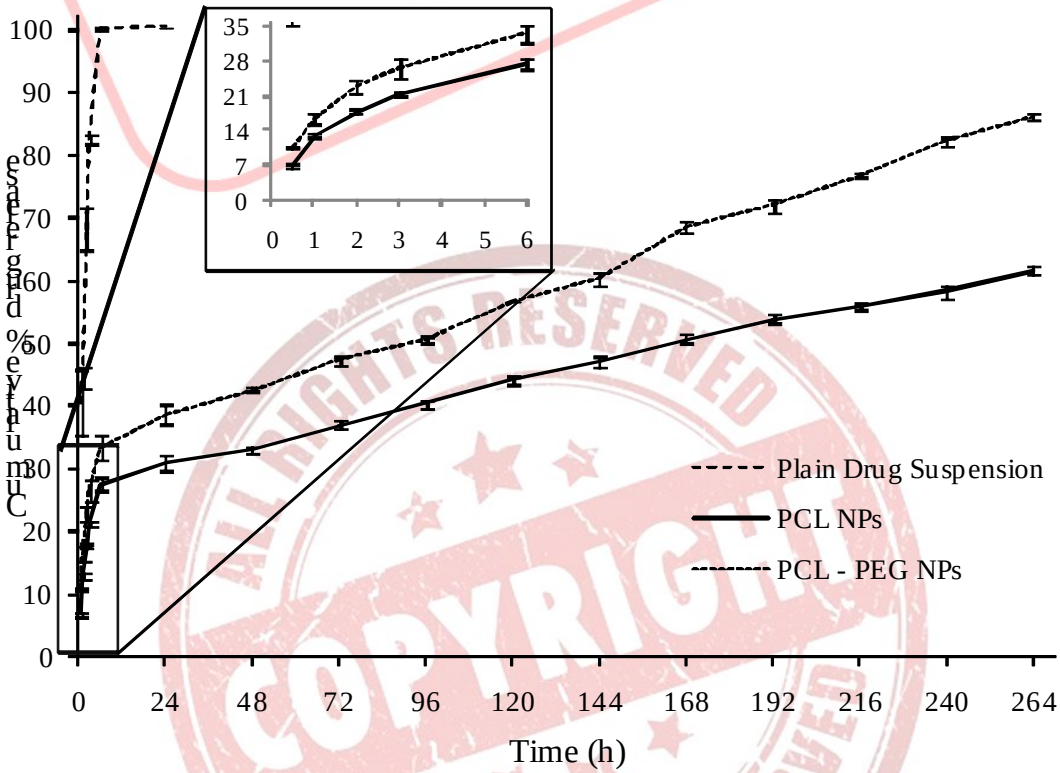

Figure 4.47 Drug release profile of EXE from plain drug suspension, cPCL NPs and pegylated PCL NPs across semi-permeable membrane using the dialysis bag diffusion technique in phosphate buffered saline (pH 7.4). The values represent mean ± S.D. of three batches.

4.18.5 Stability studies

Total drug content after different time intervals showed change in case of the NPs stored at room temperature to that of the NPs stored at refrigerator temperature. After different time intervals, increase in PS was observed for NPs stored at room temperature as compared to NPs stored at refrigerator temperature, which may attributed to the aggregation of polymeric particles (table 4.48). Also, drug content was found to decrease with increase in time as well as storage temperature (figure 4.48). Thus, it was concluded that the optimum temperature condition for storage of the EXE loaded cPCL NPs would be refrigerated condition (2-8 °C).

Table 4.48 Stability data of EXE loaded cPCL NPs stored at different temperature conditions

Storage time	% Drug content		Particle size (nm)	
	Room temp.	Refrigerator temp. (2–8 °C)	Room temp.	Refrigerator temp. (2–8 °C)
Initial	100	100	182.6 ± 2.9	182.6 ± 2.9
1 month	99.50 ± 0.53	99.71 ± 0.27	185.1 ± 1.9	184.5 ± 2.4
2 months	99.11 ± 0.28	99.32 ± 0.41	192.7 ± 3.8	189.4 ± 1.7
3 months	98.87 ± 0.33	99.04 ± 0.19	200.4 ± 5.4	196.4 ± 3.8

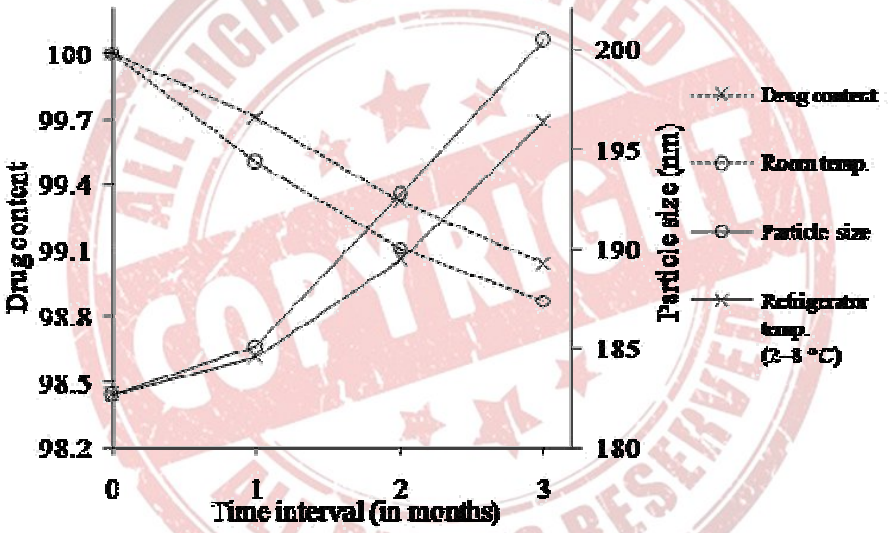

Figure 4.48 Effect of different storage conditions on drug content and PS of EXE loaded cPCL NPs.

4.19 References

Abdelwahed W, Degobert G, Stainmesse S, Fessi H. 2006. Freeze-drying of nanoparticles: formulation, process and storage considerations. Adv. Drug. Deliv. Rev. 58(15):1688-1713.

Abdul M, Ramlal S, Hoosein N. 2008. Ryanodine receptor expression correlates with tumor grade in breast cancer. Pathol. Oncol. Res. 14(2):157-160.

Aberturas MR, Hernan Perez de la Ossa D, Gil ME, Ligresti A, De Petrocellis L, Torres AI, Di Marzo V, Molpeceres J. 2011. Anandamide-loaded nanoparticles: preparation and characterization. J. Microencapsul. 28(3):200-210.

Acharya S, Dilnawaz F, Sahoo SK. 2009. Targeted epidermal growth factor receptor nanoparticle bioconjugates for breast cancer therapy. Biomaterials 30(29):5737-5750.

Adinarayana K, Ellaiah P. 2002. Response surface optimization of the critical medium components for the production of alkaline protease by a newly isolated Bacillus sp. J. Pharm. Pharm. Sci. 5(3):272-278.

Ahlin P, Kristl J, Kristl A, Vrečer F. 2002. Investigation of polymeric nanoparticles as carriers of enalaprilat for oral administration. Int. J. Pharm. 239(1–2):113-120.

Akhnazarova S. 1982. Experiment optimization in chemistry and chemical engineering. Moscow: Mir Publications.

Armstrong AN, James KC. 1996. Pharmaceutical experimental design and interpretation. Bristol, USA: Taylor and Francis Publishers.

Avgoustakis K, Beletsi A, Panagi Z, Klepetsanis P, Livaniou E, Evangelatos G, Ithakissios DS. 2003. Effect of copolymer composition on the physicochemical characteristics, in vitro stability, and biodistribution of PLGA–mPEG nanoparticles. Int. J. Pharm. 259(1–2):115-127.

Bae S, Shoda M. 2005. Statistical optimization of culture conditions for bacterial cellulose production using Box-Behnken design. Biotechnol. Bioeng. 90(1):20-28.

Barichello JM, Morishita M, Takayama K, Nagai T. 1999. Encapsulation of hydrophilic and lipophilic drugs in PLGA nanoparticles by the nanoprecipitation method. Drug Dev. Ind. Pharm. 25(4):471-476.

Behan N, Birkinshaw C, Clarke N. 2001. Poly n-butyl cyanoacrylate nanoparticles: a mechanistic study of polymerisation and particle formation. Biomaterials 22(11):1335-1344.

Bolton S, Bon C. 1997. Pharmaceutical statistics: practical and clinical applications. New York: Marcel Dekker Inc.

Box GEP, Hunter WG, Hunter WS. 1978. Statistics for experimenters: An introduction to design, data analysis, and model building. New York: John Wiley and Sons.

Box GEP, Wilson KB. 1951. On the experimental attainment of optimum conditions. J. Roy. Stat. Soc. 13:1-45.

Breda M, Pianezzola E, Benedetti MS. 1993. Determination of exemestane, a new aromatase inhibitor, in plasma by high-performance liquid chromatography with ultraviolet detection. J. Chromato. 620(2):225-231.

Causes of death in India Srs. 2009. Registrar general of India and centre for global health research. New Delhi: Government of India.

Chacon M, Molpeceres J, Berges L, Guzman M, Aberturas MR. 1999. Stability and freeze-drying of cyclosporine loaded poly(D,L lactide-glycolide) carriers. Eur. J. Pharm. Sci. 8(2):99-107.

Chaudhari KR, Kumar A, Khandelwal V, Ukawala M, Manjappa AS, Mishra AK, Monkkonen J, Murthy RSR. 2012. Bone metastasis targeting: A novel approach to reach bone using Zoledronate anchored PLGA nanoparticle as carrier system loaded with Docetaxel. J. Controlled Rel. 158(3):470-478.

Chaudhari KR, Shah N, Patel H, Murthy R. 2010. Preparation of porous PLGA microspheres with thermoreversible gel to modulate drug release profile of water-soluble drug: bleomycin sulphate. J. Microencapsul. 27(4):303-313.

Chowdhury S, Ellis PA. 2005. Recent advances in the use of aromatase inhibitors for women with postmenopausal breast cancer. J. Br. Menopause Soc. 11(3):96-102.

Clemett D, Lamb HM. 2000. Exemestane: a review of its use in postmenopausal women with advanced breast cancer. Drugs 59(6):1279-1296.

Corrigan OI, Li X. 2009. Quantifying drug release from PLGA nanoparticulates. Eur. J. Pharm. Sci. 37(3-4):477-485.

Darbandy SM, Bakhtiary A, Taheri H. 2011. Novel and efficient catalyst for the synthesis of caprolactone. 2nd International Conference on Chemical Engineering and Applications. Maldives: IACSIT Press, Singapore. 125-129.

Das M, Sahoo SK. 2012. Folate decorated dual drug loaded nanoparticle: role of curcumin in enhancing therapeutic potential of nutlin-3a by reversing multidrug resistance. Plos One 7(3):e32920.

De Jong WH, Borm PJ. 2008. Drug delivery and nanoparticles:applications and hazards. Int. J. Nanomedicine 3(2):133-149.

Derakhshandeh K, Soheili M, Dadashzadeh S, Saghiri R. 2010. Preparation and in vitro characterization of 9-nitrocamptothecin-loaded long circulating nanoparticles for delivery in cancer patients. Int. J. Nanomed. 5:463-471.

Derringer G, Suich R. 1980. Simultaneous optimization of several response variables. J. Quality Technol. 12(4):214-219.

Dowsett M. 1998. Theoretical considerations for the ideal aromatase inhibitor. Breast Cancer Res. Treat. 49 Suppl 1:S39-44; discussion S73-S77.

Dubernet C. 1995. Thermoanalysis of microspheres. Thermochimica Acta 248(0):259-269.

Feng S, Huang G. 2001. Effects of emulsifiers on the controlled release of paclitaxel (Taxol) from nanospheres of biodegradable polymers. J. Controlled Rel. 71(1):53-69.

Fessi H, Puisieux F, Devissaguet JP, Ammoury N, Benita S. 1989. Nanocapsule formation by interfacial polymer deposition following solvent displacement. Int. J. Pharm. 55(1):R1-R4.

Fonseca C, Simoes S, Gaspar R. 2002. Paclitaxel-loaded PLGA nanoparticles: preparation, physicochemical characterization and in vitro anti-tumoral activity. J. Controlled Rel. 83(2):273-286.

George Box DB. 1960. Some new three level designs for the study of quantitative variables. Technometrics 2:455-475.

Henderson IC, Canellos GP. 1980. Cancer of the breast: the past decade (first of two parts). N. Engl. J. Med. 302(1):17-30.

Jain NK, Ram A. 2011. Development and characterization of nanostructured lipid carriers of oral hypoglycemic agent: selection of surfactants. Int. J. Pharm. Sci. Rev. and Res. 7(2):125-130.

Johannessen DC, Engan T, Di Salle E, Zurlo MG, Paolini J, Ornati G, Piscitelli G, Kvinnsland S, Lonning PE. 1997. Endocrine and clinical effects of exemestane (PNU 155971), a novel steroidal aromatase inhibitor, in postmenopausal breast cancer patients: a phase I study. Clin. Cancer Res. 3(7):1101-1108.

Joshi SA, Chavhan SS, Sawant KK. 2010. Rivastigmine-loaded PLGA and PBCA nanoparticles: preparation, optimization, characterization, in vitro and pharmacodynamic studies. Eur. J. Pharm. Biopharm. 76(2):189-199.

Kashi TS, Eskandarion S, Esfandyari-Manesh M, Marashi SM, Samadi N, Fatemi SM, Atyabi F, Eshraghi S, Dinarvand R. 2012. Improved drug loading and antibacterial activity of minocycline-loaded PLGA nanoparticles prepared by solid/oil/water ion pairing method. Int. J. Nanomed. 7:221-234.

Kenneth WY, Mak MGSY, Wah Koon Teo. 1995. Formulation and optimization of two culture media for the production of tumour necrosis factor-β in Escherichia coli. J. Chem. Technol. Biotechnol. 62(3):289-294.

Kumar A, Sawant K. 2013. Encapsulation of exemestane in polycaprolactone nanoparticles: optimization, characterization, and release kinetics. Cancer Nano. 4(4-5):57-71.

Kwon HY, Lee JY, Choi SW, Jang Y, Kim JH. 2001. Preparation of PLGA nanoparticles containing estrogen by emulsification–diffusion method. Coll. Surf. A: Physicochemical and Engineering Aspects 182(1–3):123-130.

Lacoulonche F, Gamisans F, Chauvet A, Garcia ML, Espina M, Egea MA. 1999. Stability and in vitro drug release of flurbiprofen-loaded poly-epsilon-caprolactone nanospheres. Drug Dev. Ind. Pharm. 25(9):983-993.

Lam CX, Savalani MM, Teoh SH, Hutmacher DW. 2008. Dynamics of in vitro polymer degradation of polycaprolactone-based scaffolds: accelerated versus simulated physiological conditions. Biomed. Mater. 3(3):034108.

Levison KK, Takayama K, Isowa K, Okabe K, Nagai T. 1994. Formulation optimization of indomethacin gels containing a combination of three kinds of cyclic

monoterpenes as percutaneous penetration enhancers. J. Pharm. Sci. 83(9):1367-1372.

Lonning PE. 1998. Pharmacological profiles of exemestane and formestane, steroidal aromatase inhibitors used for treatment of postmenopausal breast cancer. Breast Cancer Res. Treat. 49 Suppl 1:S45-52; discussion S73-S77.

Mainardes RM, Evangelista RC. 2005. Praziquantel-loaded PLGA nanoparticles: preparation and characterization. J. Microencapsul. 22(1):13-24.

Mak KWY, Yap MGS, Teo WK. 1995. Formulation and optimization of two culture media for the production of tumour necrosis factor-β in Escherichia coli. J. Chem. Technol. Biotechnol. 62(3):289-294.

McPherson K, Steel CM, Dixon JM. 2000. ABC of breast diseases. Breast cancer-epidemiology, risk factors, and genetics. BMJ 321(7261):624-628.

Mehta AK, Yadav KS, Sawant KK. 2007. Nimodipine loaded PLGA nanoparticles: formulation optimization using factorial design, characterization and in vitro evaluation. Curr. Drug Deliv. 4(3):185-193.

Mendes GD, Hamamoto D, Ilha J, Pereira Ados S, De Nucci G. 2007. Anastrozole quantification in human plasma by high-performance liquid chromatography coupled to photospray tandem mass spectrometry applied to pharmacokinetic studies. J. Chromato. 850(1-2):553-559.

Miller AJ. 1984. Selection of subsets of regression variables. J. R. Stat. Soc. Ser. A. 147:389-425.

Misra R, Sahoo SK. 2010. Intracellular trafficking of nuclear localization signal conjugated nanoparticles for cancer therapy. Eur. J. Pharm. Sci. 39(1-3):152-63.

Montgomery DC. 2004. Introduction to factorial designs. New York: John Wiley and Sons. 392-426 p.

Moraes CM, de Matos AP, de Paula E, Rosa AH, Fraceto LF. 2009. Benzocaine loaded biodegradable poly-(d,l-lactide-co-glycolide) nanocapsules: factorial design and characterization. Mater. Sci. Eng.: B 165(3):243-246.

Musumeci T, Ventura CA, Giannone I, Ruozi B, Montenegro L, Pignatello R, Puglisi G. 2006. PLA/PLGA nanoparticles for sustained release of docetaxel. Int. J. Pharm. 325(1-2):172-179.

Myer RH, Khuri AI, Carter WH. 1989. Response surface methodology: 1966-1988. Technometrics 31:137-157.

Myer RH, Montogomery DC. 2002. Response Surface Methodology: Process and product optimization using designed experiment. New York: John Wiley and Sons.

Nanjwade BK, Manjappa AS, Murthy RSR, Pol YD. 2009. A novel pH-triggered in situ gel for sustained ophthalmic delivery of ketorolac tromethamine. Asian J. Pharm. Sci. 4(3):189 - 199.

Paolicelli P, Prego C, Sanchez A, Alonso MJ. 2010. Surface-modified PLGA-based nanoparticles that can efficiently associate and deliver virus-like particles. Nanomedicine 5(6):843-853.

Peppas NA. 1985. Analysis of Fickian and non-Fickian drug release from polymers. Pharm Acta Helv 60(4):110-111.

Quintanar-Guerrero D, Allemann E, Fessi H, Doelker E. 1998. Preparation techniques and mechanisms of formation of biodegradable nanoparticles from preformed polymers. Drug Dev. Ind. Pharm. 24(12):1113-1128.

Rahman Z, Zidan AS, Khan MA. 2010. Non-destructive methods of characterization of risperidone solid lipid nanoparticles. Eur J. Pharm. Biopharm. 76(1):127-137.

Ray S. 2006. RSM: a statistical tool for process optimization. Ind. Tex. J. 117:24-30.

Ray S, Lalman JA, Biswas N. 2009. Using the Box-Benkhen technique to statistically model phenol photocatalytic degradation by titanium dioxide nanoparticles. Chem. Eng. J. 150(1):15-24.

Redhead HM, Davis SS, Illum L. 2001. Drug delivery in poly(lactide-co-glycolide) nanoparticles surface modified with poloxamer 407 and poloxamine 908: in vitro characterisation and in vivo evaluation. J. Controlled Rel. 70(3):353-363.

Sarkar K, Yang H. 2008. Encapsulation and extended release of anti-cancer anastrozole by stealth nanoparticles. Drug Deliv. 15(5):343-346.

Scott LJ, Wiseman LR. 1999. Exemestane. Drugs 58(4):675-682

Seju U, Kumar A, Sawant KK. 2011. Development and evaluation of olanzapine-loaded PLGA nanoparticles for nose-to-brain delivery: In vitro and in vivo studies. Acta Biomater 7(12):4169-4176.

Seth AK, Misra A. 2002. Mathematical modelling of preparation of acyclovir liposomes: reverse phase evaporation method. J. Pharm. Pharm. Sci. 5(3):285-291.

Shah N, Chaudhari K, Dantuluri P, Murthy RS, Das S. 2009. Paclitaxel-loaded PLGA nanoparticles surface modified with transferrin and Pluronic®P85, an in vitro cell line and in vivo biodistribution studies on rat model. J. Drug Target. 17(7):533-542.

Shi K, Cui F, Yamamoto H, Kawashima Y. 2009. Optimized formulation of high-payload PLGA nanoparticles containing insulin-lauryl sulfate complex. Drug Dev. Ind. Pharm. 35(2):177-184.

Shirakura O, Yamada M, Hashimoto M, Ishimaru S, Takayama K, Nagai T. 1991. Particle-size design using computer optimization technique. Drug Dev. Ind. Pharm. 17(4):471-483.

Snehalatha M, Venugopal K, Saha RN, Babbar AK, Sharma RK. 2008. Etoposide loaded PLGA and PCL nanoparticles II: biodistribution and pharmacokinetics after radiolabeling with Tc-99m. Drug Deliv. 15(5):277-287.

Song Z, Feng R, Sun M, Guo C, Gao Y, Li L, Zhai G. 2011. Curcumin-loaded PLGA-PEG-PLGA triblock copolymeric micelles: Preparation, pharmacokinetics and distribution in vivo. J. Colloid Interface Sci. 354(1):116-23.

Strassmer-Weippl K, Goss PE. 2003. Prevention of breast cancer using SERMs and aromatase inhibitors. J. Mammary Gland Biol. Neoplasia 8(1):5-18.

Theobald AJ. 2000. Management of advanced breast cancer with endocrine therapy: the role of the primary healthcare team. Int. J. Clin. Pract. 54(10):665-669.

Thode K, Muller RH, Kresse M. 2000. Two-time window and multiangle photon correlation spectroscopy size and zeta potential analysis--highly sensitive rapid assay for dispersion stability. J. Pharm. Sci. 89(10):1317-1324.

Tuncay M, Calis S, Kas HS, Ercan MT, Peksoy I, Hincal AA. 2000. Diclofenac sodium incorporated PLGA (50:50) microspheres: formulation considerations and in vitro/in vivo evaluation. Int. J. Pharm. 195(1-2):179-188.

von Pawel J, Gatz emeier U, Pujol JL, Moreau L, Bildat S, Ranson M, Richardson G, Steppert C, Rivière A, Camlett I. 2001. Phase II comparator study of oral versus intravenous topotecan in patients with chemosensitive small-cell lung cancer. J. Clin. Oncol. 19:1743-1749.

Wagner JM, Shimshak DG. 2007. Stepwise selection of variables in data envelopment analysis: Procedures and managerial perspectives. Eur. J. Oper. Res. 180(1):57-67.

Yadav KS, Sawant KK. 2010. Modified nanoprecipitation method for preparation of cytarabine-loaded PLGA nanoparticles. AAPS Pharmscitech 11(3):1456-1465.

Yallapu MM, Gupta BK, Jaggi M, Chauhan SC. 2010. Fabrication of curcumin encapsulated PLGA nanoparticles for improved therapeutic effects in metastatic cancer cells. J. Colloid Interface Sci. 351(1):19-29.

Yang SC, Lu LF, Cai Y, Zhu JB, Liang BW, Yang CZ. 1999. Body distribution in mice of intravenously injected camptothecin solid lipid nanoparticles and targeting effect on brain. J. Controlled Rel. 59(3):299-307.

Yee L, Blanch HW. 1993. Defined media optimization for growth of recombinant Escherichia coli X90. Biotechnol. Bioeng. 41(2):221-230.

Zhang Q, Xu W, Wang Z. 1994. Synthesis of polycaprolactone with two carboxy end groups. J. Mater. Sci. Technol. 10:351-354.

Chapter 5

PEGYLATION AND SURFACE FUNCTIONALIZATION

5.1 Materials

Anastrozole and exemestane were obtained as gift sample from Sun Pharma Advanced Research Company Ltd (SPARC), Vadodara, India. PLGA (lactide/glycolide ratio 50:50, Mol wt. 12 KDa) was obtained as a gift sample from Purac Biomaterials, Gorinchem, Netherlands. Poloxamer 188 was obtained as gift sample from BASF, Ludwigshafen, Germany. Capric/caprylic triglyceride (Capmul MCM, C8) was obtained as gift sample from Abitec Corporation, Janesville, USA. Caprolactone monomer was purchased from Sigma-Aldrich, Mumbai, India. Sulpho-NHS, 6-Coumarin was purchased from Sigma-Aldrich, Mumbai, India. Amine-PEG-carboxylic acid (Mol wt. 5000 Da) was purchased from Biomatrik, Jhegiang, China. Monoclonal antibody against estrogen receptor was purchased from Pierce antibodies, USA. THP1 cells were procured from NCCS, Pune, India. RPMI-1640, Fetal Bovine Serum (FBS), antibiotic-antimycotic, Trypsin-EDTA and PBS were purchased from Life Technologies Pvt. Ltd., New Delhi, India. 6-well plates, 96-well plates, tissue culture flask (25 and 75 cm^2), chamber slide and other sterile material for cell culture were purchased from Thermo scientific, India. EDC and NHS were purchased from Himedia, Vadodara, India. All other chemicals were of analytical reagent grade and obtained commercially.

5.2 Cell lines

Human acute monocytic leukemia cell line (THP1), was grown in RPMI-1640 medium (Gibco, Grand Island, NY, USA) supplemented with 5% (v/v) fetal bovine serum (FBS), penicillin (100 units/ml) and streptomycin (100 µg/ml) (Gibco, Grand Island, NY, USA) at 37 °C in a humidified incubator containing 5% CO_2.

5.3 Methods

5.3.1 Pegylation of nanoparticles

Pegylated nanoparticles (NPs) were prepared in similar manner as described in chapter 4 with replacement of a part of PLGA and PCL with PLGA-PEG and PCL-PEG, respectively. Five different formulations containing 0, 5, 10, 15 and 20% PLGA-PEG and PCL-PEG were prepared. Pegylated NPs were optimized based on percentage drug entrapment (PDE), particle size (PS) and phagocytic uptake studies on THP1 cells by flow cytometry. 6-Coumarin loaded NPs were also prepared in a similar way as reported previously in chapter 4 with addition of 6-Coumarin instead of ATZ/EXE. In

vitro drug release studies were performed as described in chapter 4 to compare any change in drug release due to pegylation.

5.3.2 Phagocytic uptake

Phagocytic uptake studies were performed using human acute monocytic leukemia cell line (THP1). 1 ml of THP1 cell suspension (2×10^5 cells) was incubated with 1 ml (200 µg/ml) of 6-Coumarin-loaded PLGA NPs, 6-Coumarin-loaded PCL NPs, pegylated PLGA NPs and pegylated PCL NPs (5, 10, 15, 20%) for 60, 120 and 240 min for phagocytic uptake. Cells were then centrifuged at 400×g for 5 min, re-suspended in 1× PBS and samples were analyzed using FACS. In FACS analysis, 10,000 cells were counted by measuring signal from FITC channel (FACS Canto-II, BD Biosciences, CA, USA) and analyzed by software provided with the instrument (BD FACS Diva 6.2.1 software, BD Biosciences, CA, USA).

5.3.3 Surface functionalization of NPs with ER antibody

For target specific drug delivery, coupling of ER antibody to NPs was carried out using a surface activation method [Acharya et al. 2009]. In brief, 10 mg of drug loaded NPs were dispersed in 2 ml of PBS (0.02 M, pH 7.4) followed by addition of 225 µl of EDC (1 mg/ml) and 140 µl of NHS (1 mg/ml) in to the above suspension. EDC activation was carried out by agitating the above suspension for 4 h at room temperature using a magnetic stirrer. Excess of un-reacted EDC and NHS were removed by size exclusion chromatography using Sephadex column and ER antibody (25 µl, 1 mg/ml) was added to the activated NPs. The above dispersion was agitated for 4 h at room temperature for conjugation of antibody to NPs. The prepared immunoNPs were characterized by PDE, PS, zeta potential and transmission electron microscopy.

5.4 Results and discussion

5.4.1 Physicochemical characterization of ATZ loaded PLGA NPs

ATZ loaded PLGA NPs were optimized for highest PDE and smallest PS as discussed in chapter 4. Optimized batch of ATZ loaded PLGA NPs had PDE of 62.09 ± 0.95%, PS of 145.9 ± 2.3 nm and zeta potential of -30.7 ± 1.4 mV.

5.4.2 Optimization of ATZ loaded PLGA NPs containing different PEG ratio based on PDE, PS and phagocytic uptake studies

ATZ loaded pegylated NPs were optimized based on PDE, PS and phagocytic uptake studies on THP1 cells by FACS. Physicochemical parameters of formulations with

different PEG content are summarized in table 5.1. From the results, it was observed that as the amount of PEG increased, PDE, PS and zeta potential decreased. However, the decrease in PDE, PS or zeta potential were not significant ($p>0.01$). Decrease in PS was possibly due to the presence of both hydrophilic (PEG) and hydrophobic (PLGA) end in PLGA-PEG, imparting amphiphilic nature to NPs [Avgoustakis et al. 2003; Chaudhari et al. 2012a; Chaudhari et al. 2012b; Ramanlal Chaudhari et al. 2012]. Decrease in PDE was possibly due to decreased size of the NPs and decrease in zeta potential was due to increase in PEG chains on the surface of NPs.

Table 5.1 Physicochemical characterization of ATZ loaded PLGA NPs, pegylated PLGA NPs and ImmunoNPs

Formulation	PDE (%)	PS (nm)	Zeta Potential (mV)
PLGA NPs	62.09 ± 0.95	145.9 ± 2.3	-30.7 ± 1.4
PLGA-PEG NPs (5%)	62.21 ± 1.07	142.3 ± 3.5	-31.8 ± 2.3
PLGA-PEG NPs (10%)	61.98 ± 0.87	137.7 ± 3.1	-28.6 ± 1.9
PLGA-PEG NPs (15%)	61.76 ± 1.15	135.9 ± 2.7	-24.0 ± 2.7
PLGA-PEG NPs (20%)	61.36 ± 0.99	126.6 ± 4.1	-24.1 ± 3.4
ImmunoNPs	60.85 ± 1.53	140.4 ± 3.7	-23.6 ± 4.0

The process of phagocytosis commences by two ways, first is by protein adsorption and second is by secretion of pro-inflammatory cytokines. Kanchan et al demonstrated that in vitro phagocytosis process can be simulated using macrophage cell line. After incubation of NPs with macrophage cell line, secretion level of IFN-c and IL-4 increases [Kanchan and Panda 2007; Muhlfeld et al. 2007]. 6-Coumarin is a well known fluorescent probe and is used to study phagocytic uptake of prepared NPs due to its low pH dependent solubility and good fluorescence. Here, relative uptake of 6-Coumarin loaded NPs (pegylated and non-pegylated) in human acute monocytic leukemia cell line (THP1) was performed to confirm their in vitro anti-opsonization activity. Phagocytic uptake of PLGA NPs was compared with pegylated NPs containing varied quantity of PLGA-PEG (5, 10, 15 and 20%) in terms of mean fluorescence intensity after 60, 120 and 240 min as shown in figure 5.1 (a), (b) and (c), respectively. Pegylated NPs displayed greater resistance to phagocytic uptake than non-pegylated NPs. After 60 min, uptake of

PLGA NPs was 1.32, 2.38 and 9.34 times more than PLGA-PEG (5%), PLGA-PEG (15%) and PLGA-PEG (20%) NPs (figure 5.2). When phagocytic uptake of NPs was studied at three different time points, it was found that phagocytosis increased in a time dependent manner. However, overall uptake decreased with increase in PEG content due to increased hydrophilicity of NPs. These results are in accordance with earlier reports [Chaudhari et al. 2012c; Mosqueira et al. 1999]. The uptake of PLGA NPs is also affected by their surface charge. Cationic particles are more efficiently up taken by phagocytes as compared to negatively charged particles. This is because the ionic attraction between the positively charged particles and negatively charged cell surface causes efficient binding and facilitate the internalization process [Josephson et al. 1999]. As pegylated NPs exhibited negative zeta potential (-24.1 ± 3.4 mV), we can assume that they will successfully avoid phagocytosis and hence will be long circulating.

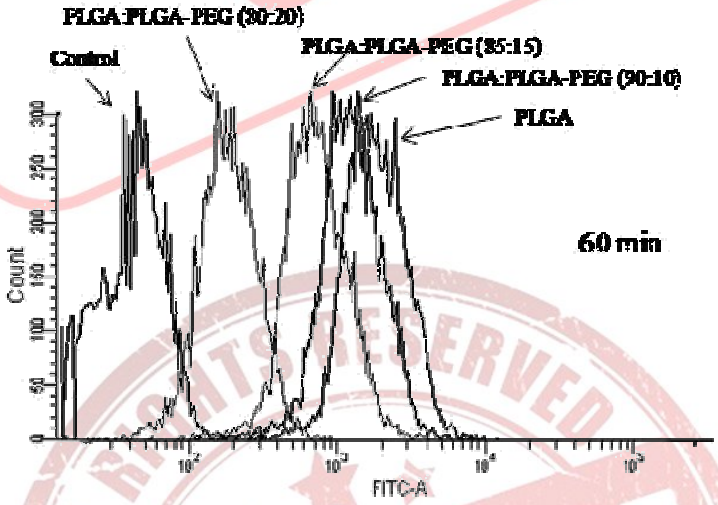

(a)

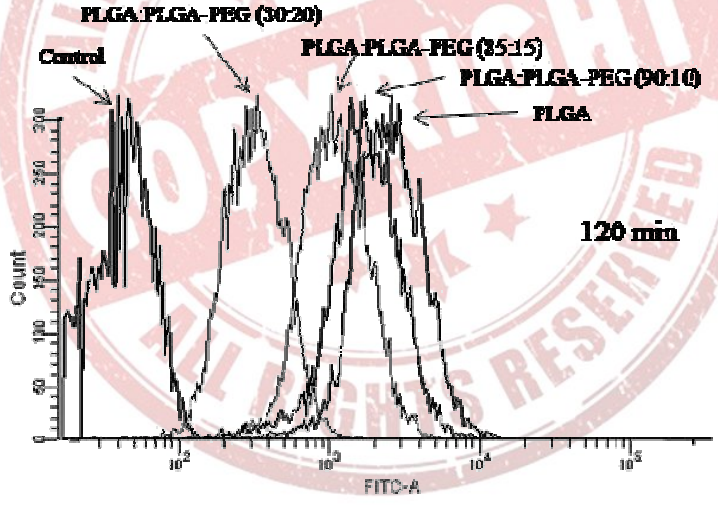

(b)

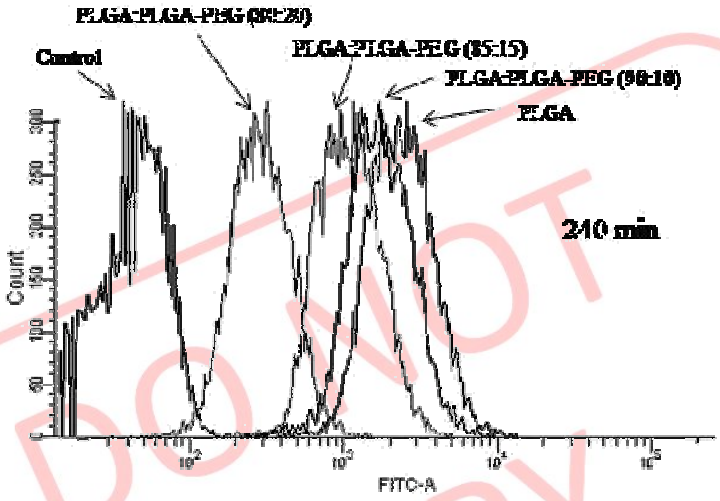

(c)

Figure 5.1 Phagocytic uptake histograms of 6-Coumarin loaded NP formulations by human acute monocytic leukemia cell line (THP1) after incubation for (a) 60, (b) 120 and (c) 240 min using FACS.

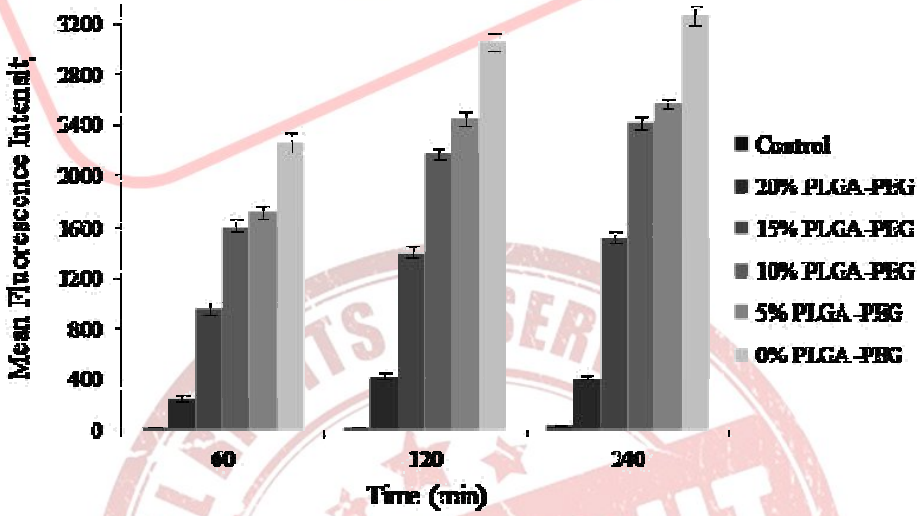

Figure 5.2 Phagocytic uptake of 6-Coumarin loaded PLGA and pegylated PLGA NPs using Human acute monocytic leukemia cell line, THP1 after incubation for 60, 120 and 240 min using FACS. Data presented as Mean ± SD, n=3

The in vitro drug release studies from different nanoparticulate formulations were performed in PBS pH 7.4. Pegylated NPs showed faster release as compared with non-pegylated NPs. In vitro release of ATZ from drug suspension and NPs is shown in figure 5.3. Within 3 h, 82.56 ± 0.623% drug release occurred from plain drug suspension, whereas only 24.14 ± 0.316% and 28.90 ± 1.03% drug released from PLGA and pegylated PLGA NPs, reaching 48.02 ± 0.566% and 60.29 ± 0.85% after 120 h and 64.9 ±

0.249% and 83.04 ± 0.55% after 240 h, respectively, indicative of sustained release. The drug release from NPs followed biphasic release model with an initial burst release for about 3 h followed by sustained release for more than 240 h. Pegylated PLGA NPs showed faster release of drug when compared to PLGA NPs due to the presence of hydrophilic PEG chains around the NPs, causing increased diffusion of water to the core of particles. The regression coefficient of the plot of log M_t/M_∞ versus log t was found to be 0.948 and 0.956 with value of release exponent (n) as 0.255 and 0.264, respectively for PLGA and pegylated PLGA NPs. The n value is the release exponent which characterizes the transport mechanism and if its value is less than 0.5, it indicates Fickian release. Hence, it can be concluded that the release of ATZ from NPs was by Fickian diffusion.

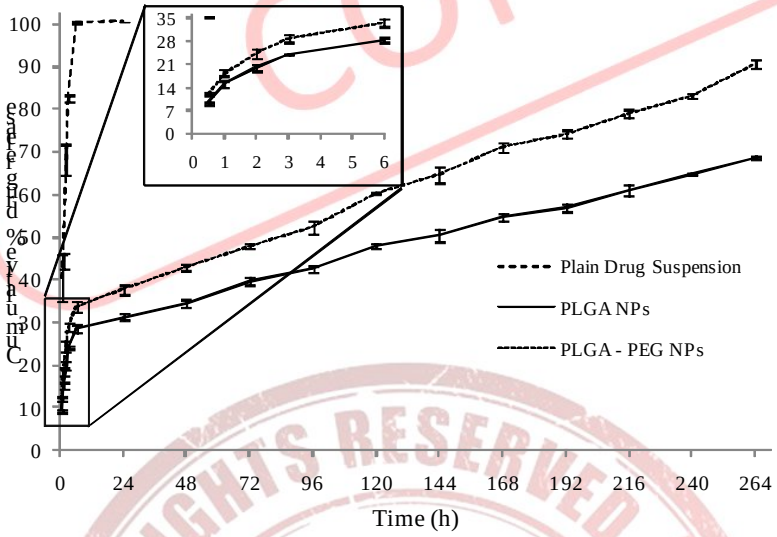

Figure 5.3 Drug release profile of ATZ from plain drug suspension, PLGA NPs and pegylated PLGA NPs across semi-permeable membrane using the dialysis bag diffusion technique in phosphate buffered saline (pH 7.4). The values represent mean ± S.D. of three batches.

5.4.3 Physicochemical characterization of ImmunoNPs

ATZ loaded pegylated PLGA NPs were conjugated with anti-estrogen receptor monoclonal antibody for targeting breast tumor by two-step EDC-NHS activation method. In this method, amino group of monoclonal antibody was conjugated to carboxyl groups of PEG through an amide bond formation [Kocbek P 2007]. It was estimated that approximately 54 Ab molecules were present on each NP [Olivier et al. 2002].

ATZ was successfully loaded in pegylated PLGA NPs prior to Ab conjugation (61.29 ± 1.18%) and no significant loss in drug content was observed after surface functionalization with Ab (60.62 ± 0.54%). However, slight increase in PS was observed which increased from 126.6 ± 4.1 to 140.4 ± 3.7 nm with no significant change in zeta potential from -24.1 ± 3.4 to -23.6 ± 4.0 mV. Poly dispersity index before and after Ab conjugation was less than 0.1 indicating mono-dispersity of particles. A similar trend was observed by Das et al. and Tseng et al. when they conjugated antibody on PLGA and gelatin NPs, respectively [Das and Sahoo 2011; Tseng et al. 2007]. TEM image showed discrete spherical particles with monodisperse size of about 100 nm (figure 5.4). The higher hydrodynamic diameter of NPs achieved by dynamic light scattering (Zetasizer NanoZS) analysis as compared to the size obtained by TEM analysis is possibly contributed by the hydration of the surface associated PEG.

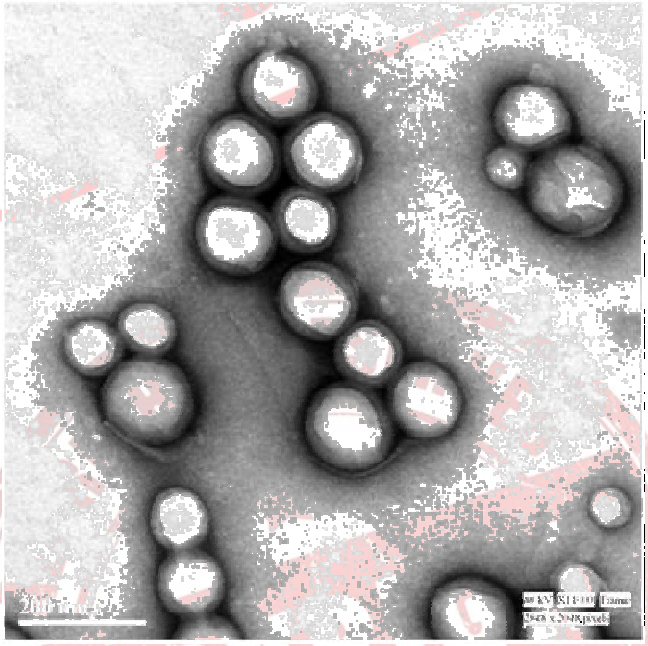

Figure 5.4 TEM image of ATZ loaded pegylated PLGA ImmunoNPs.

5.4.4 Physicochemical characterization of EXE loaded PCL NPs

EXE loaded PCL NPs were optimized for highest percentage drug entrapment (PDE) and smallest particle size (PS) as discussed in chapter 4. Optimized batch of EXE loaded PCL NPs had PDE of 84.07 ± 2.02%, PS of 182.6 ± 3.8 nm and zeta potential of -33.8 ± 2.1 mV.

5.4.5 Optimization of EXE loaded PCL NPs containing different PEG ratio based on PDE, PS and phagocytic uptake studies

Physicochemical parameters of NPs with different PEG content are summarized in table 5.2. From the results, it was observed that as the amount of PEG increased, PDE, PS and zeta potential decreased. However, the decrease in PDE, PS or zeta potential were not significant ($p<0.01$).

Table 5.2 Physicochemical characterization of EXE loaded cPCL NPs, pegylated PCL NPs and ImmunoNPs

Formulation	PDE (%)	PS (nm)	Zeta Potential (mV)
PCL NPs	84.07 ± 2.02	182.6 ± 3.8	-33.8 ± 2.1
PCL-PEG NPs (5%)	84.12 ± 1.12	184.1 ± 2.4	-33.3 ± 1.6
PCL-PEG NPs (10%)	83.58 ± 1.25	179.1 ± 4.1	-31.7 ± 1.3
PCL-PEG NPs (15%)	83.20 ± 0.92	173.7 ± 3.5	-29.6 ± 3.1
PCL-PEG NPs (20%)	82.73 ± 1.19	168.9 ± 2.9	-27.1 ± 0.9
ImmunoNPs	82.11 ± 1.79	179.8 ± 4.1	-24.3 ± 1.2

Phagocytic uptake of PCL NPs were compared with pegylated NPs containing varied quantity of PCL-PEG (5, 10, 15 and 20%) in terms of mean fluorescence intensity after 60, 120 and 240 min as shown in figure 5.5 (a), (b) and (c), respectively. Pegylated NPs displayed resistance to phagocytic uptake than non-pegylated NPs. After 1 h, uptake of PCL NPs was 1.33, 2.30 and 9.06 times more than PCL-PEG (5%), PCL-PEG (15%) and PCL-PEG (20%) NPs (figure 5.6). Phagocytic uptake of NPs were performed at three different time points to determine phagocytosis kinetics and it was found that phagocytosis increased in a time dependent manner. Small increase in uptake was observed with increase in time, but overall uptake decreased with increase in PEG content as reported by Tseng et al. [Chaudhari et al. 2012c; Mosqueira et al. 1999]. As discussed previously, the phagocytic uptake study with both the pegylated polymers (PLGA and PCL) showed lesser uptake with increased concentration of PEG.

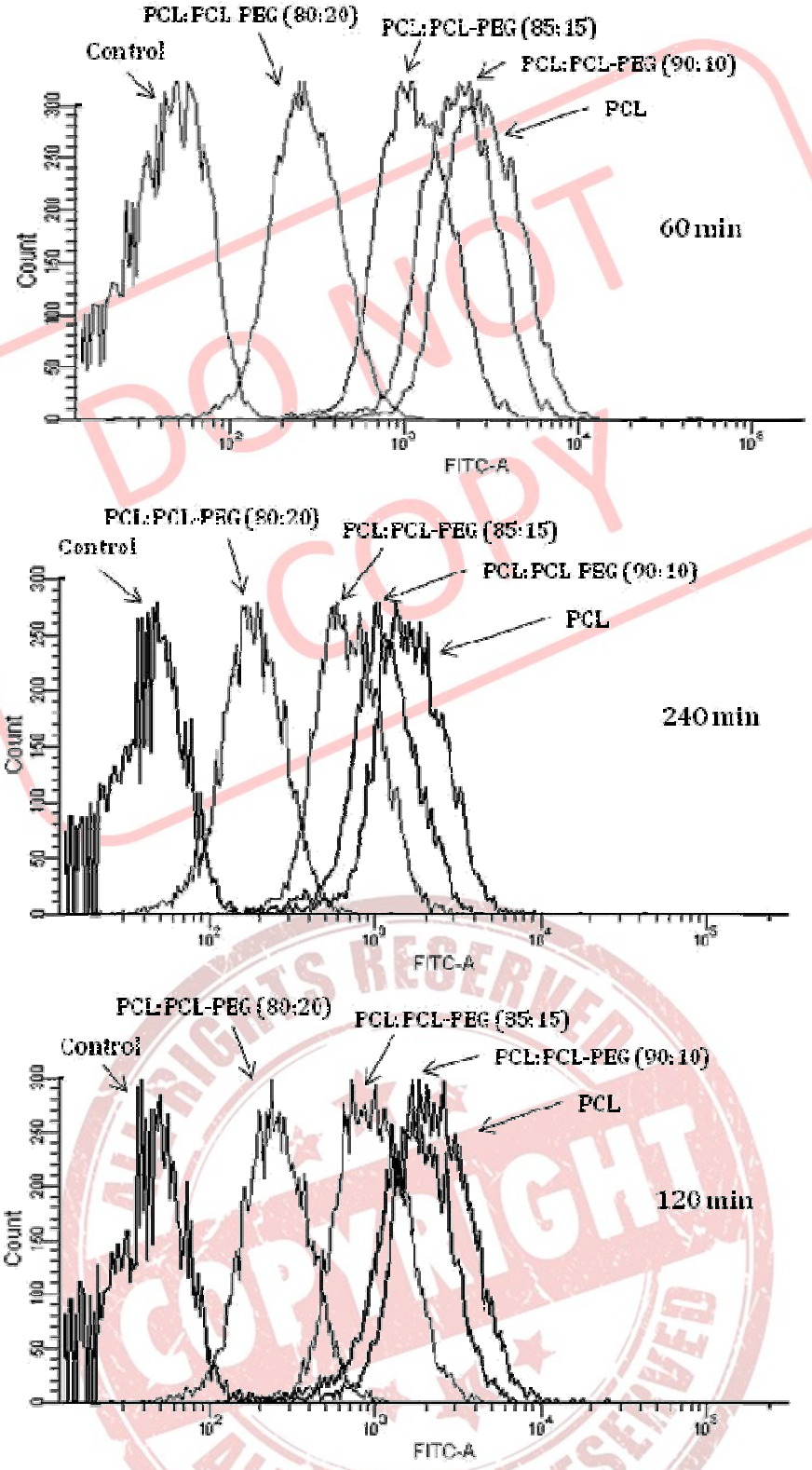

Figure 5.5 Phagocytic uptake histograms of 6-Coumarin loaded NP formulations by human acute monocytic leukemia cell line (THP1) after incubation for (a) 60, (b) 120 and (c) 240 min using FACS.

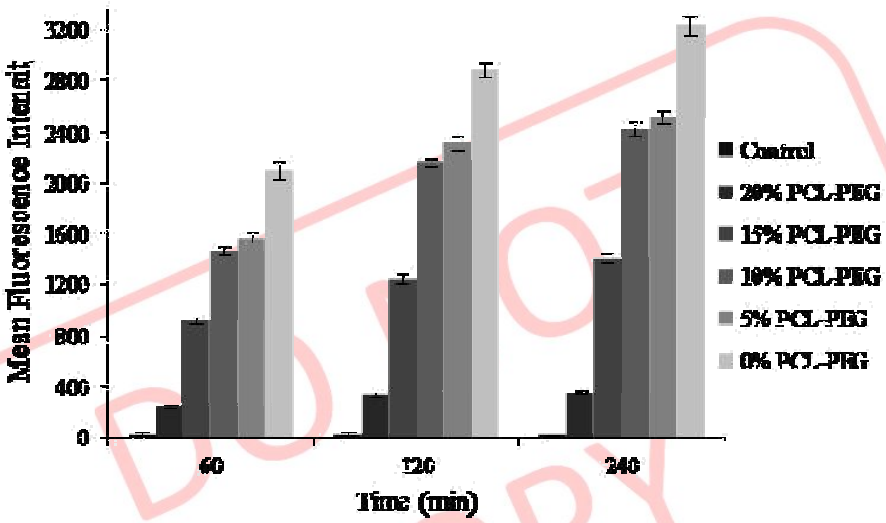

Figure 5.6 Phagocytic uptake of 6-coumarin loaded PCL and pegylated PCL NPs using Human acute monocytic leukemia cell line, THP-1 after incubation for 60, 120 and 240 min using FACS. Data presented as Mean ± SD, n=3.

The in vitro drug release studies from different nanoparticulate formulations were performed in PBS pH 7.4. Pegylated PCL NPs showed faster release as compared with non-pegylated NPs. In vitro release of EXE from drug suspension and NPs is shown in figure 5.7. Within 3 h, 71.36 ± 1.23% drug release occurred from plain drug suspension, whereas only 20.06 ± 1.31% and 24.88 ± 1.13% drug released from PCL and pegylated PCL NPs, reaching 44.89 ± 1.3% and 52.22 ± 3.1% after 120 h and 70.67 ± 1.76% and 83.26 ± 0.85% after 240 h, respectively indicative of sustained release. The drug release from NPs followed biphasic release model with an initial burst release for about 3 h followed by sustained release for more than 240 h. Pegylated PCL NPs showed faster release when compared to PCL NPs due to the presence of hydrophilic PEG chains around the NPs, causing increased diffusion of water to the core of particles. The regression coefficient of the plot of log M_t/M_∞ versus log t for PCL and pegylated PCL NPs was found to be 0.942 and 0.952 with value of release exponent (n) as 0.303 and 0.306, respectively. The n value is the release exponent which characterizes the transport mechanism and if its value is less than 0.5, it indicates Fickian release. Hence, it can be concluded that the release of ATZ from NPs was by Fickian diffusion.

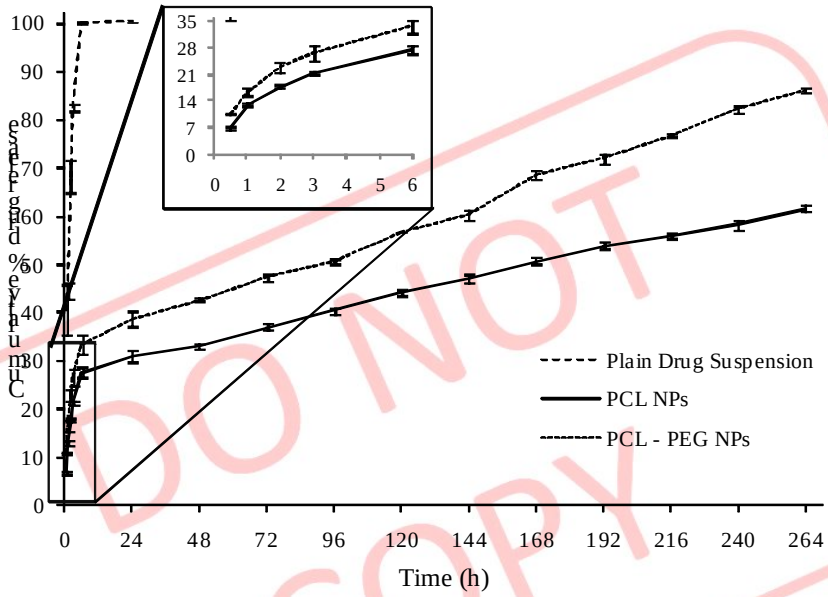

Figure 5.7 Drug release profile of EXE from plain drug suspension, PCL NPs and pegylated PCL NPs across semi-permeable membrane using the dialysis bag diffusion technique in phosphate buffered saline (pH 7.4). The values represent mean ± S.D. of three batches.

5.4.6 Physicochemical characterization of ImmunoNPs

EXE loaded pegylated PCL NPs were conjugated with anti-estrogen receptor monoclonal antibody for targeting breast tumor. For conjugation of Ab to pegylated PCL NPs, two-step EDC-NHS activation method was used. In this method, amino groups of monoclonal antibody were conjugated to carboxyl groups of PEG through an amide bond formation [Kocbek P 2007]. It was estimated that approximately 67 Ab molecules were present on each NP [Olivier et al. 2002].

EXE was successfully loaded in pegylated PCL NPs prior to Ab conjugation and no significant loss in drug content was observed after surface functionalization with Ab. However, slight increase in PS was observed. The PS increased from 168.9 ± 2.9 to 179.8 ± 4.1 nm with slight decrease in zeta potential from -27.1 ± 0.9 to -24.3 ± 1.2 mV. Poly dispersity index before and after Ab conjugation was less than 0.1 indicating unimodal distribution of particles. A similar trend was observed by Das et al. and Tseng et al. when they conjugated antibody on PLGA and gelatin NPs, respectively [Das and Sahoo 2011; Tseng et al. 2007]. TEM image showed discrete spherical particles with monodisperse size of about 100 nm (figure 5.8). The higher hydrodynamic diameter of

NPs achieved by dynamic light scattering (Zetasizer NanoZS) analysis as compared to the size obtained by TEM analysis is possibly contributed by the hydration of the surface associated PEG.

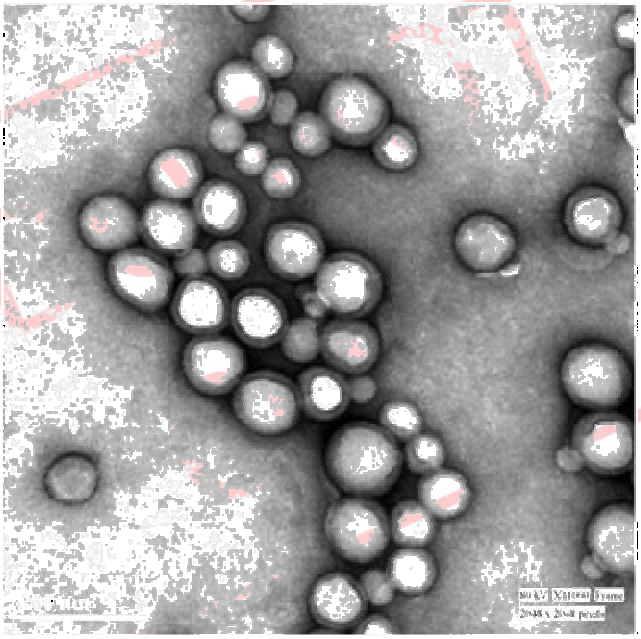

Figure 5.8 TEM image of EXE loaded pegylated PCL ImmunoNPs.

5.5 References

Acharya S, Dilnawaz F, Sahoo SK. 2009. Targeted epidermal growth factor receptor nanoparticle bioconjugates for breast cancer therapy. Biomaterials 30(29):5737-5750.

Avgoustakis K, Beletsi A, Panagi Z, Klepetsanis P, Livaniou E, Evangelatos G, Ithakissios DS. 2003. Effect of copolymer composition on the physicochemical characteristics, in vitro stability, and biodistribution of PLGA–mPEG nanoparticles. Int. J. Pharm. 259(1–2):115-127.

Chaudhari KR, Kumar A, Khandelwal VKM, Mishra AK, Monkkonen J, Murthy RSR. 2012. Targeting efficiency and biodistribution of zoledronate conjugated docetaxel loaded pegylated PBCA nanoparticles for bone metastasis. Advanced Functional Materials 22(19):4101-4114.

Chaudhari KR, Kumar A, Megraj Khandelwal VK, Ukawala M, Manjappa AS, Mishra AK, Monkkonen J, Ramachandra Murthy RS. 2012. Bone metastasis targeting: A novel

approach to reach bone using Zoledronate anchored PLGA nanoparticle as carrier system loaded with Docetaxel. J. Controlled Rel. 158(3):470-478.

Chaudhari KR, Ukawala M, Manjappa AS, Kumar A, Mundada PK, Mishra AK, Mathur R, Monkkonen J, Murthy RS. 2012c. Opsonization, biodistribution, cellular uptake and apoptosis study of PEGylated PBCA nanoparticle as potential drug delivery carrier. Pharm. Res. 29(1):53-68.

Das M, Sahoo SK. 2011. Epithelial cell adhesion molecule targeted nutlin-3a loaded immunonanoparticles for cancer therapy. Acta. Biomater. 7(1):355-369.

Josephson L, Tung CH, Moore A, Weissleder R. 1999. High-efficiency intracellular magnetic labeling with novel superparamagnetic-Tat peptide conjugates. Bioconjug. Chem. 10(2):186-191.

Kanchan V, Panda AK. 2007. Interactions of antigen-loaded polylactide particles with macrophages and their correlation with the immune response. Biomaterials 28(35):5344-5357.

Kocbek P, Obermajer N, Cegnar M, Kos J, Kristl J. 2007. Targeting cancer cells using PLGA nanoparticles surface modified with monoclonal antibody. J. Controlled Rel. 120(1-2):18-26.

Mosqueira VC, Legrand P, Gref R, Heurtault B, Appel M, Barratt G. 1999. Interactions between a macrophage cell line (J774A1) and surface-modified poly (D,L-lactide) nanocapsules bearing poly(ethylene glycol). J. Drug Target. 7(1):65-78.

Muhlfeld C, Rothen-Rutishauser B, Vanhecke D, Blank F, Gehr P, Ochs M. 2007. Visualization and quantitative analysis of nanoparticles in the respiratory tract by transmission electron microscopy. Part. Fibre Toxicol. 4:11.

Olivier JC, Huertas R, Lee HJ, Calon F, Pardridge WM. 2002. Synthesis of pegylated immunonanoparticles. Pharm. Res. 19(8):1137-1143.

Tseng CL, Wang TW, Dong GC, Yueh-Hsiu Wu S, Young TH, Shieh MJ, Lou PJ, Lin FH. 2007. Development of gelatin nanoparticles with biotinylated EGF conjugation for lung cancer targeting. Biomaterials 28(27):3996-4005.

Chapter 6

CELL CULTURE STUDIES

6.1 Introduction

After the preliminary studies of formulation preparation and characterization, the final objective was to deliver these nanoparticulate carriers by parenteral route to animals. But before the animal studies, the formulations should be evaluated for their safety and efficacy at cell culture level. The aim of the study was to evaluate prepared NPs for cancer chemotherapy with a view to explore the possible effects of particle size, conjugation and particle surface coating on the cell uptake. Hence, the cell uptake, cytotoxicity studies, cell cycle analysis and apoptosis studies were taken up prior to in-vivo studies. Cell uptake studies were carried out using 6-Coumarin (lipophilic fluorescent dye) loaded NPs with the aim of finding whether the NPs are internalized into the cells and to determine the intracellular concentrations of the loaded dye.

6.1.1 Cellular uptake

The primary advantage in using macromolecules as drug delivery vehicles is their mechanism of cellular internalization. The cell membrane is naturally impermeable to complexes larger than 1 kDa; however, cells possess a variety of active internalization mechanisms to accommodate cellular entry of large molecular complexes. Here, the cell membrane will invaginate to engulf molecules and extracellular fluid in an intracellular membrane bound vesicle or endosome, which will subsequently travel through the cell, a process known as endocytosis [Castino et al. 2003]. NPs may reside near the membrane or directly interact with membrane proteins to enable their retention in these vesicles. Analogous to the attachment of drug moieties to high molecular weight carriers, agents such as antibodies and high affinity ligands can be surface conjugated in order to exploit direct membrane interactions and target these complexes to specific cell populations in organ systems. Targeting macromolecular complexes with high affinity ligands specific to membrane proteins, namely receptors, can aid in regulating not only the cellular recognition of these carriers but also the trafficking pathway and subcellular localization within the cell [Sly and Vogler 2002].

The major objective for targeted drug delivery includes enhancing drug accumulation at the target site as well as reducing the non-selective uptake of toxic agents. In order to target drugs to specific tissue systems within the body, drug molecules can be directly attached to a targeting agent or complexed with a vehicle, or macromolecule, that contains targeting moieties. Macromolecules can be bioengineered to incorporate a

variety of synthetic and natural compounds including drugs, ligands, and radionuclides [Bareford and Swaan 2007].

6.1.2 Cytotoxicity studies

The MTT (3-(4,5-dimethylthiazole-2-yl)-2,5-diphenyltetrazoliumbromide) and the ATP (adenosine triphosphate) assays are widespread methods to assess cell viability. MTT is reduced by mitochondrial dehydrogenases in living cells to a blue-magenta colored formazan crystals. The absorption of dissolved formazan in the visible region correlates with the number of intact alive cells. Cytotoxic compounds are able to damage and destroy cells, and thus decrease the reduction of MTT to formazan [Mosmann 1983]. One remarkable disadvantage of the MTT assay is that damaged mitochondria may still be able to reduce MTT to formazan [Sieuwerts et al. 1995]. This could lead to a rightward shift of the concentration-response (absorption) curves. Damaged mitochondria could further evolve from sharp formazan crystals/needles and alter the reduction of MTT to formazan. Thus, the formation of cell/mitochondria damaging formazan needles was prevented by microscopic supervision of needle formation and led to an optimized incubation time for MTT of 50-70 min. Furthermore, more than 1 enzyme involved in oxidative/reductive metabolism may play a role in the reduction of MTT to formazan [Loveland et al. 1992]. The development of the MTT assay as a homogeneous assay was, however, a major achievement since washing steps during the MTT assay were associated with the loss of less attached damaged and living cells leading to a higher degree of variation.

6.1.3 Apoptosis

Apoptosis is a process of programmed cell death that may occur in multicellular organisms. Biochemical events lead to characteristic cell changes and death. Cells undergoing apoptosis show characteristic morphological and biochemical features. The characteristics include chromatin aggregation, nuclear and cytoplasmic condensation, while necrosis displays a direct injury to the cell. Determination of cell death mechanism is important to compare effectiveness of NP formulations. Apoptosis study of prepared NPs was conducted using Annexin V staining procedure in MCF7 cell line. This assay takes advantage of the fact that phosphatidylserine (PS) is translocated from the inner (cytoplasmic) leaflet of the plasma membrane to the outer (cell surface) leaflet soon after the induction of apoptosis. Annexin V protein has a strong and specific affinity for PS which can be used as a probe for estimation [Susin et al. 2000].

6.1.4 Cell cycle analysis

Analysis of replication state in a population of cells can be achieved by fluorescence labelling of the nuclei of cells in suspension and then analyzing the fluorescence properties of each cell in the population. The distribution of DNA in the cell replication state was studied by flow cytometry [Panyam and Labhasetwar 2003; Vega et al. 2006]. Quiescent and G1 cells will have one copy of DNA and will therefore have 1× fluorescence intensity.

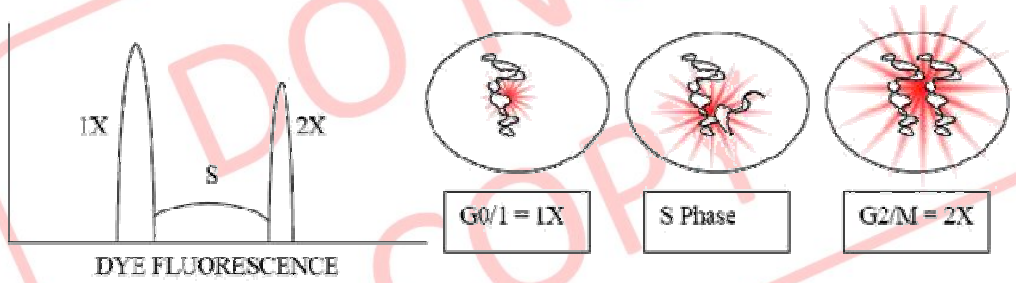

Figure 6.1 Schematic presentation of principle for cell cycle analysis using DNA intercalating florescence probe in flow cytometry.

Cells in G2/M phase of the cell cycle will have two copies of DNA and accordingly will have 2× intensity. Since the cells in S phase are synthesizing DNA they will have fluorescence values between the 1× and 2× populations (figure 6.1). The resulting histogram consists of three populations: two Gaussian curves (1× and 2× peaks) and the S phase population. Adjacent populations overlap each other. Because of this, a modelling program is required to de-convolute the populations and assign percentage values to each population. Expert and subjective review of the modelling software's cell cycle phase percentage assignment is the final stage of cell cycle analysis prior to reporting the results.

6.2 Materials

Sulpho-NHS and 6-Coumarin dye were purchased from Sigma-Aldrich, Mumbai, India. Monoclonal antibody against estrogen receptor was purchased from Pierce antibodies, Rockford, IL, USA. All other chemicals were of analytical reagent grade and obtained commercially. RPMI-1640, MEM, Fetal Bovine Serum (FBS), antibiotic-antimycotic, Trypsin-EDTA and PBS were purchased from Life Technologies India Pvt. Ltd., New Delhi, India. 6-well plates, 96-well plates, tissue culture flask (25 and 75 cm^2), chamber

slide and other sterile material for cell culture were purchased from Thermo scientific, Mumbai, India. Annexin V-FITC apoptosis detection kit was obtained from BD Pharmingen, CA, USA. Hoechst stain was purchased from Invitrogen, Mumbai, India. EDC and NHS were purchased from Himedia, Vadodara, India.

6.3 Cell lines

MCF7 and MDAMB231 cells were procured from NCCS, Pune, India. Estrogen receptor positive, MCF7 cell line, was cultured in MEM medium (Gibco, Grand Island, NY, USA) supplemented with 10% (v/v) FBS. Estrogen receptor negative, MDAMB231 cell line, was cultured in RPMI-1640 medium supplemented with 10% (v/v) FBS. All cell lines were supplemented with penicillin (100 units/ml) and streptomycin (100 µg/ml) (Gibco, Grand Island, NY, USA) at 37 °C in a humidified incubator containing 5% CO_2.

6.4 Methods

6.4.1 Receptor expression analysis by Western Blot

A comparative expression of estrogen receptor in breast cancer cell lines (MCF7 and MDAMB231) was estimated by Western Blot analysis [Van Maerken et al. 2006]. Briefly, 2.5×10^5 cells of different cell lines (MCF7 and MDAMB231) were seeded in culture flask (75 cm^2, Nunc, India) and allowed to reach confluency. Thereafter, the cells were trypsinized and collected by centrifugation. The cells were lysed in lysis buffer (150 mM NaCl, 1% NP-40, 1% sodium deoxycholate, 0.1% SDS, 50 mM Tris-HCL, pH 7.5, 2 mM EDTA) containing 1% protease inhibitor cocktail (Sigma Aldrich, USA) and incubated for 30 min. Subsequently, the lysates were centrifuged (10,000 rpm for 10 min at 4 °C), and the supernatants were used for further analysis. Protein concentration was determined by Bradford's method [Bradford 1976]. Aliquots of each sample containing 60 µg proteins were resolved on a SDS-polyacrylamide gel, by electrophoresis at 40 mA for 2 h and transferred to 0.45 µm polyvinylidene difluoride membranes (Millipore, USA). Membranes were then probed with primary antibodies specific to ER diluted at 1:2000 v/v. The membranes were washed three times with PBS containing 1% tween-80 and probed with goat anti-mouse secondary antibody. Protein bands were detected using chemiluminescence and densitometric analysis was carried out using Quantity one Quantitation software (Bio-Rad, USA).

6.4.2 Qualitative cellular uptake by fluorescent microscopy

5×10^4 MCF7 cells were seeded in chamber slides and allowed to attach and grow. After 48 h, the cells were incubated with 1 ml, 10 µg/ml 6-Coumarin, 6-Coumarin loaded PLGA NPs, 6-Coumarin loaded PCL NPs, pegylated PLGA NPs, pegylated PCL NPs, pegylated PLGA ImmunoNPs and pegylated PCL ImmunoNPs for 2 h. Adhered cells were washed with 1× PBS and treated with 1 ml (1 µg/ml) Hoechst 33342 for 15 min. Cells were again washed with 1× PBS and visualized under fluorescent microscope (Leica, DMLB, Weltzar, Germany) using FITC and DAPI filters.

6.4.3 Quantitative cellular uptake by flow cytometry

1×10^5 MCF7 cells were seeded on 6-well plate and allowed to attach and grow. After 24 h, cells were incubated with 1 ml of medium containing 100 µg/ml 6-Coumarin, 6-Coumarin loaded PLGA NPs, PCL NPs, pegylated PLGA NPs, pegylated PCL NPs, pegylated PLGA ImmunoNPs and pegylated PCL ImmunoNPs for 30, 60 and 90 min. Cells with only medium were used as respective controls. At the end of the incubation period, the cell monolayer was washed three times with cold 1× PBS to eliminate excess of dye or NPs, which were not taken up by the cells and then trypsinized. Cells were collected by centrifugation at 400×g (Eppendorf centrifuge, USA) and analyzed in FACS (FACS Canto-II, BD Biosciences, CA, USA) using software provided with the instrument (BD FACS Diva 6.2.1 software, BD Biosciences, CA, USA) for total amount of NPs uptake by 10,000 cells.

6.4.4 In vitro cytotoxicity studies by MTT Assay

MTT assay was done to evaluate the mitochondrial activity according to the method of Mosmann [Mosmann 1983]. MCF7 cells were seeded in 96-well plate (7000 cells/well) and allowed to attach and grow. After 24 h, the medium was removed and replaced with 100 µl medium containing different concentration of NPs and incubated for different time periods (6, 24, 48 h). After incubation, treatment media was removed and cells were treated with 100 µl (5 mg/ml) of MTT dye [3-(4,5-dimethylthiazoyl-2-yl)-2,5-diphenyltetrazolium bromide] 3 h prior to completion of incubation periods. The medium from each well was discarded and resulting formazan crystals were solubilized in 200 µl of dimethylsulphoxide and quantified by measuring absorbance at 550 nm in multiwell plate reader (SYNERGY-HT, Bio-Tek, Winooski, Vermont, USA) using KC4 software.

6.4.5 In vitro apoptosis study

2×10^5 MCF7 cells were seeded on 6-well plates and allowed to attach and grow for 24 h. Cells were incubated with 2 ml media containing 1 µM ATZ solution, ATZ loaded PLGA NPs, PLGA-PEG NPs, PLGA-PEG ImmunoNPs, PCL NPs, PCL-PEG NPs and PCL-PEG ImmunoNPs for 24 and 48 h. Cells were also incubated with 2 ml media containing 1 µM EXE solution, EXE loaded PLGA NPs, PLGA-PEG NPs, PLGA-PEG ImmunoNPs, PCL NPs, PCL-PEG NPs and PCL-PEG ImmunoNPs for 24 and 48 h. After incubation, cells were harvested and washed. Incubation media, washing buffer and trypsin-EDTA treated cell were collected together and centrifuged at 1,500 rpm for 5 min. Cells were suspended in 100 µl binding buffer and stained with Annexin-FITC (2 µl), mixed well using vortex shaker and incubated at room temperature, protected from light for 15 min. After incubation, propidium iodide (PI, 2 µl, 50 µg/ml) was added and incubated at 4 °C for 10-15 min. After incubation, 200 µl of additional binding buffer was added, and suspension was analyzed using FACS at Texas red and FITC channel (FACS Canto-II, BD Biosciences, CA, USA) using software provided with the instrument (BD FACS Diva 6.2.1 software, BD Biosciences, CA, USA). The intensity plot of FITC vs. Texas Red was sectioned in four quarters to differentiate stained and unstained cells. Based on four quarters, percentage of cells in early apoptotic phase (FITC positive and PI negative), late apoptotic phase (FITC and PI positive) and necrotic phase (FITC negative and PI positive) were recorded.

6.4.6 Cell cycle analysis by flow cytometry

2×10^5 MCF7 cells were seeded on 6-well plate and allowed to attach and grow for 24 h. Cells were incubated with 2 ml media containing 1 µM ATZ solution, ATZ loaded PLGA-PEG NPs, PLGA-PEG ImmunoNPs, PCL-PEG NPs and PCL-PEG ImmunoNPs for 24 h. Cells were also incubated with 2 ml media containing 1 µM EXE solution, EXE loaded PLGA-PEG NPs, PLGA-PEG ImmunoNPs, PCL-PEG NPs and PCL-PEG ImmunoNPs for 24 h. After incubation, medium was aspirated in to individual tubes. Cells were washed with 1× PBS and harvested with 200 µl of trypsin-EDTA, later 500 µl of complete medium was added to quench the trypsin activity. Cells were collected together in to the same tubes where the medium was aspirated earlier and centrifuged at 500×g for 5 min. The cell pellet was washed twice with PBS and centrifuged. Cells were re-suspended in 1 ml ethanol (70%) for fixing and kept at -20 °C for 30 min. Cells were centrifuged and were lysed in 250 µl 1× PBS containing 0.2% triton X 100 and incubated at 4 °C for 30 min.

They were again centrifuged and re-suspended in 500 µl 1× PBS containing 20 µl RNAse (10 mg/ml) and incubated at 37 °C for 30 min. Cells were then centrifuged and re-suspended in 500 µl of 1× PBS containing 10 µl propidium iodide (1 mg/ml) and incubated for 10-15 min at 4 °C. Thereafter, cells were analyzed on FACS by recording signal from Texas red channel (FACS Canto-II, BD Biosciences, CA, USA) using software provided with the instrument (BD FACS Diva 6.2.1 software, BD Biosciences, CA, USA). Histogram of count vs. intensity was made to calculate ratio of cells under G0/G1 (2n), S (2n+), G2/M phase (4n) and under apoptosis (2n-).

6.5 Results and discussion

6.5.1 Receptor expression in cell lines

The drug loaded ImmunoNPs were prepared with the objective of receptor mediated endocytosis in ER positive breast tumor cells for preferential accumulation of drug at tumor site. To achieve this, expression levels of ER in breast cancer cell lines, MCF7 and MDAMB231 were assessed by Western Blotting. The results confirmed the expression of ER in MCF7 cell line and absence of this receptor in MDAMB231 cell line (figure 6.2). Thus, MCF7 and MDAMB231 cell line served as positive control and negative control for further experiments, respectively.

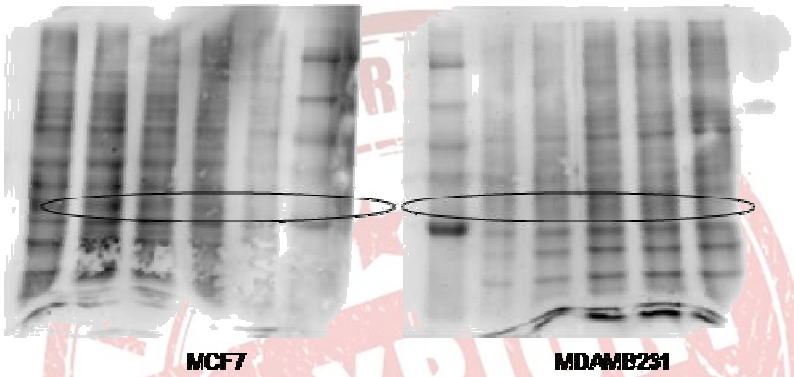

Figure 6.2 Receptor expression analyses in cell lines.

6.5.2 Qualitative and quantitative cellular uptake

Fluorescent property of 6-Coumarin was used for comparative intracellular uptake of NPs in MCF7 cell line by flow cytometry and fluorescent microscopy. The relative extent of PLGA NPs, pegylated PLGA NPs, pegylated PLGA ImmunoNPs, PCL NPs, pegylated PCL NPs and pegylated PCL ImmunoNPs was calculated using mean fluorescent index (MFI) and is shown in figure 6.3, 6.4, 6.5 and 6.6. As evident from figure 6.3, MFI of pegylated

PLGA ImmunoNPs was 1039.10 ± 17.77 which was more than 3 times than that of PLGA NPs (318.27 ± 21.69) after 180 min (table 6.1). Furthermore, pegylated PLGA ImmunoNPs showed about 2 times more uptake when compared with pegylated PLGA NPs (599.95 ± 25.17) at same time point due to receptor mediated endocytosis. As shown from figure 6.5, MFI of pegylated PCL ImmunoNPs is 1261.62 ± 39.27 which is about twice than that of PCL NPs (730.19 ± 38.68) after 180 min (table 6.2). Furthermore, ImmunoNPs showed about 1.32 times more uptake when compared with pegylated PCL NPs (956.45 ± 33.45) at same time point. Intracellular uptake was found to increase with time for all formulations from 60 to 180 min.

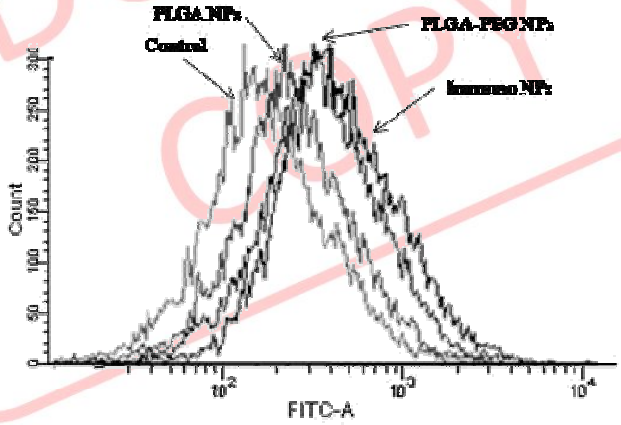

Figure 6.3 Quantitative intracellular uptake histograms of 6-Coumarin loaded PLGA NPs, pegylated PLGA NPs and ER antibody conjugated ImmunoNPs by MCF7 cells using flow cytometry.

The intracellular uptake of NPs was also dependent on the incubation time. The fluorescence intensity increased gradually with the incubation time and so also the uptake of NPs, indicating time dependent uptake. Results clearly indicate the enhanced cellular uptake of ImmunoNPs than un-conjugated systems. Figure 6.4 represents the quantitative uptake study of PLGA NPs, pegylated PLGA NPs and pegylated PLGA NPs by fluorescent microscopy. Figure 6.6 represents the quantitative uptake study of PCL NPs, pegylated PCL NPs and ImmunoNPs by fluorescent microscopy. Our results confirmed that NPs showed augmented fluorescence activity which was found to be maximum with cells treated with ImmunoNPs after 2 h of incubation. The images were consistent with those presented in the flow cytometry analysis as shown in figure 6.7 and 6.8.

The enhanced therapeutic activity of the ImmunoNPs assessed in terms of cellular uptake efficiency of the carrier system clearly demonstrated that uptake of ImmunoNPs

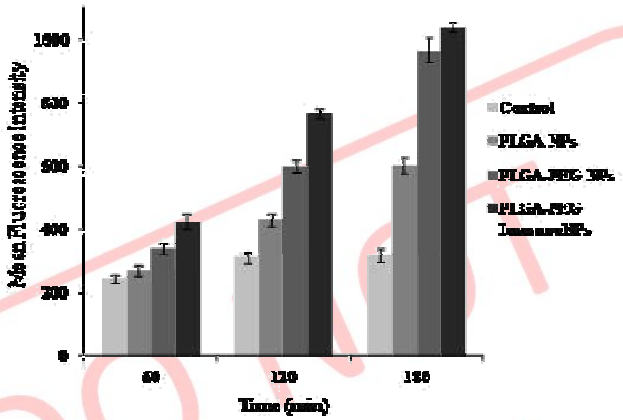

Figure 6.4 Quantitative intracellular uptake of 6-Coumarin loaded PLGA NPs, pegylated PLGA NPs and ER antibody conjugated ImmunoNPs by MCF7 cells using flow cytometry. Uptake was calculated by measuring MFI and represented as mean ± S.D. (n=3)

Table 6.1 Intracellular uptake of 6-Coumarin loaded PLGA NPs, pegylated PLGA NPs and ER antibody conjugated ImmunoNPs by MCF7 cells using flow cytometry. Uptake was calculated by measuring MFI and represented as mean ± S.D. (n=3)

Treatment	Mean Fluorescence Intensity		
	60 min	120 min	180 min
Control	243.8 ± 16.1	310.6 ± 20.1	318.3 ± 21.6
PLGA NPs	270.3 ± 16.9	430.6 ± 19.5	599.9 ± 25.2
PLGA-PEG NPs	340.6 ± 18.8	597.8 ± 18.1	965.7 ± 39.0
PLGA-PEG ImmunoNPs	423.9 ± 24.5	765.0 ± 14.3	1039.1 ± 17.8

was significantly greater than that of the un-conjugated particle and non-pegylated formulations. The greater uptake of ImmunoNPs can be explained on the basis of ER expression in cells and specificity of ER receptor mediated binding of ImmunoNPs. Moreover, the enhanced uptake level of ImmunoNPs can be attributed to the lesser exocytosis of the conjugated system than un-conjugated NPs [Sahoo and Labhasetwar 2005]. Together, all these contribute to the greater intracellular retention of ImmunoNPs. Thus, higher cellular uptake observed with ImmunoNPs is attributed to their greater intracellular delivery by receptor mediated endocytosis.

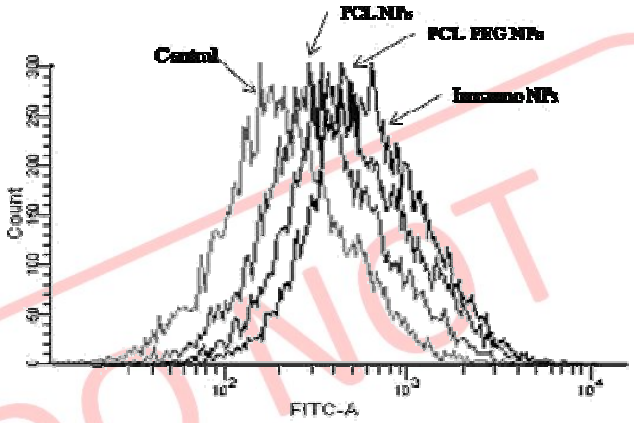

Figure 6.5 Quantitative intracellular uptake histograms of 6-Coumarin loaded PCL NPs, pegylated PCL NPs and ER antibody conjugated ImmunoNPs by MCF7 cells using flow cytometry.

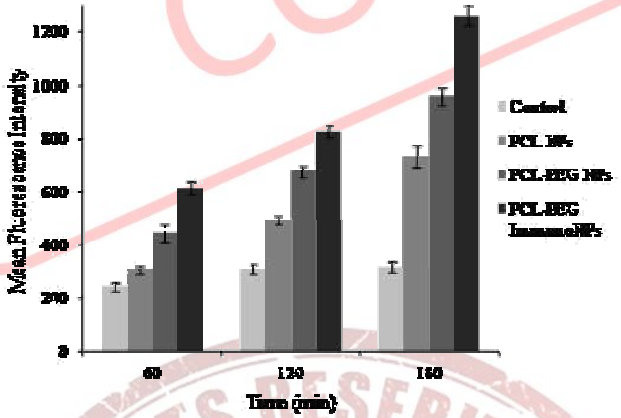

Figure 6.6 Quantitative intracellular uptake of 6-Coumarin loaded PCL NPs, pegylated PCL NPs and ER antibody conjugated ImmunoNPs by MCF7 cells using flow cytometry. Uptake was calculated by measuring MFI and represented as mean ± S.D. (n=3)

Table 6.2 Intracellular uptake of 6-Coumarin loaded PCL NPs, pegylated PCL NPs and ER antibody conjugated ImmunoNPs by MCF7 cells using flow cytometry. Uptake was calculated by measuring MFI and represented as mean ± S.D. (n=3)

Treatment	Mean Fluorescence Intensity		
	60 min	120 min	180 min
Control	243.8 ± 16.1	310.6 ± 20.1	318.3 ± 21.6
PCL NPs	307.1 ± 16.6	493.8 ± 16.4	730.2 ± 38.7
PCL-PEG NPs	446.0 ± 31.2	676.0 ±21.1	956.4 ± 33.5
PCL-PEG ImmunoNPs	613.7 ± 24.6	823.9 ± 19.5	1261.6 ± 39.3

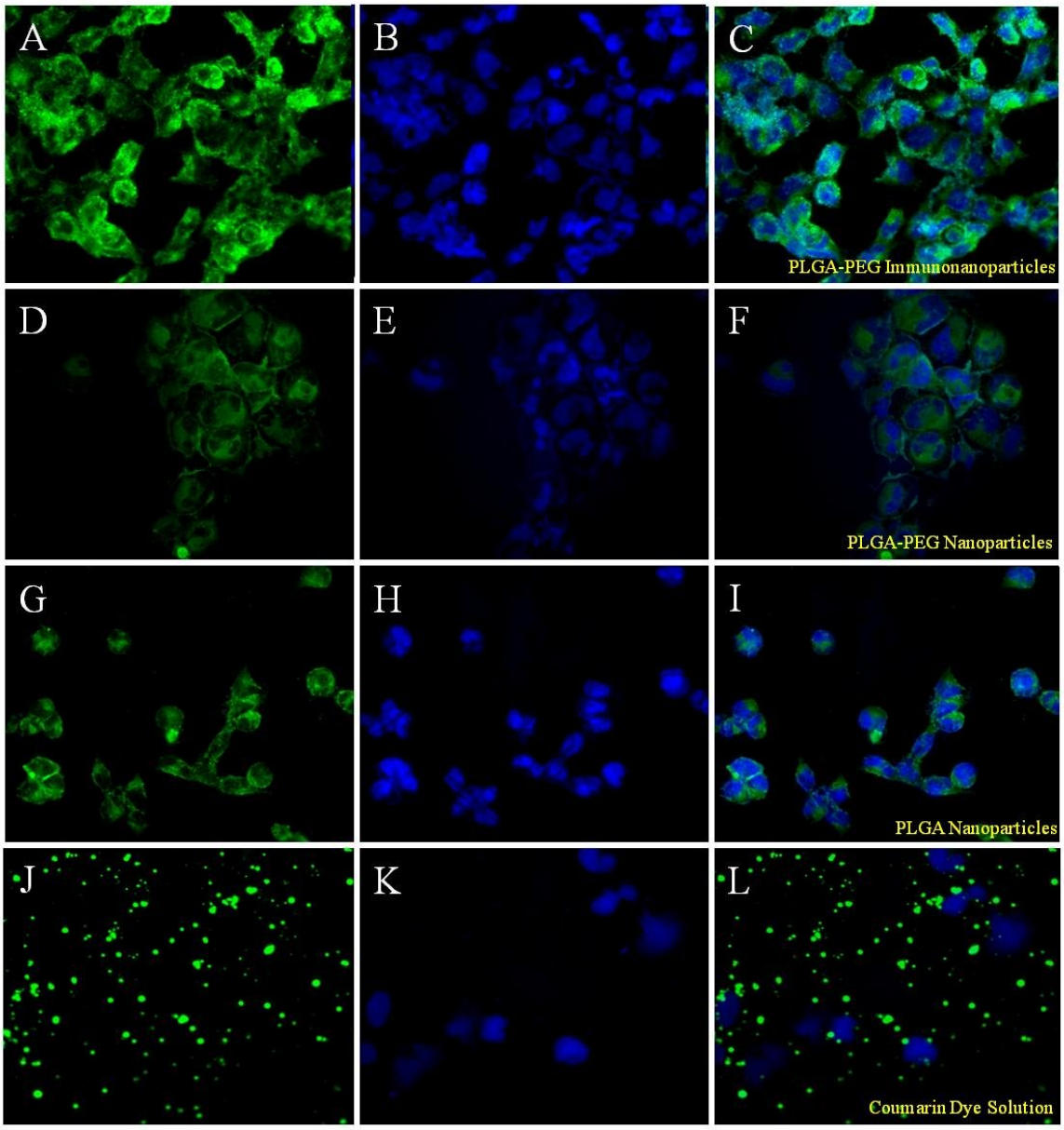

Figure 6.7 Qualitative cellular uptake of PLGA NPs, pegylated PLGA and ImmunoNPs using fluorescent microscope. (A-C) ImmunoNPs; (D-F) pegylated PLGA NPs; (G-I) PLGA NPs; (J-L) 6-Coumarin dye solution; (B, E, H and K) nucleus stained using Hoechst 33342; (C, F, I and L) overlapping images.

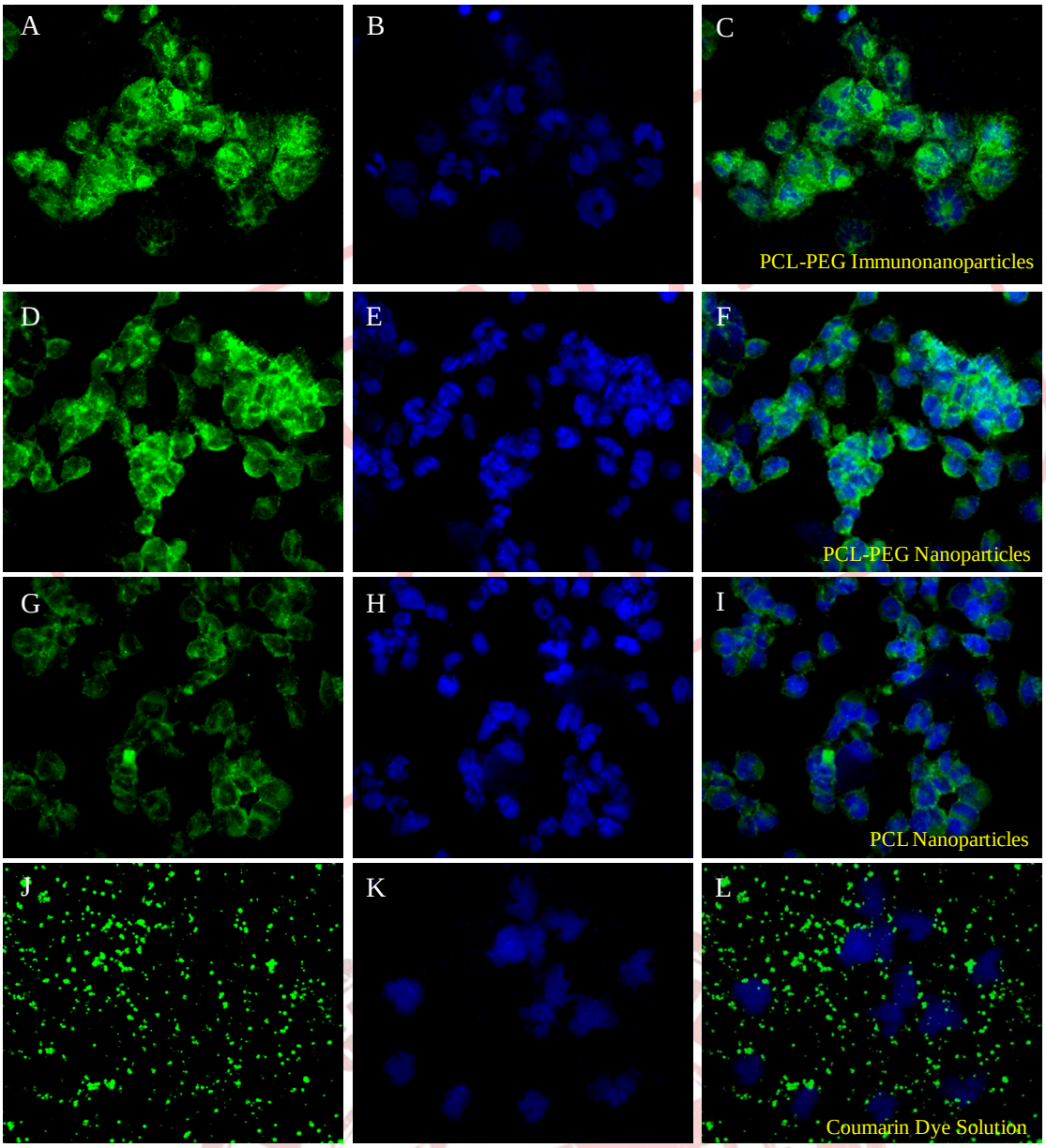

Figure 6.8 Qualitative cellular uptake of PCL NPs, pegylated PCL NPs and ImmunoNPs using fluorescent microscope. (A-C) ImmunoNPs; (D-F) pegylated PCL NPs; (G-I) PCL NPs; (J-L) 6-Coumarin dye solution; (B, E, H and K) nucleus stained using Hoechst 33342; (C, F, I and L) overlapping images.

6.5.3 In vitro cytotoxicity studies by MTT Assay

In vitro cytotoxicity studies were performed on ER positive (MCF7) as well as ER negative (MDAMB231) cell line by MTT assay and it demonstrated that ER antibody conjugated NPs showed higher anti-proliferative effect than un-conjugated NPs at all concentrations and at all time points in MCF7 cells. Cytotoxicity curve and IC_{50} value

were determined for ATZ, ATZ PLGA NPs, ATZ PLGA-PEG NPs and ATZ PLGA-PEG ImmunoNPs (figure 6.9, table 6.3). Blank Pegylated PLGA NPs (without ATZ) were also evaluated for cytotoxicity and found to be non-toxic. The IC_{50} value for ER positive cells treated with PLGA-PEG ImmunoNPs was found to be 163.65, 51.93 and 27.69 times lower than ATZ, ATZ PLGA NPs, ATZ PLGA-PEG NPs respectively, after 6 h of treatment. Exposure for 48 h further lowered the IC_{50} value by 3.6 times to 0.08 μM which was 8.25 times less in comparison with ATZ PLGA-PEG NPs. The enhanced cytotoxic effect of ATZ PLGA-PEG ImmunoNPs could be attributed to higher uptake via receptor mediated endocytosis. To confirm receptor mediated endocytosis, cytotoxicity studies were also performed on receptor negative cells (MDAMB231) and results clearly indicated that the effect of different NPs on MDAMB231 cells when compared to MCF7 cells. No significant toxicity was found on MDAMB231 cells. Thus, the enhanced cytotoxic activity of PLGA-PEG ImmunoNPs for MCF7 cells as compared with MDAMB231 cells clearly demonstrates the high affinity of ImmunoNPs towards ER positive cancer cells. Moreover, pegylated NPs showed comparatively more cytotoxicity towards MDAMB231 cells than PLGA NPs which indicated the role of pegylation in improving the efficacy of the NPs due to presence of hydrophilic PEG chains on the NPs [Chaudhari et al. 2012c]. However, no significant difference in % viability of these ER negative cells was observed after exposure to ATZ PLGA-PEG NPs and PLGA-PEG ImmunoNPs.

In vitro cytotoxicity studies of ATZ, ATZ PCL NPs, ATZ PCL-PEG NPs and ATZ PCL-PEG ImmunoNPs were performed on ER positive (MCF7) as well as ER negative (MDAMB231) cell line and it demonstrated that ER antibody conjugated NPs showed higher anti-proliferative effect than un-conjugated NPs at all concentrations and at all time points in MCF7 cells. Cytotoxicity curve and IC_{50} value were determined and presented in figure 6.10 and table 6.3. Blank Pegylated PCL NPs (without ATZ) were also evaluated for cytotoxicity and found to be non-toxic. The IC_{50} value for ER positive cells treated with PCL-PEG ImmunoNPs was found to be 158.2, 26.73 and 4.27 times lower than ATZ, ATZ PCL NPs, PCL-PEG NPs respectively, after 6 h of treatment. Exposure for 48 h further lowered the IC_{50} value by 6 times to 0.05 μM which was more than 6.6 times less in comparison with ATZ PCL-PEG NPs. To confirm receptor mediated endocytosis, cytotoxicity studies were also performed on receptor negative

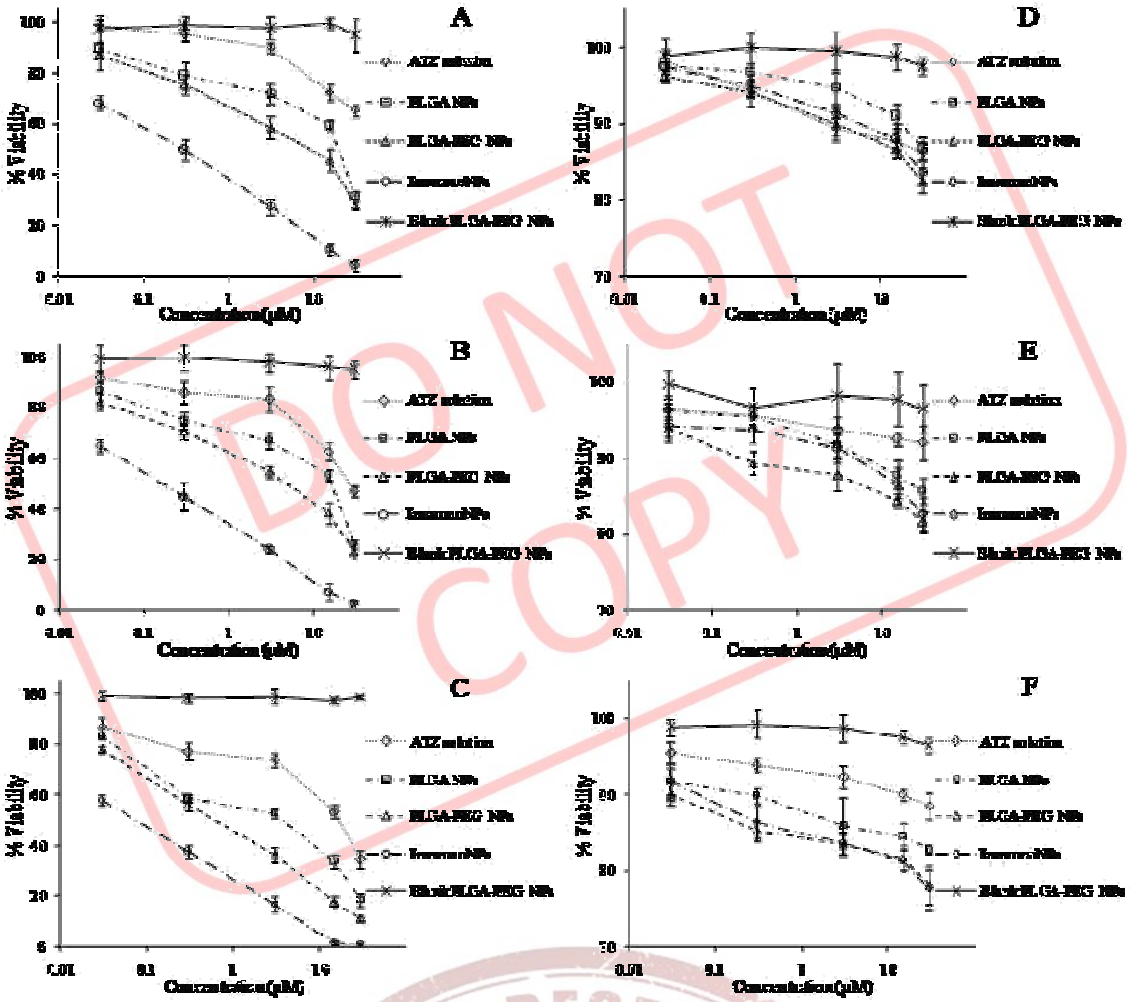

Figure 6.9 Cytotoxicity of ATZ loaded formulations (solution, PLGA NPs, PLGA-PEG NPs, ImmunoNPs) and blank PLGA-PEG NPs on MCF7 (A,B,C) and MDAMB231(D,E,F) cells after exposure for 6 h (A, D), 24 h (B, E) and 48 h (C, F).

cells (MDAMB231) and results clearly indicated that the effect of different NPs on MDAMB231 cells when compared to MCF7 cells. No significant toxicity was found on MDAMB231 cells. Thus, the enhanced cytotoxic activity of PCL-PEG ImmunoNPs for MCF7 cells as compared with MDAMB231 cells clearly demonstrates the high affinity of ImmunoNPs towards ER positive cancer cells. Moreover, pegylated NPs showed comparatively more cytotoxicity towards MDAMB231 cells than PCL NPs which indicated the role of pegylation in improving the efficacy of the NPs due to presence of hydrophilic PEG chains on the NPs [Chaudhari et al. 2012c]. However, no significant difference in % viability of these ER negative cells was observed after exposure to ATZ PCL-PEG NPs and PCL-PEG ImmunoNPs.

Table 6.3 Cytotoxicity of ATZ loaded formulations tested on MCF7 cell line (IC_{50} value)

	ATZ	ATZ PLGA NPs	ATZ PLGA-PEG NPs	ATZ PLGA-PEG ImmunoNPs	ATZ PCL NPs	ATZ PCL-PEG NPs	ATZ PCL-PEG ImmunoNPs
6 h	47.46	15.06	8.03	0.29	8.02	1.28	0.30
24 h	24.66	11.21	5.40	0.20	6.52	0.91	0.28
48 h	14.21	3.56	0.66	0.08	3.38	0.33	0.05

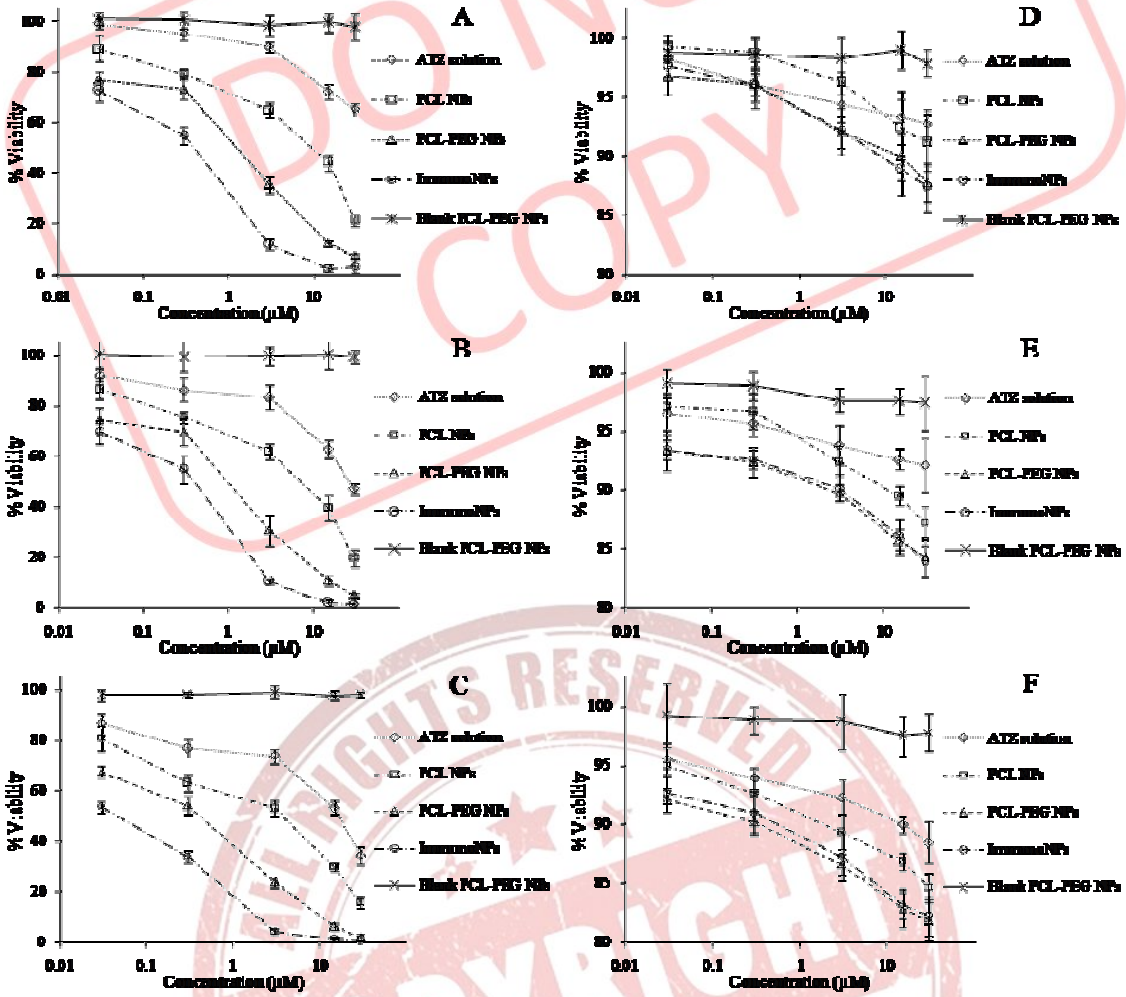

Figure 6.10 Cytotoxicity of ATZ loaded formulations (solution, PCL NPs, PCL-PEG NPs, ImmunoNPs) and blank PCL-PEG NPs on MCF7 (A,B,C) and MDAMB231 (D,E,F) cells after exposure for 6 h (A, D), 24 h (B, E) and 48 h (C, F).

In vitro cytotoxicity studies of EXE, EXE PLGA NPs, EXE PLGA-PEG NPs and EXE PLGA-PEG ImmunoNPs were performed on ER positive (MCF7) as well as ER negative (MDAMB231) cell line and it demonstrated that ER antibody conjugated NPs showed

higher anti-proliferative effect than un-conjugated NPs at all concentrations and at all time points in MCF7 cells. Cytotoxicity curve and IC_{50} value were determined and presented in figure 6.11 and table 6.4. Blank Pegylated PLGA NPs (without EXE) were also evaluated for cytotoxicity and found to be non-toxic. The IC_{50} value for ER positive cells treated with PLGA-PEG ImmunoNPs was found to be 7.5, 4.4 and 2.1 times lower than EXE, EXE PLGA NPs, EXE PLGA-PEG NPs respectively, after 48 h of treatment. To confirm receptor mediated endocytosis, cytotoxicity studies were also performed on receptor negative cells (MDAMB231) and results clearly indicated that the effect of different NPs on MDAMB231 cells when compared to MCF7 cells. No significant toxicity was found on MDAMB231 cells. Thus, the enhanced cytotoxic activity of EXE PLGA-PEG ImmunoNPs for MCF7 cells as compared with MDAMB231 cells clearly demonstrates the high affinity of ImmunoNPs towards ER positive cancer cells. Moreover, pegylated NPs showed comparatively more cytotoxicity towards MDAMB231 cells than EXE PLGA NPs which indicated the role of pegylation in improving the efficacy of the NPs due to presence of hydrophilic PEG chains on the NPs [Chaudhari et al. 2012c]. However, no significant difference in % viability of these ER negative cells was observed after exposure to EXE PLGA-PEG NPs and EXE PLGA-PEG ImmunoNPs

In vitro cytotoxicity studies of EXE, EXE PCL NPs, EXE PCL-PEG NPs and EXE PCL-PEG ImmunoNPs were performed on ER positive (MCF7) as well as ER negative (MDAMB231) cell line and it demonstrated that ER antibody conjugated NPs showed higher anti-proliferative effect than un-conjugated NPs at all concentrations and at all time points in MCF7 cells. Cytotoxicity curve and IC_{50} value were determined and presented in figure 6.12 and table 6.4. Blank Pegylated PCL NPs (without EXE) were also evaluated for cytotoxicity and found to be non-toxic. The IC_{50} value for ER positive cells treated with EXE PCL-PEG ImmunoNPs was found to be 7.7, 4.18 and 2.12 times lower than EXE, EXE PCL NPs, PCL-PEG NPs respectively, after 48 h of treatment. To confirm receptor mediated endocytosis, cytotoxicity studies were also performed on receptor negative cells (MDAMB231) and results clearly indicated that the effect of different NPs on MDAMB231 cells when compared to MCF7 cells. No significant toxicity was found on MDAMB231 cells. Thus, the enhanced cytotoxic activity of EXE PCL-PEG ImmunoNPs for MCF7 cells as compared with MDAMB231 cells clearly demonstrates the high affinity of ImmunoNPs towards ER positive cancer cells. Moreover, pegylated NPs showed comparatively more cytotoxicity towards MDAMB231 cells than PCL NPs which

indicated the role of pegylation in improving the efficacy of the NPs due to presence of hydrophilic PEG chains on the NPs [Chaudhari et al. 2012c]. However, no significant difference in % viability of these ER negative cells was observed after exposure to EXE PCL-PEG NPs and EXE PCL-PEG ImmunoNPs.

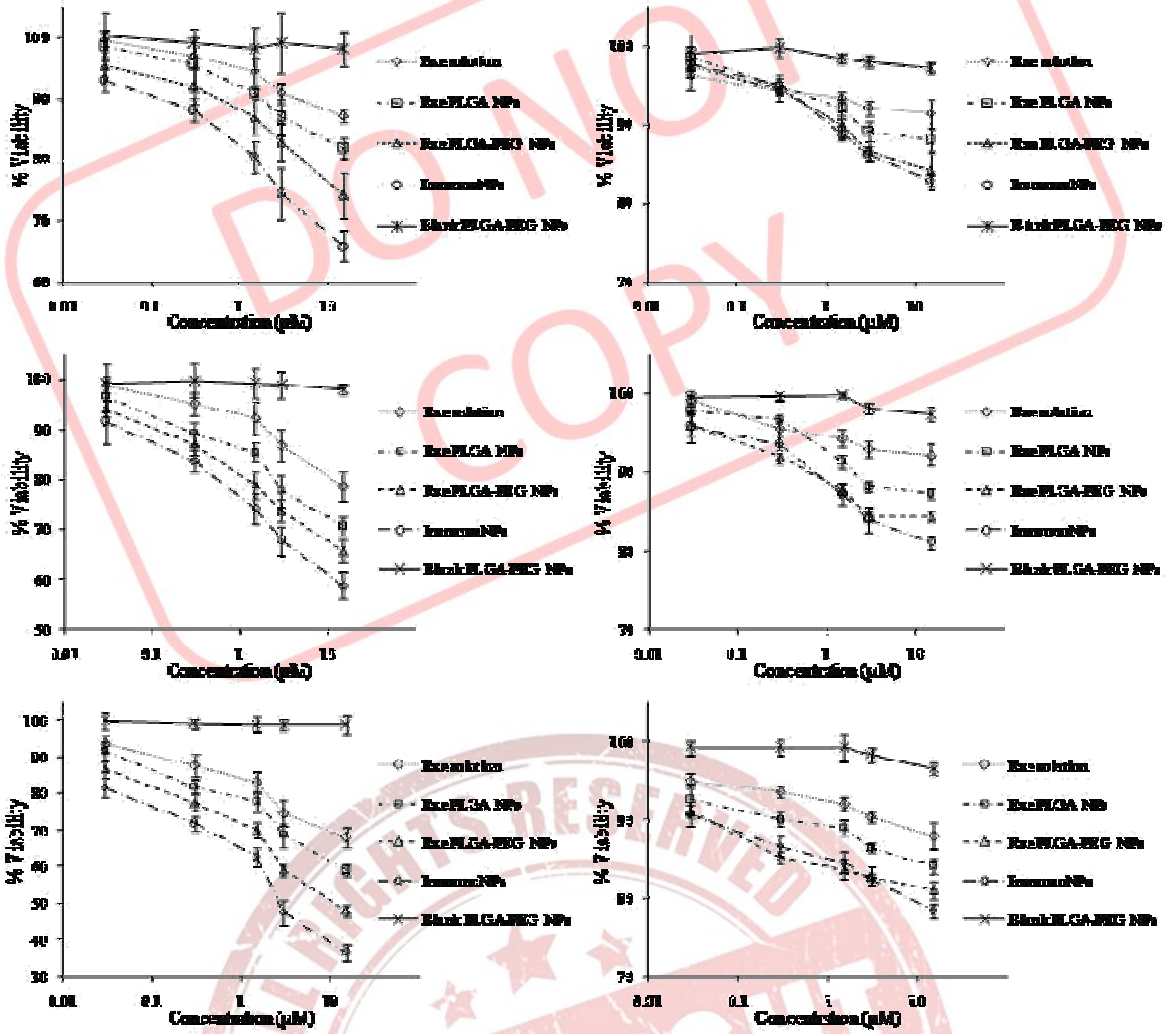

Figure 6.11 Cytotoxicity of EXE loaded formulations (solution, PLGA NPs, PLGA-PEG NPs, ImmunoNPs) and blank PLGA-PEG NPs on MCF7 (A,B,C) and MDAMB231 (D,E,F) cells after exposure for 6 h (A, D), 24 h (B, E) and 48 h (C, F).

Table 6.4 Cytotoxicity of EXE loaded formulations tested on MCF7 cell line (IC_{50} value)

	EXE	EXE PLGA NPs	EXE PLGA-PEG NPs	EXE PLGA-PEG ImmunoNPs	EXE PCL NPs	EXE PCL-PEG NPs	EXE PCL-PEG ImmunoNPs
6 h	28.84	18.24	11.21	6.44	15.21	9.68	6.27
24 h	15.5	8.66	6.14	3.86	8.61	6.19	3.84
48 h	7.24	4.20	1.96	0.96	3.93	1.99	0.94

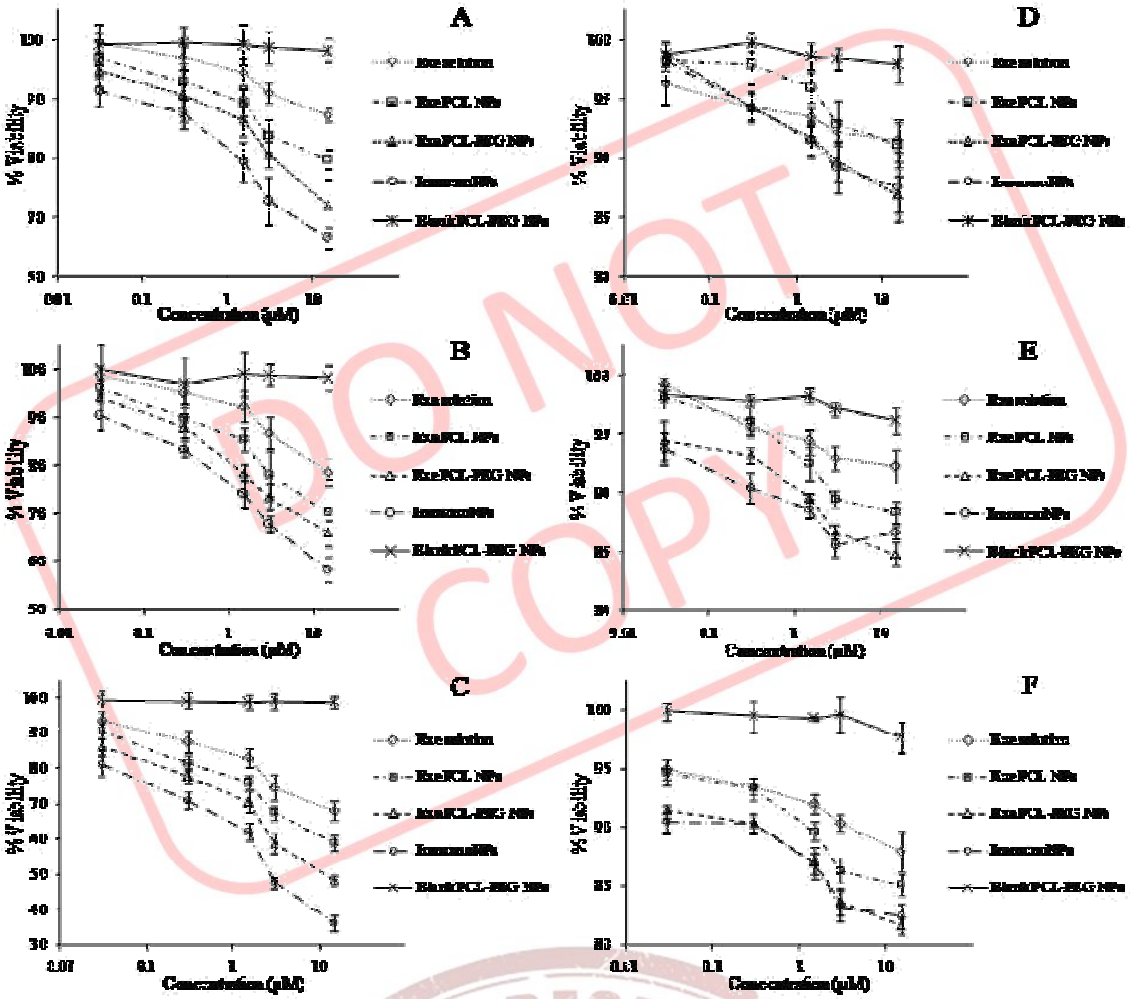

Figure 6.12 Cytotoxicity of EXE loaded formulations (solution, PCL NPs, PCL-PEG NPs, ImmunoNPs) and blank PCL-PEG NPs on MCF7 (A,B,C) and MDAMB231 (D,E,F) cells after exposure for 6 h (A, D), 24 h (B, E) and 48 h (C, F).

6.5.4 Apoptosis studies

Apoptosis studies were carried out using annexin V procedure to determine whether drug loaded NPs caused apoptosis or necrosis of MCF7 cells. The membrane phospholipid, phosphatidylserine is translocated from the inner cytoplasm of the plasma membrane to the outer cell surface soon after the induction of apoptosis, and annexin V protein has a strong, specific affinity for phosphatidylserine, while the membranes of dead and damaged cells are permeable to propidium iodide and allows identifying the late apoptotic cells and necrotic populations. The results showed significant fraction of necrotic, early and late apoptotic population of cells after exposure with ATZ drug solution, ATZ loaded PLGA NPs, PLGA-PEG NPs and PLGA-PEG

ImmunoNPs. Control group treated with PBS showed only 1.6% and 3.6% cells in apoptotic phases after 24 and 48 h respectively. After 24 h of exposure with ATZ drug solution only 5.4% cells were in apoptotic phase (early and late apoptosis) whereas exposure with ATZ PLGA NPs, PLGA-PEG NPs and PLGA-PEG ImmunoNPs showed 32.6%, 43.7% and 60.9% cells in apoptotic phase which increased to 37.3%, 50.5% and 56.4%, respectively (figure 6.13, table 6.5). After 24 h of exposure with ATZ PCL NPs, PCL-PEG NPs and PCL-PEG ImmunoNPs showed 8%, 18% and 23.2% cells in apoptotic phase which increased to 12%, 34.7% and 53.8% after 48 h respectively (figure 6.14, table 6.6). With increase in exposure time to 48 h, the percentage of cells in early apoptotic phase decreased, at the same time percentage of cells in late apoptotic phase were found to be increased. This is possibly due to conversion of early apoptotic phase into late apoptotic phase. Similarly, percentage of cells undergone necrosis also increased with time but in less proportion than apoptosis indicating apoptosis as the possible mode of cell death. The augmented apoptotic activity of ImmunoNPs in comparison to ATZ drug solution and un-conjugated NPs can be correlated with the results of quantitative uptake showing higher endocytosis. Apoptotic signals were possibly activated by ImmunoNPs at very low concentration than drug solution or un-conjugated NPs. Targeted drug delivery showed enhanced apoptosis due to receptor mediated endocytosis which resulted in higher concentration of drug available for action at target site [Chaudhari et al. 2012b; Chaudhari et al. 2012c]. Sustained cytoplasmic delivery of ATZ from NPs coupled with ER antibody resulted in more enhanced therapeutic potency of the NPs by apoptosis than un-conjugated NPs or drug solution. Thus, ImmunoNPs were able to cause significant increase in programmed cell death when compared with ATZ drug solution or un-conjugated nanoparticulate preparations, thus supporting the hypothesis that ER antibody conjugated ImmunoNPs can serve as an effective delivery system for breast tumor targeting [Chaudhari et al. 2012b; Chaudhari et al. 2012c].

The results showed significant fraction of necrotic, early and late apoptotic population of cells after exposure with EXE solution, EXE loaded PLGA NPs, PLGA-PEG NPs and PLGA-PEG ImmunoNPs. Control group treated with PBS showed only 0.2% and 0.4% cells in apoptotic phases. After 24 h of exposure, EXE PLGA NPs, PLGA-PEG NPs and PLGA-PEG ImmunoNPs showed 13.0%, 26.5% and 36.6% cells in apoptotic phase which

Table 6.5 Apoptosis studies in MCF7 cell line after treatment of (a) Control (PBS), (b) ATZ solution, ATZ loaded (c) PLGA, (d) PLGA-PEG and (d) PLGA-PEG ImmunoNPs using FACS technique.

Treatment	24 h				48 h			
	Q1	Q2	Q3	Q4	Q1	Q2	Q3	Q4
Control	0.0	0.6	98.4	1.0	0.2	3.1	96.1	0.5
ATZ solution	1.0	3.9	93.5	1.5	1.7	5.3	92.3	0.7
PLGA NPs	2.2	21.4	65.2	11.2	2.6	25.6	60.1	11.7
PLGA-PEG NPs	3.4	37.8	52.9	5.9	2.0	48.0	47.5	2.5
PLGA-PEG ImmunoNPs	3.2	48.9	35.9	12.0	5.4	56.3	38.1	0.1

Table 6.6 Apoptosis studies in MCF7 cell line after treatment of (a) Control (PBS), (b) ATZ solution, ATZ loaded (c) PCL, (d) PCL-PEG and (d) PCL-PEG ImmunoNPs using FACS technique.

Treatment	24 h				48 h			
	Q1	Q2	Q3	Q4	Q1	Q2	Q3	Q4
Control	0.0	0.6	98.4	1.0	0.2	3.1	96.1	0.5
ATZ solution	1.0	3.9	93.5	1.5	1.7	5.3	92.3	0.7
PCL NPs	3.1	5.5	88.8	2.5	5.5	11.7	75.3	0.3
PCL-PEG NPs	6.7	17.7	75.3	0.3	7.8	33.8	57.5	0.9
PCL-PEG ImmunoNPs	12.3	22.9	64.4	0.3	1.4	44.9	44.8	8.9

increased to 17.3%, 42.3% and 67.5%, respectively (figure 6.15, table 6.7). After 24 h of exposure with EXE PCL NPs, PCL-PEG NPs and PCL-PEG ImmunoNPs showed 9.8%, 25.7% and 35.4% cells in apoptotic phase which increased to 16.6%, 41.6% and 70.2% after 48 h respectively (figure 6.16, table 6.8). With increase in exposure time to 48 h, the percentage of cells in early apoptotic phase decreased, at the same time percentage of cells in late apoptotic phase were found to be increased. This is possibly due to conversion of early apoptotic phase into late apoptotic phase. Similarly, percentage of cells undergone necrosis also increased with time but in less proportion than apoptosis indicating apoptosis as the possible mode of cell death. The augmented apoptotic activity of ImmunoNPs in comparison to EXE drug solution and un-conjugated NPs can be correlated with the results of quantitative uptake showing higher endocytosis.

Apoptotic signals were possibly activated by ImmunoNPs at very low concentration than drug solution or un-conjugated NPs. Targeted drug delivery showed enhanced apoptosis due to receptor mediated endocytosis which resulted in higher concentration of drug available for action at target site [Chaudhari et al. 2012b; Chaudhari et al. 2012c]. Sustained cytoplasmic delivery of EXE from NPs coupled with ER antibody resulted in more enhanced therapeutic potency of the NPs by apoptosis than un-conjugated NPs or drug solution. Thus, ImmunoNPs were able to cause significant increase in programmed cell death when compared with EXE drug solution or un-conjugated nanoparticulate preparations, thus supporting the hypothesis that ER antibody conjugated ImmunoNPs can serve as an effective delivery system for breast tumor targeting [Chaudhari et al. 2012b; Chaudhari et al. 2012c].

Table 6.7 Apoptosis studies in MCF7 cell line after treatment of (a) Control (PBS), (b) EXE solution, EXE loaded (c) PLGA, (d) PLGA-PEG and (d) PLGA-PEG ImmunoNPs using FACS technique.

Treatment	24 h				48 h			
	Q1	Q2	Q3	Q4	Q1	Q2	Q3	Q4
Control	0.1	0.2	99.7	0.0	0.2	0.4	99.3	0.0
EXE solution	2.9	0.6	96.4	0.0	6.3	0.3	93.3	0.0
PLGA NPs	4.5	9.7	82.5	3.3	7.8	13.8	74.9	3.5
PLGA-PEG NPs	4.0	14.7	69.6	11.8	1.5	22.1	56.2	20.2
PLGA-PEG ImmunoNPs	0.9	22.3	62.4	14.3	0.3	39.5	32.2	28.0

Table 6.8 Apoptosis studies in MCF7 cell line after treatment of (a) Control (PBS), (b) EXE solution, EXE loaded (c) PCL, (d) PCL-PEG and (d) PCL-PEG ImmunoNPs using FACS technique.

Treatment	24 h				48 h			
	Q1	Q2	Q3	Q4	Q1	Q2	Q3	Q4
Control	0.1	0.2	99.7	0.0	0.2	0.4	99.3	0.0
EXE solution	2.9	0.6	96.4	0.0	6.3	0.3	93.3	0.0
PCL NPs	3.9	7.2	86.3	2.6	6.9	12.5	76.5	4.1
PCL-PEG NPs	3.1	14.2	71.2	11.5	2.4	21.6	55.9	20.0
PCL-PEG ImmunoNPs	1.6	21.4	63.1	14.0	0.5	44.8	29.3	25.4

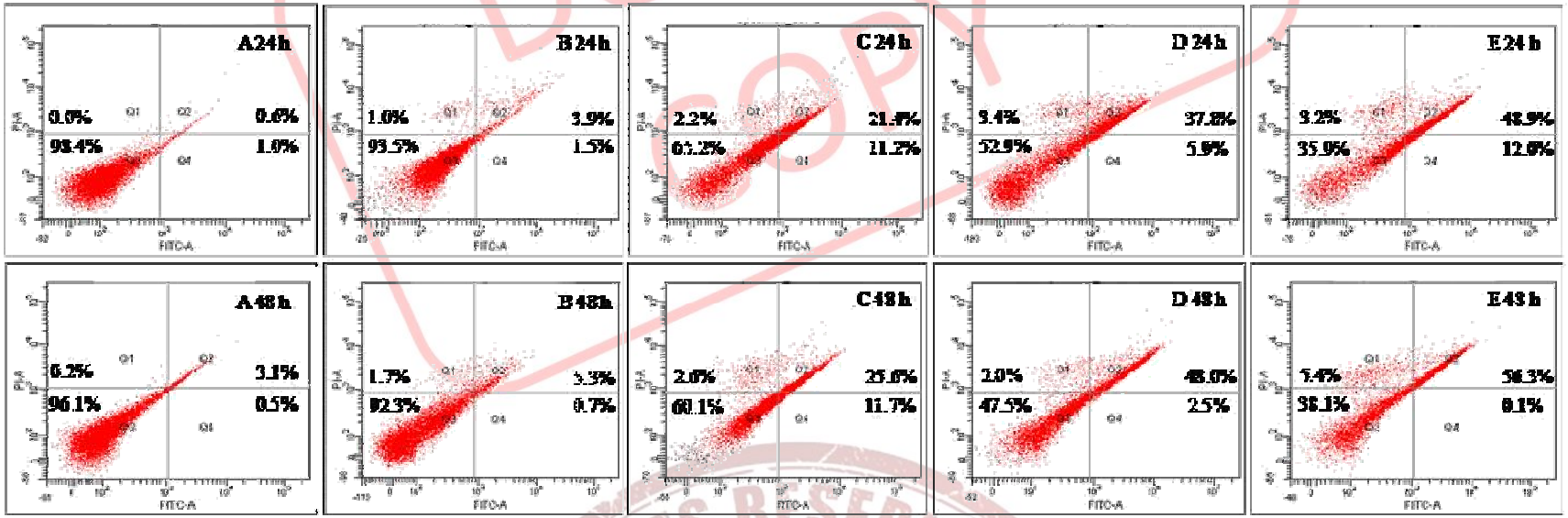

Figure 6.13 Apoptosis estimation in MCF7 cell line after exposure of Control (PBS), A; ATZ Solution, B; ATZ PLGA NPs, C; ATZ PLGA-PEG NPs, D; and ATZ PLGA-PEG ImmunoNPs, E; for 24 and 48 h by Annexin V-FITC and PI staining using FACS technique. Necrotic cells FITC (-) PI (+), Late apoptosis FITC (+) PI (+), Live FITC (-) PI (-), Early apoptotis FITC (+) PI (-).

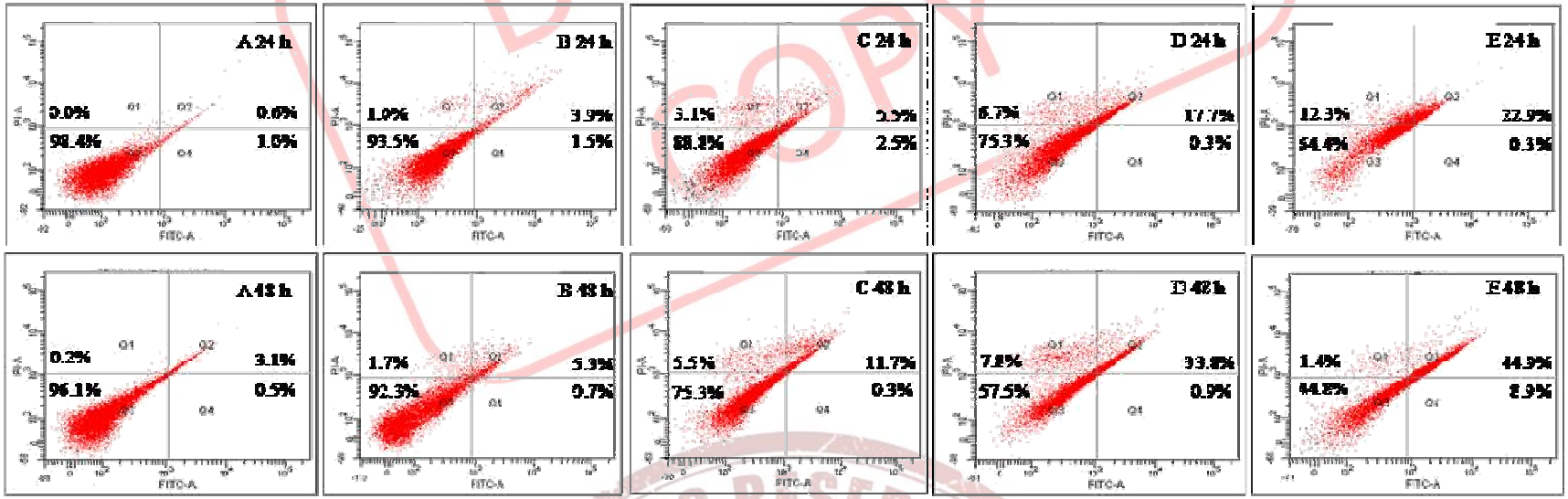

Figure 6.14 Apoptosis estimation in MCF7 cell line after exposure of Control (PBS), A; ATZ Solution, B; ATZ PCL NPs, C; ATZ PCL-PEG NPs, D; and ATZ PCL-PEG ImmunoNPs, E; for 24 and 48 h by Annexin V-FITC and PI staining using FACS technique. Necrotic cells FITC (-) PI (+), Late apoptosis FITC (+) PI (+), Live FITC (-) PI (-), Early apoptotis FITC (+) PI (-).

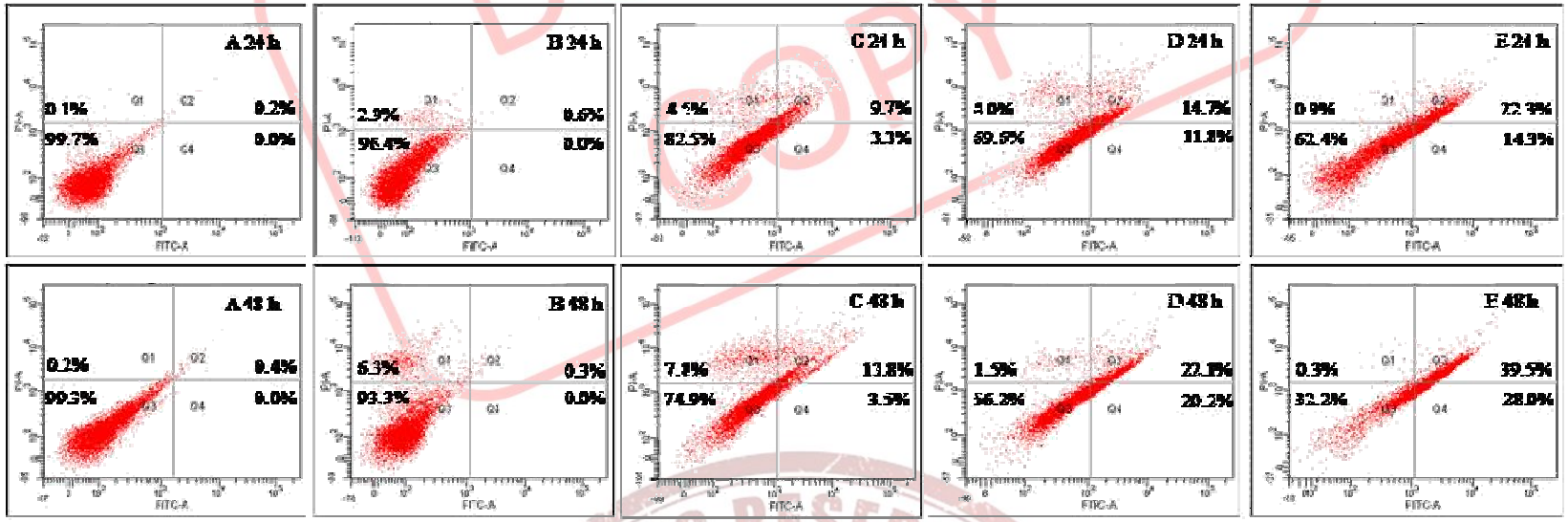

Figure 6.15 Apoptosis estimation in MCF7 cell line after exposure of Control (PBS), A; EXE Solution, B; EXE PLGA NPs, C; EXE PLGA-PEG NPs, D; and EXE PLGA-PEG ImmunoNPs, E; for 24 and 48 h by Annexin V-FITC and PI staining using FACS technique. Necrotic cells FITC (-) PI (+), Late apoptosis FITC (+) PI (+), Live FITC (-) PI (-), Early apoptotis FITC (+) PI (-).

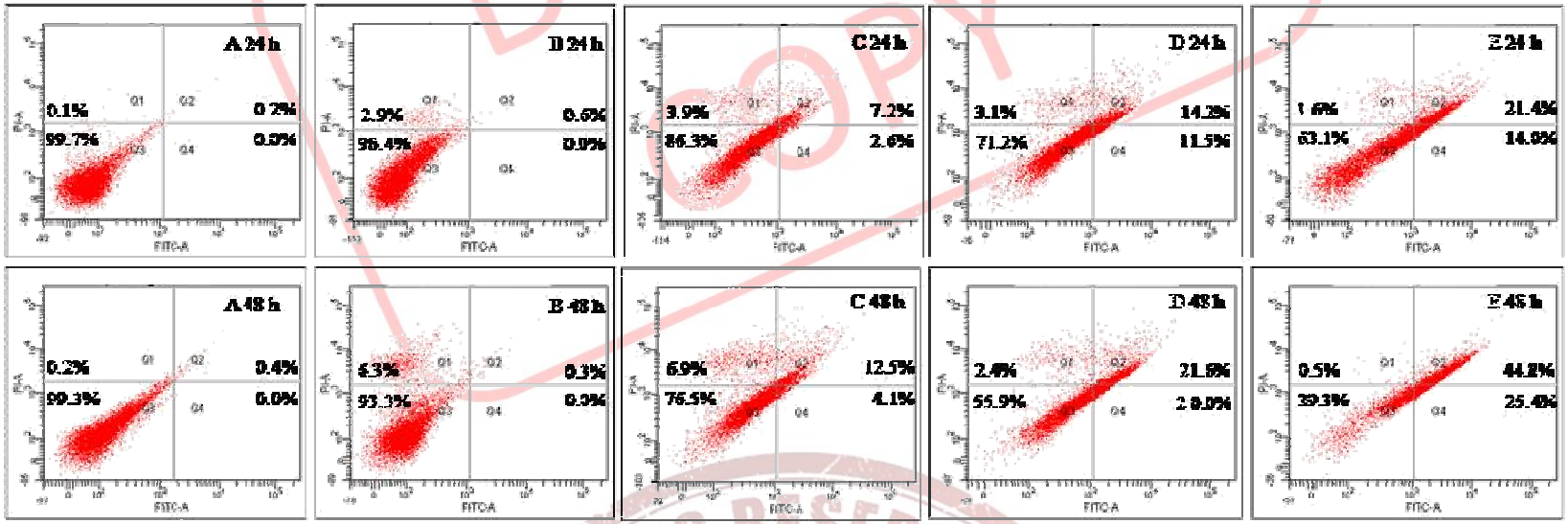

Figure 6.16 Apoptosis estimation in MCF7 cell line after exposure of Control (PBS), A; EXE Solution, B; EXE PCL NPs, C; EXE PCL-PEG NPs, D; and EXE PCL-PEG ImmunoNPs, E; for 24 and 48 h by Annexin V-FITC and PI staining using FACS technique. Necrotic cells FITC (-) PI (+), Late apoptosis FITC (+) PI (+), Live FITC (-) PI (-), Early apoptotis FITC (+) PI (-).

6.5.5 Cell cycle analysis

Drugs are known to act by different pharmacological actions which includes their effect on genes controlling the cell cycle and induction of pro- and anti-apoptotic genes [Panyam and Labhasetwar 2004]. Anastrozole is known to inhibit cell growth and proliferation primarily through apoptosis inducing mechanism and cell cycle arrest [Chaudhari et al. 2012a; Xanthopoulos et al. 2005] . Hence, we investigated whether the pharmacological action of anastrozole would affect the proliferation of breast cancer cells by studying the distribution of DNA in cell cycle. The DNA distribution in cell cycle was studied to investigate the effect of prepared formulations on growth of MCF7 cells. Results of cell cycle analysis demonstrated that ATZ treated cells showed stronger arrest at G0/G1 phase as compared to nanoparticulate formulations. ImmunoNPs showed lesser percentage of cells at G0/G1 phase (56.4%) as compared to 69.9% and 63.6% cells in PBS (control) and ATZ treated cells. However, exposure to ImmunoNPs showed stronger arrest at G2/M phase (27.1%) which was almost 1.6 times higher than ATZ drug solution (figure 6.17, table 6.9).

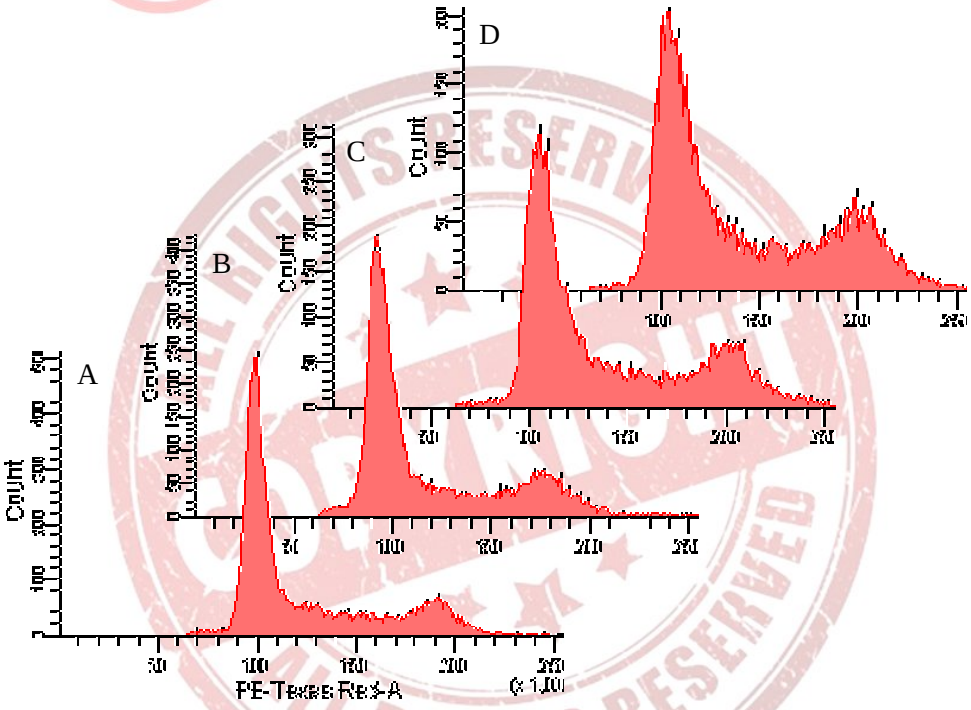

Figure 6.17 Effect of ATZ, ATZ loaded PLGA-PEG NPs and ImmunoNPs exposure on cell cycle distribution in MCF7 cells using FACS as an estimation technique.

Table 6.9 Cell cycle analysis in MCF7 cell line after treatment of (a) Control (PBS), (b) ATZ solution, ATZ loaded (c) PLGA-PEG NPs and (d) PLGA-PEG ImmunoNPs by PI staining using FACS technique.

Treatment	Phases			
	Sub G0/G1	G0/G1	S	G2/M
Control	1.4	69.9	12.7	16.0
ATZ solution	2.8	63.6	16.4	17.2
PLGA-PEG NPs	1.0	59.6	14.5	25.0
PLGA-PEG ImmunoNPs	0.9	56.4	15.6	27.1

Results of cell cycle analysis demonstrated that ATZ treated cells showed stronger arrest at G0/G1 phase as compared to nanoparticulate formulations. ImmunoNPs showed lesser percentage of cells at G0/G1 phase (50.1%) as compared to 69.9% and 63.6% cells in PBS (control) and ATZ treated cells. However, exposure to ImmunoNPs showed stronger arrest at G2/M phase (29.3%) which was almost 1.7 times higher than ATZ drug solution (figure 6.18, table 6.10).

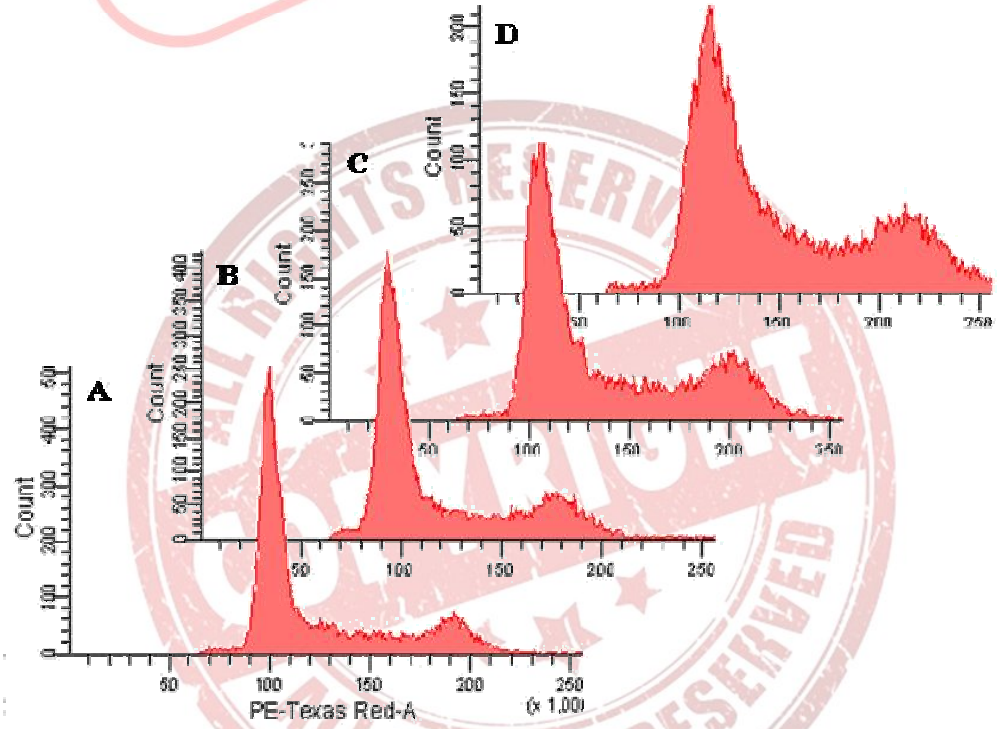

Figure 6.18 Effect of ATZ, ATZ loaded PCL-PEG NPs and ImmunoNPs exposure on cell cycle distribution in MCF7 cells using FACS as an estimation technique.

Table 6.10 Cell cycle analysis in MCF7 cell line after treatment of (a) Control (PBS), (b) ATZ solution, ATZ loaded (c) PCL-PEG NPs and (d) PCL-PEG ImmunoNPs by PI staining using FACS technique.

Treatment	Phases			
	Sub G0/G1	G0/G1	S	G2/M
Control	1.4	69.9	12.7	16.0
ATZ solution	2.8	63.6	16.4	17.2
PCL-PEG NPs	1.1	59.9	14.2	24.8
PCL-PEG ImmunoNPs	1.0	50.1	19.6	29.3

Results of cell cycle analysis demonstrated that EXE treated cells showed stronger arrest at G0/G1 phase as compared to nanoparticulate formulations. ImmunoNPs showed lesser percentage of cells at G0/G1 phase (48.2%) as compared to 68.6% and 60.2% cells in PBS (control) and EXE treated cells. However, exposure to ImmunoNPs showed stronger arrest at G2/M phase (28.5%) which was almost 1.33 times higher than EXE drug solution (figure 6.19, table 6.11).

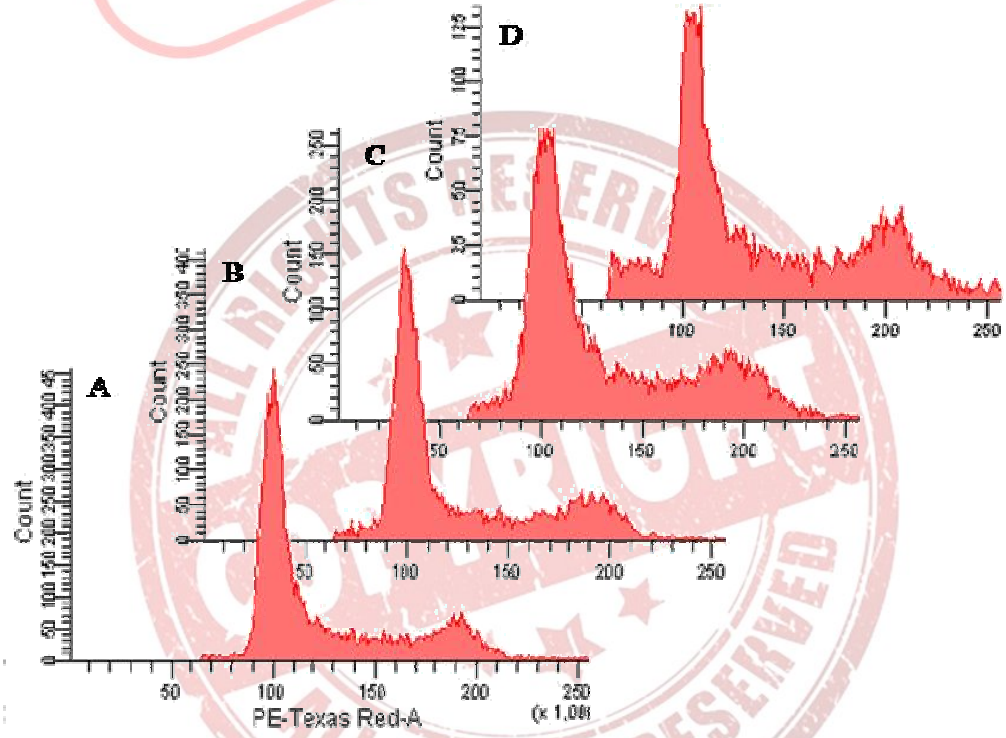

Figure 6.19 Effect of EXE, EXE loaded PLGA-PEG NPs and ImmunoNPs exposure on cell cycle distribution in MCF7 cells using FACS as an estimation technique.

Table 6.11 Cell cycle analysis in MCF7 cell line after treatment of (a) Control (PBS), (b) EXE solution, EXE loaded (c) PLGA-PEG NPs and (d) PLGA-PEG ImmunoNPs by PI staining using FACS technique.

Treatment	Phases			
	Sub G0/G1	G0/G1	S	G2/M
Control	1.5	68.6	13.1	16.8
EXE solution	2.4	60.2	15.9	21.4
PLGA-PEG NPs	2.9	53.3	19.8	24.0
PLGA-PEG ImmunoNPs	6.2	48.2	17.1	28.5

Results of cell cycle analysis demonstrated that EXE treated cells showed stronger arrest at G0/G1 phase as compared to nanoparticulate formulations. ImmunoNPs showed lesser percentage of cells at G0/G1 phase (45.3%) as compared to 68.6% and 60.2% cells in PBS (control) and EXE treated cells. However, exposure to ImmunoNPs showed stronger arrest at G2/M phase (34.2%) which was almost 1.6 times higher than EXE drug solution (figure 6.20, table 6.12).

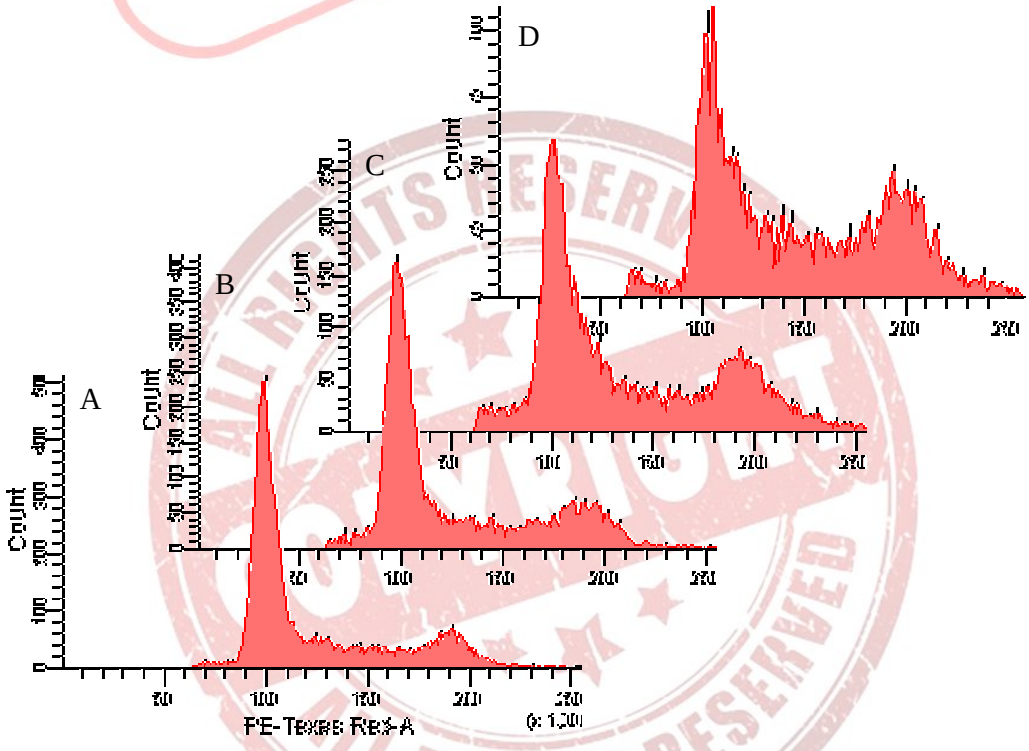

Figure 6.20 Effect of EXE, EXE loaded PCL-PEG NPs and ImmunoNPs exposure on cell cycle distribution in MCF7 cells using FACS as an estimation technique.

Table 6.12 Cell cycle analysis in MCF7 cell line after treatment of (a) Control (PBS), (b) EXE solution, EXE loaded (c) PCL-PEG NPs and (d) PCL-PEG ImmunoNPs by PI staining using FACS technique.

Treatment	Phases			
	Sub G0/G1	G0/G1	S	G2/M
Control	1.5	68.6	13.1	16.8
EXE solution	2.4	60.2	15.9	21.4
PCL-PEG NPs	4.0	56.9	13.2	25.9
PCL-PEG ImmunoNPs	2.6	45.3	17.9	34.2

Previously, it was observed by Chaudhari et al. that ligand conjugated NPs were more effective in controlling cell cycle arrest as compared to drug solution in MCF7 cells [Chaudhari et al. 2012a; Chaudhari et al. 2012b; Chaudhari et al. 2012c]. Our results suggested that higher anti-proliferative effects of ImmunoNPs on MCF7 cells may be due to decreased cell cycle progression. However, greater efficiency of ImmunoNPs in arresting more number of cells depends on the intracellular drug level in the target cells due to enhanced cellular uptake following receptor mediated endocytosis and sustained drug release as compared to drug solution and un-conjugated NPs.

6.6 References

Bareford LM, Swaan PW. 2007. Endocytic mechanisms for targeted drug delivery. Adv. Drug Deliv. Rev. 59(8):748-758.

Bradford MM. 1976. A rapid and sensitive method for the quantitation of microgram quantities of protein utilizing the principle of protein-dye binding. Anal. Biochem. 72:248-254.

Castino R, Démoz M, Isidoro C. 2003. Destination 'Lysosome': a target organelle for tumour cell killing? J. Mol. Recog. 16(5):337-348.

Chaudhari KR, Kumar A, Khandelwal VKM, Mishra AK, Monkkonen J, Murthy RSR. 2012a. Targeting efficiency and biodistribution of zoledronate conjugated docetaxel loaded pegylated PBCA nanoparticles for bone metastasis. Adv. Func. Mat. 22(19):4101-4114.

Chaudhari KR, Kumar A, Khandelwal VKM, Ukawala M, Manjappa AS, Mishra AK, Monkkonen J, Murthy RSR. 2012b. Bone metastasis targeting: A novel approach

to reach bone using Zoledronate anchored PLGA nanoparticle as carrier system loaded with Docetaxel. J. Controlled Rel. 158(3):470-478.

Chaudhari KR, Ukawala M, Manjappa AS, Kumar A, Mundada PK, Mishra AK, Mathur R, Monkkonen J, Murthy RS. 2012c. Opsonization, biodistribution, cellular uptake and apoptosis study of PEGylated PBCA nanoparticle as potential drug delivery carrier. Pharm. Res. 29(1):53-68.

Loveland BE, Johns TG, Mackay IR, Vaillant F, Wang ZX, Hertzog PJ. 1992. Validation of the MTT dye assay for enumeration of cells in proliferative and antiproliferative assays. Biochem. Int. 27(3):501-510.

Mosmann T. 1983. Rapid colorimetric assay for cellular growth and survival: application to proliferation and cytotoxicity assays. J. Immunol. Methods 65(1-2):55-63.

Panyam J, Labhasetwar V. 2003. Dynamics of endocytosis and exocytosis of poly(D,L-lactide-co-glycolide) nanoparticles in vascular smooth muscle cells. Pharm. Res. 20(2):212-220.

Panyam J, Labhasetwar V. 2004. Sustained cytoplasmic delivery of drugs with intracellular receptors using biodegradable nanoparticles. Mol. Pharm. 1(1):77-84.

Sahoo SK, Labhasetwar V. 2005. Enhanced antiproliferative activity of transferrin-conjugated paclitaxel-loaded nanoparticles is mediated via sustained intracellular drug retention. Mol. Pharm. 2(5):373-383.

Sieuwerts AM, Klijn JG, Peters HA, Foekens JA. 1995. The MTT tetrazolium salt assay scrutinized: how to use this assay reliably to measure metabolic activity of cell cultures in vitro for the assessment of growth characteristics, IC50-values and cell survival. Eur. J. Clin. Chem. Clin. Biochem. 33(11):813-823.

Sly WS, Vogler C. 2002. Brain-directed gene therapy for lysosomal storage disease: going well beyond the blood- brain barrier. Proc. Natl. Acad. Sci. USA 99(9):5760-5762.

Susin SA, Daugas E, Ravagnan L, Samejima K, Zamzami N, Loeffler M, Costantini P, Ferri KF, Irinopoulou T, Prevost MC and others. 2000. Two distinct pathways leading to nuclear apoptosis. J. Exp. Med. 192(4):571-580.

Van Maerken T, Speleman F, Vermeulen J, Lambertz I, De Clercq S, De Smet E, Yigit N, Coppens V, Philippe J, De Paepe A and others. 2006. Small-molecule MDM2

antagonists as a new therapy concept for neuroblastoma. Cancer Res. 66(19):9646-9655.

Vega F, Medeiros LJ, Leventaki V, Atwell C, Cho-Vega JH, Tian L, Claret FX, Rassidakis GZ. 2006. Activation of mammalian target of rapamycin signaling pathway contributes to tumor cell survival in anaplastic lymphoma kinase-positive anaplastic large cell lymphoma. Cancer Res. 66(13):6589-6597.

Xanthopoulos JM, Romano AE, Majumdar SK. 2005. Response of mouse breast cancer cells to anastrozole, tamoxifen, and the combination. J. Biomed. Biotechnol. 2005(1):10-19.

Chapter 7

IN VIVO BIODISTRIBUTION STUDIES

7.1 Introduction

One of the most suitable methods for studying the biodistribution is to label these NPs with radioisotopes to measure the biodistribution of radioactivity in various organs at predetermined time periods [Arulsudar et al. 2003; Babbar et al. 1991; Bhatnagar et al. 1997]. Reddy and colleagues (2004) reported the biodistribution of radiolabeled etoposide loaded lipid NPs and doxorubicin incorporated into PBCA nanocapsules [Reddy et al. 2004]. Biodistribution and anti-tumor efficacy for doxorubicin loaded NPs reported recently by Yu and colleagues (2007) showed the highest accumulation of NPs preferentially in the tumor [Yu et al. 2007]. Assessment of biodistribution of drugs and drug delivery system is very important to understand the fate of delivery system *in-vivo*. In last few years, radiolabelling has also been used to recognize the biodistribution of various delivery systems. Reports from the literature indicated the usefulness of radiolabeled formulation to study biodistribution in animals.

Among all the radioisotopes, 125-Iodine (^{125}I) can be used for the biodistribution studies and for medical diagnostic purposes due to its relatively longer half life and requires relatively low radiation dose. Examples of the half lives of some radioisotopes are given in the Table 7.1.

Table 7.1: Approximate half life of various radioisotopes.

Radioisotope	Half life (approx.)
^{81m}Kr	13 seconds
^{99m}Tc	6 hours
^{131}I	8 days
^{51}Cr	30 days
^{125}I	60 days
^{137}Cs	30 years
^{241}Am	462 years
^{226}Ra	1620 years
^{238}U	4.51×10^9 years

Radioactive isotopes of iodine have proved to be appropriated for labeling both large and small biomolecules, proteins and peptides. Several therapeutic radioisotopes used for labeling many monoclonal antibodies are available, beta emitters like iodine-131, yttrium-90, rhenium-186, rhenium-188, cupper-67 and alpha emitters like bismuth-212

and astatine-211. The choice and use of these radioisotopes are based on their physical properties, suitable chemistry, advantages and disadvantages [Weadock et al. 1990]. The preference for radioiodine, mainly iodine-131, is sustained by its well-known chemistry, easy availability and low cost.

125I due to its ideal nuclear characteristics (t1/2: 59.40 d, γ : 27.5 KeV (76.5 abundance), 35.5 KeV (6.7) for in vitro assay and studies was used for radiolabeling antibody to study pharmacokinetics of radiolabelled NPs. Radioiodination with 125I and purification of ER antibody was carried out. α-methyl Tyrosine ester (TME) was radioiodinated to serve as control. Radioiodination of biomolecules mainly proteins and peptides involve electrophilic substitution reaction at tyrosyl, histidyl or tryptophan residues. Iodine should be in +1 oxidation state to displace the H from ortho position of the phenolic ring. Oxidised species of iodine may be obtained by oxidizing iodide with agents like iodine monochloride, chloramine T or by using enzyme like HRP. In aqueous solutions, Chloramine T releases hypochlorous acid which oxidizes iodide.

I2+ H2O: H2O I + + I -

There are many methods of radiolabeling proteins with radioiodine, mostly oxidative reactions, as described by many authors [Weadock et al. 1990]. However, Chloramine-T, a mild oxidizing agent, can alter protein structure (denaturation) if exposure is prolonged. Using this procedure, the oxidizing process is terminated by addition of a reducing agent, sodium metabisulphite.

Labeling of the NPs with radioisotopes was carried out by tagging with suitable gamma emitting radioisotope. Two approaches for radiolabeling have been reported one is by attachment of the label to the polymer component prior to NP preparation and another way is to radiolabel the NP after manufacturing (Richardson et al., 1978). Radiolabeled NP have been successfully used for preclinical evaluation of pharmacokinetic parameters of nanocarrier delivery system as this can be administered to animals by different routes and its uptake in various organs can be estimated with time. Radiolabeled NP preparations have also been used successfully for imaging tumor, abscesses, ischemia and infracted region.

The procedure for biodistribution studies mainly involves attachment of ^{125}I with the antibody or α-methyl tyrosine ester which can be further conjugated to the delivery system under examination. The effective binding of the radio-labeled complex is assessed by quality control tests. Radio-labeled complex is then administered to the

animal depending on the mode of administration and the target organ. After administration of the radio-labeled complex, biodistribution can be studied either by sacrificing the animal at various time points and measuring the radioactivity in different organs.

7.2 Materials

α-methyl Tyrosine ester and chloramine T was obtained from Sigma Aldrich, Mumbai, India. PD10 columns were procured from GE healthcare. Mumbai, India

7.3 Methods

7.3.1 Radioiodination of antibody

Radioiodination was carried out by adding 0.05 M phosphate buffer pH 7.5 (30 µl) to antibody solution (25 µl) followed by addition of 18.5 MBq of 125I. Chloramine T was used as oxidizing agent (10 µl, 2 mg/ml in 0.05 M phosphate buffer, pH 7.5). After addition of chloramine T, reaction was stopped after 90 sec by addition of sodium metabisulphate (50 µl, 2 mg/ml in 0.05 M phosphate buffer, pH 7.5). To the above solution, KI (100 µl, 1 mg/ml in 0.05 M phosphate buffer) was added and mixed properly. Similarly radioiodination of α-methyl tyrosine ester (5 µl, 1 mg/ml in methanol) was carried out.

7.3.2 Determination of labeling efficiency by electrophoresis

Electrophoresis was carried out to check radioiodination of antibody and TME to calculate the yield of reaction. Whatman paper strips (3 mm) were first equilibrated with 0.025 M phosphate buffer pH 7.5. Reaction mixture for radiolabelled antibody and radiolabelled TME was spotted at the centre of paper strips and electrophoresis was carried out for 1 h at 240 V.

7.3.3 Purification of radiolabeled antibody

Commercially available PD10 column was equilibrated with 4 times column volume of 0.05 M phosphate buffer. Reaction mixture (250 µl) was loaded on the column. Purified antibody was eluted with 0.05 M phosphate buffer containing 0.5% BSA. Fractions of 1 ml/tube up to 20 tubes were collected and counted in NaI (Tl) counter. About 99% of activity was observed in fraction 5 and 6 while free iodide was observed at 12-15 fractions 1%. Electrophoresis of fraction 6 and 7 was carried out to ensure purity of column fractions.

7.3.4 Conjugation of iodinated antibody and TME on NPs

Iodinated antibody and TME was surface functionalized on NPs as described in chapter 5 (Section 5.3.3).

7.3.5 Stability of radiolabelled conjugates

Stability of the conjugated ^{125}I to antibody and tyrosine was determined after 24 h by electrophoresis. Electrophoresis was carried out as described previously (Section 7.3.2).

7.3.6 Biodistribution studies

All experiments conducted on animals were approved by Committee for the Purpose of Control and Supervision of Experiments on Animals (CPCSEA), Ministry of Social Justice and Empowerment, Government of India, New Delhi, India. Balb/c mice (aged 4 to 5 months), weighing between 25 to 30 g were selected for the study on the basis of randomization technique. Three mice were used at each time point for each formulation. The mice were divided into four groups. Group 1 received ^{125}I-Tyr PLGA NPs, group 2 received ^{125}I-ER Ab PLGA NPs, group 3 received ^{125}I-Tyr PCL NPs and group 4 received ^{125}I-ER Ab PCL NPs administered intravenously via tail vein. The mice were sacrificed at different time intervals of 3 and 24 h post-administration, and blood was collected via cardiac puncture. Different organs including heart, lungs, liver, spleen, kidney, stomach, intestine, uterus, muscle and bone were dissected and weighed. The activity associated with organs/tissues was measured in a flat type NaI (Tl) scintillation counter (ECIL, India). The mean of this radioactivity was used to obtain the total injected radioactivity in each animal. The radioactivity present in each organ/tissue was interpreted as percentage of activity per gram of the tissue (%A/g).

Injection dose at time (t) = [(Total activity before inj. – total activity of empty syringe) – background counts]

$$\% \text{ Activity per gram of the tissue} = \frac{(\text{Organ counts} \times 100)}{(\text{Organ weight} \times \text{injected dose})}$$

7.3.7 Statistical Analysis

All data are reported as mean ± SD (standard deviation) and the difference between the groups were tested using Student's t-test at the level of $p < 0.05$. Statistical evaluation were compared using ANOVA and differences greater at $p < 0.05$ were considered significant.

7.4 Results and Discussion

7.4.1 Stability of iodinated complexes

Results of electrophoresis indicates the initial binding capacity of ^{125}I to tyrosine and antibody of 100% and 99.67%, respectively. After 24, the stability studies of 125I with tyrosine and antibody conjugated to NPs was performed. The results showed more than 90% stability of the conjugates indicating high binding capacity (Table 7.2).

Table 7.2 Stability of iodinated complexes after 24 h.

	Initial		After 24 h			
	Ab	Tyr	PLGA Tyr	PLGA Ab	PCL Tyr	PCL Ab
Bound fractions	144047	446657	26834	5158	10152	3081
	537840	949848	72965	22798	71367	19655
	107955	687611	4150	10697	23921	9004
	41338	59693	344	5481	324	3755
	19022	6150	145	1386	229	896
	17703	4334	97	190	117	137
Unbound fractions	1995	28	93	70	223	1693
	716	20	1795	2299	2183	1454
	158	25	1451	1101	634	674
	39	26	65	215	15	13
% Bound	99.67	100.00	96.85	92.54	97.20	90.50
% Unbound	0.33	0.00	3.15	7.46	2.80	9.50

7.4.2 Biodistribution studies

Biodistribution of ^{125}I-Tyr PLGA NPs, ^{125}I-ER Ab PLGA NPs, ^{125}I-Tyr PCL NPs and ^{125}I-ER Ab PCL NPs following i.v. administration in swiss mice were performed and the radioactivity was estimated at predetermined time point for 3 and 24 h. The results obtained are shown in table 7.3 for PLGA NPs and table 7.5 for PCL NPs. The concentration of formulation in each organ/tissue/blood following i.v. injection of NPs was shown in figure 7.1 for PLGA NPs and figure 7.2 for PCL NPs in bar graph. The ratios

of bio-distribution in liver, blood, and uterus were calculated and tabulated in table 7.4 for PLGA NPs and table 7.6 for PCL NPs.

7.4.2.1 Biodistribution of ^{125}I-Tyr PLGA NPs and ^{125}I-ER Ab PLGA NPs

The biodistribution data reveals higher initial rapid uptake by liver, which was 1.77 ± 0.32% for PLGA NP and 2.51 ± 0.44% for immunoNPs after 3 h post injection. ImmunoNPs were available more in circulatory system as compared to non-targeted NPs (5 times and about 8 times after 3 and 24 h, respectively). Non-targeted NPs are not retained in uterus as %ID/g decreased from 0.58 ± 0.34% to 0.10 ± 0.18% which is about 6 times ($p < 0.05$), whereas in case of immunoNPs %ID/g value was increased by more than 2 times from 0.63 ± 0.13% to 1.29 ± 0.28% after 3 and 24 h respectively ($p < 0.05$). Distribution of immunoNPs was increased by more than two times after 24 h as compared to 3 h. When distribution of targeted immunoNPs was compared with non-

Table 7.3 Biodistribution of ^{125}I labeled Tyrosine and ER antibody conjugated PLGA NPs and the radioactivity was measured after 3 and 24 h post injection. The values represented as mean ± SD. Radioactivity is expressed as percent of administered dose per gram of tissue or organ.

Organ	% Dose/g of organ			
	PLGA-NPs Tyr (3 h)	PLGA-NPs Tyr (24 h)	PLGA-NPs ER Ab (3 h)	PLGA-NPs ER Ab (24 h)
Liver	1.77 ± 0.32	0.31 ± 0.02	2.51 ± 0.44	1.57 ± 0.29
GIT	1.51 ± 0.29	0.09 ± 0.01	1.65 ± 0.14	0.35 ± 0.08
Stomach	1.91 ± 0.52	0.07 ± 0.03	17.98 ± 3.02	0.44 ± 0.15
Kidneys	2.60 ± 0.96	0.12 ± 0.10	2.54 ± 0.47	0.97 ± 0.15
Heart	1.60 ± 0.31	0.01 ± 0.10	1.32 ± 0.25	0.41 ± 0.15
Lungs	1.09 ± 0.15	0.06 ± 0.07	2.28 ± 1.18	0.84 ± 0.04
Spleen	0.49 ± 0.90	0.14 ± 0.14	2.02 ± 0.50	0.61 ± 0.16
Uterus	0.58 ± 0.34	0.10 ± 0.18	0.63 ± 0.13	1.29 ± 0.28
Blood	0.84 ± 0.62	0.23 ± 0.17	4.40 ± 0.75	1.82 ± 0.52
Muscle	8.99 ± 4.3	1.09 ± 0.70	7.13 ± 1.76	3.23 ± 0.57
Bone	6.64 ± 6.95	5.06 ± 4.82	7.71 ± 2.05	4.15 ± 2.36

targeted formulations, the uterus uptake was found to be slightly but not significantly higher which later increased to 13 times after 24 h which was a very significant increase. This result shows a clear active targeting of prepared immunoNPs which was found absent in case of long circulatory pegylated NPs.

Table 7.4 Different ratio between the tissue/organ of ^{125}I labeled Tyrosine and ER antibody conjugated PLGA NPs.

Ratio of % Dose/g of organ	PLGA-NPs Tyr (3 h)	PLGA-NPs Tyr (24 h)	PLGA-NPs ER Ab (3 h)	PLGA-NPs ER Ab (24 h)
Liver to blood ratio	2.11	1.35	0.57	0.86
Blood to uterus ratio	1.45	2.3	6.98	1.41

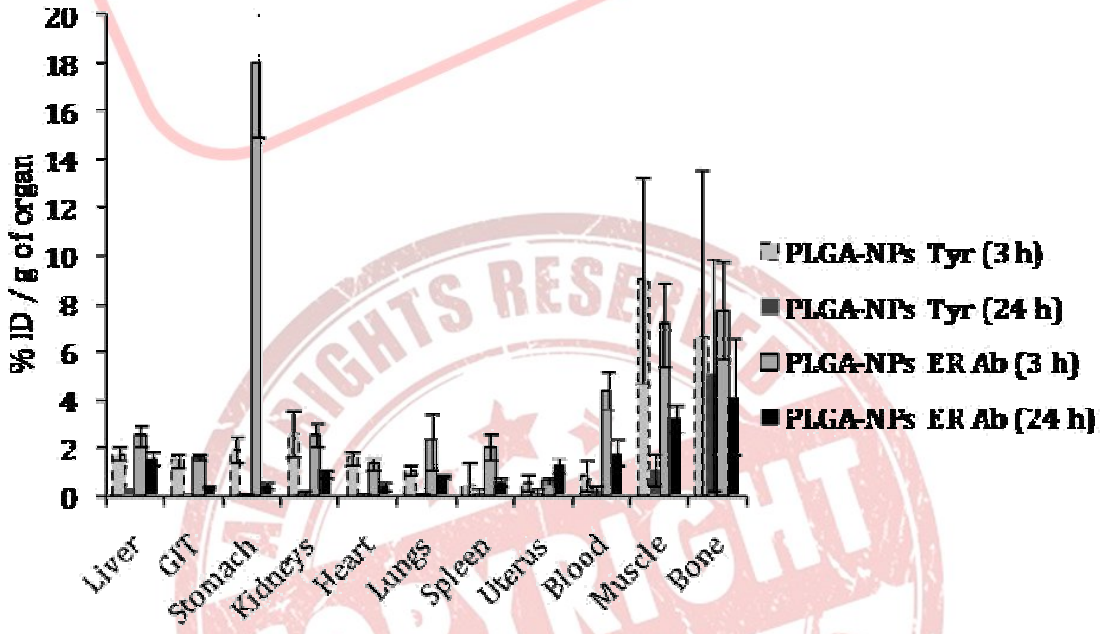

Figure 7.1 Biodistribution of ^{125}I labeled Tyrosine and ER antibody conjugated PLGA NPs and the radioactivity was measured after 3 and 24 h post injection. The values represented as mean ± SD. Radioactivity is expressed as percent of administered dose per gram of tissue or organ.

From the results of liver to blood distribution ratio, significant difference between the two formulations can be observed. Value of liver to blood ratio of above 1 signifies that

higher liver uptake of NPs as compared to circulating particles. Targeted NPs showed liver to blood ratio below 1 at both the time points indicating more NPs in circulation than uptaken by liver. Blood to uterus ratio of the injected NPs was found to be lower in case of non-targeted NPs indicating non-targetability of the NPs without antibody conjugation. The higher values of this ratio after 3 h is possibly because of more number of immunoNPs are present in circulation. The overall %ID/g activity present in uterus was 13 times more as discussed previously which clearly demonstrates the active targeting of the immunoNPs.

7.4.2.2 Biodistribution of ^{125}I-Tyr PCL NPs and ^{125}I-ER Ab PCL NPs

The biodistribution data of ^{125}I labeled Tyrosine and ER antibody conjugated PCL NPs reveals lower uptake by liver, which was 3.79 ± 0.46% and 1.44 ± 0.30% for immunoNPs ($p < 0.01$) and 7.50 ± 0.68% and 3.20 ± 1.22% for non-targeted NPs after 3

Table 7.5 Biodistribution of ^{125}I labeled Tyrosine and ER antibody conjugated PCL NPs and the radioactivity was measured after 3 and 24 h post injection. The values represented as mean ± SD. Radioactivity is expressed as percent of administered dose per gram of tissue or organ.

Organ	% Dose/g of organ			
	PCL-NPs Tyr (3 h)	PCL-NPs Tyr (24 h)	PCL-NPs ER Ab (3 h)	PCL-NPs ER Ab (24 h)
Liver	7.50 ± 0.68	3.20 ± 1.22	3.79 ± 0.46	1.44 ± 0.30
GIT	6.43 ± 0.95	0.62 ± 0.24	1.30 ± 0.32	0.53 ± 0.03
Stomach	1.67 ± 0.60	0.79 ± 0.32	15.28 ± 6.97	0.89 ± 0.13
Kidneys	1.44 ± 0.40	1.06 ± 0.39	2.62 ± 0.24	1.10 ± 0.14
Heart	1.37 ± 0.27	0.93 ± 0.04	1.20 ± 0.06	1.17 ± 0.27
Lungs	1.51 ± 0.31	0.76 ± 0.12	2.62 ± 0.30	1.19 ± 0.52
Spleen	4.81 ± 1.06	2.98 ± 1.51	3.30 ± 0.51	1.91 ± 0.37
Uterus	0.32 ± 0.19	0.28 ± 0.19	0.38 ± 0.11	3.49 ± 0.55
Blood	4.21 ± 0.79	1.59 ± 0.56	5.15 ± 0.96	1.75 ± 0.18
Muscle	6.14 ± 2.80	5.18 ± 0.88	5.30 ± 1.24	5.79 ± 1.92
Bone	6.52 ± 1.63	9.17 ± 2.63	8.07 ± 0.39	11.62 ± 4.99

and 24 h ($p < 0.01$), respectively post injection. The overall distribution of immunoNPs in liver was low at both the time points. Along with liver uptake other RES organ, i.e. spleen also showed less distribution of immunoNPs (3.30 ± 0.51%, 3 h and 1.91 ± 0.37%, 24 h) than non-targeted NPs (4.81 ± 1.06%, 3 h and 2.98 ± 1.51, 24 h) ($p < 0.05$) after both the time points. Similar to distribution of PLGA NPs, more concentration of immunoNPs was present in circulation after both the time points, as shown in table 7.4. No significant difference in uterus uptake was observed after 3 h (1.2 times higher uptake of immunoNPs as compared to non-targeted nanoparticulate system), which incrased to about 12.5 folds after 24 h.

Table 7.6 Different ratio between the tissue/organ of ^{125}I labeled Tyrosine and ER antibody conjugated PCL NPs.

Ratio of % Dose/g of organ	PCL-NPs Tyr (3 h)	PCL-NPs Tyr (24 h)	PCL-NPs ER Ab (3 h)	PCL-NPs ER Ab (24 h)
Liver to blood ratio	1.78	2.01	0.74	0.82
Blood to uterus ratio	13.16	5.68	13.55	0.5

From the results of liver to blood distribution ratio, significant difference between the two formulations can be observed. Value of liver to blood ratio of above 1 signifies that higher liver uptake of NPs as compared to circulating particles. Targeted NPs showed liver to blood ratio below 1 at both the time points indicating more NPs in circulation than uptaken by liver.

No significant difference was found in distribution of NPs in uterus after 3 h. However, blood to uterus ratio of the injected NPs was found to be lower in case of non-targeted NPs indicating non-targetability of the NPs without antibody conjugation. The higher value of this ratio after 3 h is possibly because of more number of immunoNPs are present in circulation and not reached the organ. After 24 h, blood to uterus ratio was 0.5 indicating higher concentration of immunoNPs in uterus than in blood. The overall %ID/g activity present in uterus was more than 12 times which clearly demonstrates the active targeting of the immunoNPs.

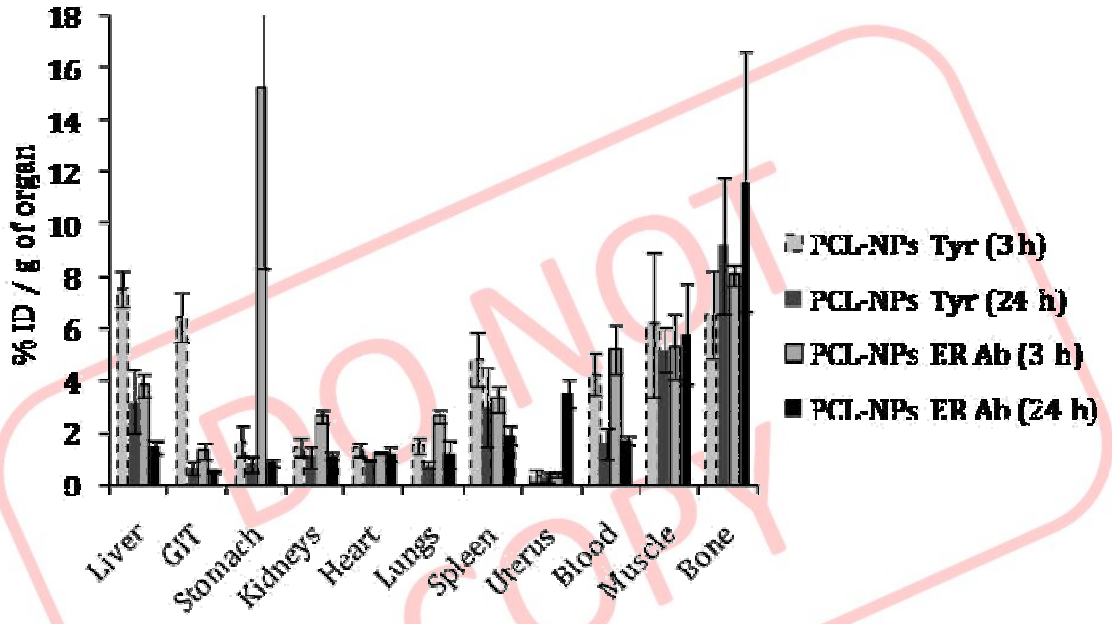

Figure 7.2 Biodistribution of ^{125}I labeled Tyrosine and ER antibody conjugated PCL NPs and the radioactivity was measured after 3 and 24 h post injection. The values represented as mean ± SD. Radioactivity is expressed as percent of administered dose per gram of tissue or organ.

7.5 References

Arulsudar N, Subramanian N, Mishra P, Sharma RK, Murthy RS. 2003. Preparation, characterisation and biodistribution of 99mTc-labeled liposome encapsulated cyclosporine. J Drug Target 11(3):187-196.

Babbar A, Kashyap R, Chauhan UP. 1991. A convenient method for the preparation of 99mTc-labelled pentavalent DMSA and its evaluation as a tumour imaging agent. J Nucl Biol Med 35(2):100-104.

Bhatnagar A, Singh AK, Babbar A, Soni NL, Singh T. 1997. Renal imaging with 99Tc(m)-dextran. Nucl Med Commun 18(6):562-566.

Reddy LH, Sharma RK, Murthy RS. 2004. Enhanced tumour uptake of doxorubicin loaded poly(butyl cyanoacrylate) nanoparticles in mice bearing Dalton's lymphoma tumour. J Drug Target 12(7):443-451.

Weadock KS, Sharkey RM, Varga DC, Goldenberg DM. 1990. Evaluation of a remote radioiodination system for radioimmunotherapy. J Nucl Med 31(4):508-511.

Yu JJ, Lee HA, Kim JH, Kong WH, Kim Y, Cui ZY, Park KG, Kim WS, Lee HG, Seo SW. 2007. Bio-distribution and anti-tumor efficacy of PEG/PLA nano particles loaded doxorubicin. J Drug Target 15(4):279-284.

Chapter 8

SUMMARY AND CONCLUSION

8.1 Summary

Breast cancer is the most frequently diagnosed form of cancer and second leading cause of death in women. The incidence of breast cancer is still rising, and the disease remains largely incurable once it becomes malignant. Estrogen is important factor in development of breast cancer. When it binds with estrogen receptor, it becomes activated resulting in stimulation of tumor growth. This receptor has been found to be overexpressed in about 70-80% of the breast cancer patients. Despite the significant progress in the development of anticancer technology, there is still no common cure for patients suffering from with this malignant disease. Traditional chemotherapy relies on the premise that rapidly proliferating cancer cells are more likely to be killed by a cytotoxic drug. However, in reality, cytotoxic agents have very little or no specificity as very less concentration of drug reaches tumor site, which leads to systemic toxicity. Current treatment methods either reduce estrogen levels or block estrogen-receptor using aromatase inhibitors or anti-estrogens. However, the lack of specificity of currently available chemotherapeutic agents constitutes a major obstacle to the treatment of cancer. In addition, the long-standing problem of chemotherapy is the lack of tumor-specific treatments. Therefore, targeting is required to ensure high efficiency of the drug at tumor site with reduced side effects when dealing with drugs that are presumed to kill cancer cells along with healthy cells. The drug loaded polymeric nanoparticles can be tagged with specific ligands like monoclonal antibodies by synthetic or biochemical means to form a tumor-selective conjugate. Administration of such conjugates leads to the accumulation of drug loaded nanoparticles preferentially in the tumor without significant distribution to normal tissues, leading to high specificity and reduced systemic toxicity. The reduction or prevention of side effects can also be achieved by controlled release. Nanoparticulate drug delivery systems provide a better penetration of the particles inside the body as their size allows delivery via intravenous injection or other routes. The nanoscale size of these particulate systems also minimizes the hypersensitive reactions at the injection site. nanoparticles may be targeted to the growing vasculature serving the growing cancer or to the cancer cells themselves. Targeted delivery utilizes unique phenotypic features of diseased tissues and cells in order to concentrate the drug at the location where it is needed. Active targeting utilizes biologically specific interactions including antigen–antibody and ligand–receptor

binding and may seek drug uptake by receptor mediated endocytosis through association of the drug or drug carrier with such antigen or ligand.

Estrogens and progesterone are important factors in the development of breast cancer. The majority of breast tumors found in postmenopausal women contain estrogen receptor (ER) while tumors in younger women often lack this protein. Approximately 70% of all breast cancers retain the estrogen receptor α (ERα, encoded by ESR1) and the progesterone receptor. When estrogen receptor binds estrogen, it becomes activated and can interact with the genes of the cell, resulting in the activation of selected sets of responsive genes. This results in changes in the synthesis of specific RNA's and proteins involved in the regulation of cell proliferation, differentiation and physiological functions. Although normal breast tissue retains estrogen receptor, the amount of this protein produced in positive breast carcinomas is significantly higher. This may account for some of the differences seen in the abnormal growth of various tumors and tumor cell lines when compared to normal breast tissue development.

An alternate strategy to endocrine therapy, which specifically inhibits binding of E2 to the ER, is to inhibit the production of E2 by blocking the cytochrome p450 aromatase enzyme, the rate-limiting enzyme that converts androgens (i.e., testosterone and androstenedione) to estrogens (i.e., E2 and estrone). Anastrozole is one of the second generation Type II (nonsteroidal) aromatase inhibitors which act by binding reversibly to the enzyme and competitively inhibiting binding of the substrate androstenedione. Steroidal inhibitors are competitive-substrate mimics of androstenedione. Exemestane, an irreversible steroidal inhibitor, which bind with high affinity to the binding site of aromatase and are converted to a covalently bound intermediate. The benefits of using aromatase inhibitors over tamoxifen, are believed to be the complete deprivation of E2 and thus better efficacy for ERα-positive breast cancer. Recent clinical data have clearly demonstrated that anastrozole is more effective than tamoxifen as first-line treatment in patients with metastatic breast cancer. Two very small trials demonstrated a significantly increased clinical response rate in patients with ER-positive, HER2-positive cancers treated with preoperative aromatase inhibitors compared to preoperative tamoxifen. This led to a widely accepted hypothesis that aromatase inhibitors were a better choice than tamoxifen in patients with ER-positive, HER2-positive cancers. Hence, the present investigation was aimed at conjugation with estrogen receptor antibody with the objective of ligand based targeting of nanoparticles. The objective of

this study is to develop nanoparticulate drug delivery system composed of biocompatible and biodegradable polymers like poly(lactic co-glycolic acid) and poly(ε-caprolactone), using anticancer drugs (anastrozole, exemestane) for enhancing tumor uptake by ligand (antibody) specific breast targeting and thereby, reducing systemic side-effects of the drug.

Analytical method for the estimation of drugs

The reported HPLC method was used to analyze the content of anastrozole and exemestane separately with some modifications. The standard calibration curve was developed in mobile phase in the range of 1 to 50 µg/ml and linearity was obtained. The retention time obtained was 5.2 ± 0.1 min for anastrozole and 5.0 ± 0.1 min for exemestane.

Preparation of Conjugates and nanoparticles

Caprolactone was successfully polymerized to Polycaprolactone containing carboxylic group and this was confirmed by TLC, FTIR and GPC. Both the polymers (PLGA and PCL) were PEGylated using amine-PEG-carboxylic acid by amide bond formation between carboxylic group present in polymers and amine group present in PEG. Free carboxylic group in PEG was further utilized for formulation of antibody conjugated nanoparticles (Immunonanoparticles) by conjugation with amine group present in antibody. Each reaction step as well as purification step were monitored by TLC using 100% ethyl acetate as a mobile phase and iodine as a spotting reagent. PLGA-PEG and PCL-PEG were successfully characterized by FTIR, NMR and GPC.

Anastrozole loaded PLGA nanoparticles were optimized for high entrapment efficiency and lowest particle size using 3^3 full factorial design. The independent variables were drug:polymer ratio, polymer concentration and surfactant concentration. The optimum formulation offered by the software (Design Expert 8.0) based on desirability was found at 0.68, 1, and -1 level of drug:polymer ratio, polymer concentration in organic phase and surfactant concentration in aqueous phase respectively. The results of dependent variables from the software were found to be 61.39% for percentage drug entrapment and 144.68 nm for particle size at these levels which is as per our desired criteria. The calculated desirability factor for offered formulations was 0.990. The optimized batch of anastrozole loaded PLGA nanoparticles was found to have zeta potential of -30.7 ± 1.4 mV. DSC and TEM studies indicated absence of any drug-polymer interaction and spherical nature of nanoparticles, respectively. Pegylated nanoparticles were optimized

based on percentage drug entrapment, particle size and phagocytic uptake studies on THP1 cells by FACS. From the results, it was observed that as the amount of PEG increased, percentage drug entrapment, particle size and zeta potential decreased. Anastrozole was successfully loaded in pegylated PLGA nanoparticles prior to Ab conjugation (61.29 ± 1.18%) and no significant loss in drug content was observed after surface functionalization with Ab (60.62 ± 0.54%). However, slight increase in particle size was observed which increased from 126.6 ± 4.1 to 140.4 ± 3.7 nm with slight decrease in zeta potential from -24.1 ± 3.4 to -23.6 ± 4.0 mV. The in vitro drug release studies from different nanoparticulate formulations were performed in PBS pH 7.4. Pegylated nanoparticles showed faster release as compared with non-pegylated nanoparticles. Within 3 h, 82.56 ± 0.62% drug release occurred from plain drug suspension, whereas only 24.14 ± 0.31% and 28.90 ± 1.03% drug released from PLGA and pegylated PLGA nanoparticles, reaching 48.02 ± 0.56% and 60.29 ± 0.85% after 120 h and 64.9 ± 0.24% and 83.04 ± 0.55% after 240 h from PLGA and pegylated PLGA nanoparticles, respectively indicative of sustained release. In-vitro drug release showed biphasic pattern exhibiting Fickian diffusion based release mechanism.

Anastrozole loaded PCL nanoparticles were optimized for high entrapment efficiency and lowest particle size using 3^3 full factorial design. The optimum formulation offered by the software based on desirability was found at 1.0, 0.69, and -1.0 level of drug:polymer ratio, polymer concentration and surfactant concentration respectively. The results of dependent variables from the software were found to be 70.21% for percentage drug entrapment and 200 nm for particle size at these levels which is as per our desired criteria. The calculated desirability factor for offered formulations was 0.965, which was near to 1 and indicates suitability of the designed factorial model. The optimized batch of anastrozole loaded PCL nanoparticles was found to have zeta potential of -32.1 ± 1.1 mV. DSC studies indicated spherical nature of nanoparticles and DSC thermogram of drug, polymers, physical mixtures and nanoparticles indicated no chemical interaction amongst them. In vitro release of anastrozole from plain drug suspension and nanoparticles after 3 h exhibited 82.56 ± 0.62% drug released from plain drug suspension, whereas only 21.36 ± 0.41% and 26.57 ± 1.81% drug release occurred from PCL nanoparticles and pegylated PCL nanoparticles, reaching 44.14 ± 0.69% and 56.71 ± 0.67% after 120 h and 58.22 ± 0.99% and 82.21 ± 0.74% after 240 h from PCL and pegylated PCL nanoparticles, respectively indicative of sustained release.

The drug release from nanoparticles followed biphasic release model with an initial burst release in about first 3 h followed by sustained release for more than 240 h. The regression coefficient of the plot of log M_t/M_∞ versus log t for nanoparticles was found to be 0.935 and 0.957 with value of release exponent (n) as 0.273 and 0.275 for PCL and pegylated PCL nanoparticles. The n value is the release exponent which characterizes the transport mechanism and if its value is less than 0.5, it indicates Fickian release.

Exemestane loaded PCL nanoparticles were optimized for high entrapment efficiency and low particle size using Box-Behnken design. The independent variables were drug:polymer ratio, amount of polymer and volume of organic phase. The optimum formulation offered by the Design Expert 8.0.3 software based on desirability was found at 0.43, -0.68, and 0.27 level of drug:polymer ratio, amount of polymer and volume of organic phase, respectively. The calculated desirability factor for offered formulations was 1, which indicated suitability of the designed factorial model. The results of dependent variables from the software were found to yield 83.96% percentage drug entrapment and 180.51 nm particle size at these levels. Data analysis using student's 't' test revealed that there was no statistically significant difference ($p<0.05$) between experimentally obtained values and predicted values by regression analysis and hence, it confirms the utility of the established contour plots and reduced polynomial equation in the preparation of nanoparticles. The optimized batch of exemestane loaded cPCL nanoparticles was found to have zeta potential of -33.8 ± 2.1 mV. TEM image showed discrete spherical particles with monodisperse size of about 100 nm. DSC studies indicated absence of any drug-polymer interaction. Phagocytic uptake of PCL nanoparticles was compared with pegylated nanoparticles containing different quantity of PCL-PEG (5, 10, 15and 20%) in terms of mean fluorescence intensity. Pegylated nanoparticles displayed resistance to phagocytic uptake when compared to non-pegylated nanoparticles. Among various tested formulations, PCL-PEG (20%) showed minimum uptake by THP1 cells. After 1 h, uptake of PCL nanoparticles was 1.33, 2.30 and 9.06 times more than PCL-PEG (5%), PCL-PEG (15%) and PCL-PEG (20%) nanoparticles. Exemestane was successfully loaded in pegylated PCL nanoparticles prior to Ab conjugation and no significant loss in drug content was observed after surface functionalization with Ab (82.11 ± 1.79%). However, slight increase in particle size was observed. The particle size increased from 168.9 ± 2.9 to 179.8 ± 4.1 nm with slight decrease in zeta potential from -27.1 ± 0.9 to -24.3 ± 1.2 mV. Poly dispersity index

before and after Ab conjugation was less than 0.1 indicating unimodal distribution of particles. Pegylated PCL nanoparticles showed faster release as compared with non-pegylated nanoparticles. Within 3 h, 71.36 ± 1.23% drug release occurred from plain drug suspension, whereas only 20.06 ± 1.31% and 24.88 ± 1.13% drug released from PCL and pegylated PCL nanoparticles, reaching 44.89 ± 1.3% and 52.22 ± 3.1% after 120 h and 70.67 ± 1.76% and 83.26 ± 0.85% after 240 h from PCL and pegylated PCL nanoparticles, respectively indicative of sustained release.

Exemestane loaded PLGA nanoparticles were optimized for high entrapment efficiency and low particle size using Box-Behnken design. The optimum formulation offered by the Design Expert 8.0.3 software based on desirability was found at 0.41, -0.09 and 0.75 levels of X_1, X_2 and X_3 respectively. The calculated desirability factor for offered formulations was 1, which indicated suitability of the designed factorial model. The results of dependent variables from the software were found to yield 78.37% percentage drug entrapment and 162.28 nm particle size at these levels. Calculated t value ($t_{calculated}$) for percentage drug entrapment and particle size was found to be 0.6411 and 0.0699, respectively which was less than the tabulated t value of 2.9199 which indicates that there was no statistically significant difference ($p<0.05$) between experimentally obtained values and predicted values by regression analysis and hence confirms the utility of the established contour plots and reduced polynomial equations in the preparation of nanoparticles. The optimized batch of exemestane loaded cPCL nanoparticles was found to have zeta potential of -29.5 ± 1.4 mV. TEM image reveals that the particles were discrete, round and uniform in shape with diameters in the range of 80–100 nm. DSC studies indicated absence of any drug-polymer interaction. In vitro release of exemestane from drug suspension and nanoparticles showed 71.36 ± 1.23% drug release occurred from plain drug suspension, whereas only 25.18 ± 0.56% and 20.21 ± 0.23% drug released in 3 h from PLGA and pegylated PLGA nanoparticles, reaching 48.05 ± 0.94% and 54.25 ± 0.23% after 120 h and 71.4 ± 1.23% and 73.9 ±0.86% after 240 h from PLGA and pegylated PLGA nanoparticles, respectively indicative of sustained release. The drug release from nanoparticles followed biphasic release model with an initial burst release for about 3 h followed by sustained release for more than 240 h. The regression coefficient of the plot of log M_t/M_∞ versus log t for PLGA and pegylated PLGA nanoparticles was found to be 0.935 and 0.984 with value of release exponent (n) as 0.271 and 0.312, respectively indicating Fickian release.

No significant difference between predicted and observed responses was observed in check point analysis with very less normalized error in all the optimization statistical designs.

Nanoparticles were lyophilized using different cryoprotectants like trehalose, sucrose, lactose and mannitol. Out of these, sucrose was found to be the best cryoprotectants causing minimum increase in particle size after re-constitution.

A comparative expression of estrogen receptor in breast cancer cell lines (MCF7 and MDAMB231) was estimated by Western blot analysis. The results confirmed the presence of estrogen receptors in MCF7 cells and absence of the same in MDAMB231 cells.

The 6-coumarin dye acts as a better fluorescent probe due to its low pH-dependent solubility and high fluorescence activity. Using the intrinsic fluorescence property of 6-Coumarin, a comparative analysis of intracellular uptake behavior of 6-Coumarin loaded immunonanoparticles, PEGylated and non-PEGylated nanoparticles were performed in MCF7 cell line by flow cytometry (Quantitative) and fluorescence microscopy (Qualitative). The relative extent of cellular uptake of native 6-Coumarin, 6-Coumarin loaded PEGylated and non-PEGylated nanoparticles, and 6-Coumarin loaded immunonanoparticles was calculated in terms of mean fluorescence intensity (MFI) exhibited by the cells. The fluorescence microscopy results clearly indicate that cellular uptake of nanoparticles were in the order of immunonanoparticles > PEGylated nanoparticles > non-PEGylated nanoparticles > 6-Coumarin which was confirmed by quantitative uptake studies by flow cytometry.

Flow cytometry studies indicated the relative extent of PLGA nanoparticles, pegylated PLGA nanoparticles and immunonanoparticles was calculated using mean fluorescent index (MFI). MFI of pegylated PLGA immunonanoparticles was 1039.10 ± 17.77 which was more than 3 times than that of PLGA nanoparticles (318.27 ± 21.69) after 180 min. Furthermore, pegylated PLGA immunonanoparticles showed about 2 times more uptake when compared with pegylated PLGA nanoparticles (599.95 ± 25.17) at same time point due to receptor mediated endocytosis. The MFI of pegylated PCL immunonanoparticles is 1261.62 ± 39.27 which is about 2 times than that of PCL nanoparticles (730.19 ± 38.68) after 180 min. Furthermore, immunonanoparticles showed about 1.32 times more uptake when compared with pegylated PCL nanoparticles (956.45 ± 33.45) at same time point. Intracellular uptake was found to increase with time for all

formulations from 60 to 180 min. The intracellular uptake of nanoparticles was also dependent on the incubation time. The fluorescence intensity increased gradually with the incubation time and so the uptake of nanoparticles. Results clearly indicates the enhanced cellular uptake of immunonanoparticles than un-conjugated nanoparticles.

In vitro cytotoxicity studies were carried out at different concentration of nanoparticles (0.03, 0.3, 3, 15 and 30 μM) and incubated for different time periods (6, 24, 48 h) with drug solution, blank nanoparticles and drug loaded PEGylated, non-PEGylated and immunonanoparticles. The toxicities by drug loaded immunonanoparticles were found to be significant as compared to drug loaded PEGylated and non-PEGylated nanoparticles in MCF7 cells. Toxicity by all the drug loaded nanoparticulate systems was significant when compared with drug solution in MCF7 cells. . The IC_{50} value for ER positive cells treated with PLGA immunonanoparticles was found to be 165.28, 52.44 and 27.95 times lower than anastrozole, anastrozole loaded PLGA nanoparticles and PLGA-PEG nanoparticles respectively, after 6 h of treatment. Exposure for 48 h further lowered the IC_{50} value by 3.46 times to 0.0828 μM which was 8 times less in comparison with PLGA-PEG nanoparticles.

The IC_{50} value for ER positive cells treated with PCL-PEG ImmunoNPs was found to be 158.2, 26.73 and 4.27 times lower than ATZ, ATZ PCL NPs, PCL-PEG NPs respectively, after 6 h of treatment. Exposure for 48 h further lowered the IC_{50} value by 6 times to 0.05 μM which was more than 6.6 times less in comparison with ATZ PCL-PEG NPs. To confirm receptor mediated endocytosis, cytotoxicity studies were also performed on receptor negative cells (MDAMB231) and results clearly indicated that the effect of different NPs on MDAMB231 cells when compared to MCF7 cells. No significant toxicity was found on MDAMB231 cells. Thus, the enhanced cytotoxic activity of PCL-PEG ImmunoNPs for MCF7 cells as compared with MDAMB231 cells clearly demonstrates the high affinity of ImmunoNPs towards ER positive cancer cells.

In vitro cytotoxicity studies were carried out at different concentration of nanoparticles (0.03, 0.3, 1.5, 3 and 15 μM) and incubated for different time periods (6, 24, 48 h) with drug solution, blank nanoparticles and drug loaded PEGylated, non-PEGylated and immunonanoparticles. The IC_{50} value for ER positive cells treated with exemestane loaded PLGA-PEG Immunonanoparticles was found to be 7.5, 4.4 and 2.1 times lower than exemestane, exemestane PLGA nanoparticles, exemestane PLGA-PEG nanoparticles

respectively, after 48 h of treatment. The IC_{50} value for ER positive cells treated with Immunonanoparticles was found to be 4.7, 3.1 and 1.8 times lower than that of exemestane, exemestane PCL nanoparticles and exemestane PCL-PEG nanoparticles after 48 h exposure respectively. To confirm receptor mediated endocytosis, cytotoxicity studies were also performed on receptor negative cells (MDAMB231) and results clearly indicated that the effect of different nanoparticles on MDAMB231 cells when compared to MCF7 cells. No significant toxicity was found on MDAMB231 cells. Thus, the enhanced cytotoxic effect of immunonanoparticles could be attributed by higher uptake via receptor mediated endocytosis.

Different drugs are known to have a variety of pharmacological actions, including their effect on genes controlling the cell cycle and induction of pro- and anti-apoptotic genes. Drug loaded nanoparticles inhibit cell growth and proliferation primarily through cell cycle arrest and apoptosis inducing mechanism. Cell cycle analysis demonstrates the arrests of cell cycle by drug solution and drug loaded nanoparticulate formulations at different phases like G1 phase, S phase or G2 phase.

Results of cell cycle analysis demonstrated that anastrozole treated cells showed stronger arrest at G0/G1 phase as compared to nanoparticulate formulations. immunonanoparticles showed lesser percentage of cells at G0/G1 phase (50.1%) as compared to 69.9% and 63.6% cells in PBS (control) and anastrozole treated cells. However, exposure to immunonanoparticles showed stronger arrest at G2/M phase (29.3%) which was almost 1.7 times higher than anastrozole drug solution. The treatment with anastrozole, anastrozole PCL-PEG nanoparticles, Immunonanoparticles to MCF7 cells showed a S, G2/M arrest of (16.4, 17.2%), (14.2, 24.8%), and (19.6, 29.3%) compared to control (12.7, 16.0%).

Results of cell cycle analysis demonstrated that exemestane treated cells showed stronger arrest at G0/G1 phase as compared to nanoparticulate formulations. Immunonanoparticles showed lesser percentage of cells at G0/G1 phase (45.3%) as compared to 68.6% and 60.2% cells in PBS (control) and exemestane treated cells. However, exposure to PLGA-immunonanoparticles showed stronger arrest at G2/M phase (34.2%) which was almost 1.6 times higher than exemestane drug solution. The results indicated that exemestane loaded PCL Immunonanoparticles showed a significant G2/M arrest compared to control, exemestane solution and PCL-PEG

nanoparticles. The arrest was almost 1.6 times greater than the drug solution which correlates with the findings that ligand conjugated nanoparticles were more effective in controlling the cell cycle phases as compared to drug solution in MCF7 cells.

To assess the ability of immunonanoparticles to induce apoptosis in MCF7 cell lines, apoptosis study was conducted using standard Annexin V staining procedure. The intensity plot of FITC vs. Texas Red was sectioned in four quarter to differentiate stained and unstained cells. Based on four quarters percentage of cells in early apoptotic cells (FITC positive and PI negative), late apoptosis (FITC and PI positive), necrotic (FITC negative and PI positive) and live cells (FITC and PI negative) were calculated. The results demonstrated higher fraction of total cell death in MCF7 cell line treated with immunonanoparticles than un-conjugated nanoparticles or native drug in solution following site-specific sustained release pattern. No difference in total cell death treated by immunonanoparticles or un-conjugated nanoparticles in MDAMB231 cells was observed. The augmented apoptotic activity of immunonanoparticles in receptor positive cells (MCF7) can be correlated with the cellular uptake results showing higher endocytosis of immunonanoparticles.

The results showed significant fraction of necrotic, early and late apoptotic population of cells after exposure with anastrozole solution, anastrozole loaded PLGA nanoparticles, PLGA-PEG nanoparticles and immunonanoparticles. Control group treated with PBS showed only 1.6% and 3.6% cells in apoptotic phases. After 24 h of exposure with anastrozole solution, only 5.4% cells were in apoptotic phase (early and late apoptosis) whereas exposure with anastrozole loaded PLGA nanoparticles, PLGA-PEG nanoparticles and immunonanoparticles showed 32.6%, 43.7% and 60.9% cells in apoptotic phase. With increase in exposure time to 48 h, the percentage of cells in early apoptotic phase decreased, at the same time percentage of cells in late apoptotic phase were found to be increased. This is possibly due to conversion of early apoptotic phase into late apoptotic phase

The treatment with different nanoparticles formulations to MCF7 cells showed a significant increase in necrotic and late apoptotic population after 24 h. whereas after 48 h of exposure the necrotic population got decreased with an increase in early and late apoptosis explaining apoptosis as the possible mode of cell death. The population statistics after 24 h treatment of PCL-PEG nanoparticles, immunonanoparticles

exhibited a necrotic and late apoptotic population of (6.7 and 17.7%) and (12.3 and 22.9%) respectively compared to the drug solution (1.0 and 3.9%). However, 48 h exposure showed an increase in early and late apoptotic population of (0.9 and 33.8%) and (8.9 and 44.9%) than the drug solution (0.7 and 5.3%). Previous studies explained the role of estrogen in inducing breast cancer proliferation and prevention of apoptotic stimulation. Estrogen deprivation or exposure to anti-estrogens (aromatase inhibitors) leads to apoptotic cell death in MCF7 tumors.

The results showed significant fraction of necrotic, early and late apoptotic population of cells after exposure with exemestane solution, exemestane loaded PLGA nanoparticles, PLGA-PEG nanoparticles and PLGA-PEG Immunonanoparticles. Control group treated with PBS showed only 0.2% and 0.4% cells in apoptotic phases. After 24 h of exposure, exemestane PLGA nanoparticles, PLGA-PEG nanoparticles and PLGA-PEG Immunonanoparticles showed 13.0%, 26.5% and 36.6% cells in apoptotic phase which increased to 17.3%, 42.3% and 67.5%, respectively. After 24 h of exposure with exemestane PCL nanoparticles, PCL-PEG nanoparticles and PCL-PEG immunonano-particles showed 9.8%, 25.7% and 35.4% cells in apoptotic phase which increased to 16.6%, 41.6% and 70.2% after 48 h respectively.

The results showed significant fraction of necrotic, early and late apoptotic cell population after exposure (24 and 48 h) to all exemestane formulations whereas control group treated with PBS showed only 0.2% and 0.4% cells in apoptotic phases. After 24 h of exposure with exemestane PCL nanoparticles, PCL-PEG nanoparticles and Immunonanoparticles, 9.8%, 25.7% and 35.4% cells were seen in apoptotic phase which increased to 16.6%, 41.6% and 70.2% respectively after 48 h.

The higher anti-proliferative activity of immunonanoparticles than PEGylated/non-PEGylated formulation in MCF7 cells is the outcome of decreased cell cycle progression. No significant difference in anti-proliferative activity by immune-nanoparticles and PEGylated/non-PEGylated formulations in MDAMB231 cells were observed. However, greater efficiency of immunonanoparticles in arresting more number of receptor positive cells (MCF7 cells) can be explained on the basis of the intracellular drug levels at the site of action (due to enhanced cellular uptake following receptor mediated endocytosis) for a longer period of time (following sustain release) than drug and unconjugated nanoparticles.

The result depicts the presence of a significant fraction of early apoptotic, advanced/late apoptotic and necrotic cell population following treatment with drugs, drug loaded PEGylated nanoparticles and Immunonanoparticles. In MCF7 cells, a higher population of early apoptotic cells and late apoptotic cells was observed in the case of immunonanoparticles but un-conjugated nanoparticles showed less early apoptotic or late apoptotic cell population. Disclosing the effect of immunonanoparticles in inducing apoptosis in receptor positive cell line (MCF7), flow cytometry results depict a higher fraction of apoptotic cells in the case of cells treated with immunonanoparticles than with PEGylated nanoparticles or drug solution. It is noteworthy to emphasize that MCF7 cells treated with immunonanoparticles showed augmented apoptotic activity compared to MDAMB231 cells which shows receptor mediated uptake of immunonanoparticles.

Radiolabeling of nanocarrier systems was performed to study their organ distribution pattern and its fate in vivo. The iodination of tyrosine and ER Ab was successfully performed and found to be stable even after 24 h. The nanoparticles were radiolabeled with ^{125}I and these radiolabeled complexes were intravenously administered to study blood clearance and biodistribution in mice model. In vivo animal studies results showed clear advantage of immunonanoparticles over other non-targeted formulation in term of lower blood clearance and high uterus concentration and prolong plasma half life. The biodistribution studies showed that immunonanoparticles distributed more in uterus which contains ER than other organs. This remarkable targeting efficiency was resulted because of affinity of ER antibody towards these organs. Thus, here we conclude that these nanoparticulate systems will work as a novel tool for ER positive tumors and can be used to deliver therapeutically active substance successfully in conditions such as breast cancer.

8.2 Conclusion

The goal of this study was to design PEGylated and antibody conjugated PLGA/PCL nanoparticulate system for targeting of anticancer drugs, anastrozole and exemestane to breast tumor. Both formulations were PEGylated for longer circulation half life and better tumor retention. FTIR, NMR and GPC reports demonstrated the successful conjugation. DSC studies indicated absence of any interaction. In vitro release studies indicated sustained release property of nanoparticles. Sucrose was found to be the best

cryoprotectant for these formulations as it showed good reconstitution property without significant change in particle size. Images of TEM has shown that the particles are spherical in shape and uniform in size distribution with no visible aggregation which is in relevance with data obtained from particle size analysis by Malvern Zetasizer. Phagocytic uptake studies of PEGylated and non-PEGylated nanoparticles on human acute monocytic leukemia cell line, THP-1 showed significant reduction in macrophage uptake of PEGylated nanoparticles and thus providing longer circulation half life. In vitro cell line studies have been performed to evaluate effectiveness of the formulation on cancer cells. Immunonanoparticles showed significant increase in cell cytotoxicity, apoptosis, cell uptake, and cell cycle arrest in comparison to only drug solution or PEGylated nanoparticles.

However, we need to conduct elaborate toxicological studies, preclinical studies and further investigations in human beings under clinical conditions before they can be commercially exploited.